THE UNIVERSITY of LIVERPOOL

Chromatic Driver Fatigue Monitoring System

Thesis submitted in accordance with the requirements of the University of Liverpool for the degree of Doctor in Philosophy by

Alex Koh Ker Keong

November 2008

Abstract

Sleep related vehicle accidents have been under publicised but remains as one of the main causes of road traffic accidents, as much as drink driving. This research aims to reduce this worldwide problem by developing a system to monitor fatigue driving. The thesis describes the research into the application of chromatic data processing techniques to detect early physiological and physical indicators of fatigue.

Physiological factors that influence drivers are based on the duration of the drive, how much rest they have throughout the journey and the quality of sleep they had prior to the drive. The physiological indicator algorithm of the system is developed to take account of these factors and calculates the tiredness level. The chromatic technique is then used to analyse the results to establish trends and signatures of early fatigue situations where a warning system can be introduced. The chromatic signatures of fatigue have been established using results from 20 road tests conducted by professional drivers.

Physical indicators such as early drowsy driving are detected by monitoring the behaviour of the vehicle. Micro sleep (e.g. head nodding, slow eye-blinking) can lead to lane drifting and vehicle swerving. These events are being regarded as early physical signs of sleepy driving. The main sensor for detecting the lateral yaw motion of the vehicle is a miniaturised gyroscope. Chromatic analysis is applied to the gyroscope output to identify and differentiate fatigue related events (e.g. swerves and lane drifting) from normal driving (e.g. left and right turning, roundabouts and bumpy roads)

Combining the extracted information of the physiological and physical indicators, a Chromatic Fatigue Driving System can be developed as a fail safe system which monitors and alerts driver during critical fatigue conditions.

Acknowledgements

For the past three years I have enjoyed the research work and gained skills that will prepare me for my career path ahead. I am very grateful for all the support everyone have given me through the ups and downs.

I would like to express my gratitude to Prof Jones who has helped and taught me so much. Thank you for the generous amount of time that you have patiently spent guiding me and talking through the challenges at work

Many thanks to all my colleagues in CIMS who have journeyed with me I will always remember the laughter and jokes in the G03 labs. Jing Zhang, Illias Rallis, Raj Kolupula, Anthony Deakin, Ken Wong, Yang Lihua, Nicola Telfer, Ian Thomas, Duncan Smith, Al Lawal, Joe Spencer, Paul Calton. I will miss working with you guys.

I would like to dedicate this to my Mom, Dad and Sister. Without the loving support from you all I would never have gone this far in life. You are always there for me every second from the day I was born. I love you all very much!

To my family members in Brunei, thank you very much for supporting me all these years of my life. Without you I will never have achieved so much in life. Love you all very much.

I must also thank my Evelyn Pang, for being with me all this time, supporting and strengthening me mentally when I was down. My successes are always sweet with you around me.

Lastly I will like to thank my beloved Grandpa! We will always miss you!

Table of Contents

ABSTRACT 2

ACKNOWLEDGEMENTS 3

TABLE OF CONTENTS 4

LIST OF FIGURES 8

LIST OF TABLES 11

CHAPTER 1 12

INTRODUCTION 12

1.1 Research Overview 12

1.2 Current Research and Technologies 13

1.3 Research Contributions 14

1.4 Research Objectives and Benefits 15

1.5 Thesis Outline 16

CHAPTER 2 17

LITERATURE REVIEW OF PREVIOUS WORK 17

2.1 Introduction 17

2.2 Fatigue related vehicle driving 17
2.2.1 Statistical Aspects 17
2.2.2 Time factor effects 19
2.2.3 Microsleeps 20

2.3 Monitoring Strategies for Fatigue Related Driving 21

2.4 Information Acquisition from Sensing Device 24

2.5 Sensor: Piezoelectric Vibrating Gyroscope 26

2.6 Chromatic Monitoring Technique 29
2.6.1 Introduction 29
2.6.2 Review of signal processing aspects of chromatic monitoring 29
2.6.3 Chromatic Processing Algorithm 30
2.6.4.1 Time Stepping 36

2.7 Summary 37

CHAPTER 3 38

EXPERIMENTAL SYSTEMS 38

3.2 Composite System (ASTiD) 39
3.2.1 Introduction 39
3.2.2 Overview of the Composite System 39
3.2.3 Installation of the composite system 43

3.3 Gyroscope System 43
3.3.1 Introduction 43
3.3.2 Overview of the Gyroscope system structure. 44
3.3.3 Data Acquisition 44
3.3.4 Software Development 45

3.4 Sensor Deployment 46
3.4.1 Dashboard Implementation 46
3.4.2 Steering Wheel Deployment 47
3.5 Video Capturing System 48

3.6 Summary 49

CHAPTER 4 50

EXPERIMENTAL METHODOLOGIES 50

AND TESTS PROCEDURE 50

4.2 Composite system (ASTiD) 51
4.2.1 The Experimental methods 51
4.2.2 Experimental Tests 55

4.3 Gyroscope System - Dashboard Implementation 56
4.3.1 The methodology of the system 56
4.3.2 Normal Driving Manoeuvres 57
4.3.3 Fatigue-related driving manoeuvres 59
4.3.4 Mode base driving 62
4.3.5 Experiments Conducted 63
4.3.6 Summary of Test Conditions 65

4.4 Gyroscope System - Steering Wheel Unit 65
4.4.1 Experimental methods of the steering wheel system 65
4.4.2 Normal Driving 66
4.4.3 – Fatigue-Related Driving 68
4.4.4 Experiments Performed 69
4.4.5 Summary 70

CHAPTER 5 ..... **71**

EXPERIMENTAL RESULTS **71**

5.2 Composite System Results **72**
5.2.1 Introduction 72
5.2.2 Unprocessed Data Results 72
5.2.2 Duration data results 74

5.3 Dashboard Unit Results (Gyroscope System) **76**
5.3.1 Introduction 76
5.3.2 Normal driving manoeuvre results 76
5.3.3 Results for fatigue related driving 80
5.3.4 Mode based driving results 82
5.3.5 Further Road test Experiments 83

5.4 Steering Wheel Results **87**
5.4.1 Introduction 87
5.4.2 Laboratory Steering Wheel results 87
5.4.3 Vehicle Steering Wheel results (Road test) 88

5.5 Summary **89**

CHAPTER 6 ..... **91**

CHROMATIC ANALYSIS AND DISCUSSION OF RESULTS **91**

6. 2 Chromatic Analysis of the Composite System Signal **92**
6.2.1 Introduction 92
6.2.2 Application of the Chromatic Processing technique 92
6.2.2.1 Chromatic Filtering 93
6.2.2.2 Chromatic parameters representation 95
2. Interpretation of L 96
6.2.3 Chromatic Analysis of the Composite System 98
6.2.3.1 Chromatic analysis of the Physiological Tiredness Score (PTS) 99
6.2.3.3 Comparison between the chromatic analysis of PTS and DTS 102

6.3 Chromatic Analysis of the Dashboard System Signals **103**
6.3.1 Introduction 103
6.3.2 Application of Chromatic analysis 103
6.3.2.1 Chromatic Filtering 103
6.3.2.2 Chromatic Transformation 106
6.3.2.3 Comparison of normal and fatigue related driving manoeuvres 107
6.3.3 Chromatic Analysis of the Dashboard unit System 110
6.3.3.1. Analysis for detection of event using the chromatic threshold level 111
6.3.3.2. Mode based driving effects. 115

6.4 Chromatic Analysis of the Steering Wheel system **119**
6.4.1.1 Analysis of the laboratory steering wheel results 119
6.4.1.2 Discussion of the road test result 120

6.5 Combination of physiological and physical factors. **125**
6.5.2 Combination of Physiological and Physical Alarm system. 126

6.6 Summary **128**

CHAPTER 7 ..... **130**

CONCLUSIONS AND FUTURE WORK 130

7.1 Conclusions 130

7.2. Future Work 133

PUBLICATIONS 134

REFERENCES 158

APPENDICES 169

List of Figures

FIGURE 2.2.3.1. SELF-REPORTED CONSEQUENCES OF DRIVERS FALLING ASLEEP. N=1061. [SAGBERG, 1999] ... 21
FIGURE 2.6.3.1 FLOW CHART FOR CHROMATIC PROCESSING OF DATA AND SIGNALS ... 30
FIGURE 2.6.3.1.1 OVERLAPPING RESPONSES OF THREE FILTERS WITH EQUAL WIDTH (R_w, G_w AND B_w) ... 31
FIGURE 2.6.3.3.1 CHROMATIC MAPPING WITH: H-S AND H-L POLAR DIAGRAMS [ZHANG, 2004] ... 34
FIGURE 2.6.3.4.1 CHROMATIC PROCESSING OF TWO SIGNAL A AND B AND THEIR REPRESENTATION ON CHROMATIC POLAR DIAGRAMS H-S AND H-L ... 35
FIGURE 2.6.4.1 FILTERS TIME STEPPED WITH A STEP PERIOD T ... 36
FIGURE 3.2.2.1 – OVERVIEW OF THE COMPONENTS STRUCTURE AND SENSORS USED FOR THE COMPOSITE SYSTEM (ASTID) ... 39
FIGURE 3.2.2.2 SPECIFICATIONS OF THE CERAMIC GYROSCOPE ... 40
FIGURE 3.2.2.3 - CIRCADIAN RHYTHM DEFAULT PLOT FOR VARIOUS SLEEPING CONDITIONS ... 41
THE QUALITY OF SLEEP JUDGEMENT (B) "GOOD", "POOR", "BAD" IS INPUTTED INTO THE ASTID UNIT BY THE DRIVER PRIOR TO COMMENCING THE DRIVE. THIS IDENTIFIES THE APPROPRIATE CIRCADIAN RHYTHM CURVE (FIGURE 3.2.2.3) TO BE APPLIED BY THE UNIT FOR THAT PARTICULAR JOURNEY [HORNE, 2001] ... 41
FIGURE 3.2.2.4 – COMPOSITE SYSTEM DISPLAYING THE TIREDNESS LEVEL OF 5/6 (WARNING LEVEL) ... 42
FIGURE 3.2.2.5 – THE LED UNIT WITH THE 6 DIFFERENT LED INDICATORS ... 42
FIGURE 3.2.3.1 – DIAGRAM SHOWING THE REAR VIEW OF THE COMPOSITE UNIT WITH THE POWER SUPPLY CABLES. ... 43
FIGURE 3.2.3.2 – SHOWING AN ASTID UNIT INSTALLED ... 43
ONTO THE UNIVERSAL DIM SLOT OF THE DASHBOARD. [PERNIX, 2005] ... 43
FIGURE 3.3.1.1 – OVERALL STRUCTURE OF THE GYROSCOPE SYSTEM ... 44
FIGURE 3.3.4.1 - FLOWCHART OF THE GYROSCOPE SYSTEM SOFTWARE ... 45
FIGURE 3.4.1.1 –IMPLEMENTATION OF THE GYROSCOPE SYSTEM ON THE DASHBOARD OF A VEHICLE ... 46
[KOH ET AL 2007] ... 46
FIGURE 3.4.1.2 – MOUNTING OF A GYROSCOPE ON A VEHICLE DASHBOARD ... 47
(A) OVERHEAD VIEW OF VEHICLE WITH THE GYROSCOPE PLACED HORIZONTALLY ... 47
(B) FRONT VIEW OF VEHICLE WITH THE GYROSCOPE DETECTING THE YAW ANGLE OF THE VEHICLE ... 47
FIGURE 3.4.2.1 – GYROSCOPE INSTALLATION ON A LABORATORY BASED STEERING WHEEL ... 47
FIGURE 3.4.2.2 –MOUNTING OF A GYROSCOPE ONTO A VEHICLE STEERING WHEEL ... 48
(A) OVERHEAD VIEW OF THE STEERING WHEEL WITH THE GYROSCOPE SYSTEM ... 48
(B) FRONT VIEW OF THE STEERING WHEEL WITH THE GYROSCOPE SYSTEM ATTACHED ... 48
FIGURE 3.5.2 – DIAGRAM SHOWS 4 FRAME SHOT OF TURNING ON THE STEERING WHEEL ... 49
FIGURE 4.2.1.1 - OVERALL STRUCTURE OF THE TEST PROCEDURE FOR THE COMPOSITE SYSTEM ... 51
FIGURE 4.2.1.2 – FIGURE SHOWS THE VARIOUS CIRCADIAN RHYTHMS IN RELATION WITH THE QUALITY OF SLEEP ON PREVIOUS NIGHT. THE Y-AXIS SHOWS THE PHYSIOLOGICAL TIREDNESS SCORE AGAINST TIME OF DAY FOR 24H CLOCK CYCLE. ALARM THRESHOLD IS SET AT 0.95 INDICATED IN RED DOTTED LINE ... 52
FIGURE 4.2.1.3 SHOWS THE VEHICLE DRIVEN FROM MOTORWAY MODE TO TOWN MODE. THE GRAPH IS PLOTTED FOR GYROSCOPE OUTPUT AGAINST TIME. ... 54
FIGURE 4.2.2.1 – NORMAL VEHICLE MANOEUVRES ... 58

(A) LEFT AND RIGHT TURNING EXAMPLES 58
(B) CAR-PARKING EXAMPLES 58
(C) VEHICLE NEGOTIATING A ROUNDABOUT 58
(D) PITCH AND ROLL MOVEMENT OF A VEHICLE 58
FIGURE 4.3.3.1 – VEHICLE MOVEMENT WHEN ALERTED BY RUMBLE STRIP 60
FIGURE 4.3.5.1 – MAP SHOWS THE ROUTE (BLUE ROUTE) FROM THE STARTING POINT (A) AND FINISHING POINT (B) 64
FIGURE 4.4.2.1 FRONT VIEWS OF THE STEERING WHEEL MOVEMENTS 67
(A) LEFT OR RIGHT TURN (~90^0) 67
(B) PARKING AND HANDLING OF VEHICLE (0~360^0, MAX 540^0) 67
(C) NEGOTIATING ROUNDABOUT (MAINTAINED AT ~ 45^0) 67
FIGURE 4.4.3.1 FATIGUE RELATED DRIVING WHEEL ROTATION 68
(A) COMPARISON OF ANGULAR CHANGES FOR ALERT AND FATIGUE CHANGES 68
(I) ALERT (II) FATIGUE 68
(B)SWERVE REACTION 68
FIGURE 5.2.2.2. DIFFERENCE GRAPH OF THE RAW DATA (FIGURE 5.2.2.1). 75
(DIFFERENCE GRAPH = RAW DATA – CIRCADIAN RHYTHM) 75
(A, B, C, D –DRIVERS. 1, 2, 3, 4, 5-SECTORIAL REGIONS OF INCREASING TIREDNESS) 75
[KOH ET AL 2007] 75
FIGURE 5.3.2.1. GYROSCOPE OUTPUT SHOWING SIGNAL FEATURES OF 2 DIFFERENT MANOEUVRES: PARKING AND HANDLING (0-1.5MIN) & LEFT AND RIGHT TURNING (1.5-3MIN) 77
FIGURE 5.3.2.2. GYROSCOPE OUTPUT SHOWING SIGNAL FEATURES OF VEHICLE NEGOTIATING ROUNDABOUTS 78
FIGURE 5.3.2.3. GYROSCOPE OUTPUT SHOWING SIGNAL FEATURES OF VEHICLE NEGOTIATING ON A SPEED BUMP 79
FIGURE 5.3.2.4 GYROSCOPE OUTPUT SHOWING SIGNAL FEATURES OF VEHICLE ACCELERATION AND DECELERATION 80
FIGURE 5.3.3.2. ENLARGED VERSIONS OF THE SECTION OF FIGURE 5.3.3.1 82
(A) 2 SWERVES 'S1' AND 'S2' 82
(B) 2 LANE DRIFTING 'D1' AND 'D2' 82
FIGURE 5.3.4.1. GYROSCOPE OUTPUT SHOWING DIFFERENT SIGNALS ASSOCIATED WITH VARIOUS DRIVING MODES 83
FIGURE 5.3.5.1 UNPROCESSED GYROSCOPE OUTPUTS FOR EXPERIMENTAL TESTS 86
(A) TEST 2 86
(B) TEST 3 86
(C) TEST 6 86
FIGURE 5.4.2.1 –GYROSCOPE OUTPUT FROM THE LABORATORY STEERING WHEEL TEST 87
FIGURE 5.4.3.1 –GYROSCOPE OUTPUT SIGNALS:- 88
(A) THE DASHBOARD UNIT (EXPERIMENTAL NO 8) 88
(B) THE STEERING WHEEL SYSTEM 88
FIGURE 6.2.2.1 DEPLOYMENT OF THE CHROMATIC RGB FILTERS ONTO THE COMPOSITE SYSTEM OUTPUT RESULTS OF FIGURE 5.2.2.1. (FILTER IS CONFIGURED AT 75 MINS TIME STEPPED 1 MINUTE). [KOH ET AL 2007] 93
FIGURE 6.2.2.2 4 DIFFERENT FORMS OF SIGNALS FOR THE COMPOSITE SYSTEM 94
(A) INCREASING TIREDNESS 94
(B) DECREASING TIREDNESS 94
(C) RESTING TROUGH 94
(D) PEAK TIREDNESS 94
FIGURE 6.2.2.2.1 – CORRESPONDENCE BETWEEN SECTORS OF A H-L DIAGRAM AND THE TYPE OF LINEARITY OF A SIGNAL 96

FIGURE 6.2.2.2.2– EFFECT OF INCREASING SIGNAL AMPLITUDE GRADIENT UPON THE OUTPUTS OF R, G, B.... 97
FIGURE 6.2.2.2.3– H-L DIAGRAM SHOWING THE EFFECT OF INCREASING SIGNAL GRADIENTS..... 97
FIGURE 6.2.3.1.1 - CHROMATIC POLAR- DIAGRAM H-L FOR THE OVERALL OUTPUT SIGNAL OF FIGURE 5.2.2.1. 99
(DIFFERENT SYMBOLS CORRESPONDS TO VARIOUS DRIVERS A-D, FIGURE 5.2.2.1) [KOH ET AL 2007]..... 99
FIGURE 6.3.3.1. CHROMATIC POLAR-DIAGRAMS OF H-L FOR THE DIFFERENCE DATA OF FIGURE 5.2.2.2. 101
(DIFFERENT SYMBOLS INDICATE DIFFERENT STAGES OF FIGURE 5.2.2.2) [KOH ET AL 2007]..... 101
FIGURE 6.3.2.1.1 DEPLOYMENT OF THE THREE OVERLAPPING FILTERS (R, G AND B) EACH WITH A WIDTH OF 0.66S AND A TOTAL TIME WINDOW OF 1.32..... 106
(A) FATIGUE RELATED EVENT (S1) FROM FIGURE 5.3.3.2 (A)..... 106
(B) LEFT TURN 1 FROM FIGURE 5.3.2.1 106
(C) ROUNDABOUT 2 FROM FIGURE 5.3.2.2..... 106
FIGURE 6.3.2.2.1 CHROMATIC S AND L ON THE SWERVE 1 EXPERIMENTAL OUTPUT FROM FIGURE 5.3.3.2 (A)107
(S=SPREAD, L=STRENGTH ~ SHADED AREA) 107
FIGURES 6.3.2.3.1 CHROMATIC PARAMETER VALUES FOR DIFFERENT TYPES OF MANOEUVRES..... 109
(A) CHROMATIC L COMPARISON FOR DIFFERENT MANOEUVRES 109
(B) CHROMATIC S COMPARISON FOR DIFFERENT MANOEUVRES..... 109
FIGURE 6.3.3.1 FLOW CHART FOR THE REAL TIME FATIGUE EVENT DETECTOR..... 110
FIGURE 6.3.3.1.1 CHROMATIC OF L AND S AS FUNCTIONS OF JOURNEY TIME FOR THE TABLE 5.3.5.1..... 112
(A) TEST 2..... 112
(B) TEST 3..... 112
(C) TEST 6..... 112
FIGURE 6.3.3.2.1 FLOW CHART FOR THE REAL TIME FATIGUE EVENT DETECTOR WITH MODE BASE DRIVING. 116
FIGURE 6.4.1.1.1 EVENTS DETECTION FOR THE TEST RESULTS OF FIGURE 5.4.2.1..... 120
FIGURE 6.4.1.2.1 – TIME VARIATION OF CHROMATIC ANALYSIS PARAMETERS FOR THE TEST RESULTS OF FIGURE 5.4.3.1 121
(A)DASHBOARD UNIT (EXPT NO. 8)..... 121
(B) STEERING WHEEL SYSTEM..... 121
(A) 122
FIGURE 6.4.1.2.2 – COMPARISON OF THE CHROMATIC RESULTS FOR SWERVE (S1) FROM FIGURE 6.4.1.2.1 122
(A)DASHBOARD UNIT (EXPT NO. 8)..... 122
(B) STEERING WHEEL SYSTEM..... 122
(A) 123
FIGURE 6.4.1.2.3 – COMPARISON OF THE CHROMATIC RESULTS FOR LANE DRIFTING (D1) FROM FIGURE 6.4.1.2.1..... 123
(A)DASHBOARD UNIT (EXPT NO. 8)..... 123
(B) STEERING WHEEL SYSTEM..... 123

List of Tables

TABLE 4.2.1.1 FIGURE SHOWS THE SCORE ADDED PER MINUTE FOR THE TOWN AND MOTORWAY MODE DRIVING. DEPENDING ON WHICH HOUR THE DRIVER IS IN DIFFERENT SCORE LEVEL WILL BE ADDED TO THE PTS. 53

TABLE 4.2.1.2 FIGURE SHOWS THE SCORE REDUCTION PER MINUTE ACCORDING TO THE DURATION THE VEHICLE IS IN STOP MODE 53

TABLE 4.2.1.3 DIFFERENT MODES REPRESENTED BY AVERAGE GYROSCOPE FOR THE LAST MINUTE OF A DRIVE 54

TABLE 4.2.2.1 – SUMMARY OF TESTS CONDUCTED WITH THE COMPOSITE SYSTEM (ASTID). 56

TABLE 5.3.5.1 – SUMMARY OF THE DASHBOARD IMPLEMENTATION TESTS (SAME ROUTE) 84

TABLE 6.3.2.1.1 LIST FOR NORMAL MANOEUVRES AND FATIGUE RELATED MANOEUVRES WITH TIME DURATION OF EVENTS AND GYROSCOPE OUTPUT (V) FROM SECTION 5.3 104

TABLE 6.3.2.3.1 THRESHOLD LEVELS FOR THE FATIGUE RELATED MANOEUVRES 109

TABLE 6.3.3.1.1 SUMMARY OF EVENT DETECTED DURING TEST 2, 3 AND 6. THE EVENT DETECTED CONSISTS OF SWERVES, LANE DRIFTING AND FALSE POSITIVES. 113

TABLE 6.3.3.1.2 SUMMARY EVENTS DETECTED, FALSE POSITIVES AND EVENTS MISSED FOR ALL 16 EXPERIMENTS FROM TABLE5.3.5.1 115

TABLE 6.3.3.2.1 AVERAGE GYROSCOPE OUTPUTS FOR DIFFERENT DRIVING MODES 116

TABLE 6.3.3.2.1 SHOWS THE COMPARISON OF THE RESULTS OF MODE BASE DRIVING INTRODUCED 117

TABLE 6.5.1 QUANTIFICATION OF PHYSICAL TIREDNESS FACTOR BASED UPON THE NUMBER OF EVENTS DETECTED BY A GYROSCOPE AND SHOWING THE VARIOUS ALARM LEVELS. 126

TABLE 6.5.2.1 COMBINATION OF PHYSIOLOGICAL AND PHYSICAL INDICATORS OR DRIVING FATIGUE 128

Chapter 1

Introduction

1.1 Research Overview

Fatigue in the context of human behaviour is a temporary loss of strength and energy resulting from hard physical or mental work. Furthermore fatigue can be accumulated throughout the daily human activities which is also affected by the quality of sleep of the previous night **[Gandevia et al, 1995; Hawley and Reilly, 1997; Hagberg 1981]**. Studies of the human body biological circadian clock have shown that there are two dips and troughs in a 24hour clock cycle. The human body feels most tired in the early hours of the morning (0200h-0400h) and mid afternoon (1400h-1600h) **[Halberg et al, 2003]**.

There is an increasing awareness in the role of human fatigue in reducing the effectiveness of performing everyday tasks such as vehicle driving. Drowsy driving encompasses several aspects; falling asleep while driving or simply not paying attention due to fatigue which is caused by the lack of sleep. Statistical research for road accidents have shown that there are at least 20% in Britain and 11.4% in Italy which are sleep related. **[Horne and Reyner, 1995; Gabarino et al, 2001; Blincoe et al, 2002]**. Most of these sleep related accidents occurs at three major times i.e. at 0200h, 0600h and 1600h which are related to the Circadian rhythm of the human body **[Horne, 2001]**. Most of these accidents are caused by men under the age of 30 **[Horne and Baulk, 2003]**. Sleep related accidents are largely dependent on the time

of the day and this accounts for a significant proportion of these accidents occurring on motorways and under monotonous road conditions **[Reyner and Horne 2000]**.

The effect of driving while fatigued causes impairment such as lane drifting during micro-sleeps, followed by vehicle lane corrections **[Risser et al, 2000; Reyner and Horne 1998 a]**. Most drivers are often not motivated to take a break or have a nap when becoming tired, but rather prefer to engage in several activities in order to try and keep awake. However research has shown such activities such as opening the window, increasing the volume of the radio, can only postpone sleep for a few minutes **[Reyner and Horne 1998 b]**. On the other hand, a nap of at least 15 minutes is very effective and enables a driver to continue driving in an alert and vigilant condition for a considerable period **[Reyner and Horne 1997]**.

Driver fatigue is recognised to be among the most important causative factors in road crashes, on par with alcohol, speeding and inattention **[Sagberg et al, 2004]**. Also, most drivers are unaware of the fact that alcohol intake can exacerbate the driving impairment caused by sleep deprivation **[Horne et al, 2003]**. Other causes which can worsen sleep related accidents are drivers with sleep apnoea problems. Sleep apnoea is a medical condition characterised by temporary breathing interruptions during sleep. Patients with sleep apnoea may claim to have a good 8 hours sleep the night before, but are often have poor quality sleep due to the frequent interruptions. They may experience a more rapid onset of sleepiness when driving compared to healthy individuals falling asleep at the wheel due to sleep deprivation **[Turkingtona et al, 2001]**.

1.2 Current Research and Technologies

Driving fatigue management system aims to improve the driver's awareness of driving fatigue thereby reducing driving impairment such as lane drifting and swerving **[Dinges, 2005]**. Currently there is a huge need to provide assistive monitoring for vehicle operators to reduce these potential fatigue related accidents. Such monitoring system is designed to detect early warning signs of fatigue. It is discovered that early signs of fatigue can be identified by microsleeps **[Horne et al,**

2003], rate of eye blinking **[Johns 2003b]** and erratic driving behaviour **[Dinges, 2005]**. Incorporation of these features into the monitoring systems are required for early detection of fatigue driving.

Fatigue management technologies are being increasingly developed and validated in controlled laboratory settings, which is the initial step of validation. Examples of research technologies conducted in a controlled laboratory environment include vehicle driving simulators **[Muzet 2004; Reyner and Horne 2000]**, Electroencephalogram (recording of the electrical activity of the brain) **[Jammes, 2006; Wright 2006]**, Electro-Oculogram (recording of the electrical activity of the eyes) **[Johns 2003a; Evinger et al, 1991]**, video image processing equipment **[Horne et al, 2003]** and Steering Entropy (measure of steering wheel outcome in driving performance caused by microsleeps) **[Sagberg, 1999; Paul et al, 2005 a; Reyner and Horne 1998 a]**.

1.3 Research Contributions

In this thesis, the research focuses on how to transfer these technologies to improve driver alertness in an operational environment such as real road conditions. A monitoring system is developed to improve and manage the driver alertness whilst driving on real road condition. To achieve this, the research acknowledges the two important factors in sleep research: 'Physiological' and 'Physical factors'. The physiological factor needs an understanding of the human biological clock which affects driver tiredness at various time of the day **[Halberg et al, 2003]**. The physical factor is to understand the early physical indicators of fatigue build up while driving **[Reyner and Horne 2000]**.

The focal point of the physiological factor is the application of circadian rhythm whereby time of the day can affect driver alertness. The circadian rhythm is also affected by other factors such as duration of the drive, road monotonousness and quality of sleep the previous night **[Reyner and Horne 2000]**. These factors are taken into consideration to develop a system to monitor the physiological areas of driving fatigue. The designed system is known as the 'Composite System'

For the physical factors, Horne and Reyner have stressed that a vehicle driver in a fatigued state displays erratic driving behaviour **[Horne et al, 2003]**. Paul also states that steering entropy is a good indicator of increasing erratic steering behaviour during microsleeps **[Paul et al, 2005 a]**. Dinges agrees and confirms that possible early physical indicators are lack of activity on the steering wheel due to microsleeps which causes lane drifting on the road followed by driver corrective reaction (eg. Swerve) **[Dinges, 2005]**. Therefore the movement and patterns from the fatigue driving behaviour plus steering wheel activity will be the factors contributing to the physical aspects of the research. The system designed to monitor the early physical indicators of fatigue driving is called the 'Gyroscope System'

1.4 Research Objectives and Benefits

There is an under-development of driving fatigue management technologies other than in a controlled laboratory environment. Thus the main objective of this research is to develop such a system to operate in real road conditions which is also unobtrusive to the driver and the vehicle specifications (such as the steering wheel). The system should only act as an advisory system and not interfere with the driver during operation.

The main purpose of the two systems, Composite System and the Gyroscope System, is to monitor the fatigue level of the driver and to detect early signs of fatigue. The key objectives of the research development are:-

1. Unobtrusive design to the driver and the vehicle specifications
2. Economical cost factor
3. Acts as an advisory system to the driver
4. Implements both Physiological and Physical factors
5. Live monitoring and operates in actual traffic conditions

The two system (Composite and Gyroscope system) will produce complex data output which needs to be processed and represented in a simple form for easy interpretation. With the results output from the physiological (Composite system) and physical

(Gyroscope system) system there is a need to process these complex data output and represent the information in a simple representative approach. A novel technique developed by the CIMS research group in the University of Liverpool which fits this purpose, is called the 'Chromatic Processing' technique. This is a unique signal processing technique which applies three overlapping Gaussian filter and divides the data into three parameter; H, L and S **[Jones et al. 2000]**. H indicates the dominant signal information, L indicates the strength of the signal and S indicates the spread of the signal **[Zhang et al. 2004]**. With these parameters specific information can be characterised and identified within the data provided **[Wong et al. 2006]**. This key advantage is the early diagnosis of such fatigue events which can lead to prognosis of sleepy driving and with alarm indication.

1.5 Thesis Outline

The thesis has been structured into seven chapters. Chapter 2 discusses the background research of the current market systems for identifying sleepy driving and provides a theoretical review of chromatic methodology. Chapter 3 provides information on the design of the two experimental system; composite system (physiological indicator) and gyroscope system (physical indicator). Chapter 4 is about the methodology, the test procedures on how the design system operates. Chapter 5 displays the experimental results. Chapter 6, discusses the analysis of the experimental result using the chromatic processing technique. Further details on how the alarm system is implemented to detect early signs of fatigue are also discussed in this chapter. Finally the conclusion and further work, Chapter 7, summarises the work that has been undertaken to date and the research outcomes. It also suggests future areas for work development.

Chapter 2

Literature review of previous work

2.1 Introduction

This chapter presents a review of fatigue related driving accidents, current monitoring technologies and scientific factors of fatigue driving. It considers physiological aspects such as Circadian rhythms and physical factors such as driving behaviour and vehicle swerving. The need for a versatile yet efficient information extraction approached is considered and which can accommodate both physiological and physical aspects. One such candidate is the chromatic monitoring approach **[Jones et al. 2000]**. The nature and properties of this approach are reviewed. A miniature vibrating gyroscope is the main sensor applied in the system for the detection of early physical indicators of fatigue. The basic fundamentals of the gyroscope theory are also described.

2.2 Fatigue related vehicle driving

2.2.1 Statistical Aspects

Respondents in a recent survey of Irish motorists were asked if they had experienced extreme tiredness while driving in the past 12 months **[National Sleep Foundation, 2001]**. Almost 2 in every 5 motorists said they had experienced driver fatigue in the

past year and 1 in 8 admitted to having nodded off at the wheel of their vehicle at least once. The report also indicated that motorists in Ireland were not aware that is a major cause of road accidents with only 1.5% citing it as a number one cause. The danger is further compounded by the fact that 3 in every 7 extremely tired drivers do not stop to take a break and 1 in every 3 of these take no remedial action at all. These figures are alarming in light of that fact that 86.9 % of motorists surveyed said they believed they were excellent or good drivers **[National Sleep Foundation, 2001].**

According to the National Sleep Foundation's 2002 *Sleep in America* poll, about one-half of adult drivers - some 100 million people – admitted that they have driven feeling drowsy, while 17 percent, about 32 million people admitted that they had actually fallen asleep at the wheel. The National Highway Traffic Safety Administration in United States (NHTSA) conservatively estimates that 100,000 police-reported crashes each year are the direct result of driver fatigue each year, resulting in an estimated 1,550 deaths, 71,000 injuries and $12.5 billion in monetary losses including diminished productivity and property loss **[Stutts et al, 1999].**

In the UK, the Department of Transport estimates that on average the cost of a sleep crash is about £1.2 million **[RAC, 2003]**. In 1999 the Australian Transport Safety Bureau (ASTB) estimated that driver tiredness resulted in about 30% of all fatal crashes and 15% of serious injuries. The average cost of a fatality is approximately $1.7 million and about $400,000 for serious injury **[Australian Transport Safety Bureau, 1996]**.

Furthermore, information from the New York department of motor vehicle states that drowsiness and fatigue may play a role in crashes that are often attributed to other causes. About one million crashes annually (1 in 6 of all crashes) are thought to be caused by driver inattention due to sleepiness. Sleep deprivation and fatigue make these lapses of attention more likely to occur **[New York State Department of Motor Vehicles , 2007]**.

2.2.2 Time factor effects

The relative risk among lorry drivers to have a crash during the night hours (2000h to 0800h) is twice the risk during daytime (0800h to 2000h). Furthermore the risk during the night hours increased fourfold if the driver had driven for 11 hours or more **[Hamelin, 1987]**. Thus, there seems to be a combined effect of time of day and time on duty where the percentage of single-vehicle crashes were at a maximum at 0400h and a minimum at 1900h, with a 25 times higher risk at the time of maximum risk compared to the time of minimum **[Mackie and Miller, 1978]**. A comparison of risk at different times of the day, taking the traffic volume into account, showed the risk between 0300h and 0400h to be 13 times the minimum risk **[Kecklund and Åkerstedt, 1995]**. There is four times more risk of crashes with trucks at 0500h compared to 1900h **[Federal Motor Carrier Safety Administration, 2000]**.

Although the risk is highest during the night, there is also a peak in sleep-related crashes during the afternoon. Thus from the report it can be conducted that the time-of-day variation in sleep-related crashes mirrors the well-known circadian rhythm. According to the rhythm, humans are naturally sleepier and have reduced alertness not only late at night but also in the afternoon **[Horne and Reyner, 1995]**.

Circadian rhythms have evolved so that biological processes governing daily activities (like sleeping and digestion) are in the right state at the right time of day. Bright light (typically brighter than most artificial lighting) is the main stimulus by which the body clock is 'set' (eating times also have some influence). For example melatonin is a hormone influencing the sleep-wake cycle **[Altun, 2007]**. The increase of melatonin level tells the body it is time to sleep. When the eye detects light, melatonin production is suppressed. Although artificial light and Information and Communication Technology (ICT) allow people to work at any time, circadian rhythms have not changed. They take time to adapt to new routines and can adjust only by around an hour a day **[Foster and Kreitzman 2004]**. This may be why jetlag is associated not only with sleep loss, but with gastrointestinal problems and loss of appetite: different parts of the body take different lengths of time to adapt. **[Postnote, 2005]**

2.2.3 Microsleeps

Falling asleep while driving under monotonous driving conditions accounts for a significant proportion of accidents **[Reyner and Horne 2000]**. Times of day (circadian) effects are profound, and are as important in determining driver sleepiness as is the duration of a drive **[Halberg et al, 2003, Reyner and Horne 1998b]**.

Microsleeps are an indicator of excessive daytime sleepiness and have been associated with poor simulated driving performance **[Risser et al., 2000]**. The hypothesis is that a microsleep increases the potential for deviation from a driving lane because steering is temporarily neglected. This potential is especially strong when steering is neglected when negotiating a road curve or during periods in which the vehicle is perturbed by lateral disturbances, such as strong wind gusts, road canter, or bumps and ruts in the road surface. During microsleeps, these disturbances cause the vehicle to drift towards the lane edge; drivers then jerk awake and respond with a corrective steering action that is more aggressive than what is observed during wakeful driving **[Paul et al, 2005 b]**. Steering entropy is particularly designed to identify and quantify these larger and faster than normal corrective actions and is thus expected to provide a selective and sensitive metric to identify microsleeps and quantify their consequences with the lane deviation resulting from the microsleep **[Paul et al, 2005 a]**.

A Norwegian study showed that 4 per cent of microsleep incidents result in a crash, most of which were running-off-the-road crashes (3.5%) **[Sagberg, 1999]**. This is consistent with the finding that the most frequent non-crash consequence of microsleep was crossing near the side rumble strip (right edge). This occurred much more frequently than crossing either the lane dividing line (centre line) or the carriageway divider (left edge) line, as shown in Figure 2.2.3.1.

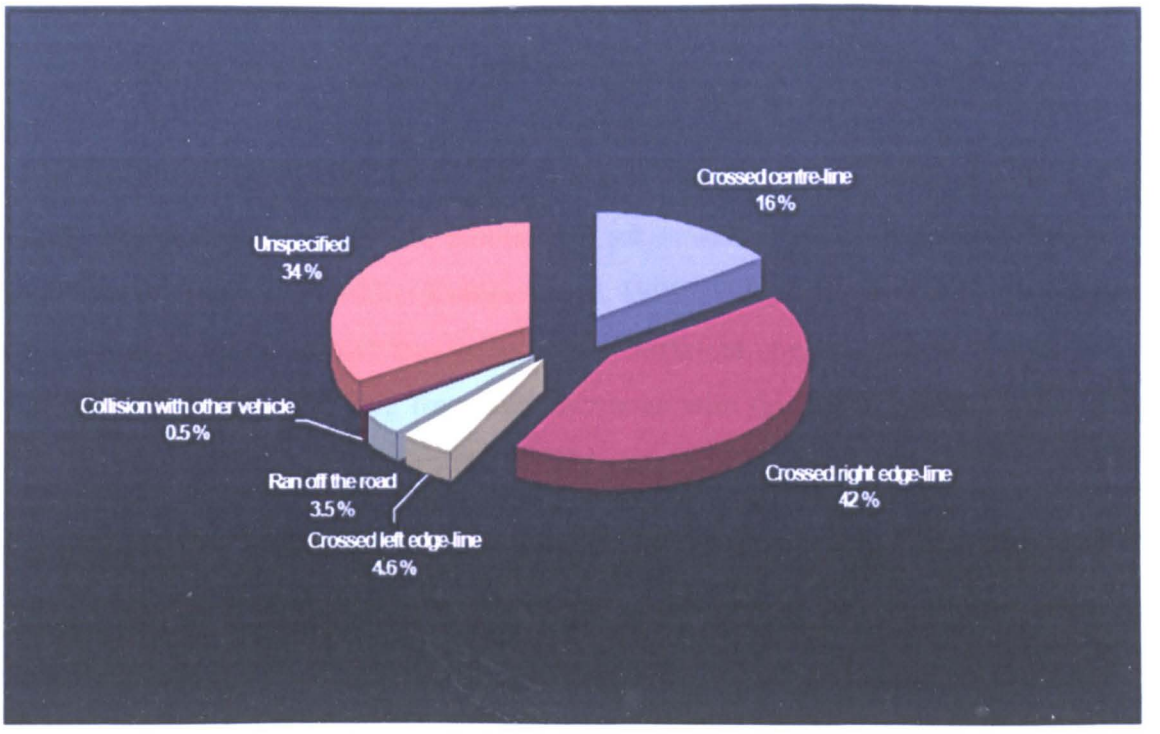

Figure 2.2.3.1. Self-reported consequences of drivers falling asleep. N=1061. [Sagberg, 1999]

2.3 Monitoring Strategies for Fatigue Related Driving

1. Laboratory Car Driving Simulator

Studying drowsy drivers in a laboratory driving environment is the preferred option due to safety hazard issues **[Staner et al, 2005]**. The driving simulator consists of a real vehicle with moving platforms and produces movements similar to those of a real car. There is a 3-screen system which gives 120 degrees viewing angle of the computer simulated road conditions **[Muzet, 2004]**.

It is comparatively easy in the laboratory to have sleep-deprived people, to use alcohol, to use medications, to shift the time for sleep period, to have people sleeping during the day and be active during the night **[Muzet 2004; Reyner and Horne 2000, Horne et al, 2003]**. The driving simulator makes it possible to approach some particular driver states, especially those that are dangerous in real traffic. However the driving simulator is far from a real driving experience as it ignores effects such as traffic stress, weather conditions, road conditions, speed bumps and other important situations which will influence the fatigue level when driving. The driver may also

have stronger motivation to maintain vigilance during real road driving compared to the driving simulator.

2. Eye and Eyelid detection.

From research, the eye and eyelid movements act as indicators of drowsiness during vehicle operation **[Johns 2003a; Evinger et al, 1991]**. Different parameters of eyelid activity can be measured, and they reflect partly different phenomena and influences during a sleepy drive. Blinking frequency increases with time on task and decreases with increased alertness level **[Johns 2003b]**. Eye closure duration increases with sedating or relaxing substances and with increasing daytime sleepiness (caused by Circadian rhythm); there is a gradual transition to long eye closures **[Johns 2003b]**.

However Miles (1929) discovered that eye closure can be delayed so that drivers are asleep with their eyes open which casts doubts about the effectiveness of eye closure detectors **[Miles, 1929]**. The rates of eye blinking are accurate in determining the fatigue level of a driver **[Stern et al, 1994]**, but driver blinking can be affected by the outside road lighting, sunlight, oncoming headlights, in-vehicle air temperatures and state of the ventilation system **[Reyner and Horne, 1997]**.

3. ECG and EEG measures

Electrocardiogram (ECG) is a record of the electrical activity of the myocardium which allows diagnosis of cardiac abnormalities **[Cooper, 1986]**. Electroencephalography (EEG) is a test used to detect and record the electrical activity generated by the brain **[Epstein, 1983]**. In most sleep research institutes around the world, ECG and EEG equipments are used on the driving simulator during experimental trials. These are used to gather data online whilst driving along with the body temperature **[Jammes, 2006]**. Amongst all possible data which could be acquired, the EEG is an important source of data on the level of vigilance. From the recorded information of the EEG, there are distinct differences in the data between a fully awake and a fatigue driver **[Jammes, 2006; Wright 2006]**.

However these systems are suitable for the laboratory environment only, there are many difficulties in transferring these technologies to real vehicles on the road due to obtrusiveness to driver, cost factor, and difficulties of usage.

4. Steering Entropy

A microsleep is a period of sleep lasting from milliseconds to a few seconds. It often occurs as a result of a sleep debt or mental fatigue. Microsleep becomes extremely dangerous when it occurs during situations when continual alertness is demanded for instance whilst driving a motor vehicle **[Risser et al, 2000; Paul et al, 2005 b]**. Paul defines steering entropy as the measure of steering wheel outcome in driving performance caused by microsleeps. The study of steering entropy is capable of defining decrements in driving performance caused by microsleep **[Paul et al, 2005 a]**. The knowledge gained from steering entropy shows that increased erratic steering behaviour occurs during microsleep episodes in drivers. Paul strongly suggests that microsleeps can provide a real-time marker for identifying physical factors of fatigue **[Paul et al, 2005 a]**.

Further research should address the physical driving performance which links to the steering wheel entropy behaviour, vehicle lane deviation and time to lane crossing **[Sagberg, 1999; Paul et al, 2005 a; Reyner and Horne 1998 a]**. An intelligent driver fatigue indicator system should be an unobtrusive monitoring system. The system should contain vital information such as driving patterns (lateral drifting) with integration of information on driver sleep (loss) status, time of day Circadian rhythm and monotonous driving conditions. These factors are important building blocks for constructing an intelligent monitoring system to provide countermeasures towards sleepy driving.

2.4 Information Acquisition from Sensing Device

The two types of sensors commonly used for detecting physical motions of a vehicle are accelerometers and gyroscopes. An accelerometer is a device for measuring the acceleration of a body in a particular direction or linear motion **[Nasiri, 2003]**. It is most commonly used as an instrument to measure the accelerations and decelerations generated by a vehicle **[Norton 1989]**. A gyroscope is a device for measuring angular rate rotation or maintaining orientation, based on the principle of conservation of angular momentum **[Green and Krakauer 2003; Burdess 1994]**. Applications for gyroscopes are very broad, some examples of which are; vehicle stability control, stabilisation in digital cameras and camcorders, motion control of hydraulic equipment or robots, platform stabilization in avionics and many more **[Burdess 1994; Nasiri, 2003].**

In the market today there are 4 common types of gyroscope sensors for various types of applications:-

1. **Spinning Mass Gyroscope** - A classical gyroscope, that has a mass spinning steadily with a free movable axis (so called gimbal) .When the gyro is tilted, a Gyroscopic effect causes precession (motion orthogonal to the direction of tilt) on the rotating mass axis, hence indicating the angle through which it has rotated **[Schilovsky, 1992].**

2. **Fibre Optic Gyroscope** – Applies the interference of light to detect movements. Optical gyroscopes, with virtually no moving parts, are replacing mechanical gyroscopes in commercial jetliners, booster rockets, and orbiting satellites **[Pavlath, 1994]**

3. **Gas rate Gyroscope** - Gas rate gyro sprays gas onto heated wires. When rotation occurs the spray is curved leading to a change in the temperature of the wires **[Dau et al; 2005]**

4. **Vibrating Gyroscope** - Utilises an oscillating mass in place of a spinning mass to sense angular rates. The mass oscillates back and forth through a fixed angle **[Yang 1998]**. One particular form of vibrating gyroscope is the piezoelectric type, whereby the mechanical rotational movements generate an output voltage by the piezoelectric elements **[H.Y.Fang 2000].**

Out of these four types, the vibrating gyroscope is selected because of its miniature size, low cost factor and low power consumption. These miniatures gyroscopes are used to measure angular rate (The rate of change of angular displacement with respect to time) **[Yang 1998]**. The vibrating gyroscope is used as a sensing device to measure angular rate in reference to the yaw movements in the vehicle in order to give an early signs of fatigue. The early signs of fatigue can be identified from erratic driving behaviour such as lane drifting and swerving **[Paul et al, 2005 a; Dinges, 2005].**

Low cost piezoelectric type vibrating gyroscopes have been developed for the automotive industry to measure the angular rate of the yaw axis **[H.Y.Fang 2000]**. One example is in the vehicle braking system. Current braking systems, ABS (automatic braking system), rely on the equalisation of all four wheel speeds during braking. Under ideal conditions, this results in safe controlled braking **[Masayoshi and Hedrick 1995]**. Nevertheless, it is still possible, in some circumstances, for the car to spin. In order to prevent the car spinning, it is first necessary to measure the angular rate of rotation (reference to yaw axis) and then to change the actuation controls to brake accordingly **[Masayoshi and Hedrick 1995]**. The angular rate is measured by the piezoelectric gyroscope which helps to improve road safety in this particular application.

2.5 Sensor: Piezoelectric Vibrating Gyroscope

Traditional mechanical gyroscopes are based on the inertia of a rotating rigid body where the device is a spinning wheel or disk whose axle is free to assume any orientation **[Guohong He et al, 1999]**. The advantages of the design and development of the vibrating gyroscope is its miniature size and low cost factor. **[Apostolyuk 2006]**. These miniaturized vibrating gyroscopes use vibrating mechanical elements (proof-mass) to sense rotation. They have no rotating parts that require bearings and hence they can be easily miniaturized and batch fabricated using micromachining techniques **[Apostolyuk 2006]**.

For vibrating gyroscopes, the excitation and detection of vibrations can be achieved via electrostatic or piezoelectric devices **[H.Y.Fang 2000]**. Manufacturing vibratory gyroscopes with piezoelectric material has been a more popular choice due to the wide variety of piezoelectric materials available, such as quartz, PZT (leat zirconate-titanate) PVDF (polymer-film) and several others **[Guohong He et al, 1999; H.Y.Fang 2000]**.

Piezoelectric materials have the property of producing a charge change, hence a D field change in response to a mechanical strain and vice versa. Their properties may therefore be described by the following equations:-

$$T_{ij} = c_{ijkl}S_{kl} - e_{kij}E_k, \quad D_i = e_{ijk}S_{jk} + \varepsilon_{ij}E, \qquad \text{--(1)}$$

$$S_{ij} = (u_{i,j} + u_{j,i})/2, \quad E_i = -\phi_{,i}, \qquad \text{--(2)}$$

where,

T_{ij} is the stress tensor,

S_{ij} is the strain tensor,

D_i is the electric displacement vector,

E_i is the electric field vector,

C_{ijkl}, e_{kij} and e_{ij} are the elastic, piezoelectric and dielectric constant

ε_{ijk} is the permutation tensor

u_i is the mechanical displacement vector

ϕ is the electric potential

The structures of piezoelectric gyroscopes are simple, being based upon a piezoelectric plate being excited in the direction of the electrical polarisation of the material to produce the mechanical vibration **[Apostolyuk 2006]**.

Consider a piezoelectric body rotated at a constant angular rate. A reference frame is attached to the body and rotating with it. Piezoelectric gyroscopes undergo small vibrations in the rotating frame **[Yang 1998]**. The mathematical equations describing the piezoelectric effect in the rotating frame need to incorporate both Coriolis and centrifugal forces in the equations in the inertial frame **[Yang 2000]**. If the reference frame rotates at a constant angular velocity $\Omega_j = \Omega\varsigma_j$ then the stress tensor T_{ij} and electric displacement vector D_i of equations (1) and (2) are given by the following equations:

$$T_{ji,j} - 2\rho\varepsilon_{ijk}\Omega_j\dot{u}_k - \rho(\Omega_i\Omega_j u_j - \Omega_j\Omega_j u_i) + O(\Omega^2) = \rho\ddot{u}_i, \quad \text{--(3)}$$

$$D_{i,i} = 0, \quad \text{--(4)}$$

Where ρ is the mass density and Ω_j is the angular velocity vector. (Superimposed dot indicates time derivative. Summation convention for repeated tensor indices and the convention that a comma followed by an index denotes partial differentiation with respect to the coordinate associated with the index are used). The terms involving Ω_j represent the sum of the Coriolis and centrifugal forces. $O(\Omega^2)$ are due to the initial fields **[Yang 2000]**.

Because piezoelectric gyroscopes are small (of the order of 10mm), their operating frequency ω_0 is high, usually of the order of 10 kHz or higher **[Yang 2005]**. Piezoelectric gyroscopes are used to measure an angular rate Ω much smaller than its resonant frequency ω_0. In this case, the centrifugal force due to rotation – which is

proportional to Ω^2 - is much smaller compared to the Coriolis force that is proportional to $\omega_0 \Omega$. Therefore the effect of rotation on the motion of piezoelectric gyroscopes is dominated by the Coriolis force **[Yang 2005]**

.

2.6 Chromatic Monitoring Technique

2.6.1 Introduction

The 'Chromatic Monitoring' approach is concerned with the integration of data collection, information extraction, data presentation. The realisation of each function involves the use of non-collimated or overlapping procedures which are seamlessly matched to each other **[Jones et al. 2000]**. The approach has also been used for data mining **[Brazer et al, 2001]**. For example, multiple sensors are often involved and their responsivities overlap. The data processing involves filters with overlapping responses in the measurement domain (which may be optical, acoustic, mass, space etc.). The information is then quantified in terms of various waveform attributes such as amplitude, dominating range and data spread **[Brazer et al, 2001]**.

The present research focuses on the application of chromatic concepts for processing data outputted from a conventional physical sensor (a gyroscope) and empirically established physiological data (i.e. diurnal patterns of fatigue). Information is then combined from each data set to give an overall quantification level of fatigue for a driver (i.e. when driving a road vehicle).

Another aspect of the chromatic approach may be regarded as a form of signal processing i.e. the analysis, interpretation and manipulation of signals **[James, 1996]** which may originate from various sources e.g. ECG, Radar, etc.

2.6.2 Review of signal processing aspects of chromatic monitoring

The chromatic methodology may be traced back to the work of Moon and Spencer (1981) and further elaborated by Jones et al (2000). Processing based upon chromatic principles may be applied for discriminating information and to present results in a simplified quantitative manner **[Wong et al. 2006]**. This approach involves filtering signals using a set of three filters (R, G and B) with overlapping responses. The output of these filters are then transformed into three chromatic parameters H, L and S **[Zhang et al. 2004]** which represents the signal defining features. The method may be

regarded as originating from a manifestation of a particular form Gabor Transform signal representation **[Jones et al. 2000]**.

The processing aspect of the chromatic approach has been used for extracting information from complex signals, which occur in many branches of medicine and engineering. Such signals may occur as pulses in the circulation of blood in the human body **[Deakin at al 2005]**, by faulty impeller blades on a mechanical pump **[Deakin at al 2005]** or localised faults on the rotating tyre of road vehicles **[Du, 2004]**. The chromatic processing technique has advantages in using simple algorithms, efficient data representation to identify signatures of events **[Zhang et al. 2004]** and a high level of traceability. Traceability is the ability to trace (identify and measure) all the stages that led to a particular point in a process **[Y Hino et al, 2007]**

For the present research, the processing aspects of the chromatic approach **[Jones and Russell, 1993; Jones et al, 2000]** are applied for extracting relevant information from complex data relating to both human physiological trends (circadian rhythm) and physical indicators required from gyroscopic signals produced by angular changes resulting from the yaw movements of a road vehicle.

2.6.3 Chromatic Processing Algorithm

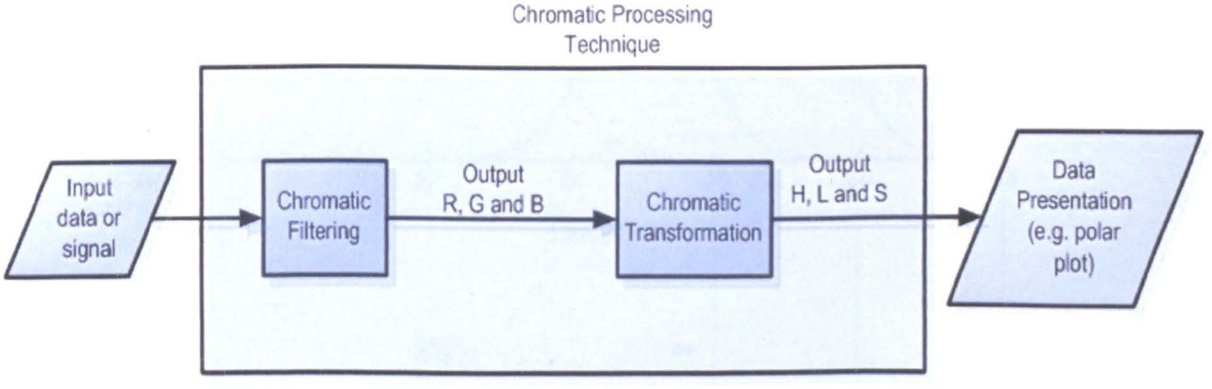

Figure 2.6.3.1 Flow chart for chromatic processing of data and signals

The basic concept of chromatic processing involves two main procedures, which are chromatic filtering and chromatic transformation to yield chromatic parameters

[Zhang et al. 2004]. The chromatic parameters are usually presented on polar diagrams from which trends can be conveniently observed. A flow chart of this procedure is given on figure 2.6.3.1

2.6.3.1 Chromatic Filtering

The chromatic filtering involves three filters (R, G and B) with overlapping responses which may be Gaussian, triangular etc in nature **[Zhang et al. 2004]**. A data set or signal having a complex structure can then be conveniently defined by only three parameters determined from the outputs of the three filters (R, G and B). Figure 2.6.3.1.1 shows three time based filter responses, each Gaussian in nature and overlapping at half width at maximum magnitude for all three processors R, G and B **[Wong et al. 2006]**. All three processors have equal width (w).

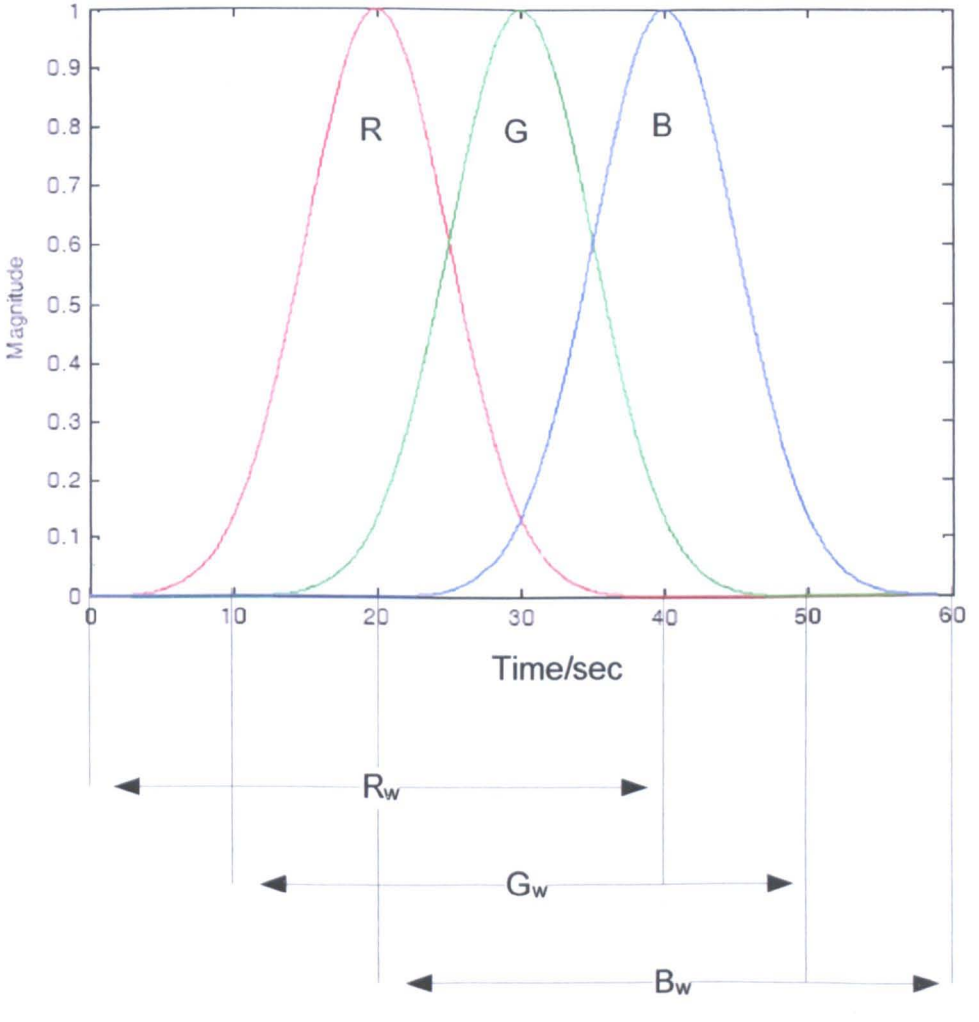

Figure 2.6.3.1.1 Overlapping responses of three filters with equal width (R_w, G_w and B_w)

These three over-lapping filters are superimposed onto a signal for analysis. Signals may be analysed either in the time domain as on figure 2.6.3.1.1 or frequency domain (horizontal axis) **[Du, 2004]**. The vertical axis parameter of the signal can be represented as voltage, current, capacitance, flow rate, depending on the application.

Before such signals are chromatically processed, they need to be normalised onto a common range from 0 to 1 **[Zhang, 2004]**. Normalisation is a mathematical process that adjusts for differences among data from varying sources in order to create a common basis for comparison **[James, 1996]**. One form of normalisation is given by the following equation:-

$$\text{Normalisation Parameter} = \frac{\text{Amplitude of parameter at one instance}}{\text{Maximum amplitude of parameter over entire signal duration}}$$

Following normalisation the signal is chromatically filtered (figure 2.6.3.1.1) to yield outputs from each filter according to **[Wong et al, 2005]** :-

$$\left\{\begin{array}{l} r = \sum_{t=1} R_w(t).w \\ g = \sum_{t=1} G_w(t).w \\ b = \sum_{t=1} B_w(t).w \end{array}\right\} \quad \text{---------- Eqn 2.6.3.1.1}$$

Where $R_w(t)$, $G_w(t)$ and $B_w(t)$ are the filter responses at time t and filter width (w). The data amplitudes are summed with respect to time for each of the filters (R, G and B) giving only a single output per filter **[Zhang, 2004; Wong et al, 2005]**.

2.6.3.2 Chromatic Transformation

The chromatic transformation **[Zhang, 2004; Wong et al, 2005]** involves converting the r, g and b values to the chromatic parameters H, L and S according to the following formulae.

$$H = \begin{Bmatrix} 60\dfrac{g-b}{\max(r,g,b)-\min(r,g,b)}, if\ r = \max \\ 60\left[2+\dfrac{b-r}{\max(r,g,b)-\min(r,g,b)}\right], if\ g = \max \\ 60\left[4+\dfrac{r-g}{\max(r,g,b)-\min(r,g,b)}\right], if\ b = \max \end{Bmatrix} \qquad (Eqn-2.6.3.2.1)$$

$$L = \frac{\max(r,g,b)+\min(r,g,b)}{2} \qquad (Eqn-2.7.2.2)$$

$$S = \frac{\max(r,g,b)-\min(r,g,b)}{\max(r,g,b)+\min(r,g,b)} \qquad (Eqn-2.7.2.3)$$

The chromatic parameter H represents the region on the horizontal axis of figure 2.6.3.1.1 (i.e. time, frequency, etc) which dominates. Chromatic L represents the nominal signal strength. The larger the amplitude the a higher the L value. Chromatic S is a measure of the spread of the signal, a larger spread produces a lower S value and vice versa. **[Jones et al, 2000; Zhang, 2004]**. When chromatic filtering is applied to continuous signals in the frequency or time domain, the parameters HLS have appropriate meaning in relation to the application **[Wong et al, 2005]**.

2.6.3.3 Chromatic Data representation

The values of the chromatic parameters can be represented via the coordinates on two-dimensional chromatic polar diagrams of H-S and H-L with H the azimuthal angle, S or L the radius ($\vartheta = H \in [0^0, 360^0], r = S \in [0,1], r = L \in [0,1]$) **[Jones et al, 2000]**. The chromatic boundary encompassing all signals remains fixed as a circle of unity radius. An important property of such signal representation on the chromatic polar diagrams is that the relationship between two signals is easily visualized. The superposition of the two complex signals can also be conveniently determined using simple moment equations **[Jones et al, 2000]**.

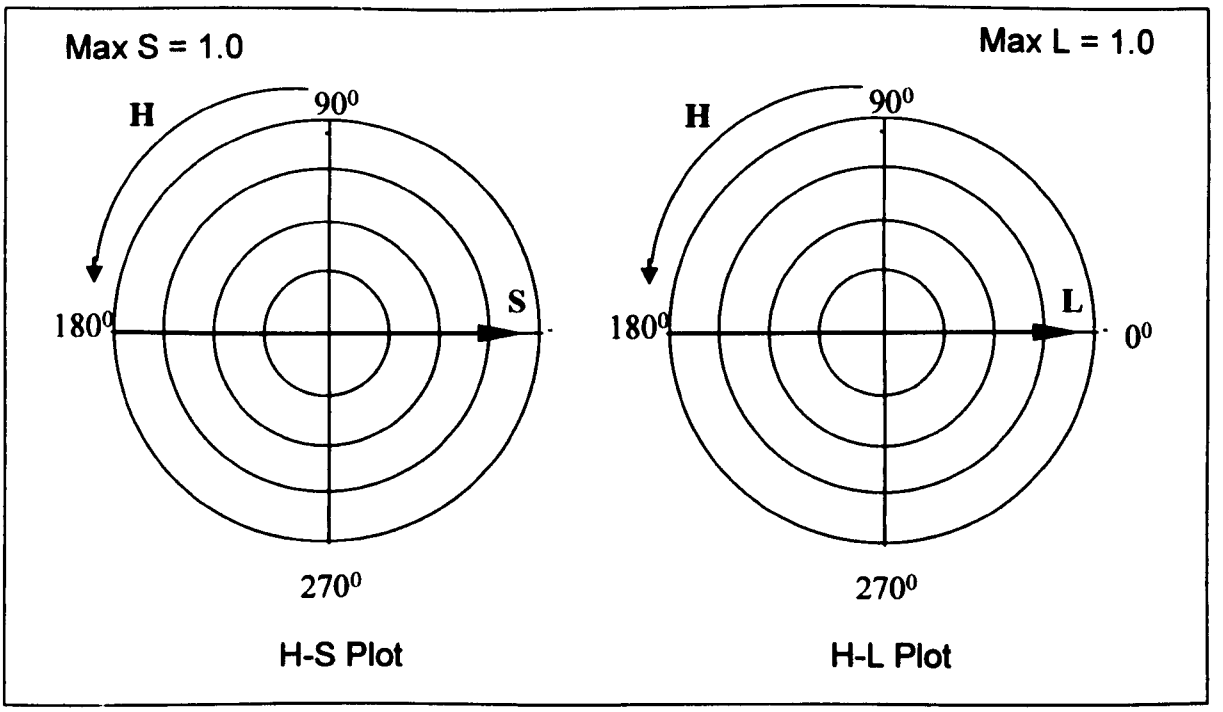

Figure 2.6.3.3.1 Chromatic mapping with: H-S and H-L polar diagrams [Zhang, 2004]

2.6.3.4 Example of the application of the method

An example of the chromatic processing approach and signal representation on two polar diagrams is given using two types of signals. This also illustrates the interpretation and meaning of the information represented by the values of the H, L and S parameters. The two example signals are shown on figure 2.6.3.4.1, where signal X has a higher amplitude and a wider spread compared to signal Y. The three overlapping Gaussian filters (R, G, and B) are applied as shown on the diagram

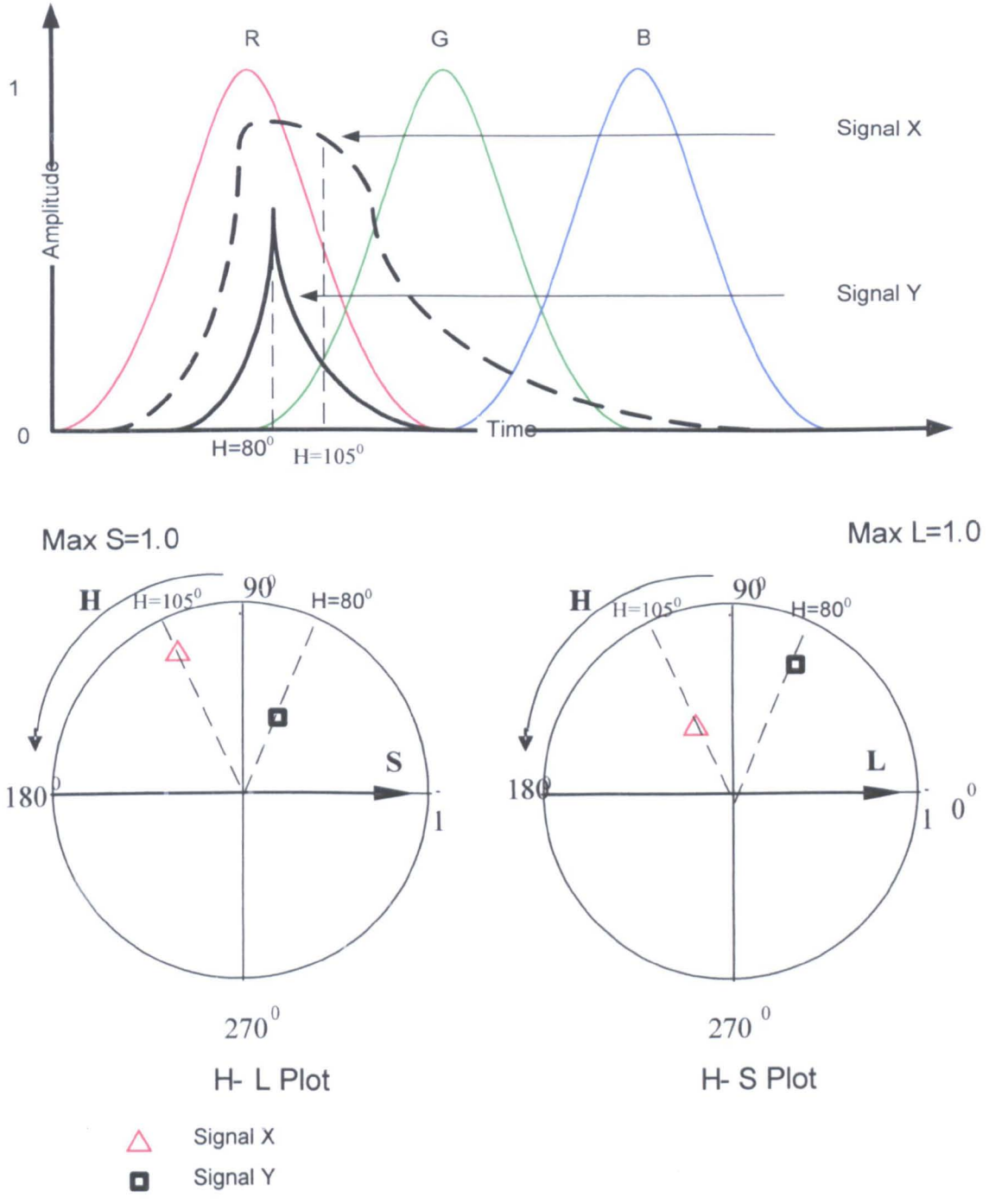

Figure 2.6.3.4.1 Chromatic processing of two signal A and B and their representation on chromatic polar diagrams H-S and H-L.

The parameter H represents the time region in which the signal is dominant. For signal A, $H=105^0$ and for signal B, $H=80^0$. Signal X is maximum at filter R and minimum at filter B. Signal Y is maximum at filter R and minimum and filter G.

The chromatic parameter L represents the nominal strength of the signal. The value of L for signal A is 0.89 and 0.45 for signal B, which means that signal A has a higher nominal strength than B.

The chromatic parameter S represents the spread of the signal. S has a value of 0.35 for signal A and 0.82 for signal B. Signal B has a higher S value than signal B because it has a smaller spread with respect to time.

2.6.4 Continuous type data

2.6.4.1 Time Stepping

It has been explained in the previous section, that the application of one set of three overlapping filters (R, G and B) will only output one set of chromatic parameter values (H, L and S). Generally the filter width (w) is chosen depending on the application. A process called 'Time Stepping' **[Jones et al, 2007]** may then be implemented in order to address the long-term continuously varying signal with the overlapping RGB filters (figure 2.6.4.1). The step size may be set, for example to be equal to the filter width. Infinite length time stepping is usually deployed for live-monitoring systems. As a result there is a sequence of chromatic parameter values produced corresponding to each time step. These values may then be displayed on H-L, H-S polar diagrams to track changes in the time varying signal (figure 2.6.4.2)

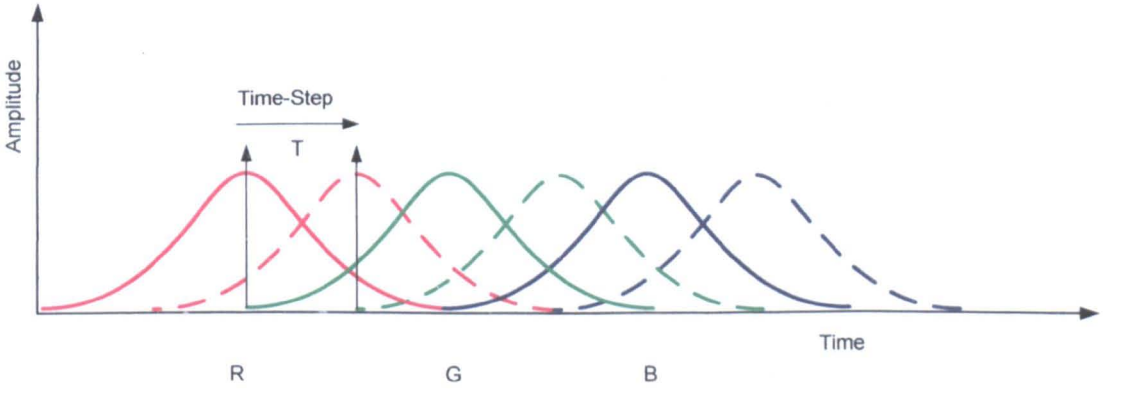

Figure 2.6.4.1 Filters time stepped with a step period T

2.7 Summary

This chapter has reviewed a number of aspects which relate to the monitoring of fatigue suffered by vehicle driver. There is statistical evidence for the serious effects of fatigue in causing road vehicle accidents. From the literature review it is understood that driving at different times of the day has an effect on the human circadian rhythm which contributes to fatigue driving. Microsleeps is a clear indicator of fatigue driving which can result in erratic driving behaviour such as lane drifting and vehicle swerving on the road due to lack of attention to the steering wheel orientation.

There have been several methods discussed for monitoring a driver's susceptibility to fatigue and microsleeps, which include eye and eyelid detection, ECG and EEG measurements and steering entropy. The latter appears to be a more promising approach since it reflects the effect of microsleeps on the actual vehicle movements.

An important need is to be able to extract relevant fatigue level indicators from the complex signals produced by the monitors utilised. The difficulty is exasperated by the need to incorporate both physiological (Circadian rhythm) and physical (lateral vehicle movement) components into the decision-making.

The miniature piezoelectric vibrating gyroscope measures the angular rate on a body to which it is attached. This is the preferred gyroscope because of its miniature size and low power consumption. The gyroscope is implemented into the design of a monitoring system as the main sensing device to detect angular rate changes with reference to the yaw movement on the vehicle. With the yaw or lateral motion of the vehicle, erratic driving can be identified when a driver is fatigued.

The processing aspect of the chromatic methodology involves two steps, chromatic filtering and chromatic transformation. The chromatic filtering involves applying three over-lapping filters to sample the signal followed by the chromatic transformation to yield the chromatic parameters (H, L and S). H represents the signal dominance on the three filters, L is the strength of the signal and S indicates the spread of the signal over the parameter space.

Chapter 3

Experimental Systems

3.1 Introduction

In this chapter, the experimental systems are described. These include the various sensors and components selected to integrate the system. There are two designed of experimental systems which have been designed for the development of the driver fatigue monitoring system, the 'Composite System' and the 'Gyroscope System'. The composite system is designed to capture fatigue driving information based on physiological factors such as the quality of sleep, influence of the circadian rhythm, duration of the drive and monotonous road conditions **[Halberg et al, 2003; Reyner and Horne, 1998b]**. The system consists of a microprocessor unit containing a complex algorithm which calculates the physiological factors indicating the fatigue level of the driver.

The gyroscope system is designed to gather fatigue driving information based on the physical aspects. These aspect encompasses the erratic driving behaviours such as lane drifting and road swerving **[Sagberg, 1999; Paul et al, 2005 a; Reyner and Horne 1998 a]**. The driving behaviours are used to identify early driving fatigue before situations becomes worse **[Dinges, 2005]**. The gyroscope system design is based on a vibrating gyroscope sensor to monitor the angular rate of the vehicle

reference to the yaw motion. The gyroscope detects the angular rate depending on where the sensor is installed on the vehicle. This system has been further applied in two different applications. The first application was a dashboard implementation whereby the system was installed on the front of the vehicle dashboard to detect lateral or yaw motion of the vehicle. The second application involved installing the gyroscope on the steering wheel to capture angular rate of the steering wheel itself.

3.2 Composite System (ASTiD)

3.2.1 Introduction

The composite system design is mainly based on the physiological research conducted by the Sleep Research Centre at Loughborough University. The abbreviation ASTiD is an acronym for 'Advisory System for Tired Drivers', whereby the system was designed to act as an advisory system to warn drivers of possible high fatigue situations **[Pernix 2005]**.

3.2.2 Overview of the Composite System

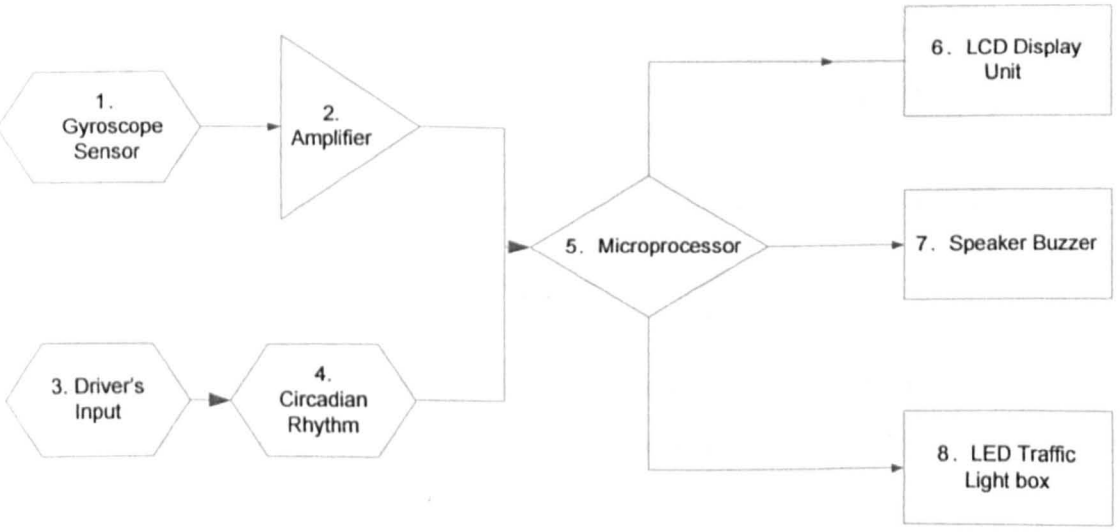

Figure 3.2.2.1 – Overview of the components structure and sensors used for the Composite System (ASTiD)

The structure of the composite system is shown in figure 3.2.2.1. The main sensor used in the system is a vibrating gyroscope which detects lateral changes of the vehicle movement. This helps to identify if the vehicle is travelling on monotonous or non-monotonous road conditions only. The driver is required to input information of

quality of sleep (shown on figure 3.2.2.3; good, poor and bad night sleep) before start, to generate the circadian rhythm for the particular driver at the time. The microprocessor contains the algorithm which analyses the information and outputs the tiredness result onto the LCD display, speaker and the external LED output.

1. Gyroscope Sensor

The gyroscope model is the NEC Tokin (CG-L43) miniature piezoelectric gyroscope. Its dimensions are only 8x15.5x5mm. Its advantages are:- a low power consumption and high sensitivity at 0.66mV/Degs/s. However the gyroscope is sensitive to temperature with a -15 to +5% change per degree.

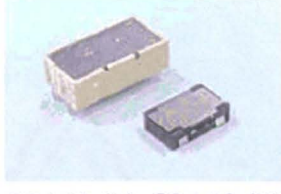

CG-L43 (L), CG-L53 (R)

	Ceramic Gyro CG-L43	Ceramic Gyro CG-L53
Dimensions (mm)	8×15.5×5	6.0×10×2.5
Oscillator dimensions (mm)	ϕ1.5×13	ϕ0.82×9
Supply voltage (V)	3	3
Sensitivity (mV/deg/s)	0.66	0.66
Output voltage at zero angular rate (mV)	-5 to +75	-5 to +75
Temperature characteristics of sensitivity (%)	-15 to +5	-15 to +5

Figure 3.2.2.2 Specifications of the ceramic gyroscope

2. Amplifier

The output voltage of the gyroscope ranges from -5mV to +75mV (figure 3.2.2.2). Since the output voltage is small, an operational amplifier is used to increase the output voltage up to a maximum value of 5 volts.

3. Driver's Input

The driver information required for the processing is:-

a) Driver's ID
b) Quality of Sleep
c) Confirmation of Date and Time

4. Circadian Rhythm

Figure 3.2.2.3 shows a typical Circadian Rhythm **[Horne, 2001]** covering a period of 24 hours. This takes the form of a tiredness score as a function of time from which a cyclical pattern is apparent. A maximum period of tiredness at night time (0200h-0400h) is followed by a maximum period of wakefulness (0900h-1100h), then a further tiredness peak (1500h) and a wakeful period (1730h-2000h). The absolute level of the Circadian rhythm decreases with the quality of sleep leading to the three curves of figure 3.2.2.3

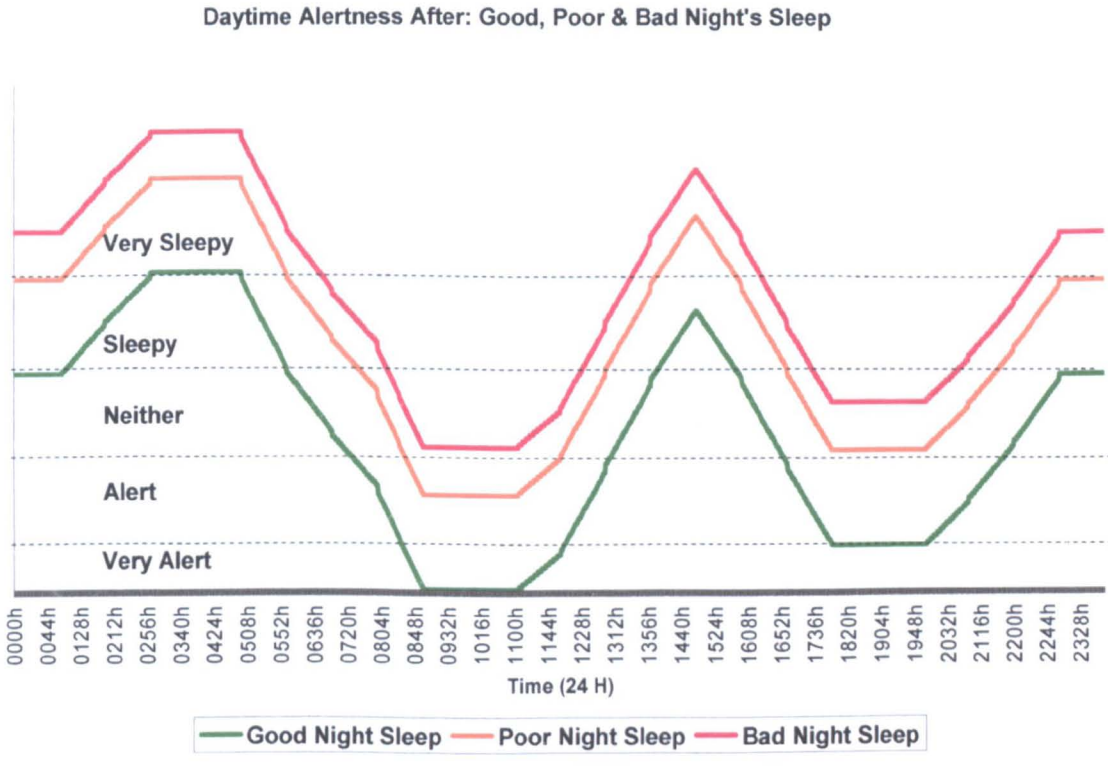

Figure 3.2.2.3 - Circadian Rhythm default plot for various sleeping conditions

The quality of sleep judgement (b) "Good", "Poor", "Bad" is inputted into the ASTiD unit by the driver prior to commencing the drive. This identifies the appropriate Circadian Rhythm curve (figure 3.2.2.3) to be applied by the unit for that particular journey [Horne, 2001].

5. Microprocessor

The microprocessor is used to perform arithmetic, logic and control operations, with the assistance of an internal memory of 512kb. The memory was designed to store a maximum of 3 to 4 days of the latest driving data and information.

6. ASTiD front panel

The LCD display unit informs the operator of the current status of tiredness level which is output from the algorithm for the specific driver. The clock is also found on the LCD display with the tiredness score level on the right.

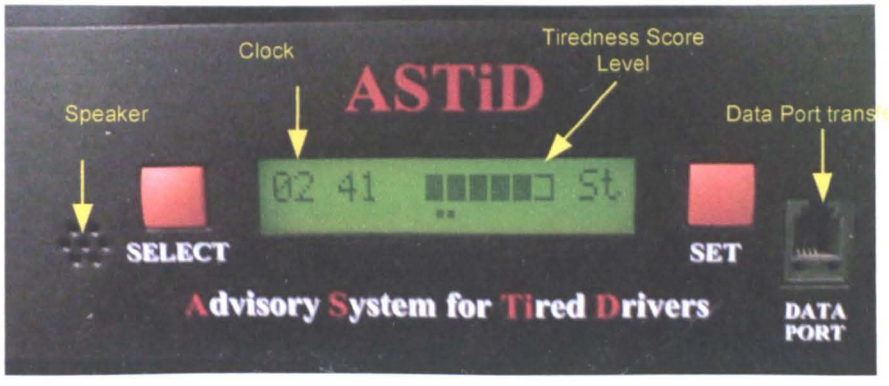

Figure 3.2.2.4 – Composite system displaying the tiredness level of 5/6 (warning level)

A small buzzer is incorporated in the unit (figure 3.2.2.1) to alert the driver if the tiredness level reaches a critical level. The data port helps to transfer information such as driver change, alarm triggered, tiredness level for the journey and the time.

7. LED external display

This is an external display fitted at the drivers eye-level on the dashboard which is also unobtrusive to the driver's road vision. It contains 6 different LED colours:-

- 3 green – indicating normal safe level
- 2 amber – indicating warning levels of tiredness
- 1 red – indicating a critical level of fatigues – which blinks simultaneously with the buzzer alarming

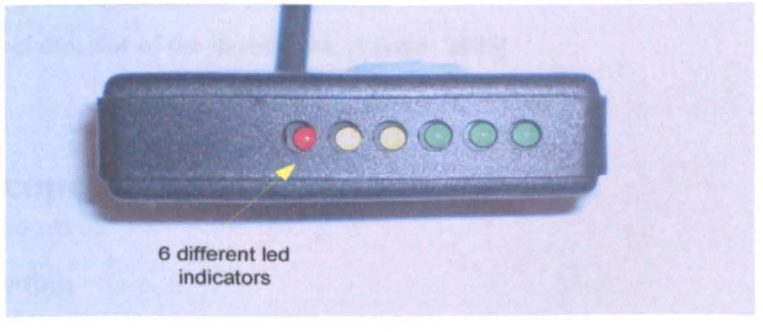

Figure 3.2.2.5 – The LED unit with the 6 different LED indicators

3.2.3 Installation of the composite system

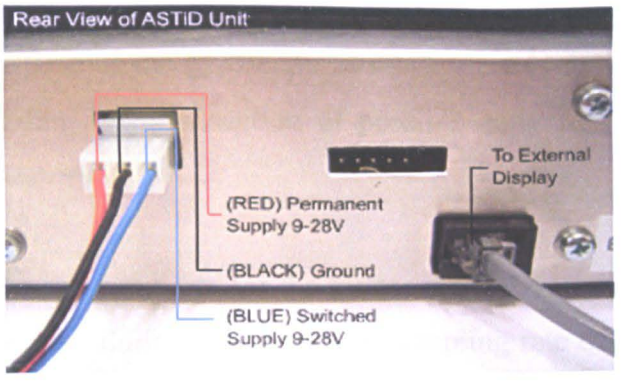

Signal name	Colour
Permanent Supply (9-28V DC) (Should not be controlled by the vehicle ignition switch)	RED
Vehicle ground (0V)	BLACK
Switched Supply (9-28V DC) (Must be connected via vehicle ignition switch)	BLUE

Current Consumption

30mA (Normal)
10mA (Waiting)
120mA (Alarm)

Figure 3.2.3.1 – Diagram showing the rear view of the composite unit with the power supply cables.

The composite system requires a supply voltage of 9-28volts from the vehicle battery. This should not affect the battery supply of the vehicle as the power consumption of the composite unit during the vehicle resting mode is 10mA (this is required by the unit's clock). The composite system is designed to fit into the universal dim-slot of the vehicle front dashboard (similar to a radio). The system is required to be placed on a flat surface firmly for the gyroscope to operate robustly.

Figure 3.2.3.2 – Showing an ASTiD unit installed onto the universal dim slot of the dashboard. [Pernix, 2005]

3.3 Gyroscope System

3.3.1 Introduction

The main sensing device used in the design of the gyroscope system is the piezoelectric vibrating gyroscope. It is the same piezoelectric gyroscope used for the

composite system and its specifications can be found figure 3.2.2.2. This type of gyroscope was selected due to its low power consumption and miniature size. The purpose of the gyroscope in this system is to detect the angular rate of the vehicle, leading to the detection of possible early fatigue events such as lane drifting and swerving.

The sampling rate for the gyroscope system is 15Hz (this was the optimal frequency reported during road trials). A sampling rate of 15Hz provides a sufficient resolution for data representation. A higher sampling rate would mean an unnecessary increase in the amount of data. At this sampling rate the gyroscope system is capable of gathering detailed information about any angular change of the vehicle.

3.3.2 Overview of the Gyroscope system structure.

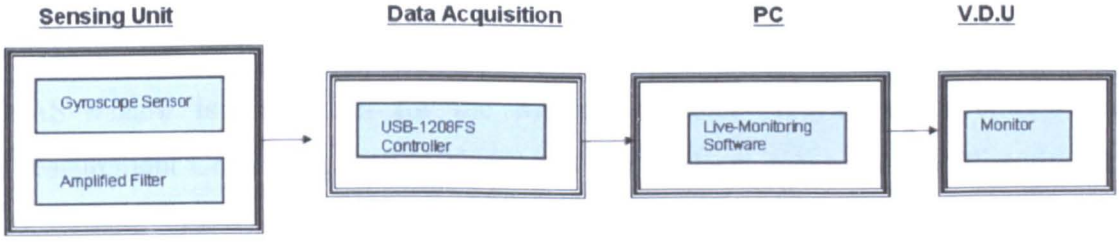

Figure 3.3.1.1 – Overall structure of the Gyroscope system

The overall designed structure of the gyroscope system is shown in figure 3.3.1.1. The main sensing unit contains an op-amp for voltage amplification. The raw data from the gyroscope is acquired by a USB 1208FS controller. This is an interface between the sensor and the computing unit which transmits the raw data to the computer for instantaneous processing. The result is then displayed on the visual unit for further observation.

3.3.3 Data Acquisition

The hardware used to transfer information from the system to the computer is the USB-1208FS. The USB-1208FS is a USB-based device that sets a new standard for low-cost, PC-based analogue and digital I/O. It provides 8 single-ended inputs with 11-bit resolution or 4 differential inputs with 12-bit resolution. The unit offers sample

rates up to 50 kilosamples/sec with 8 software selectable input ranges. The unit also provides 2 channels of 12-bit analog output, one 32-bit counter and 16 bits of digital I/O. It has a low power consumption where the power is drawn from the USB channel of the computer.

3.3.4 Software Development

Figure 3.3.4.1 - Flowchart of the gyroscope system software

Figure 3.3.4.1 shows the structure of the real-time monitoring software when the data is directly inputted into the system. The gyroscope software system utilises two separate software components simultaneously to capture and analyse the input data information.

1. DAS-Wizard

DAS-Wizard is an add-in for the Microsoft Excel program that controls the Measurement Computing USB-1208FS board and places measurements directly into the cells of an Excel worksheet. A simple dialog box enables the setting of the board to be configured to the range of cells in which to place measurements. DAS-Wizard provides seamless integration. The data can be in the format of A/D counts, volts, or temperature. A/D counts may be converted into any type of engineering units using Excel formulae.

2. Microsoft Excel

Microsoft Excel is a spreadsheet program which enables spreadsheets to be created and edited. These are used to store information in columns and rows that can then be organized and/or processed

3.4 Sensor Deployment

The 2 different applications of the gyroscope:

1. *Dashboard Implementation* - a gyroscopic sensing system that detects the yaw movements of the vehicle independent of the travelling speed of the vehicle and is unobtrusive to the driver.
2. *Steering Wheel Deployment* – a gyroscopic sensing system which is installed on the steering wheel of a vehicle in order to detect the angular movements and displacements of the steering wheel itself.

3.4.1 Dashboard Implementation

Figure 3.4.1.1 shows the installation of the gyroscope system onto the dashboard of a vehicle. The power requirement of the system can be satisfied by a 9 volt supply, from the power outlet of the vehicle.

Figure 3.4.1.1 –Implementation of the gyroscope system on the dashboard of a vehicle [Koh et al 2007]

The positioning of the gyroscope unit is an important consideration during the installation process as this affects the data outputted by the gyroscope. The system needs to be placed on a flat surface on the dashboard at approximately 0 degrees (±5~8 degrees) across the horizontal surface.

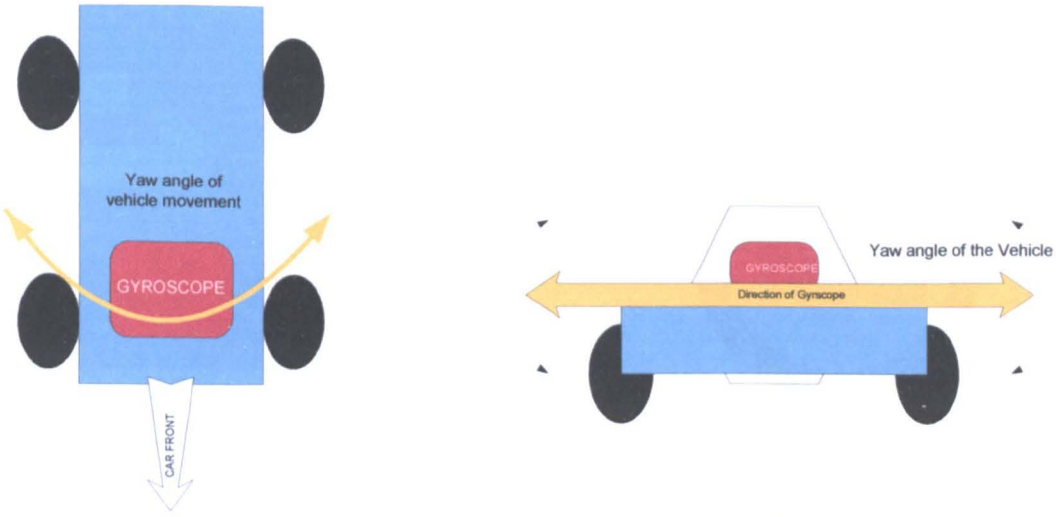

Figure 3.4.1.2 – Mounting of a gyroscope on a vehicle dashboard

(a) Overhead view of vehicle with the gyroscope placed horizontally

(b) Front view of vehicle with the gyroscope detecting the yaw angle of the vehicle

Figure 3.4.1.2 shows the positioning of the gyroscope system on a vehicle. The purpose of the horizontal position is to detect the yaw angle movement of the vehicle.

3.4.2 Steering Wheel Deployment

For deployment on the steering wheel, the gyroscope element (figure 3.3.2.2) is removed from its enclosure box and attached directly onto the steering wheel. It remains connected electrically to the monitoring electronics via an insulated cable of sufficient length to allow an unrestricted full rotation of the steering wheel.

Figure 3.4.2.1 – Gyroscope installation on a laboratory based steering wheel

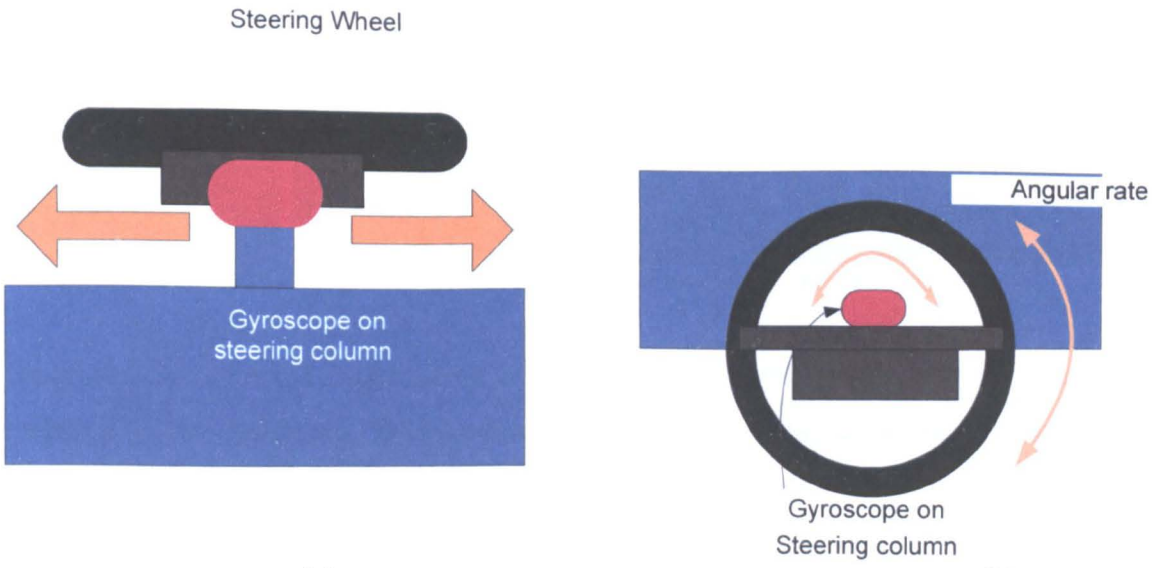

Figure 3.4.2.2 –Mounting of a gyroscope onto a vehicle steering wheel
(a) overhead view of the steering wheel with the gyroscope system
(b) Front view of the steering wheel with the gyroscope system attached

The figure 3.4.2.2 shows the positioning of the gyroscope on the steering wheel column from which the gyroscope is able to measure the angular rotation of the steering wheel.

3.5 Video Capturing System

For experiments on roads, a video capturing system was used to capture the steering wheel activities and the driver. The video capturing system was installed on the top of the dashboard in the vehicle without obstructing the driver's view of the road. It consists of a mobile phone camera with video capturing software. This camera was capable of capturing VGA resolution video at 30 frames per second with sound. A 512mb memory card was available for video recording of up to 3 hours. The advantage of a video phone camera system was that it operated from a battery, was self contained and therefore convenient to install on different vehicles. The camera model used was a 'Sony Ericsson K800i'

Figure 3.5.2 – Diagram shows 4 frame shot of turning on the steering wheel

Diagram 3.5.2 shows 4 frame views of the driver at the wheel from a video camera installed on the dashboard. This feedback information can be further used to analyse the information of the steering wheel angle to determine different activities.

3.6 Summary

The structures of two systems which have been used (composite and gyroscope systems) have been described. The composite system utilised the Circadian rhythm and other factors to determine the driver's fatigue score. The gyroscope system obtained information from the gyroscope directly to determine the angular rate of the vehicle yaw motion. Two deployments of the latter have been described, the 'Dashboard Implementation' and the 'Steering Wheel Deployment'. The installation of the dashboard implementation has been shown to be unobtrusive to the vehicle and the driver. The system was accurately positioned to measure the horizontal yaw movements only. The steering wheel deployment was with the gyroscope mounted on the steering wheel to measure it's the angular movements.

Chapter 4

Experimental Methodologies and Tests Procedure

4.1 Introduction

Experimental methodologies and tests with the two systems, composite and gyroscope system, are discussed in this chapter. The composite system has been designed to monitor the physiological factors during sleepy driving. The composite system depends on different inputs to calculate the fatigue level of the driver. Experimental tests with this system were undertaken with professional logistic truck drivers (eg. TNT and Christian Salvesan) operating the vehicle during their work shift where a physiological tiredness score (PTS) was continuously being monitored.

The two gyroscope systems (the Dashboard implementation and the Steering Wheel deployments) were tested separately despite using the same sensing unit. The gyroscope system experimental tests may be categorised into normal driving and simulated fatigue related driving manoeuvres. The normal driving manoeuvres contain driving exercises such as left and right turn, accelerating, roundabout, etc, which a driving operator would perform on any regular session. The fatigue related manoeuvres were simulations of sleepy driving situations such as lane drifting and swerving.

4.2 Composite system (ASTiD)

4.2.1 The Experimental methods

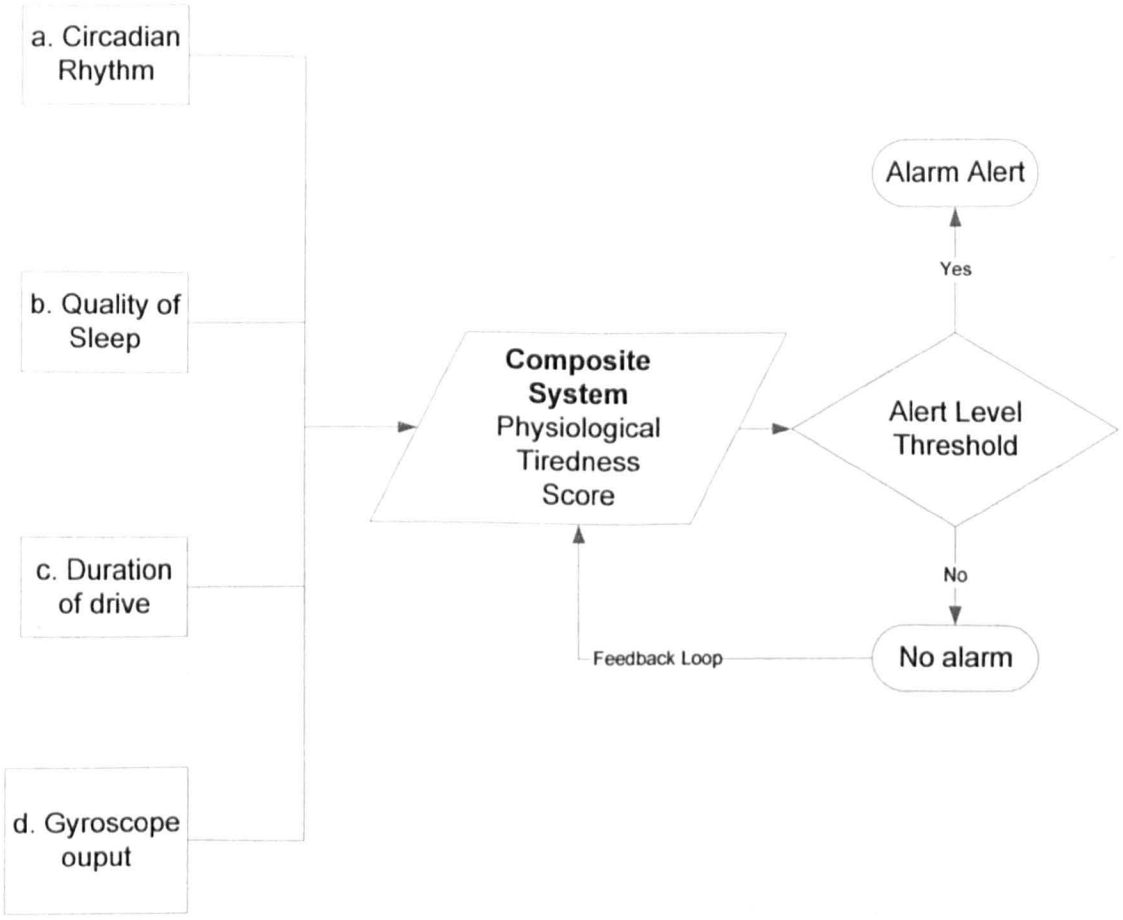

Figure 4.2.1.1 - Overall structure of the test procedure for the Composite system

The instrumentation used consisted of an Advisory System for Tired Drivers (ASTiD) **[Pernix, 2005]**. This advisory system utilised four sets of data **[Reyner and Horne, 1998]** which are:-

a. The Circadian rhythm representing diurnal variation in human tiredness
b. A driver's input about the quality of sleep before driving
c. A tiredness factor which increases with the continuous period of driving
d. A gyroscope output which indicates the driving condition to be monotonous or non-monotonous.

a. Circadian rhythm and quality of sleep

The first component for the composite system is the Circadian rhythm (a) of the driver which varied with the time of day (figure 4.2.1.2). It is an important physiological

factor as described in chapter 2.2.2 and the graph shown on figure 3.2.2.3. Figure 4.2.1.2 is a revised version of figure 3.2.2.3, where the y-axis is changed and quantified to the 'Physiological Tiredness Score' (PTS) indicator. A threshold set at 0.95 will trigger the alarm if the PTS is greater or equal to this value. The circadian rhythm **[Horne, 2001]** shows a daily cyclical pattern (figure 3.2.2) with a maximum tiredness at night time (0200h-0400h) followed by a maximum period of awakeness (0900h-1100h), a further tiredness peak (1500h) and a wakeful period (1730-2000h). The absolute level of the Circadian rhythm decreases with the quality of sleep leading to the three curves.

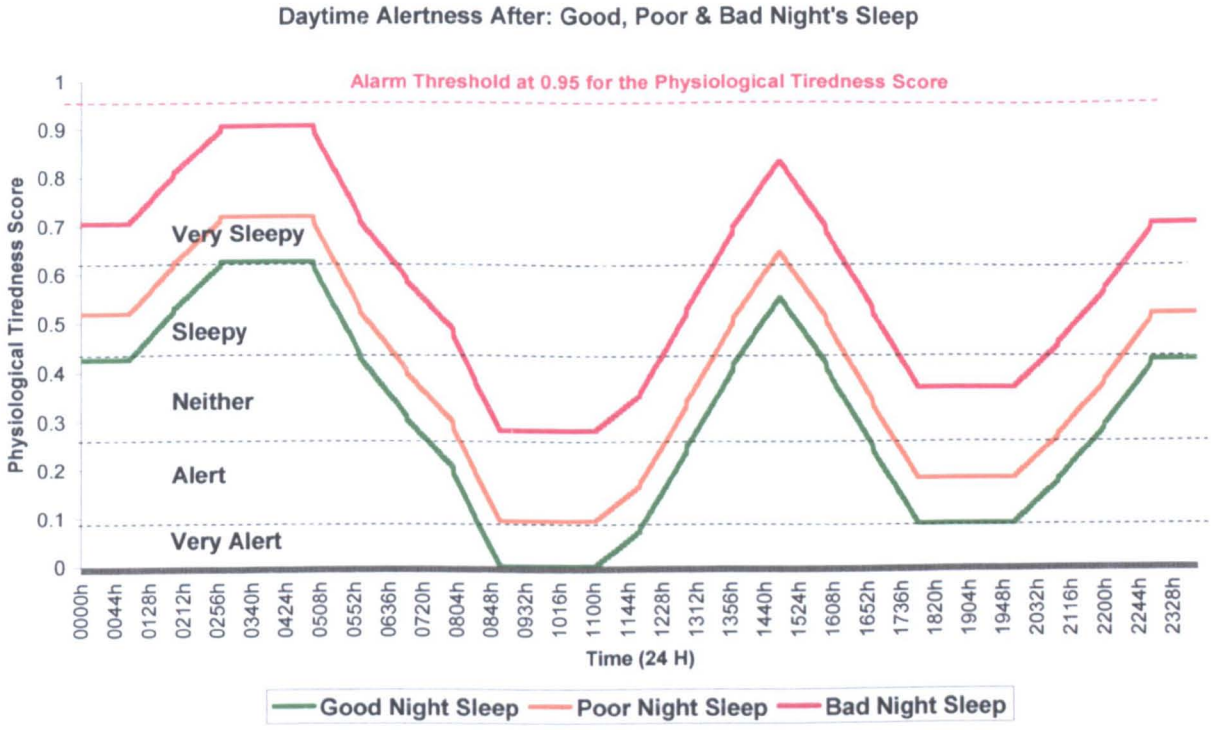

Figure 4.2.1.2 – Figure shows the various circadian rhythms in relation with the quality of sleep on previous night. The y-axis shows the physiological tiredness score against time of day for 24h clock cycle. Alarm threshold is set at 0.95 indicated in red dotted line.

b. Duration of drive

Component (c) is the component accounting for the increase in tiredness as the duration of the drive progresses **[Reyner and Horne 1998 a].** The table 4.2.1.1 shows the score added per minute depending on how long the driver has been driving (1hr, 2hrs or more). The score given also takes into account the monotonity of the driving conditions, i.e. driving vehicle is being driven in town (non-monotonous) or

motorway (monotonous) mode. For example, if the driver is driving on the 1st hour of the journey a score of 0.63×10^{-3} is added per min for town mode and 1.25×10^{-3} per minute for motorway mode. After every hour the score added per minute increases according to table 4.2.2.1 below.

Time of driving (in hours)	Town Mode (Non-monotonous)	Motorway mode (Monotonous)
1st hr	0.63×10^{-3} per min	1.25×10^{-3} per min
2nd hr	1.25×10^{-3} per min	2.50×10^{-3} per min
3rd hr	1.88×10^{-3} per min	3.75×10^{-3} per min
4th hr	2.50×10^{-3} per min	5.00×10^{-3} per min
5th hr	3.13×10^{-3} per min	6.25×10^{-3} per min
6th hr	3.75×10^{-3} per min	7.50×10^{-3} per min
7th hr	4.38×10^{-3} per min	8.75×10^{-3} per min

Table 4.2.1.1 Figure shows the score added per minute for the town and motorway mode driving. Depending on which hour the driver is in different score level will be added to the PTS.

Time of driving for the first 'x' minutes	Stop Mode
15	2.50×10^{-3} per min
20	5.00×10^{-3} per min
25	7.50×10^{-3} per min
30	10.5×10^{-3} per min
35	12.5×10^{-3} per min

Table 4.2.1.2 Figure shows the score reduction per minute according to the duration the vehicle is in Stop mode

Regular rest and stops of a minimum of 15 minutes decreases the tiredness score **[Reyner and Horne 1997].** A rest of 60 minutes removes the tiredness score completely. Table 4.2.1.2 shows the score reduction according to the duration of time the vehicle is stationary whereby there is no output from the gyroscope (stop mode).

c. Gyroscope Mode Base driving

The gyroscope component (d) plays a role in differentiating the driving mode of the vehicle from monotonous and non-monotonous driving conditions. Monotonous driving conditions are normally found on motorways and non-monotonous type conditions are normal town type driving (more information can be found in section 4.3.4). When the gyroscope detects regular manoeuvre movements then the driving mode is classified as non-monotonous driving. Monotonous driving mode is when the

gyroscope output is low indicating minimal regular movements. When there is no movement detected by the gyroscope, it switches to the stop mode.

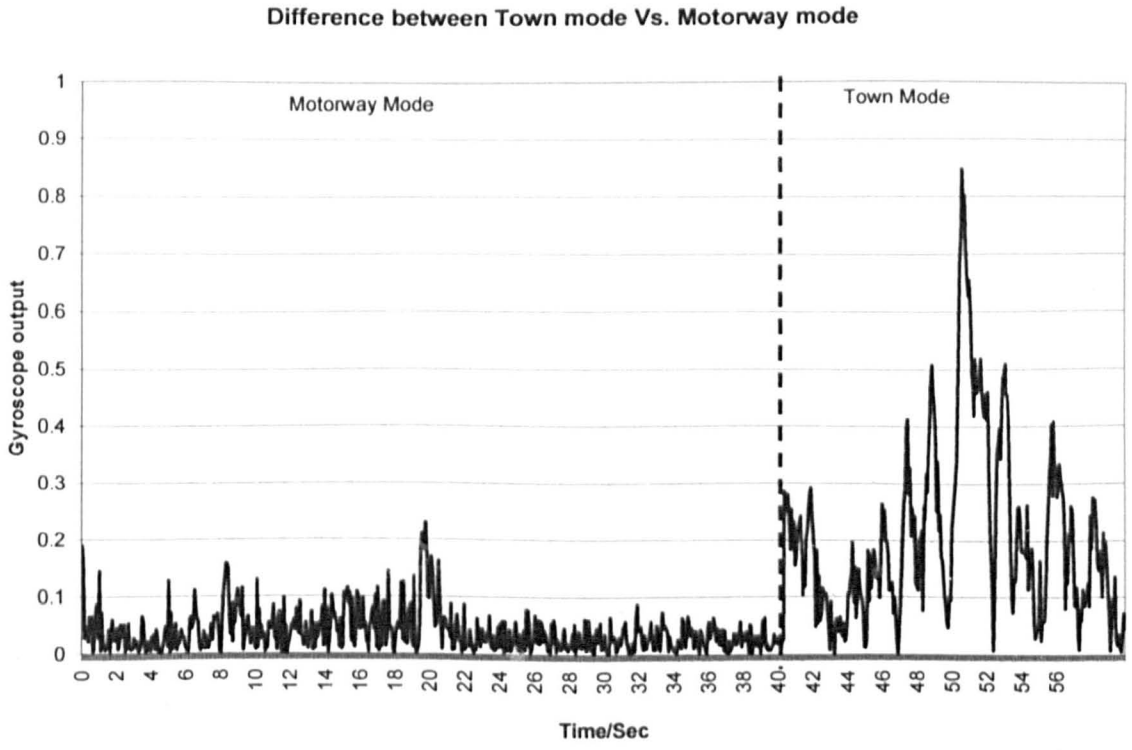

Figure 4.2.1.3 shows the vehicle driven from motorway mode to town mode. The graph is plotted for gyroscope output against time.

Figure 4.2.1.3 shows the difference in the gyroscope output between town mode and motorway mode. This output data has been RMS transformed and normalised. The y-axis represents the gyroscope output and the x-axis represent the time in seconds. The driving mode is determined by averaging the gyroscope output data for the previous one minute.

Driving Mode	Average gyroscope output for previous 1 minute
Town Mode	Gyro Output>0.25
Motorway Mode	0.001>Gyro Output>0.025
Stop Mode	Gyro Output<0.001

Table 4.2.1.3 Different modes represented by average gyroscope for the last minute of a drive

d. Physiological tiredness score (PTS)

The four components (a), (b), (c) and (d) are combined by the mathematical algorithm to calculate the physiological tiredness score. There is a threshold level of 0.95 for the critical tiredness score level, which triggers the alarm to alert the driver to this dangerous situation.

$$PTS(t) = C_{SQ}(t) + D_{dm}(t) - D_r(t) \quad \text{----------Eqn 4.2.1.1}$$

Where,

PTS (t) = Physiological Tiredness Score

$C_{SQ}(t)$ = Circadian based on sleep quality wrt time

$D_{dm}(t)$ = Duration of drive base on driving mode wrt time

$D_r(t)$ = Duration of rest wrt time

4.2.2 Experimental Tests

The first set of tests was with commercial trucks driven by professional drivers on shift duty. Experimental tests were performed with the composite system appropriately mounted on the dashboard of the commercial vehicle (figure 3.4.1.1) which was in routine use on normal roads. During such tests there were changes of drivers, rest periods and extensive road driving.

The overall output of the composite system was recorded as a function of time along with notes of major events such as time of start of driving, rest period, change of driver etc. The composite system also had inputted each driver's estimate of the quality of sleep prior to driving. Consequently test data could be retrieved after each test in the form of the time variation of the overall output of the composite system based upon the sum of the Circadian Rhythm curve appropriate to each driver, the fatigue increase with longer duration of drive in monotonous road conditions.

Table 4.2.2.1 presents a list of experimental tests conducted using the composite ASTiD unit. The types of vehicles used vary from commercial articulated trucks, van and mining trucks (caterpillar). These experimental tests were conducted during the course of the commercial vehicles undertaking their normal duties.

List of Data

	Date	Vehicle code - Journey	Vehicle Type	Duration of Journey
1	19th April 04	TNT(NG) – Driver 2	Articulated Truck	5 hrs
2	19th April 04	TNT(NG) – Driver 3	Articulated Truck	3 hrs
3	23rd March 04	TNT(AJ) - Menalesham	Articulated Truck	5hrs
4	30th March 04 31st March 04	TNT(AJ) – Newsfast Glasgow	Articulated Truck	4 hrs 3 hrs
5	20th January 04 21st January 04 26th January 04 27th January 04 30th January 04	TNT(AJ) - Thetford	Articulated Truck	3 hrs 3 hrs 4 hrs 3 hrs 6 hrs
6	21st February 04 22nd February 04	Caterpillar 797 - Chile	Mining Tuck	7 hrs 7 hrs
7	02nd February 05 04th February 05 31st March 05	Ford Van	Commercial Van	2 hrs 2 hrs 2 hrs
8	11th August 04 12th August 04 8th February 05 9th February 05 11th February 05	Christian Salvesan	Articulated Truck (multiple driver change)	24 hrs 24 hrs 24 hrs 18 hrs 24 hrs

Table 4.2.2.1 – Summary of tests conducted with the composite system (ASTiD).

4.3 Gyroscope System - Dashboard Implementation

4.3.1 The methodology of the system

The purpose of the dashboard implementation was to directly monitor and gather information of the angular rate with reference to the yaw motion of the vehicle. The main objective was to detect fatigue related manoeuvres. Fatigue related manoeuvres can be in the form of lane drifting and swerving which would not occur during normal driving circumstances **[Paul et al, 2005 a; Dinges, 2005].**

The positional installation of the gyroscope was important. The gyroscope is required to be positioned horizontally on the dashboard to measure the angular rate with reference to the yaw or lateral movements. From the dynamics of motion, yaw is the left/right rotation around the vertical axis of the vehicle. The sampling rate of the gyroscope system was set at 15Hz which provided a good resolution for fatigue manoeuvres to be recorded.

In order to understand the yaw motion of a vehicle under real road conditions via the dashboard gyroscope system, driving manoeuvres were divided into two categories. They were the normal driving manoeuvres and fatigue related driving manoeuvres. The data collected can be compared with one another in order to identify the difference in the driving characteristics.

4.3.2 Normal Driving Manoeuvres

Normal driving manoeuvres are a series of driving manoeuvres which drivers of any type of vehicle need to perform in order to run a vehicle normally on a journey. They can be classified according to the angle of change of the vehicle from its original position. The manoeuvres include:-

1. Vehicle Left or Right Turning
2. Parking and Handling of vehicle
3. Roundabout
4. Speed bumps and other types of road indicators

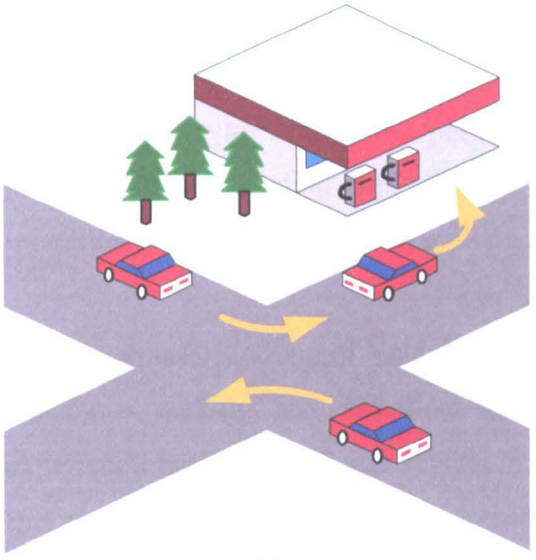

(a)

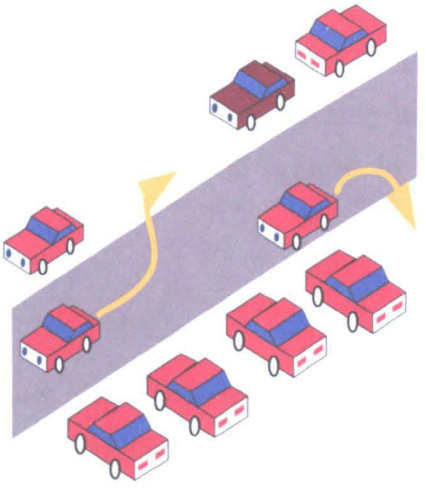

(b)

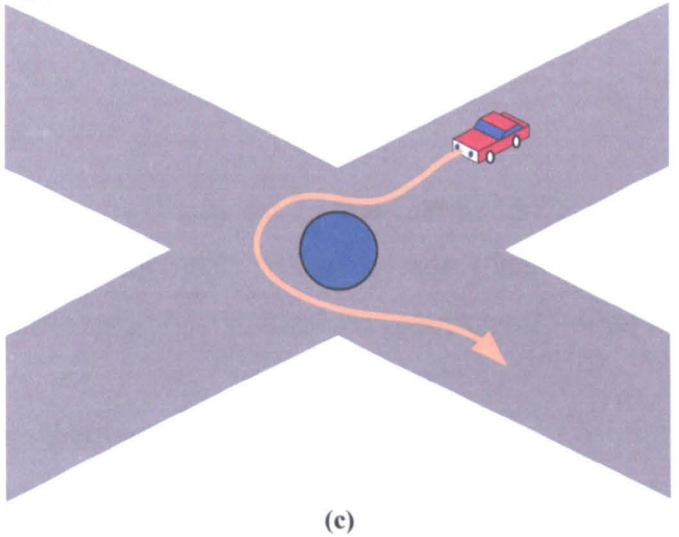

(c)

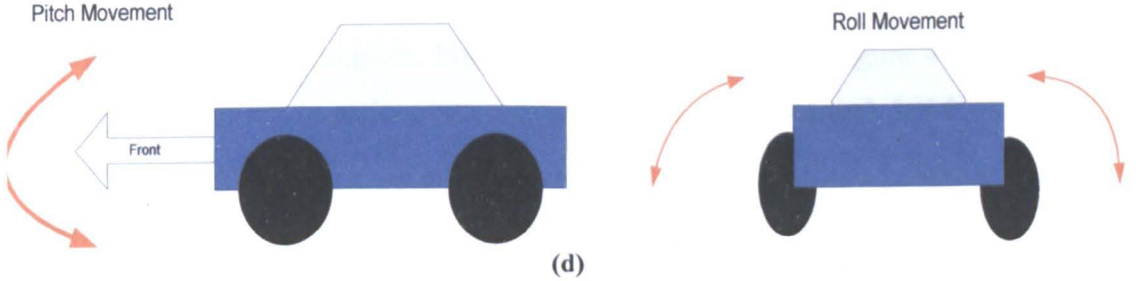

(d)

Figure 4.2.2.1 – Normal Vehicle Manoeuvres

(a) Left and right turning examples

(b) Car-Parking examples

(c) Vehicle negotiating a roundabout

(d) pitch and roll movement of a vehicle

1. Left or Right Turning

The left or right turn manoeuvre (figure 4.2.2.1a) is the most commonly used manoeuvre on the road. This particular manoeuvre can range from turning at a junction to accelerating and decelerating. This would involve a vehicle to be travelling at more than 20 to 30 mph on average.

2. Parking and Handling of Vehicle

During a parking and handling manoeuvre (figure 4.2.2.1b), the vehicle may experience both forward and reverse movement depending on the situation. During this phase the average speed of a vehicle should be below 10mph when the vehicle will conduct wide angle movements

3. Roundabout

The roundabout manoeuvre (figure 4.2.2.1c) would be similar to parking and handling because the angular displacement would be more than 45 degrees. However the average moving traffic speed on a roundabout is between 15-30mph on average

4. Speed bumps or other types of road indicators

Driving over a speed bump on the road does not in general require any change in the angular displacement of the steering wheel or the vehicle. This would only affect the pitch movement of the vehicle. Pitch is the dynamic motion (figure 4.2.2.1d) where thenose of the vehicle experience an up and down motion **[Stengel, 2004].**

Other types of road conditions include rumble strips, pot holes and cat's eyes. These also do not affect the angular displacement of the vehicle but may affect the dynamic roll motion of the vehicle. Roll motion (figure 4.2.2.1d) is the rotation around the longitudinal axis **[Stengel, 2004].**

4.3.3 Fatigue-related driving manoeuvres

The research into fatigue and sleep shows that an early indicator of driver tiredness is given by a finite number of reactions resulting in particular corrective steering actions by the driver **[Sagberg, 1999; Paul et al, 2005 a; Reyner and Horne 1998 a]**. There is a need to

better understand the capabilities of such fatigue monitoring systems with respect to their operation under real conditions.

During a road experimental test, a series of simulated fatigue-related driving manoeuvres can be conducted to gather lateral yaw movement information. Simulated fatigue driving manoeuvres include the following:-

1. Lane drifting correction
2. Swerving

1. Lane drifting correction

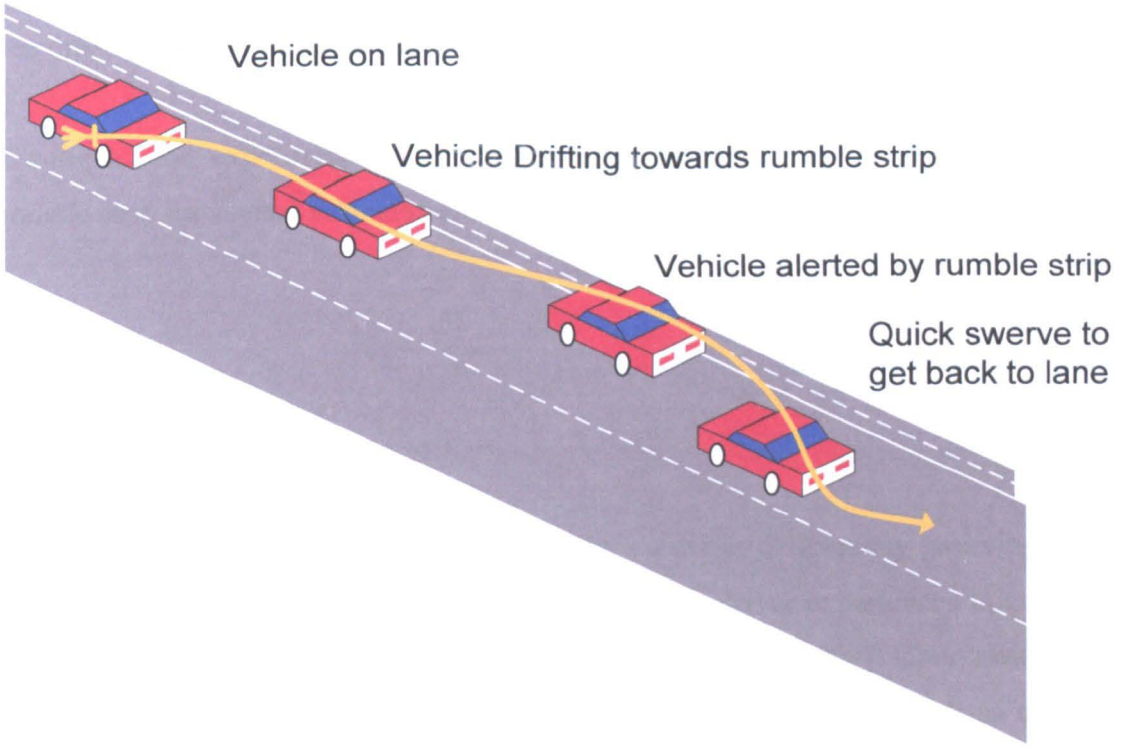

Figure 4.3.3.1 – Vehicle movement when alerted by rumble strip

During normal driving, an alert vehicle driver would voluntarily try to make small adjustments on the steering wheel to maintain a steady alignment along the road. When a vehicle driver starts to feel tired, these corrective activities reduce involuntarily, as the human body relaxes. This is an early indicator of fatigue, seconds or minutes before the driver becomes drowsy and head nodding commences, depending on the situation and individual drivers **[Horne and Baulk, 2003; Paul et al, 2005 a]**.

Lane drifting correction is an on road experimental test simulation where the steering wheel is left unattended while driving at a constant speed, which causes the vehicle to drift out of lane. This can be caused by either the uneven camber of the road or the alignment of the vehicle wheel **[Horne and Baulk, 2003; Paul et al, 2005 a]**. When the driver is aware of the lane drifting, the driver will try to correct the movement to revert back to its normal road alignment.

The rumble strip was designed to alert any vehicle driver that the vehicle was too close to the hard shoulder **[Paul et al, 2005 a]**. Running the vehicle over the rumble strip would cause loud repetitive noise via the wheel of the vehicle. This should alert the driver instantly and cause the driver to swerve back into lane.

During a road experiment, the vehicle was deliberately positioned to run on the rumble strip for several seconds before swerving back into the correct lane alignment.

2. Swerving

A road test simulation of this condition involves a driver deliberately swerving to the left, right or both. This is a sharp manoeuvre when a driver experiences micro-sleep and awakes seconds later **[Paul et al, 2005 a; Risser et al., 2000]**. Upon awakening, the driver would most likely be shocked to find himself heading towards an obstacle or going into another lane thereby overcompensating with a violent swerve.

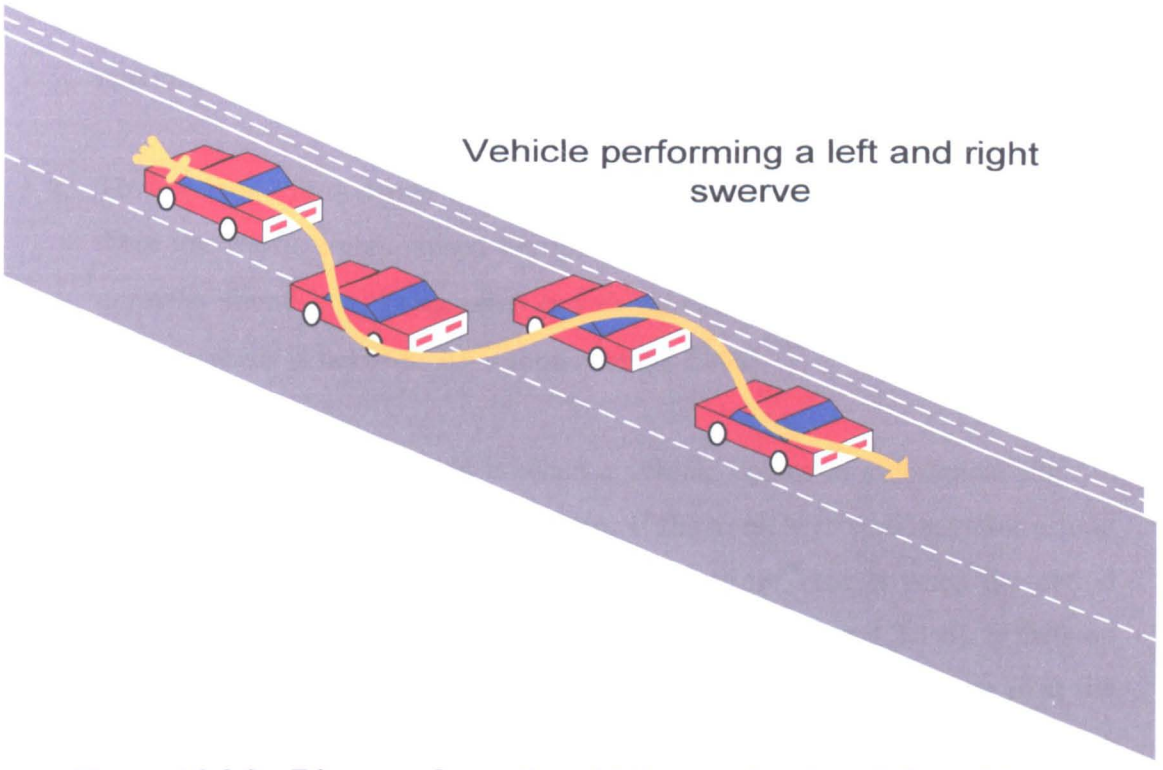

Figure 4.3.3.3 – Diagram shows the vehicle swerving from left to right.

4.3.4 Mode base driving

From sleep research studies, it is known that road vehicle drivers are most likely to become drowsy during a long monotonous journey **[Reyner and Horne 1998 a]**. Monotonous driving conditions occur when a vehicle is travelling at a fairly constant speed on a long road with a lack of manoeuvre activities (left, right turn, roundabout, traffic lights, etc.).

This type of road is normally found on motorways where there are no traffic lights, speed bumps, etc. Fatigue driving manoeuvres like lane drifting and swerving are most likely to occur during these monotonous conditions. Non-monotonous roads are town based driving where there are plenty of road manoeuvre activities (left-right turning, traffic stops, etc.) which require a certain level of alertness. Therefore the gyroscope system needs to be designed to differentiate between the 3 driving modes:-

1. Motorway Mode (M) – Monotonous road conditions where activities on the steering wheel are at minimum levels due to long lengths of straight road

ahead. These are mostly found on motorways and dual carriageways. The maximum speed limit on these roads are normally 60-70mph **[Pernix 2005]**

2. Town Mode (T) – Town mode driving is on non-monotonous roads where there are traffic lights, speed bumps and roundabouts. This type of road is normally found in built-up areas and single carriageways. The average speed on these roads is between 30-40mph **[Pernix 2005]**

3. Stop Mode (S) – Stop mode is when a vehicle comes to a complete stop. In this mode the gyroscope output is zero. If the vehicle is stationary for a long period, the implication is that the driver is resting. That is when the period alert system ceases to increase the tiredness factor (section 4.2.1 d). If the stop mode is only for a short duration this would indicate that the driver is at the traffic lights, in a traffic jam, or parking. This may be used as a transition from the 'M' to 'T' mode or vice versa. **[Pernix 2005]**

4.3.5 Experiments Conducted

Experimental data was gathered with different vehicles driven by different drivers, of different genders under different weather and traffic conditions. The participants were volunteer drivers with at least 3 years of driving experience but were non-professional drivers. There was only one professional driver participant when experiments using an articulated truck were conducted. To ensure that the data could be used for cross comparison, the same route was used each time to gather the data. Driving at different times of the day was also undertaken to ensure exposure to various traffic densities. The different experiments were conducted to show how the dashboard system adapted to different environments and other varying situations.

The route was an approximately 34 miles return trip shown in figure 4.3.5.1. This involves various driving modes (section 4.2.4), whereby the first 10 minutes of the route was in the town mode driving. The town mode had various "obstacles" such as traffic lights, turning junctions and heavy traffic conditions through out the day. The conditions of the road surface included potholes and speed bumps which enabled the

effect of vibration on the dashboard gyroscope system to be checked. The average speed for these roads was 10 to 30 mph.

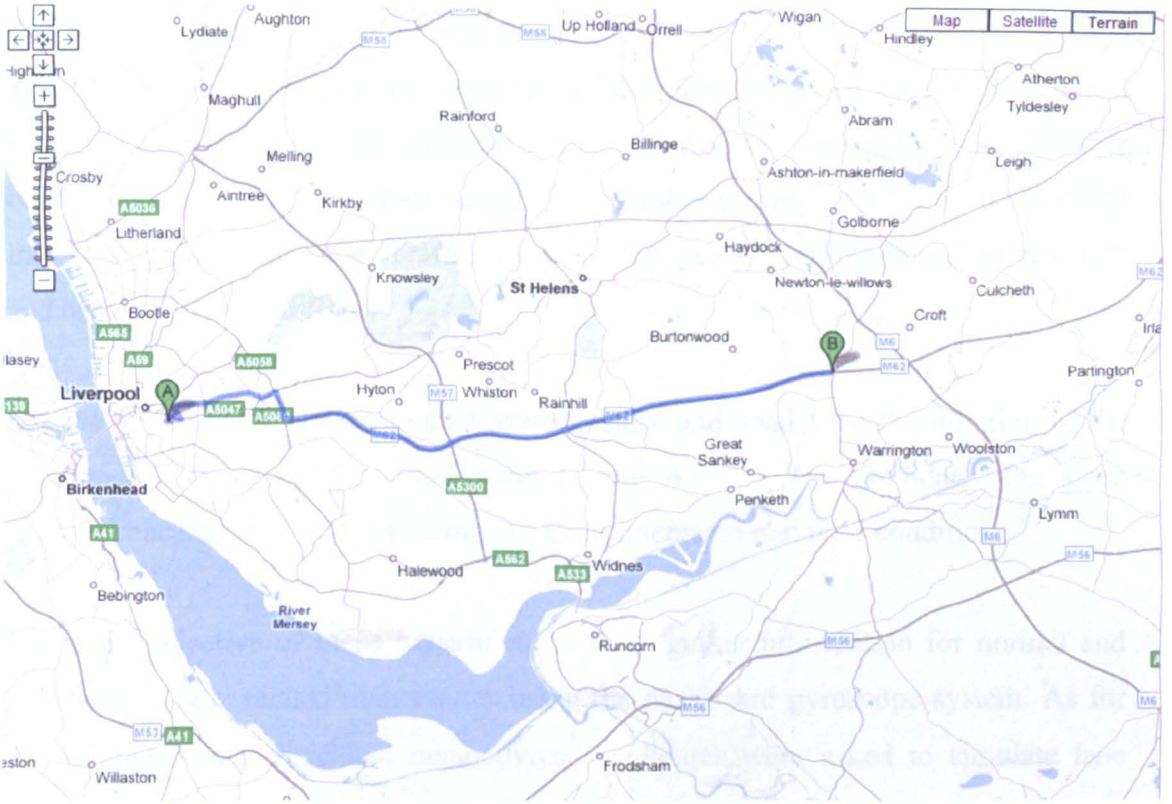

Figure 4.3.5.1 – Map shows the route (blue route) from the starting point (A) and finishing point (B).

After approximately 10 minutes the route continued onto a motorway where there were more lanes to accommodate the traffic and the speed limit of the motorway was 70mph. For these experimental tests, fatigue-related manoeuvres would only be conducted in the motorway-driving mode when fatigue driving most commonly occurs in monotonous road conditions (based on the research by Loughborough University) **[Reyner and Horne, 1997].**

The route was selected to include all three kinds of mode driving for the driver to perform various normal and fatigue-related manoeuvres. The particular route (map figure 4.3.5.1), was selected to keep consistent road conditions and distance for each experiment. Results were collected and then used for comparison and deduction.

4.3.6 Summary of Test Conditions

There were a total of 16 experiments conducted for the route identified on figure 4.3.5.1. Different drivers were selected to conduct the experiments, 5 male candidates and 2 female candidates over 16 experiments.
There were 4 different types of vehicles used throughout the experiments: Hatchback car, van, saloon car and an articulated truck. During the experiments the weather conditions and traffic conditions varied. The weather conditions have been classified into sunny, cloudy and rain. Traffic densities have been classified into light, medium and heavy traffic conditions.

For the experiments, the candidates were healthy and awake for the duration of the experimental drive on the fixed route (figure 4.3.5.1). No candidate was sleep deprived because it far too dangerous for experiments on real road conditions.

The main objective of these experiments was to gather information for normal and simulated fatigue related manoeuvres using the dashboard gyroscope system. As for the simulated fatigue related manoeuvres, candidates were asked to simulate lane drifting and swerving as shown in section 4.3.3.

A summary table of the experimental test can be found in section 5 (table 5.3.5.1)

4.4 Gyroscope System - Steering Wheel Unit

4.4.1 Experimental methods of the steering wheel system

The steering wheel unit was the second deployment of the gyroscope system whereby the miniaturised gyroscope alone was installed on the steering wheel. The purpose of this implementation was to gather possible fatigue related features from the driving signals of the steering wheel.

When the gyroscope is correctly installed on the steering wheel (as shown in section 3.4.2), output signals will be produced when the steering wheel is rotated either clockwise or anticlockwise. Therefore the output of the gyroscope would be zero if

there is no activity on the steering wheel. The various types of manoeuvres which occurred under different situations led to two categories of operation for the steering wheel: -

1. Normal Driving –The angular rotation situation is regularly changing. This driving mode consists of much non-monotonous driving. (e.g. turning, parking, etc.)
2. Fatigue Related Driving –This usually happens during the monotonous driving mode, when steering wheel movements are a minimum during a journey.

4.4.2 Normal Driving

Normal driving consisted of left and right turns, parking and handling, and negotiating roundabout. (Section 4.2.2).

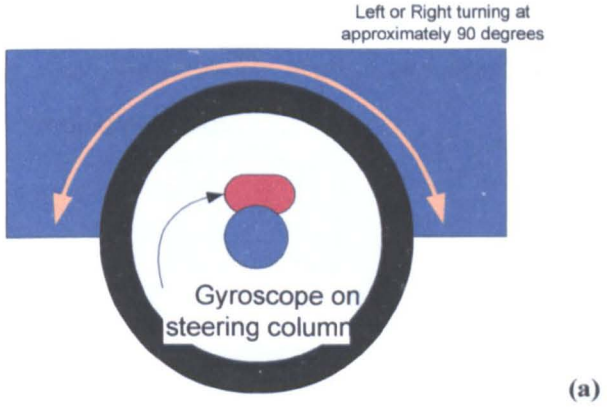

(a)

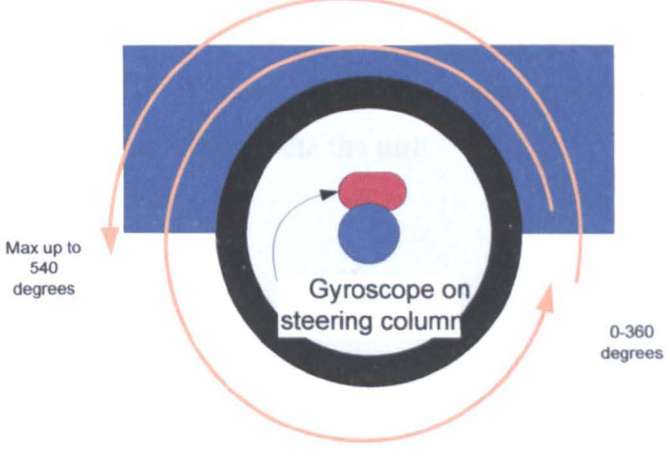

(b)

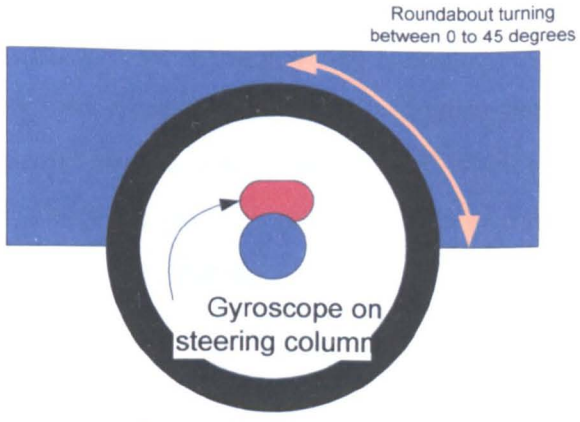

(c)

Figure 4.4.2.1 Front views of the steering wheel movements

(a) Left or right turn (~90^0)

(b) Parking and handling of vehicle (0~360^0, max 540^0)

(c) Negotiating roundabout (maintained at ~ 45^0)

1. Left or Right Turning

The left or right turning manoeuvre involves the steering wheel angle rotating up to approximately 90 degrees. This normally occurrs at a junction (with of without traffic lights) on non-monotonous type roads

2. Parking and Handling of Vehicle

The parking and handling of a vehicle is classified as a steering wheel angular displacement of more than 90 degrees up to 540 degrees at an average speed of less than 10mph. This would often occur during a car parking routine. Also when a vehicle was travelling at 10mph or less, a left and right turn will require a larger angular displacement for the vehicle to complete the turn.

3. Roundabout

During a roundabout manoeuvre the steering wheel needs to be turned through and maintained at approximately 45 degrees depending on the roundabout exit.

4.4.3 – Fatigue-Related Driving

Fatigue-related driving occurs during prolonged monotonous driving. The two key factors associated with fatigue driving under monotonous conditions which can be observed via steering wheel monitoring are lane-drifting and reaction (swerve). These early signs of fatigue occur during sleep attacks and when alert control of the steering wheel deteriorates. Sleep attacks are micro sleeps experienced by a driver when he/she feels tired **[Risser et al., 2000]**.

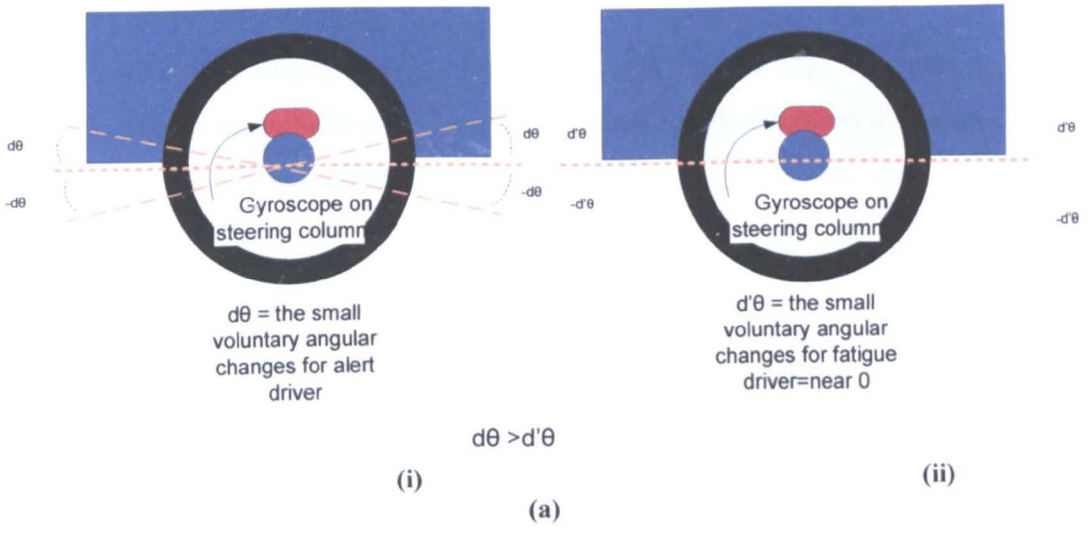

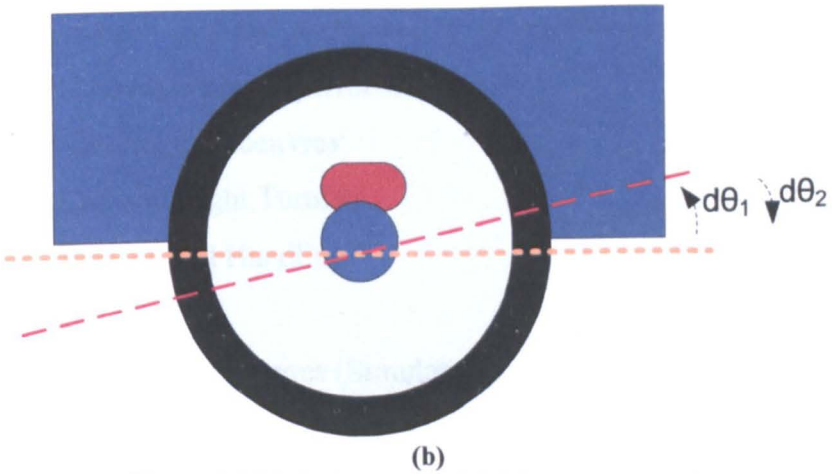

Figure 4.4.3.1 Fatigue related driving wheel rotation

(a) comparison of angular changes for alert and fatigue changes

(i) alert (ii) fatigue

(b)Swerve Reaction

1. Lane Drifting

When a driver is alert, there will be small angular changes on the steering wheel. These changes are voluntary actions by the driver to maintain a steady control of the vehicle on the road. When fatigue increases these small angular changes will reduce. Eventually the vehicle would start to drift across the road whilst the steering wheel is neglected due to micro sleep **[Paul et al, 2005 b]**. Figure 4.4.3.1 (a) shows that the changes in the angular displacement of the steering wheel for the alert driver is greater than the angular change for the fatigue driver.

2. Steering Swerving (reaction)

Vehicle swerve is a fatigue-related reaction where the driver rapidly pulls the steering wheel to readjust the vehicle to align with the road. In this situation the rate of angular change is more rapid than normal turning.

Figure 4.4.3.1(b) shows the movement of a steering wheel during a swerve. This is an example of a swerve where the vehicle may have drifted towards the right side of the road. The reaction of the driver pulls the steering wheel at $d\theta_1$ and is then followed by $d\theta_2$ to realign the steering wheel back to its original position.

4.4.4 Experiments Performed

The steering wheel gyroscope system were assessed both in a lab on a laboratory bench steering wheel unit and under real road conditions mounted on a vehicle's steering wheel. The experiments performed were:-

1. Normal Driving Manoeuvres
    a. Left and Right Turning
    b. Parking and Handling
    c. Roundabout
2. Fatigue related Manoeuvres (Simulation)
    a. Lane Drifting
    b. Swerving

4.4.5 Summary

This chapter has explained the experimental methodology and test procedures for the three experimental systems: composite system, dashboard unit and the steering wheel gyroscope. For the Composite system, professional drivers performed the experiments during actual working hours to gather real fatigue data for long duration journeys. The system operated on both physiological and physical factors.

The gyroscope system was considered in two parts; the Dashboard Unit and the Steering Wheel gyroscope. The gyroscope unit was used to detect the vehicle yaw movements and steering wheel movements respectively. The objective of using this system was to detect simulated fatigue related driving events For the dashboard unit, experiments were planned and conducted on real road conditions where different drivers, road and weather conditions could influence the experiments. The steering wheel system tests were conducted under both laboratory and real road conditions. Comparisons of both systems are presented in the analysis section.

Chapter 5

Experimental Results

5.1 Introduction

In this chapter the results collected from the two systems developed, composite and gyroscope systems will be presented. A series of graphical results will be provided to demonstrate the operations of the systems during an experimental test. The first set of results is for the Composite System (ASTiD). The tests were conducted by professional drivers and the results consist of several activities such as rest and stop breaks, driver change and fatigue alarm triggered on high physiological tiredness score (PTS).

The next system is the dashboard monitoring unit which is based on the gyroscope system. For the dashboard unit the experimental results for normal driving manoeuvre and simulated fatigue-related driving manoeuvre were collected to understand the system response. The following sets of experiments were conducted to test the performance of the system with different drivers, different vehicles, different weather conditions and traffic densities. These sets of tests were performed on the same route each time and for the same duration to maintain the consistency of the experiments.

The second deployment of the gyroscope system was installed on a steering wheel. The experimental test results for the steering wheel system are divided into two parts, laboratory test and road test results. Normal driving and simulated fatigue related manoeuvres were conducted for both the laboratory and road tests for comparison of the performance in different environments.

5.2 Composite System Results

5.2.1 Introduction

Results from a typical 24 hour test involving the driver changes obtained with the composite system are shown on figures 5.2.2.1, and 5.2.2.2 corresponding respectively to the physiological tiredness score (PTS) and the duration tiredness score (DTS) without the circadian contribution.

5.2.2 Unprocessed Data Results

The experimental results presented on figure 5.2.2.1 are for the experiment conducted on the 9th February 2005, using a Christian Salvesan articulated truck. The duration of the experiment is for the entire day (24hrs drive) conducted by 4 professional drivers on different shifts. The change in shift is indicated by the red triangle on the figure 5.2.2.1.

The graph on figure 5.2.2.1 shows the physiological tiredness score (PTS) plotted against time over the duration of 24 hours. The output result of the PTS shown is based on the mathematical algorithm equation 4.2.1.1. The calculation of the PTS is based on the four factors: quality of sleep, circadian rhythm, duration of drive and monotonous road conditions. For the experimental results on figure 5.2.2.1 all four drivers have register good quality of sleep before the operation. A change of driver is accompanied by the system resetting itself to the relevant point on the circadian rhythm. Likewise a driver resting reduces the tiredness score (section 4.2.1).

Based upon the Sleep Research conclusions of the University of Loughborough **[Reyner and Horne 1998 a]** a PTS of 0.95 is regarded as the threshold for an

unacceptably high tiredness level. This is shown as a horizontal dashed line on figure 5.2.2.1. In practice when T.S. $\geq$ 0.95 an alarm is triggered to advise the driver to stop driving.

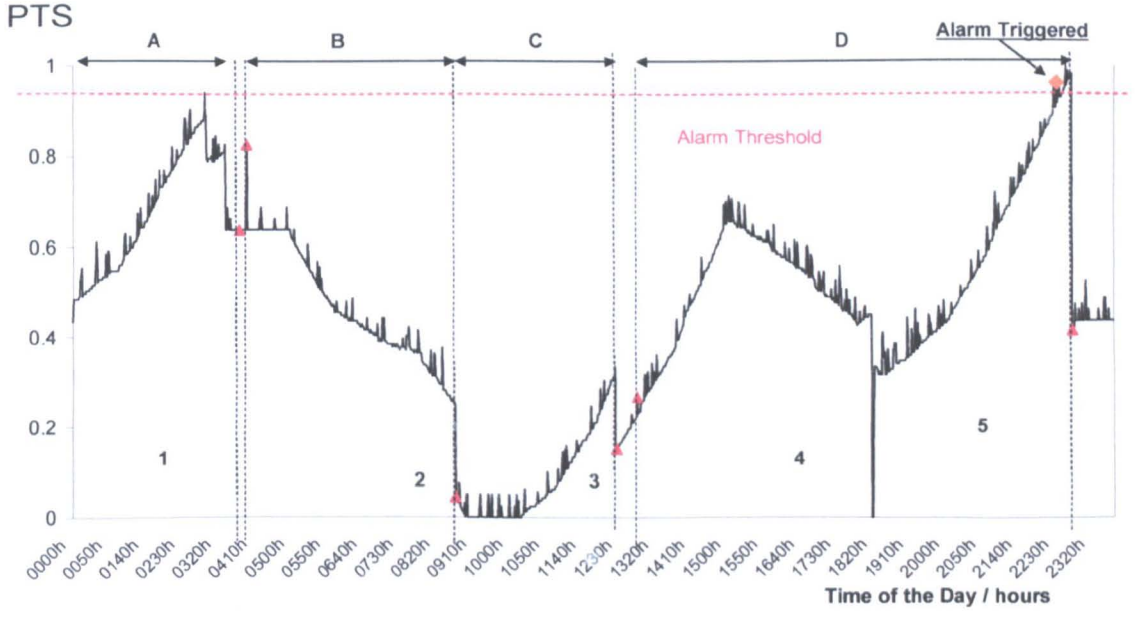

Figure 5.2.2.1. Typical Output of the ASTiD system from a typical 24 hour period test with several changes in drivers. (A, B, C, D different driver and shift periods). These output results are calculated from the mathematical formula equation 4.2.1.1 [Koh et al 2007]

The results shown on figure 5.2.2.1 above are subdivided into driver A, B C and D The four driver changes which occurred during different shift periods were at 0330h(A), 0846h(B), 1230h(C) and 2255h (D). The driving duration for driver A was from 1200h to 0330h. At approximately 0300hrs the driver's physiological tiredness score was high and was close to triggering an alarm. Rest was immediately taken and later driver B took over from 04100h to 0846h. During the rest it is shown on the graph that there is a reduction in PTS (explained in section 4.2.1 b) since the rest is more than 15 minutes **[Reyner and Horne 1997]**. After the driver, change the PTS score was resets according to the circadian rhythm based on the driver B's quality of sleep.

The graph shows that for driver B the PTS reduces over the duration of the drive, this is due to the human circadian rhythm. The driver alertness should have been improved during that time of the day **[Reyner and Horne 1997].** Driver C took over from

0846h to 1230h and the PTS result is the lowest compared to the other drivers throughout the duration of the drive.

Driver D took over at 1230h and drove for a total duration of 10 hours. Driver D rested only rested once at 1830h for approximately 30 minutes, therefore there was a drop in PTS score. There was an alarm triggered at 2233h indicated by orange diamond on the graph where the PTS score exceeded 0.95. The driver eventually stopped driving 10 minutes after the alarm.

5.2.2 Duration data results

The circadian rhythm component (figure 4.2.1a) may be removed from the physiological tiredness score (PTS) (figure 5.2.2.1) in order to observe the effects of the other factors. The formula for removing the circadian rhythm component is:-

$DTS(t) = PTS(t) - C_{SQ}(t)$ ----------Eqn 5.2.2.1

Where,

DTS (t) = Duration Tiredness Score

PTS (t) = Physiological Tiredness Score

$C_{SQ}(t)$ = Circadian based on sleep quality wrt time

Subtraction of the circadian rhythm component from the composite system output signal leads to the time varying difference DTS shown on figure 5.2.2.2. This graph shows that with a fresh driver (A, B, C, D figure 5.2.2.1) the tiredness score resets to zero. During the final phase of the day (Sector D figure 5.2.2.1) there was no driver change therefore the tiredness score remained accumulative for prolonged periods (approx. 10 hours) of driving with the alarm eventually triggered at 22.33 hours.

Five time sectors of increasing tiredness can be identified on figure 5.2.2.2 which are designated by 1, 2, 3, 4, and 5. Each refers to a different driver apart from 4 and 5 which refers to a single driver D who reset at 18.20 hours so reducing the tiredness level (from 0.6 to 0.4) yielding the two regions of tiredness 4 and 5.

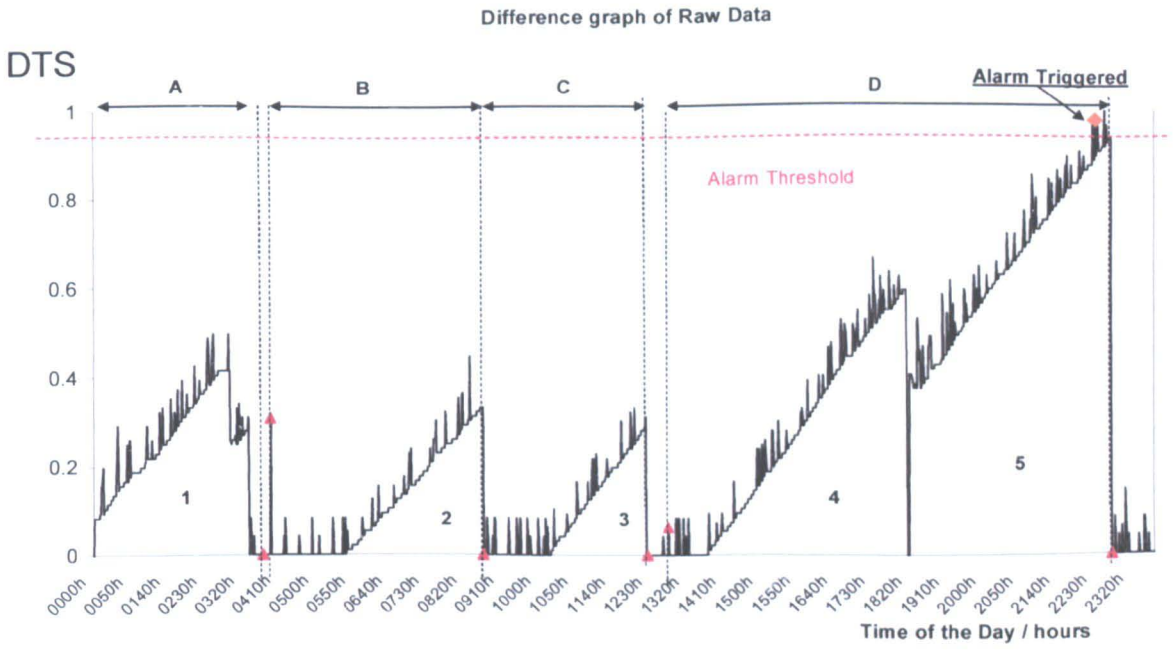

Figure 5.2.2.2. Difference graph of the raw data (Figure 5.2.2.1).

(Difference Graph = Raw Data – Circadian Rhythm).

(A, B, C, D –Drivers. 1, 2, 3, 4, 5-sectorial regions of increasing tiredness)

[Koh et al 2007]

5.3 Dashboard Unit Results (Gyroscope System)

5.3.1 Introduction

The experimental results of the dashboard unit involved the unprocessed signal from the gyroscope sensor which recorded the angular rate with reference to the yaw movement of the vehicle. In this section the experimental results are divided into four different sections:-

1. Normal driving manoeuvre results
2. Results for simulated fatigue-related driving
3. Mode based driving results
4. Further experimental results (with respect to different)
    a. Drivers
    b. Vehicles
    c. Weather conditions and Traffic density

For the gyroscope output results, there will be an offset of 0.5 on the y-axis from the origin. This is a normal feature since the gyroscope output has been purposely configured to settle on 0.5 to indicate centre positioning of the gyroscope.

For all the graphical results, the y-axis will represent the voltage of the processed gyroscope output from 0 up to 1. The horizontal x-axis represents the time in minutes.

5.3.2 Normal driving manoeuvre results

The list of monitored normal driving manoeuvres has been given in chapter 4.2.2. The results for these manoeuvres are presented in this section where the sampling rate of the gyroscope was selected as 15Hz.

1. Parking and Handling with Left and Right turning

This section presents results for the parking and handling of a vehicle with left and right turning. The vehicle used during this experiment was a van, and the experiment was conducted at a car park from which the vehicle was driven onto a road with normal road traffic conditions.

Figure 5.3.2.1 shows test results from the gyroscope of the vehicle during start-up followed by the vehicle leaving the parking bay and subsequently turning left and right. The gyroscope output was 0.5V when vehicle was stationary (section 5.3.1).

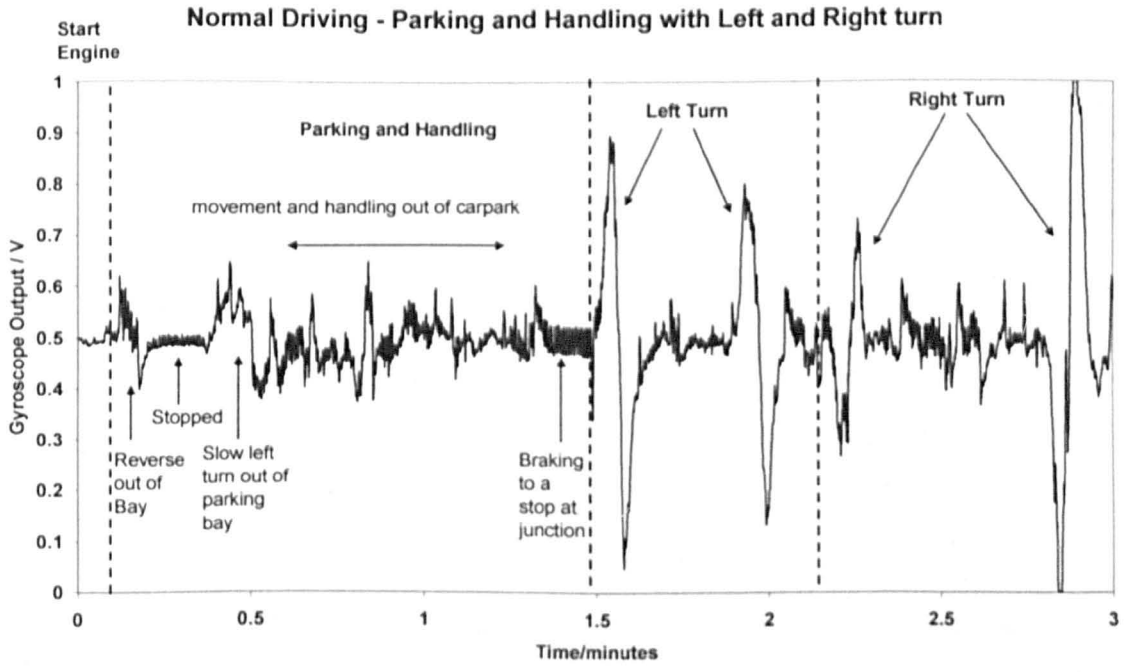

Figure 5.3.2.1. Gyroscope output showing signal features of 2 different manoeuvres: Parking and Handling (0-1.5min) & Left and right turning (1.5-3min)

After the parking and handling (0-1.5min) racking the vehicle under took a series of left and right turns on the road (1.5-3min). When the vehicle turned left the output of the gyroscope was in the range between 0.5-1V and when the vehicle turned right the output of the gyroscope was 0.5V -0V. As the vehicle turned left the gyroscopic output initially increase from 0.5V to 0.9V. Thereafter the output changed from 0.5V-0.1V indicating a movement of the vehicle in the opposite direction after the turn. The process is reversed for the vehicle turning towards the right direction.

2. Negotiating Roundabout

The result on figure 5.3.2.2 shows the vehicle negotiating a roundabout. Initially the vehicle stops at the traffic junction for about half a minute (0-0.4mins) before proceeding to the 1st roundabout after which (1-1.6mins) it proceeds to a second roundabout (1.6-2.2min). The approximate time to negotiate each roundabout is about 10~15 seconds.

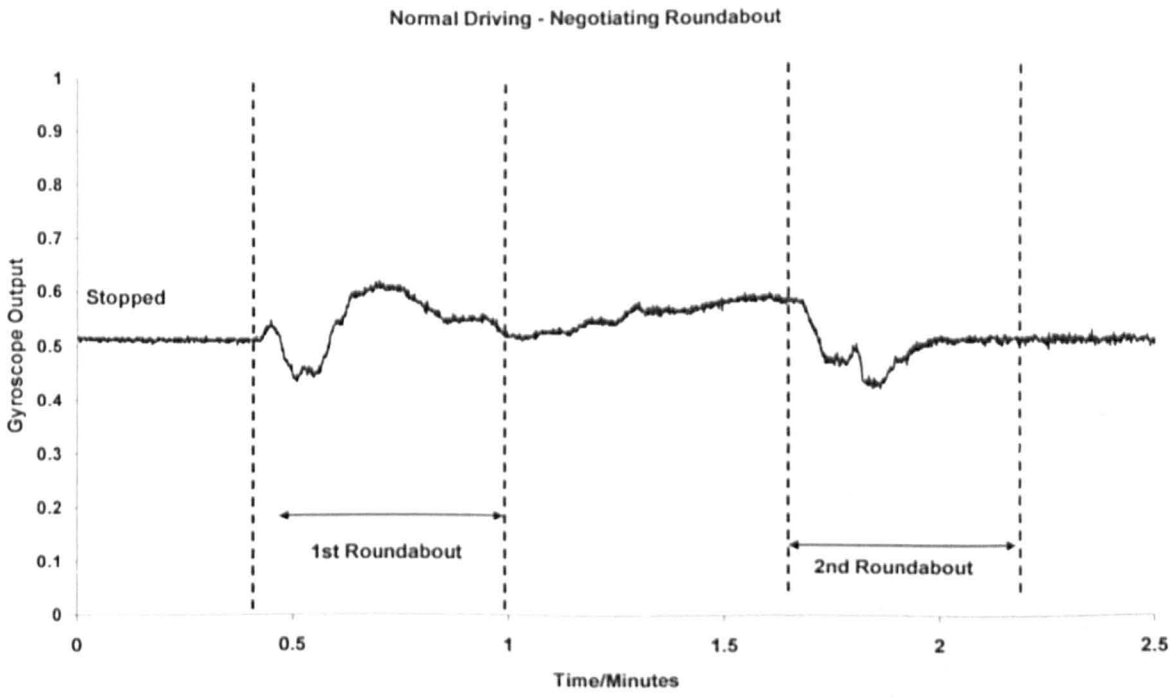

Figure 5.3.2.2. Gyroscope output showing signal features of vehicle negotiating roundabouts

3. Speed bump

Figure 5.3.2.3 shows the road test results for the vehicle negotiating a speed bump. The results demonstrate two examples of speed bumps. The time taken to complete a traverse of a speed bump is approximately 5-10 seconds. The output of the signal for the speed bump is in a range from 0.5V to 0.53V for both cases.

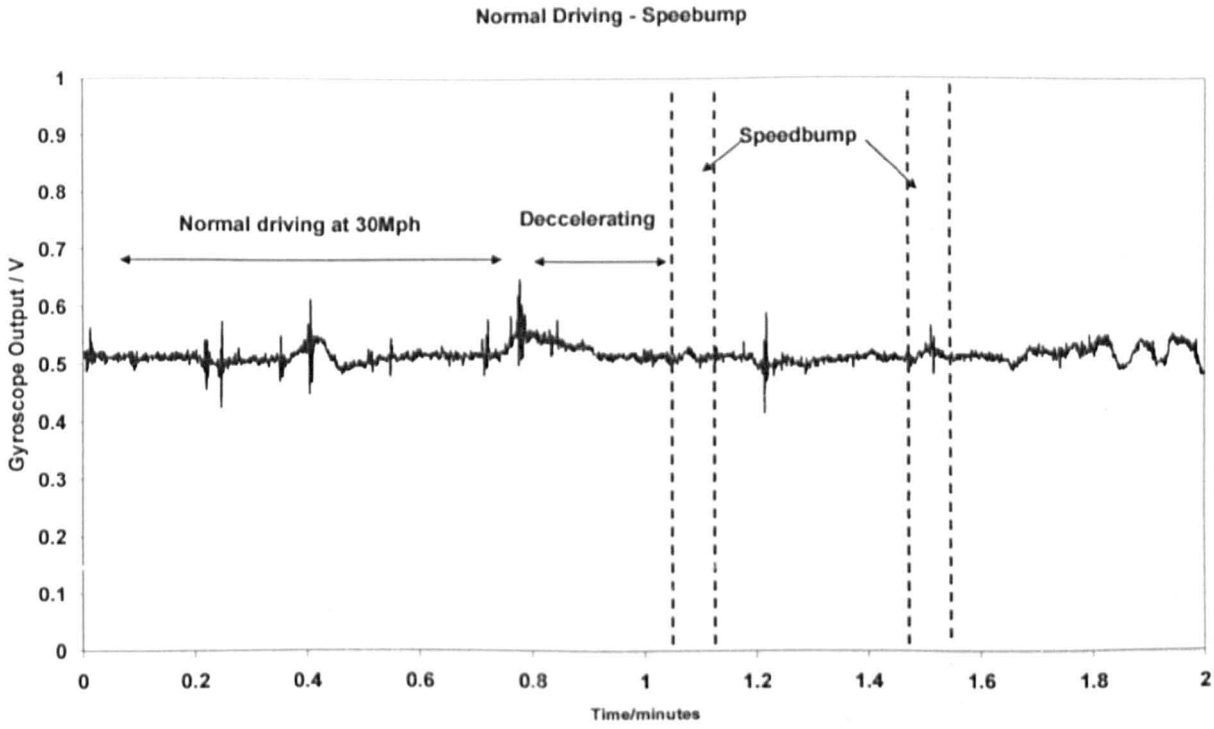

Figure 5.3.2.3. Gyroscope output showing signal features of vehicle negotiating on a speed bump

4. Acceleration and Deceleration

The results shown on figure 5.3.2.4 are when a vehicle accelerated from 0mph up to 60mph followed by the speed being maintained before decelerating to a halt. When the vehicle was stationary the gyroscope output showed no changes. As the vehicle performed the 3 point turn the parking and handling features (fig 5.3.2.1) are similar. During the acceleration of the vehicle the gyroscope output varied approximately 0.4V-0.6V, when the vehicle decelerated the variation of the gyroscope output was 0.45V-0.55V until the vehicle halted.

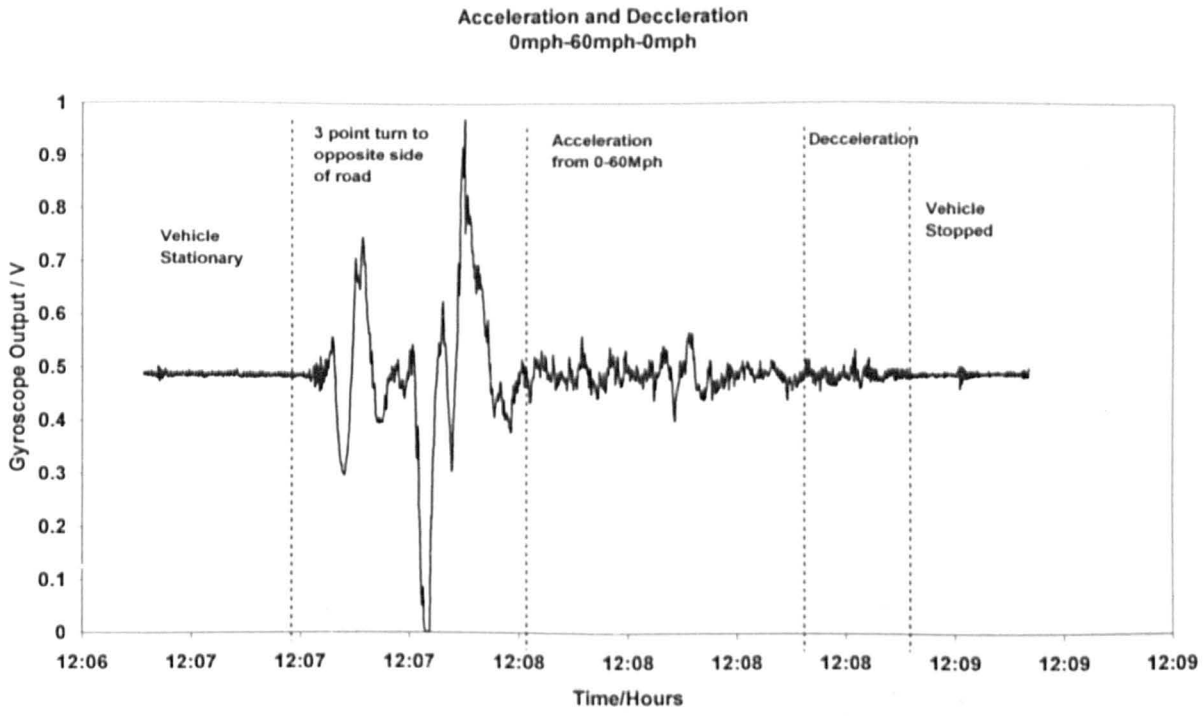

Figure 5.3.2.4 Gyroscope output showing signal features of vehicle acceleration and deceleration

5.3.3 Results for fatigue related driving

The various types of fatigue-related simulations of driving manoeuvres have been described in detail in chapter 4.2.3. The results of the fatigue related exercise, lane drifting and swerving, on a road test are presented on figure 5.3.3.1. The road test record showed that a total of 6 swerve activities (S_1-S_6) and 4 lane-drifts (D_1-D_4) were undertaken. The signals shown on figure 5.3.3.1 indicate that it is difficult to discriminate swerving and lane drifting from the other driving artefacts on the same graph.

The first two swerves and lane drifts have been enlarged for further observation and comparison on figure 5.3.3.2 (a) and (b) respectively. The vehicle used for this experimental task was a van and the sampling rate of the gyroscope system was 15Hz

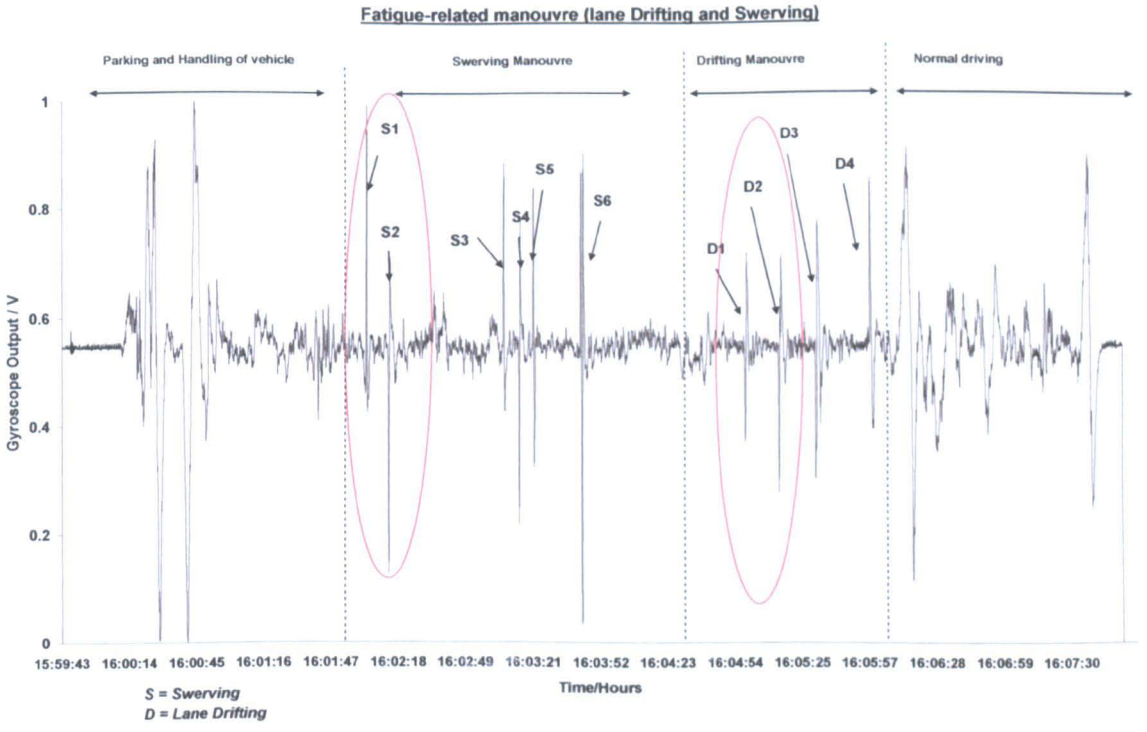

Figure 5.3.3.1. Gyroscope output showing different signals associated with fatigue related manoeuvre (Lane drifting and swerving)

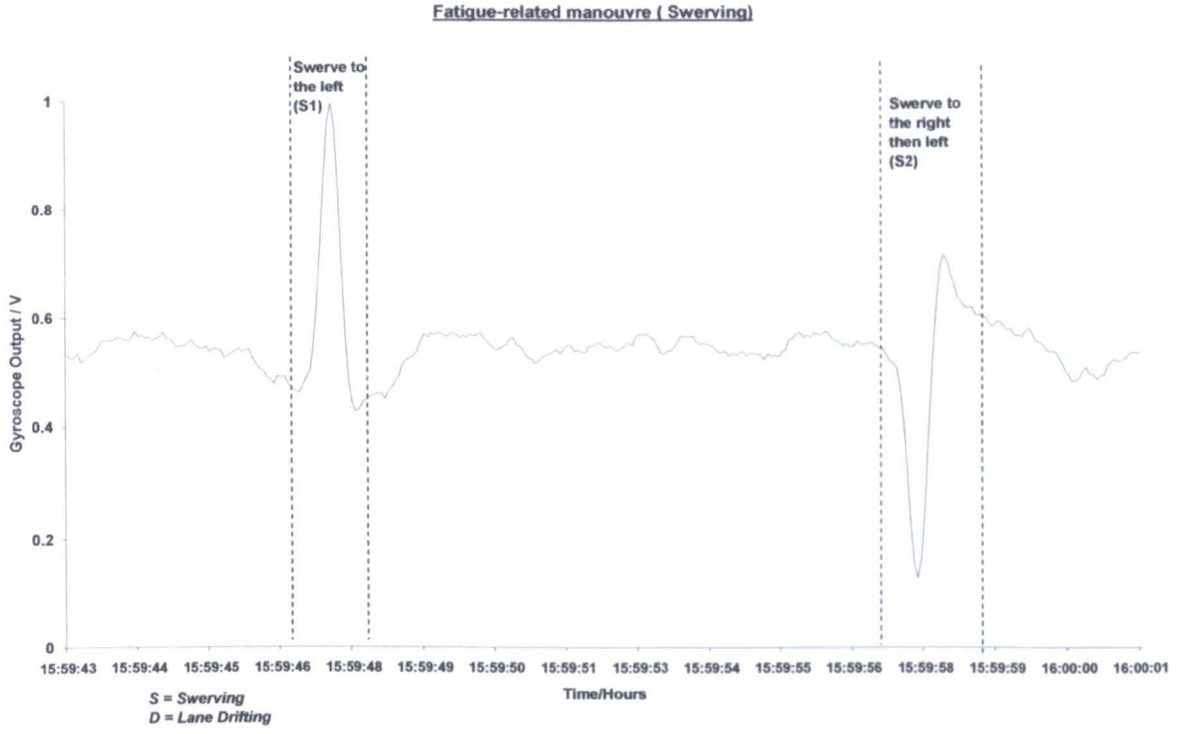

(a)

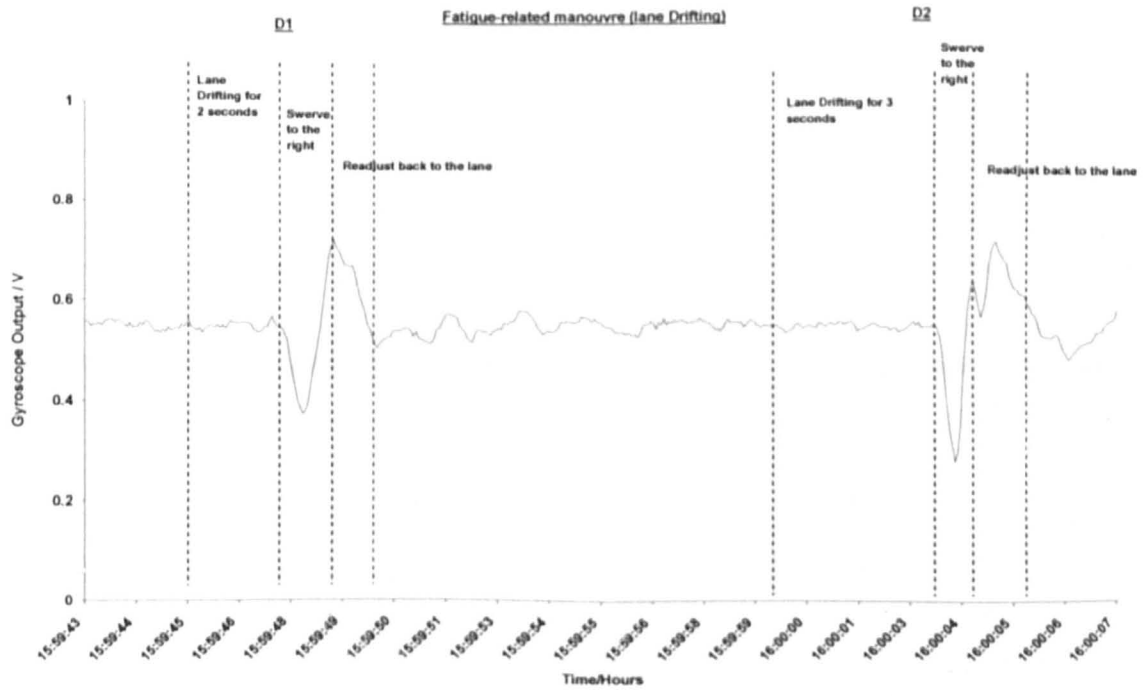

(b)

Figure 5.3.3.2. Enlarged versions of the section of figure 5.3.3.1

(a) 2 swerves 'S1' and 'S2'

(b) 2 Lane drifting 'D1' and 'D2'

5.3.4 Mode based driving results

Three driving modes, 'Town', 'Motorway' and 'Stop' modes were described in chapter 4.3.2.4. The result shown on figure 5.3.4.1 highlights the various manoeuvres occurring during the respective driving modes.

The figure indicates that the town mode driving consists of parking and handling, speed bump, normal town driving and roundabout. The motorway mode consists of driving on the motorway which can involve overtaking a vehicle, entering or leaving a slip road and vehicle switching lanes.

With the gyroscope output alone it appears difficult to classify the different driving modes and in particular to identify a fatigue driving manoeuvre when it only occurs during monotonous driving conditions.

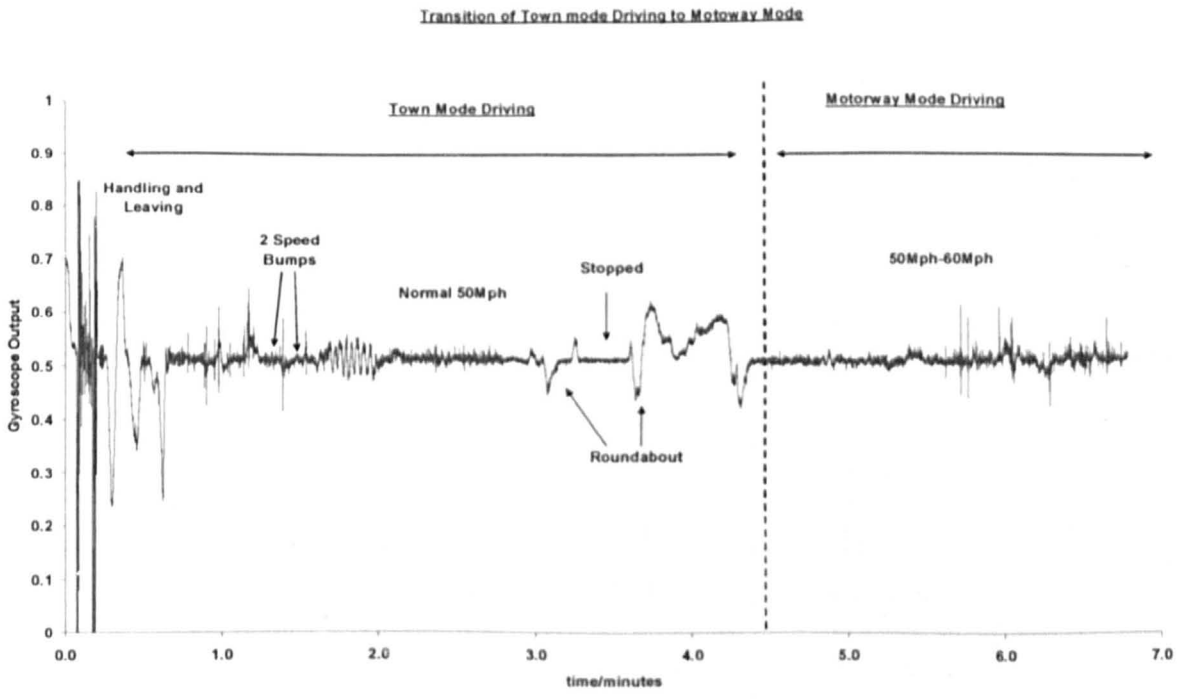

Figure 5.3.4.1. Gyroscope output showing different signals associated with various driving modes

5.3.5 Further Road test Experiments

Further experimental tests were undertaken to test and verify the performance of the dashboard gyroscope system under various conditions. These conditions included different drivers, vehicles, traffic density and weather.

A total of 16 experiments were conducted each using the same test route and experimental tasks. Each experiment lasted for approximately 40 minutes. The tests undertaken are summarised on table 5.3.5.1. The purpose of these experiments was to identify the simulated fatigue manoeuvres from other normal driving manoeuvres

The table 5.3.5.1 shows the experimental test conducted for the dashboard gyroscope unit. The last column of the table shows the number of simulated fatigue events. These events are simulated fatigue related events on real road driving conditions. The fatigue events can be either a swerving or lane drifting as described in section 4.3.3.

Test No.	Driver (M=Male) (F=Female)	Vehicle Type	Weather Conditions (Sunny, Cloudy, Rainy)	Traffic Density (Light, Medium, Heavy)	Simulated Fatigue event
1	M-1	Hatchback Car	Cloudy	Medium	4
2		Hatchback Car	Cloudy	Medium	3
3		Van	Sunny	Medium	3
4		Van	Sunny	Light	7
5		Van	Cloudy	Medium	8
6	M-2	Hatchback Car	Rainy	Medium	5
7		Van	Rainy	Medium	3
8		Van	Rainy	Heavy	7
9	M-3	Hatchback Car	Sunny	Medium	6
10		Van	Sunny	Light	7
11	M-4	Saloon Car	Rainy	Medium	9
12	M-5	Articulated Truck(Loaded)	Rainy	Heavy	4
13		Articulated Truck(Unloaded)	Sunny	Medium	4
14	F-1	Van	Sunny	Heavy	1
15		Van	Sunny	Heavy	4
16	F-2	Van	Sunny	Medium	4

Table 5.3.5.1 – Summary of the dashboard implementation tests (same route)

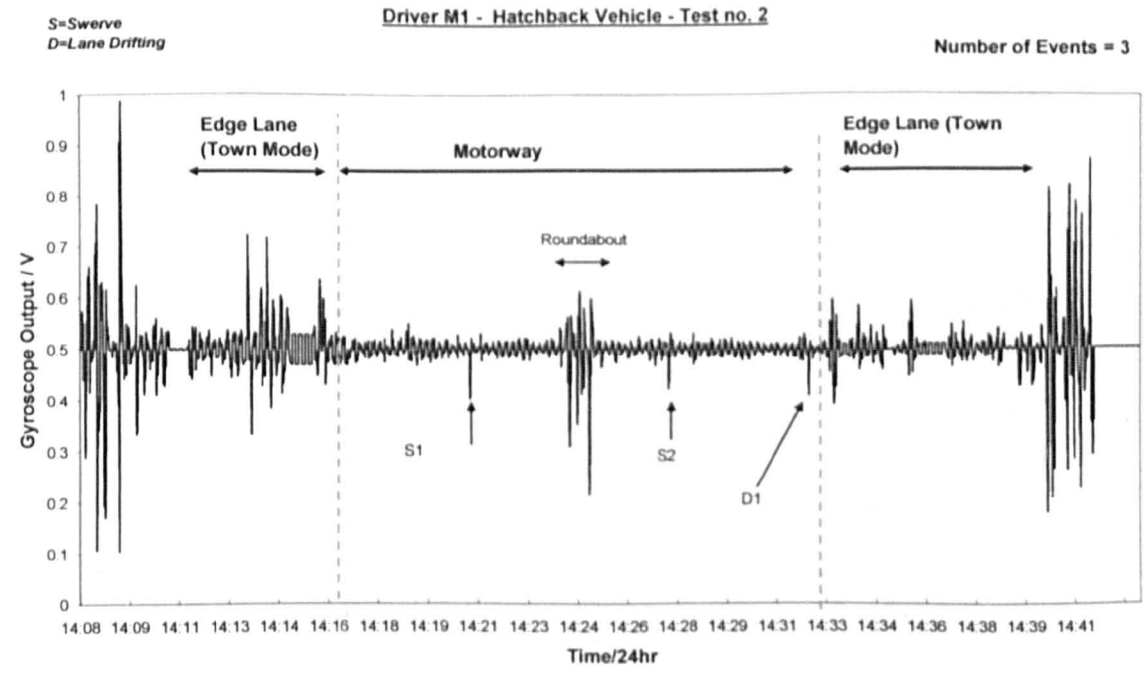
S=Swerve
D=Lane Drifting
Driver M1 - Hatchback Vehicle - Test no. 2
Number of Events = 3
Edge Lane (Town Mode)
Motorway
Edge Lane (Town Mode)
Roundabout
S1
S2
D1
Gyroscope Output / V
Time/24hr

(a)

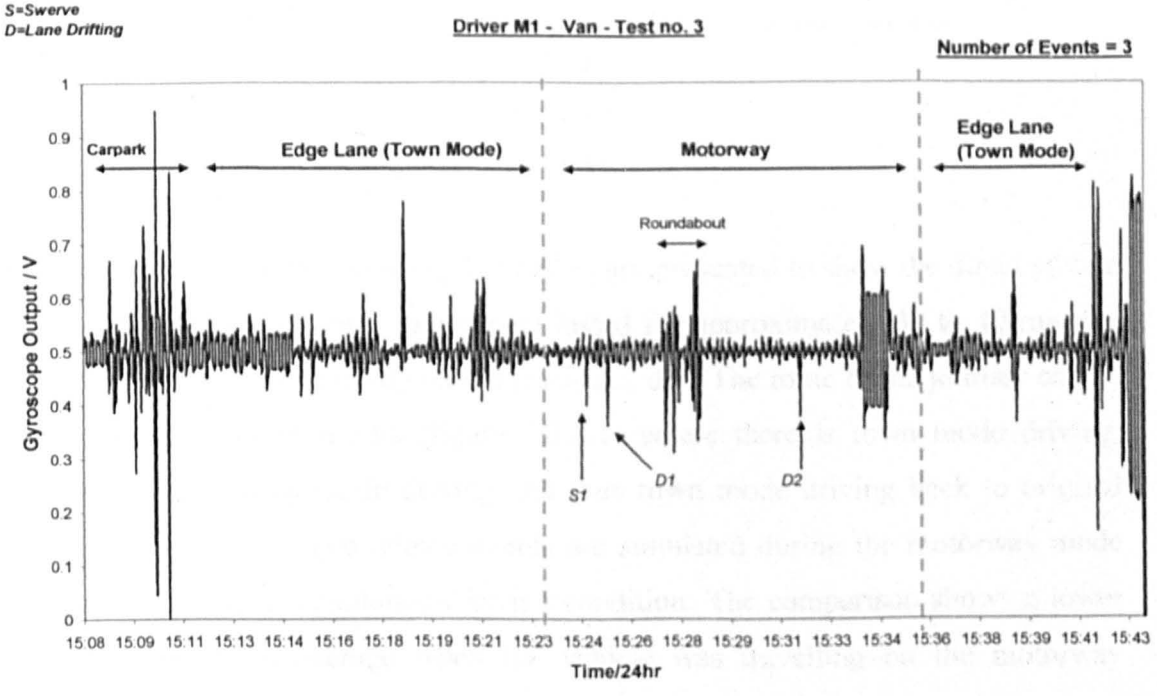
S=Swerve
D=Lane Drifting
Driver M1 - Van - Test no. 3
Number of Events = 3
Carpark
Edge Lane (Town Mode)
Motorway
Edge Lane (Town Mode)
Roundabout
S1
D1
D2
Gyroscope Output / V
Time/24hr

(b)

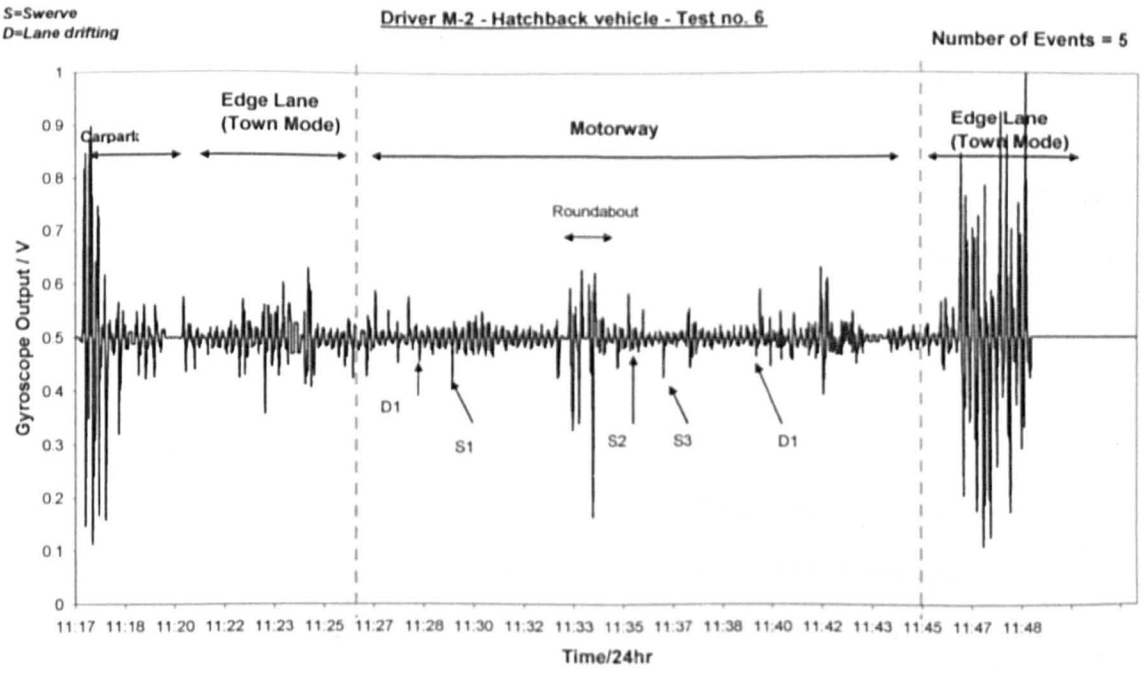

(c)

Figure 5.3.5.1 Unprocessed gyroscope outputs for experimental tests

(a) Test 2

(b) Test 3

(c) Test 6

Three different experimental tests, 2, 3 and 6, are presented to show the direct system output (Figure 5.3.5.1). Each experiment lasted for approximately 30 to 40 minutes depending on the traffic density on the particular day. The route of the journey can be observe on the output results (figure 5.3.5.1) where there is town mode driving, followed by motorway mode driving and then town mode driving back to original destination. All the fatigue related events are simulated during the motorway mode which is regarded as monotonous driving condition. The comparison shows a lower gyroscope output in average when the vehicle was travelling on the motorway compared to the town mode driving. The test 2 and 3 results shows 3 events simulated where 2 are swerves and 1 lane drifting. Test 6 shows a total of 5 events where 3 are swerves and 2 are lane drifting. Fatigue related manoeuvres (swerves and lane drifting) do not seem to be easily distinguishable from the other driving data recorded.

5.4 Steering Wheel Results

5.4.1 Introduction

The output signals from the gyroscope system installed on the steering wheel are presented in this section. Two different types of tests were conducted: the Laboratory steering wheel test and an actual road test on a vehicle steering wheel.

5.4.2 Laboratory Steering Wheel results

Figure 5.4.2.1 shows the gyroscope output results of the laboratory steering wheel test. The experimental test period is divided into 5 subsections where each section is of one minute duration and covering a different manoeuvre set.

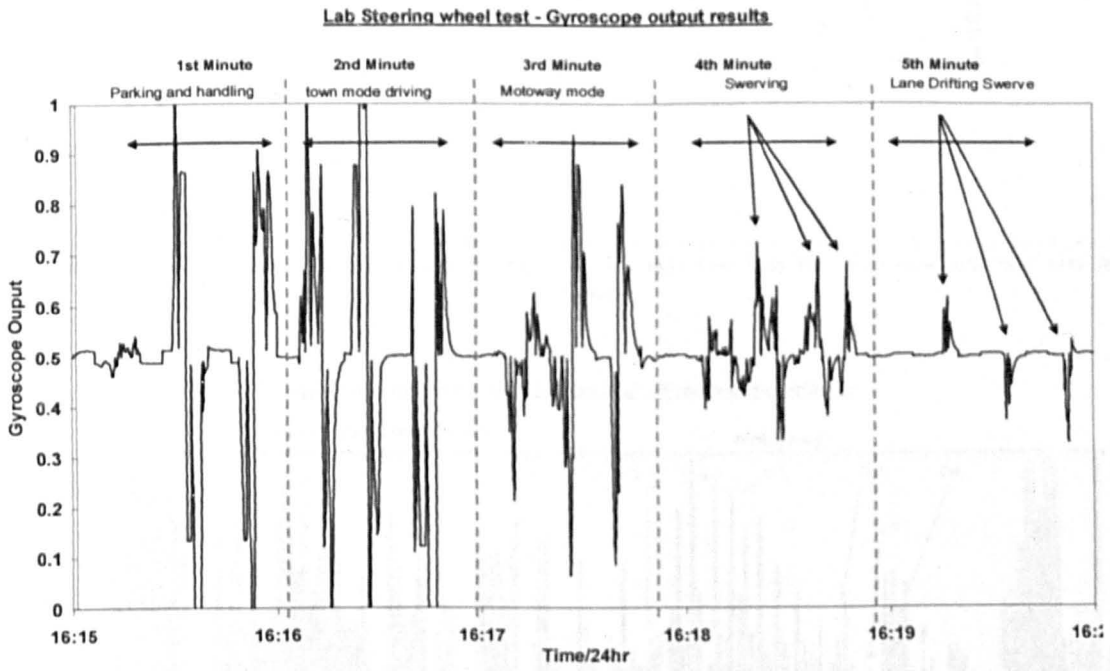

Figure 5.4.2.1 –Gyroscope output from the laboratory steering wheel test

The orders of the manoeuvre sets are as follows:-

1. Parking and Handling
2. Normal driving – Town mode driving
3. Motorway mode driving
4. Fatigue related simulations – Swerving
5. Fatigue related simulations – Lane Drifting swerving

5.4.3 Vehicle Steering Wheel results (Road test)

For the road test, the experimental journey followed the same route as that described in section 4.2.5.1.During the test phase, both the steering wheel and dashboard systems were used simultaneously to gather results which could by synchronised. These two sets of results are presented.

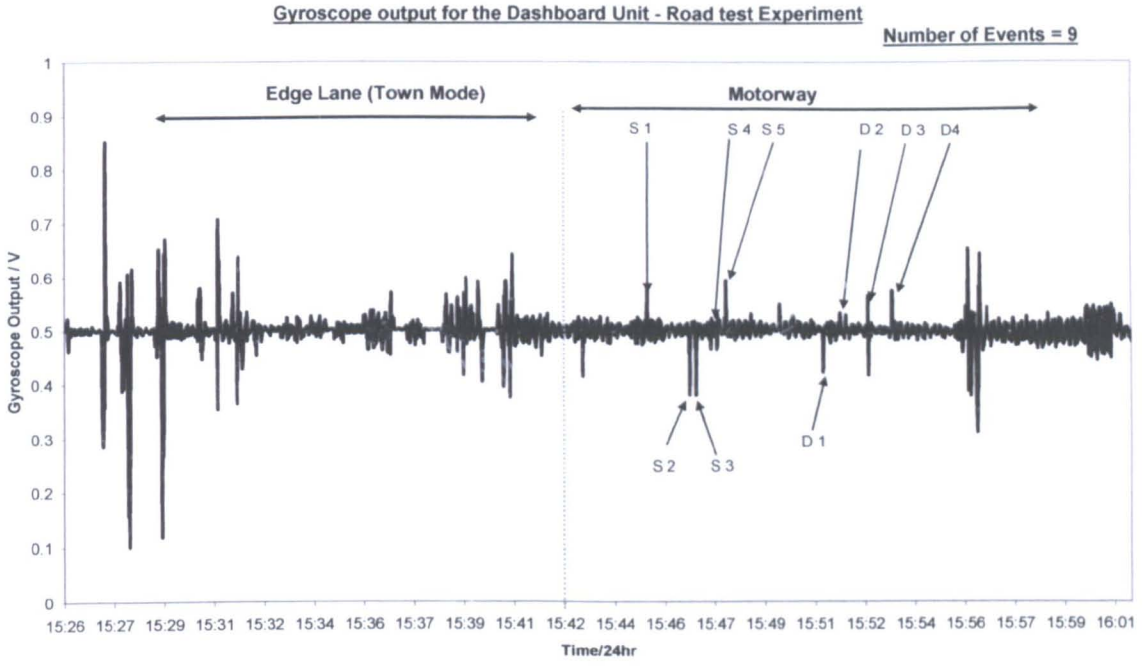

(a)

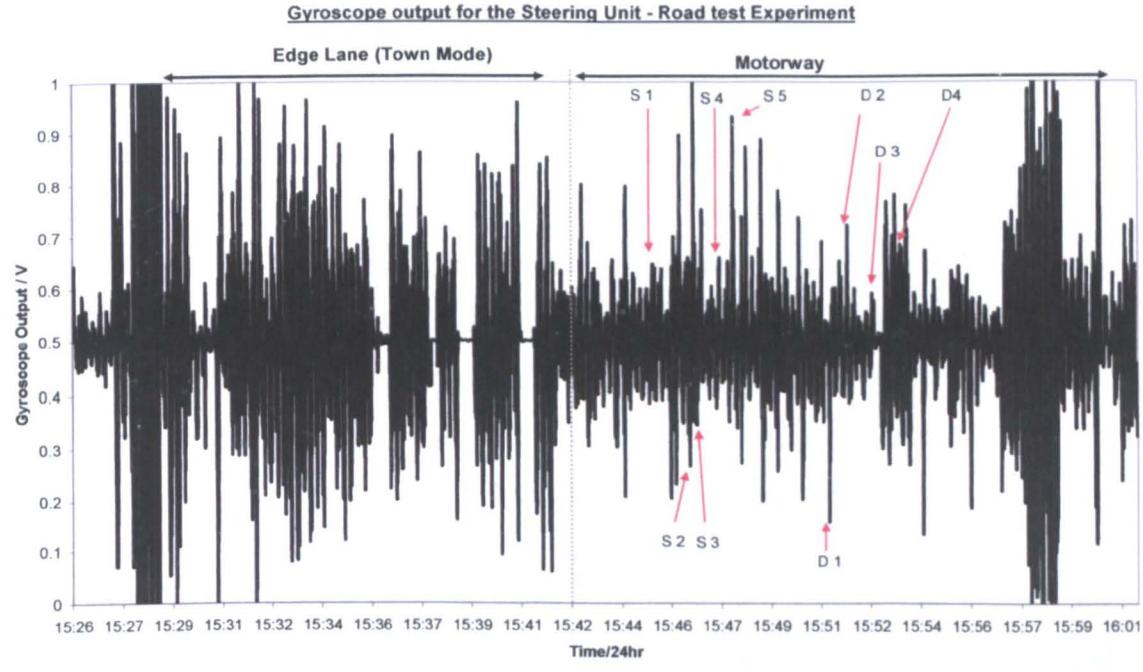

(b)

Figure 5.4.3.1 –Gyroscope output signals:-

(a) The Dashboard unit (experimental no 8)

(b) The steering wheel system

Figure 5.4.3.1(a) shows the results for the dashboard unit (expt 8) with a van where nine fatigue related events were simulated of which five were swerving activities and four were lane drifting manoeuvres. Figure 5.4.3.1(b) presents the gyroscope output from the steering wheel system during the experimental drive. The vehicle used for this task was the van. Comparing the experimental results for the two different systems, there is more background noise seen on the steering wheel system result. This is because the gyroscope on the steering wheel experienced more angular rate rotation on the steering wheel.

5.5 Summary

The gyroscope output (V) which measures the angular rate for the composite system, dashboard unit and the steering wheel system obtained from the respective road tests have been presented. The composite system measures the physiological information from the Circadian rhythm, length of driving, quality of sleep and the driving behaviour. The experimental results presented show the physiological tiredness score of four different drivers on a 24 hour driving shift. Since driver D covered the longest night shift and drove for more than 10 hours, his PTS triggered the alarm advising the driver to stop driving.

The dashboard unit was built to collect real time driving information such as normal and fatigue driving manoeuvres. From the signals gathered it is not apparent that distinguish between normal driving and simulated fatigue related driving manoeuvres can be distinguished. Also it is difficult to classify the transition of a vehicle changing from town to motorway mode. This is important since monotonous driving (motorway mode) information is required to eliminate the possibility of a fatigued driver. Further experiments were conducted for different drivers, vehicles, weather conditions and traffic conditions to investigate the performance of the dashboard system

The steering wheel system used the same principles as the gyroscope system, for detecting steering wheel motion. As for the dashboard experiments, normal and fatigue driving exercises have been conducted for both the laboratory and the vehicle units for road test. The actual road driving test results contained additional

information such as road conditions, vibrations and traffic conditions compared to the laboratory steering wheel test results. Comparison of the experimental results between the dashboard unit and steering system showed that the steering wheel system results have more background noise and also higher angular rate detected.

Chapter 6

Chromatic Analysis and Discussion of Results

6.1 Introduction

The analysis of results involves the application of the chromatic processing technique to the experimental results presented in chapter 5. The processing aspects of the chromatic methodology assist in reducing the complexity of an unprocessed raw signal produced by the monitoring system. The information may be further analysed to discriminate critical incidents from normal events. This can provide an early indication of the onset of driving fatigue.

For the composite system, the chromatic processing technique is applied to help classify and efficiently represent the data of the output signal. For this analysis, chromatic polar diagrams will be used to efficiently classify tiredness information. Details about the application of chromatic processing are discussed. The three overlapping chromatic filters are configured to identify the trend of fatigue over the

entire time period during which a vehicle is driven. These fatigue trends are the driver physiological indicators obtained from the respective circadian rhythm patterns.

The gyroscope system has been deployed in two different monitoring systems. The chromatic processing is applied to both the dashboard unit and the steering wheel system. The analysis of results shows how the fatigue related manoeuvres are discriminated from normal driving conditions. Mode based driving is an important element in the algorithm to minimise false positive event.

6. 2 Chromatic Analysis of the Composite System Signal

6.2.1 Introduction

The composite system is designed to monitor the physiological conditions of a road vehicle driver. The physiological factors are taken into account by combining the information from the circadian rhythm, quality of sleep, duration of the drive and monotonous driving conditions (section 4.2). The experimental results presented in section 5.2 are for an articulated vehicle driven by 4 different shift drivers over a 24 hour period. There were two results presented, the first was the physiological tiredness score (PTS) over the 24 hour period and the second is the difference tiredness score (DTS) over the 24 hour period (circadian rhythm absent).

The purpose of applying the chromatic processing technique is to classify and differentiate the tiredness information (e.g. driver alert and driver tired). In this section the details of how the chromatic processing technique is configured to this particular application is described. This is followed by the analysis and discussion of the results

6.2.2 Application of the Chromatic Processing technique

The chromatic processing technique explained in section 2.6 involved two steps: chromatic filtering and chromatic transformation.

6.2.2.1 Chromatic Filtering

There are two steps involved in the chromatic filtering: selection of optimum filter size and time stepping. For the first step, an optimum filter size was selected to identify the trend of tiredness. The optimum size of the chromatic filter selected for this analysis had a width of 75 minutes for each filter and 150 min (due to the overlapping) for all three filters shown on figure 6.2.2.1. This selected filter size was found (from the 20 experimental results) to be optimal for detecting relevant changes in the signals **[Koh et al, 2007]**.

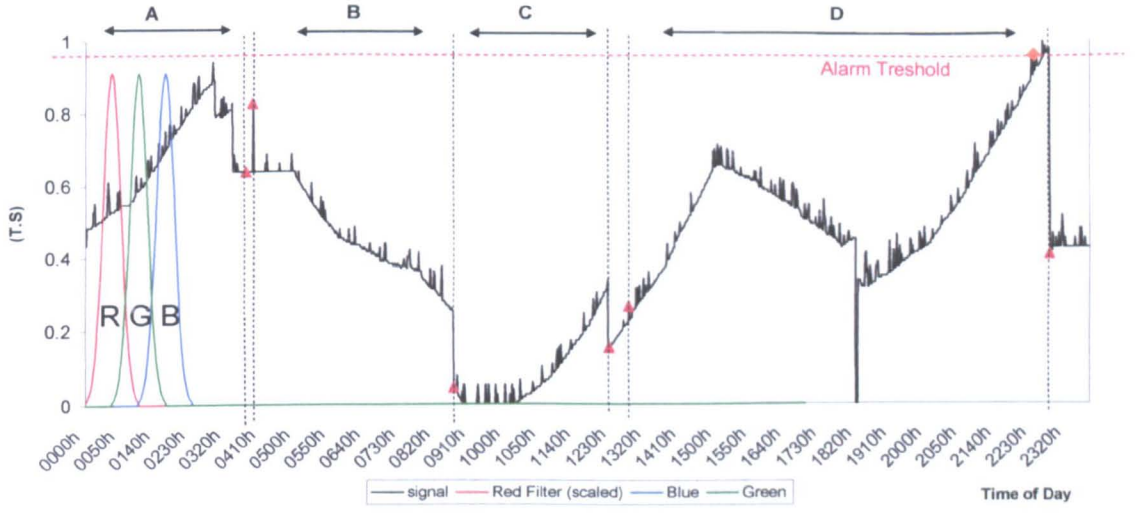

Figure 6.2.2.1 Deployment of the chromatic RGB filters onto the Composite system output results of figure 5.2.2.1. (Filter is configured at 75 mins time stepped 1 minute). [Koh et al 2007]

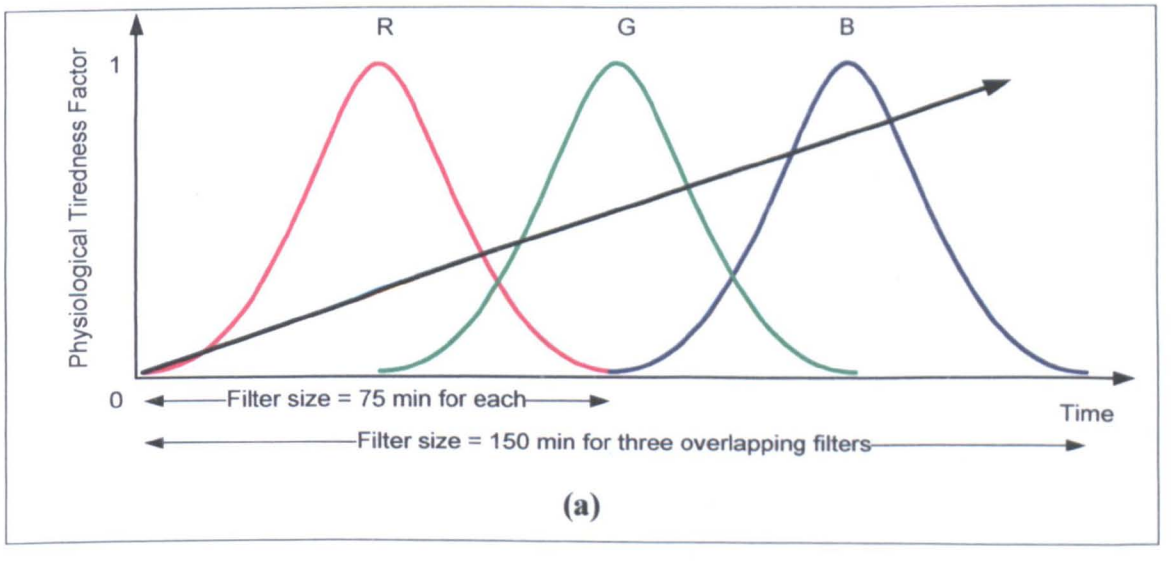

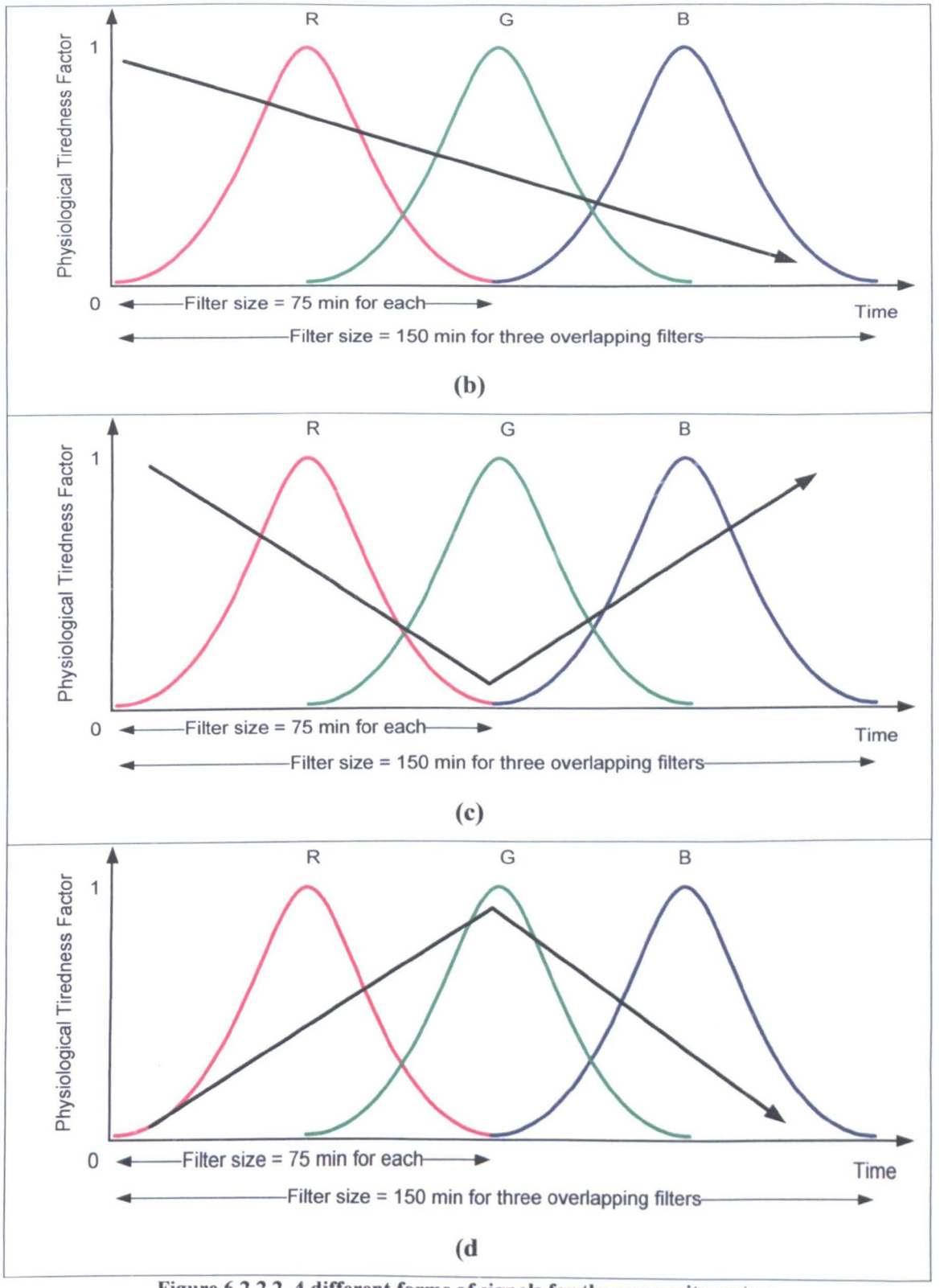

Figure 6.2.2.2 4 different forms of signals for the composite system

(a) Increasing tiredness

(b) Decreasing tiredness

(c) Resting trough

(d) Peak tiredness

There are four major forms of signals found on the experimental results which identify the changes of the tiredness score. The four forms of signals are shown on figure 6.2.2.2 (a), (b), (c) and (d) where the gradient of each signal is different from one another. Figures (a) and (b) show positive and negative gradients which indicate increasing and decreasing tiredness for the driver respectively. Figure (c) shows that the gradient reaches a minimum level which indicates that the driver is resting or that there is a decreasing circadian rhythm. Figure (d) shows the gradient increasing to a peak and then decreasing thereafter, which indicates that the tiredness reaches its maximum peak before gradual decreasing. From the experimental output results (figure 6.2.2.1), the gradient of the time variation of the signal can be used to identify the tiredness trend of the driver.

With an optimal filter size selected, a time stepping method (section 2.8.4) is required to analyse the signals for the entire time span on the data. The time stepping technique (section 2.8.4.9) is applied using a time step of 1 minute yielding a sampling rate for the composite system of 1 data point per minute. With this time stepping technique, a chromatic output is processed for each of the time steps from the experimental data received.

6.2.2.2 Chromatic parameters representation

From each chromatically filtered time step, there is a set of outputs produced, r, g and b (equation 2.6.3.1.1). Applying the chromatic transformation formula (equation 2.6.3.2.1) yields three chromatic output parameters H, L, and S which have appropriate meanings in relation to the application which serves the purpose for the information extraction **[Wong et al, 2005].**

The chromatic parameters H, L and S in this case have the following meanings.

1. Interpretation of H

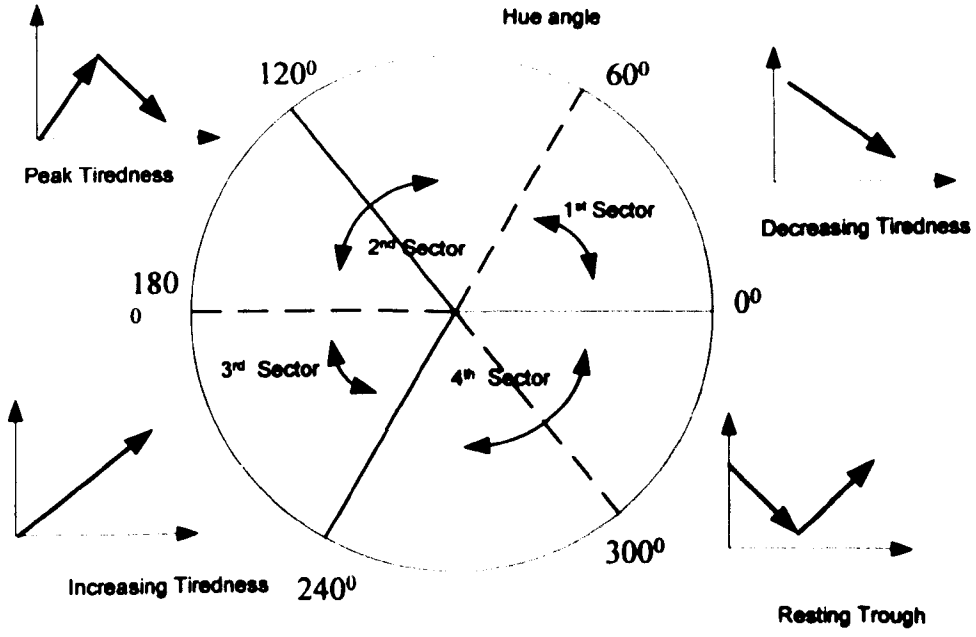

Figure 6.2.2.2.1 – Correspondence between sectors of a H-L diagram and the type of linearity of a signal

The purpose of the chromatic H parameter is to identify the dominant signal on the respective R, G and B filters **[Jones et al, 2000; Zhang, 2004]**. With the selection of the filter size shown on figure 6.2.2.2, the chromatic output H may be interpreted as a tiredness trend as follows

1st sector (H=0^0-60^0),	-	Decreasing tiredness
2nd sector (H=60^0-180^0),	-	Peak tiredness
3rd sector (H=180^0-240^0),	-	Increasing Tiredness
4th sector (H=240^0-360^0),	-	Resting trough

2. Interpretation of L

$$L = \frac{\max(r,g,b) + \min(r,g,b)}{2} (Eqn - 2.7.2.2)$$

The chromatic output L is defined as the nominal strength of the signal **[Jones et al. 2000; Zhang, 2004]**. Considering a linearly increasing signal amplitude (figure

6.2.2.2.2) the output of each processor R, G, B increases as the area beneath the signal curve increases leading an increase in the value of L. A similar argument applies to a negative gradient signal.

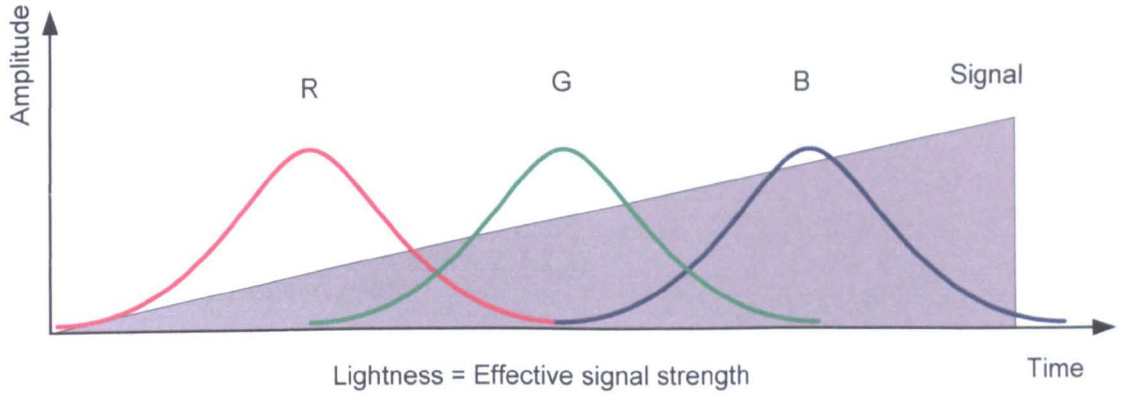

Figure 6.2.2.2.2– Effect of increasing signal amplitude gradient upon the outputs of R, G, B.

The larger the area under the signal amplitude: time (6.2.2.2.2) curve the higher the lightness value (6.2.2.2.3).

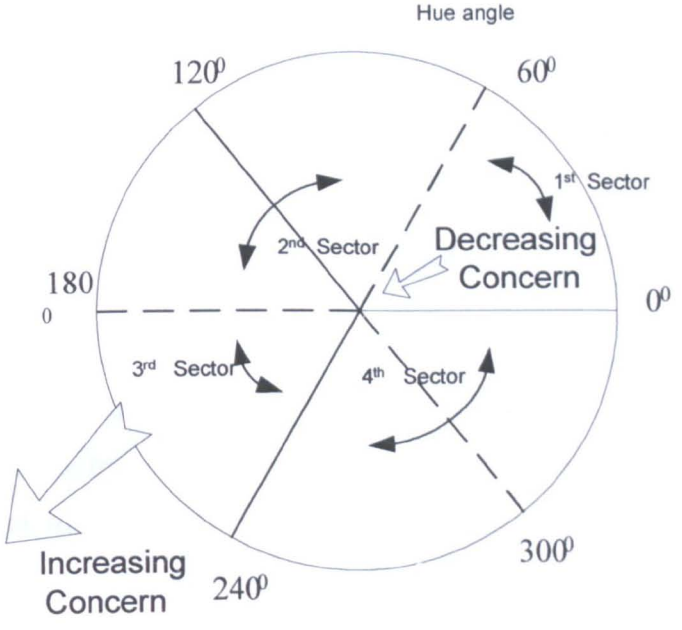

Figure 6.2.2.2.3– H-L diagram showing the effect of increasing signal gradients

It has already been shown (figure 6.2.2.2.1) that the H values within the 1st sector of a H-L polar diagram represent a decreasing tiredness regime whilst the 3rd quadrant represents an increasing tiredness regime. Therefore to interpret the physical meaning of the chromatic L parameter, attention is focused upon the first and thirds sectors. For the 1st sector (figure 6.2.2.2.3) the L values indicate the rate at which the tiredness level decreases i.e. a lower L means decreasing tiredness. Therefore it is a region of

decreasing concern. Extending the argument to the third sector which correlates with increasing tiredness, the higher the L values in this region the more rapid the increase in tiredness. This shows that the magnitude of L indicates the tiredness level being linked to the strength of the signal.

3. Interpretation of S

The chromatic formula for calculating Saturation is:

$$S = \frac{\max(r,g,b) - \min(r,g,b)}{\max(r,g,b) + \min(r,g,b)} \quad Eqn - 2.7.2.3)$$

Chromatic S is the spread of the signal. More widely spread signals will result in a low S value and vice versa. **[Jones et al, 2000; Zhang, 2004].** Chromatic S in this case is an indication of the fractional change in signal distribution in a finite time compared with a norm. A low saturation indicates smaller changes in the signal distribution.

When used in small scale time stepping mode the S parameter does not appear to yield useful information about changes in tiredness level compared with longer deviation physiological trends. Therefore the chromatic S parameter is not used for addressing the composite system.

In conclusion, it is only the H-L polar diagram which is used to extract the tiredness information so that the transformed information can conveniently highlight trends and also be in a form for amalgamation with information derived chromatically from physical measurement with a gyroscope.

6.2.3 Chromatic Analysis of the Composite System

Chromatic analysis has been used with two experimental results, physiological tiredness score plot (PTS) (figure 5.2.2.1) and difference tiredness score (DTS) plot (figure 5.2.2.2) shown in section 5.

6.2.3.1 Chromatic analysis of the Physiological Tiredness Score (PTS)

Applying chromatic processing to the physiological tiredness score graph of figure 5.2.2.1 yields the H-L polar diagram of figure 6.2.3.1.1. The chromatic H represents the nature of the gradient (e.g. increasing or decreasing) of the physiological tiredness score. The chromatic L shows the magnitude of the physiological tiredness score.

Data for each driver, designated by A-D as on figure 5.2.2.1, is distinguished by different symbols. The polar plot is divided into 4 sectors of different tiredness level regimes. Arrows are used to show the time progression.

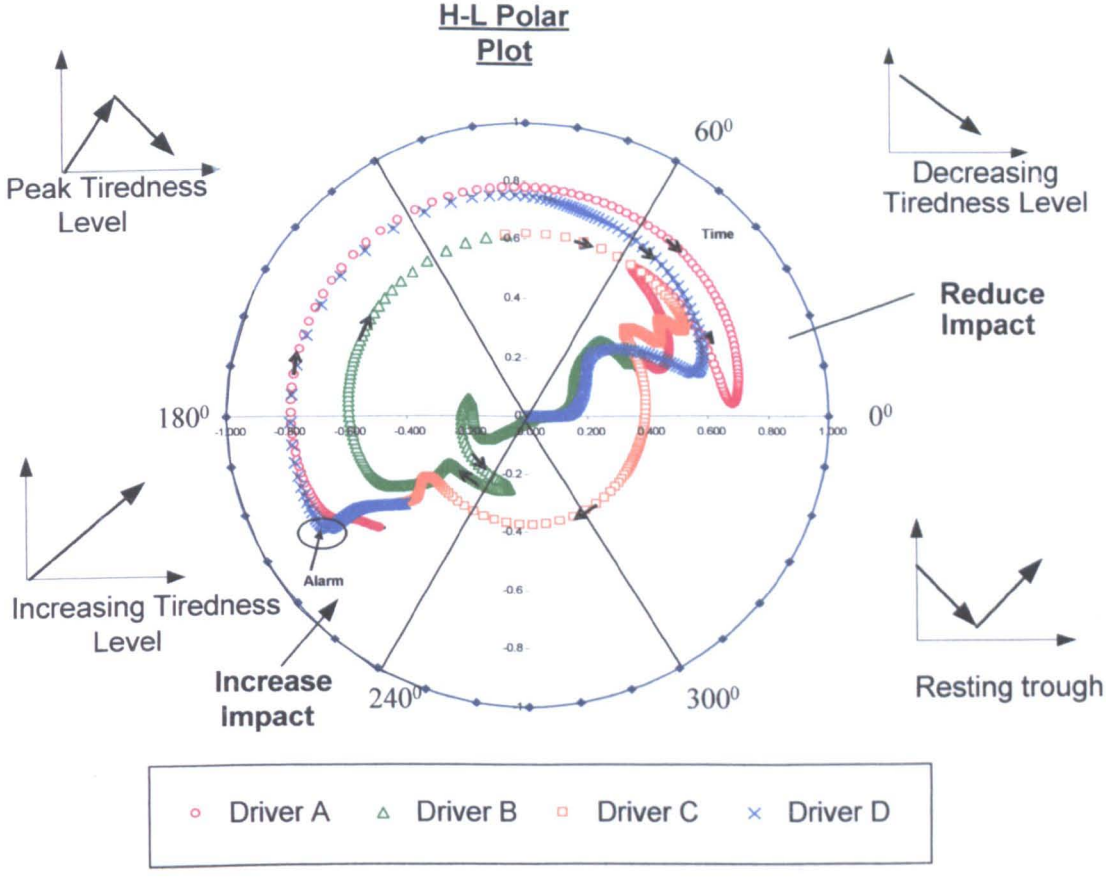

Figure 6.2.3.1.1 - Chromatic polar- diagram H-L for the overall output signal of Figure 5.2.2.1. (Different symbols corresponds to various drivers A-D, figure 5.2.2.1) [Koh et al 2007]

The 1st sector (H=0^0-60^0) shows the decreasing tiredness level for all 4 drivers (A-D) where there is a presence of decreasing gradient in the physiological tiredness score. From the result for driver B (green) the L values were tending towards zero, indicating that the driver was driving at the time of day when the circadian rhythm was decreasing i.e. between 0400h to 0900h. The results for driver D (blue) also

shows the L values tending towards zero, where there was a decrease in physiological score between 1500h and 1800h again due to the circadian rhythm. The decrease in circadian rhythm indicates that the alertness of the driver is improving which is between 0400h – 0900h and 1500h-1800h **[Horne, 2001]**.

In the 4th sector (H=300^0-360^0) the physiological tiredness score is at its lowest. For this sector the only data is from driver C. This corresponds to a maximum wakefulness period where the circadian rhythm is at its lowest throughout the day (1730h-2000h) **[Horne, 2001]**. This physiological tiredness score is the healthiest in this sector.

The 3rd sector (H=180^0-240^0) shows an increasing gradient for the physiological tiredness score. The higher the L the worse the physiological score. Driver A and D have the highest L values of 0.77 and 0.80 respectively. Driver A has high L values because the time of day during the drive is between 0200h and 0400h during which the circadian rhythm indicates most tiredness. Driver D has a very high L of 0.8 which also triggered an alarm. This is because of the time of the day and the lengthened duration of the drive. An alarm which was triggered at 2233h (figure 3) has H, L coordinates 210^0, 0.8. To reduce the physiological tiredness score the driver should be taking more rest breaks of least 15 minutes to regain alertness.

When drivers A and D experienced peak tiredness, both took action to cease driving and rest immediately. The 2nd sector (H=60^0-180^0) is the region where the physiological tiredness score reaches its peak and commences to decrease. Drivers A and D show high L values in this sector. The reason for this is because the physiological tiredness score is decreasing after the peak in the 3rd sector.

This analysis of the physiological tiredness score shows that different sectors of the H scale indicate the tiredness level of a driver with respect to the circadian rhythm. Chromatic L shows the level of the tiredness where higher L indicates greater tiredness.

6.2.3.2 Chromatic analysis of the Duration Tiredness Score (DTS)

Applying the chromatic analysis to the data of figure 5.2.2.2 yields the H-L polar diagram of figure 6.3.3.1. In this case the five different time stages of figure 5.2.2.2 (1-5) are distinguished by different symbols. These results correspond to the case whereby the circadian rhythm factor is removed from the score.

With the description of different levels of tiredness being categorised for the 4 separate sectors, trends of tiredness progression become more apparent. Chromatic H represents the sense of the gradient (eg. increasing or decreasing) of the duration tiredness score. Chromatic L shows the length of the driving duration, the longer the duration of the drive (high L), the more tired the driver.

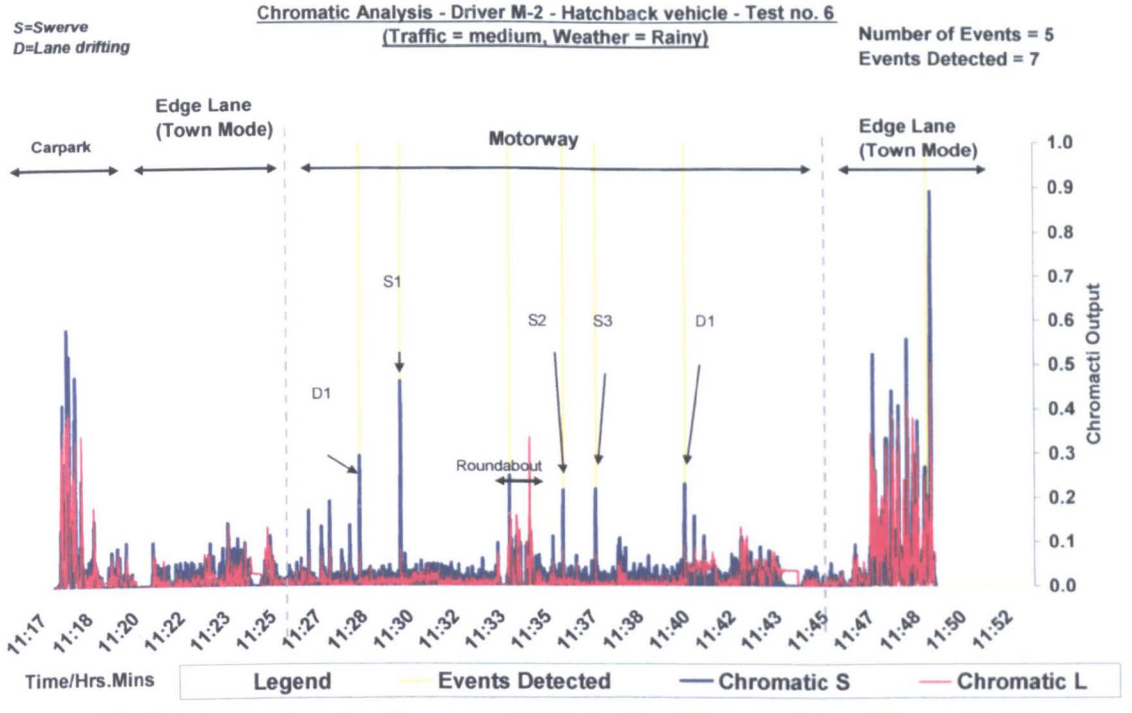

Figure 6.3.3.1. Chromatic polar-diagrams of H-L for the difference data of Figure 5.2.2.2. (Different symbols indicate different stages of figure 5.2.2.2) [Koh et al 2007]

The L values decrease in the order stage 5 (red), stage 4 (blue), stage 1 (pink), stage 2 (green) and stage 3 (orange). Thus driver C at stage 3 has the shortest duration of driving overall. The duration of driver D is divided into two stages - stage 5 (red) with the highest tiredness score and followed by stage 4 (blue).

The 4th sector (H=300^0-360^0), shows that there is only stage 4 (driver D) values where the driver D rested for a period of time. The values for drivers A, B and C are because there was no rest during duties and the tiredness score is reset once the next shift driver is registered.

An alarm was triggered at 2233h (figure 6.3.3.1) when the H, L coordinates were 210^0, 0.8 and the driver tiredness level was reaching the threshold. The high tiredness factor was due to the duration of the drive with the driver driving continuously for more than 10 hours without sufficient rest to regain alertness.

6.2.3.3 Comparison between the chromatic analysis of PTS and DTS

The above analysis shows that there are two important sectors on the polar plot in determining the tiredness level of the driver. The 1st sector (H=0^0-60^0) with low L values represents the decreasing tiredness level. The 3rd sector (H=180^0-240^0) with high L value indicates the high tiredness level when the alarm triggers at H=210^0 and L=0.8.

The physiological tiredness score calculates the driver's tiredness level including the circadian rhythm, quality of sleep factors and duration of the drive under monotonous road conditions. The duration tiredness score only includes the duration under monotonous driving conditions. Driver A only drove for a duration less than 4 hours compared to driver D who drove for a duration of approximately 10 hours in total. For the DTS chromatic analysis, the maximum L values (tiredness score) of driver D is more than twice that of driver A in the 3rd sector. Considering the circadian rhythm, the PTS chromatic analysis shows a similar maximum score of L= 0.78 (driver A) to 0.8 (driver D) on the 3rd sector. This shows that the tiredness level is as high for driving during the early hours in the morning (between 0200-0400h) for a shorter duration compared to a driver driving for a longer period during the evening (1730h-2000h) **[Horne, 2001]**).

An advantage of the chromatic polar diagram analysis is its capability for classifying the period of tiredness according to the values of H which determines the dominance of the tiredness score, and L, which determines the magnitude of the tiredness score.

Representing both these aspects on the chromatic H-L polar plot provides a convenient means for visualising and comparing trends.

6.3 Chromatic Analysis of the Dashboard System Signals

6.3.1 Introduction

The design of the dashboard unit was based on the gyroscope system to monitor the angular rate reference to the yaw motion of the vehicle. The system provided a means for monitoring the physical indicators of driving fatigue, such as swerving and lane drifting manoeuvres. The experimental results for the dashboard system, gyroscope output (V) against time, have been presented in section 5.3. In this section, chromatic processing is utilised to analyse the gyroscope output signals in order to extract and detect the fatigue related events (lane drifting and swerving) from other normal driving manoeuvres (e.g. roundabout, left and right turning)

6.3.2 Application of Chromatic analysis

The chromatic analysis described in chapter 2.6 has been used to analyse the experimental results (section 5.3) for both gyroscope systems. Details of the chromatic filtering and chromatic transformation steps are presented.

6.3.2.1 Chromatic Filtering

There are two steps involved in the chromatic filtering: selection of optimum filter size and time stepping (section 2.8). For the first step, an optimum filter size was selected to identify and discriminate fatigue related driving from normal manoeuvres. Table 6.3.2.1.1 shows the data collected from the experimental results for normal driving and fatigue related manoeuvres. The table compares the time taken for the complete manoeuvre in seconds and the gyroscope output range in volts.

Comparing normal driving and fatigue related manoeuvres; there is a distinct difference between the times taken to complete each manoeuvre. The time taken to

complete the fatigue related manoeuvres ranged from 1.00s to 1.65s. The times taken for normal driving type manoeuvres were all greater than 4s. Figure 6.3.2.1.1 shows examples of how three overlapping R, G and B filters were deployed onto time varying signals. Three examples are given which are swerve (1 (a)), left turn (1 (b)) and roundabout (2 (c)) from the table 6.3.2.1.1. Using the tabulated results, the filter widths selected were 0.66s or 1.32s for all three overlapping R, G and B filters (figure 6.3.2.1(a)). This range was selected because the filter width cover the whole time range of the events and aids the discrimination of the swerve and lane drifting events from other normal driving manoeuvres.

	Time taken for event (s)	Gyroscope output(V)
Normal Manoeuvre		
Left turn 1	4.70	0.84
Left turn 2	5.70	0.67
Right turn 1	6.70	0.47
Right turn 2	5.40	1.00
Roundabout 1	10.50	0.12
Roundabout 2	12.40	0.10
Speed bump1	5.50	0.03
Fatigue related Manoeuvre		
Swerve 1	1.00	0.56
Swerve 2	1.20	0.72
Swerve 3	1.50	0.46
Swerve 4	1.35	0.60
Swerve 5	1.15	0.35
Swerve 6	1.36	0.88
Lane drifting 1	1.20	0.33
Lane drifting 2	1.30	0.44
Lane drifting 3	1.65	0.45
Lane drifting 4	1.20	0.46

Table 6.3.2.1.1 List for normal manoeuvres and fatigue related manoeuvres with time duration of events and gyroscope output (v) from section 5.3

The gyroscope system output signal was sampled at 15Hz to capture the driving information at a sufficiently high level of resolution. The time step (section 2.8.4) for the filters was 1 step @ 1/15 to maintain the resolution of the data.

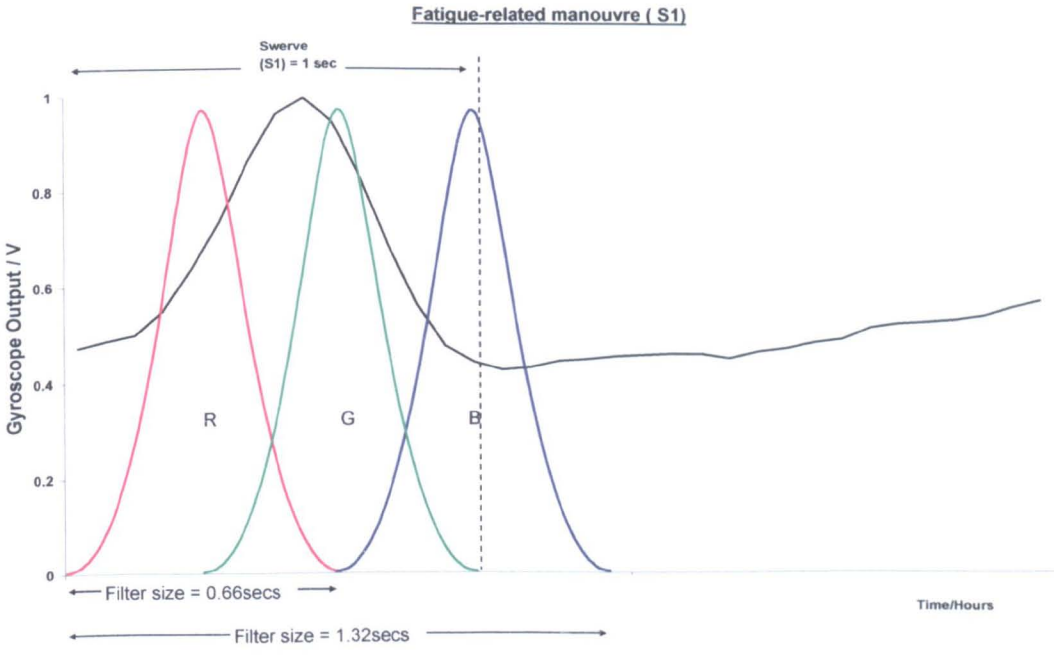
Fatigue-related manouvre (S1)
Swerve
(S1) = 1 sec
Gyroscope Output / V
1
0.8
0.6
0.4
0.2
0
R
G
B
Filter size = 0.66secs
Filter size = 1.32secs
Time/Hours

(a)

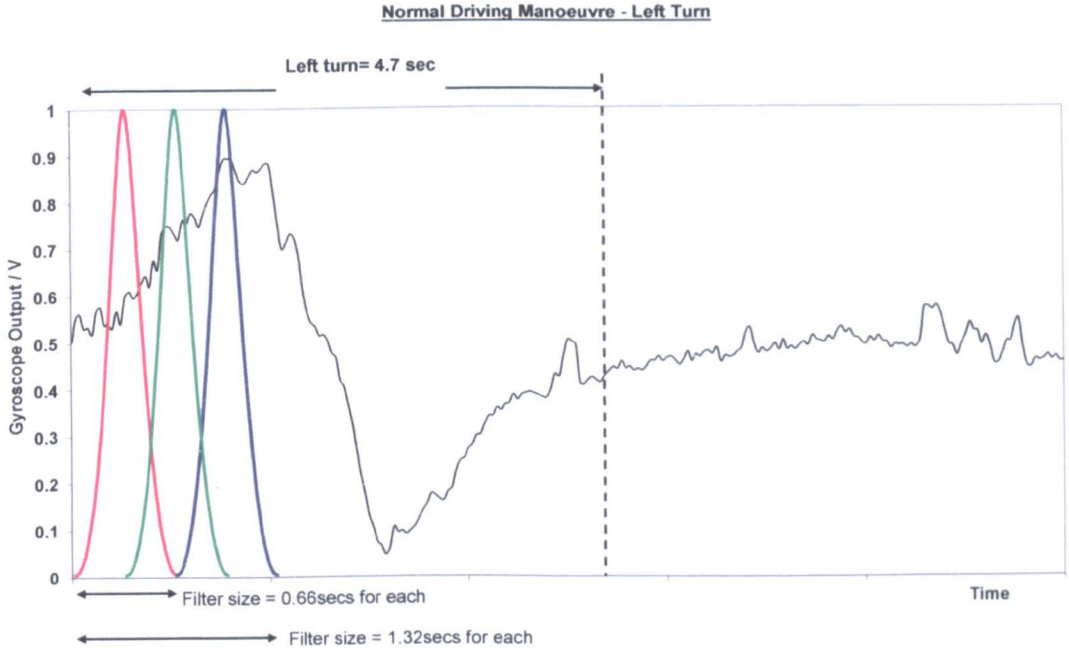
Normal Driving Manoeuvre - Left Turn
Left turn= 4.7 sec
Gyroscope Output / V
1
0.9
0.8
0.7
0.6
0.5
0.4
0.3
0.2
0.1
0
Filter size = 0.66secs for each
Filter size = 1.32secs for each
Time

(b)

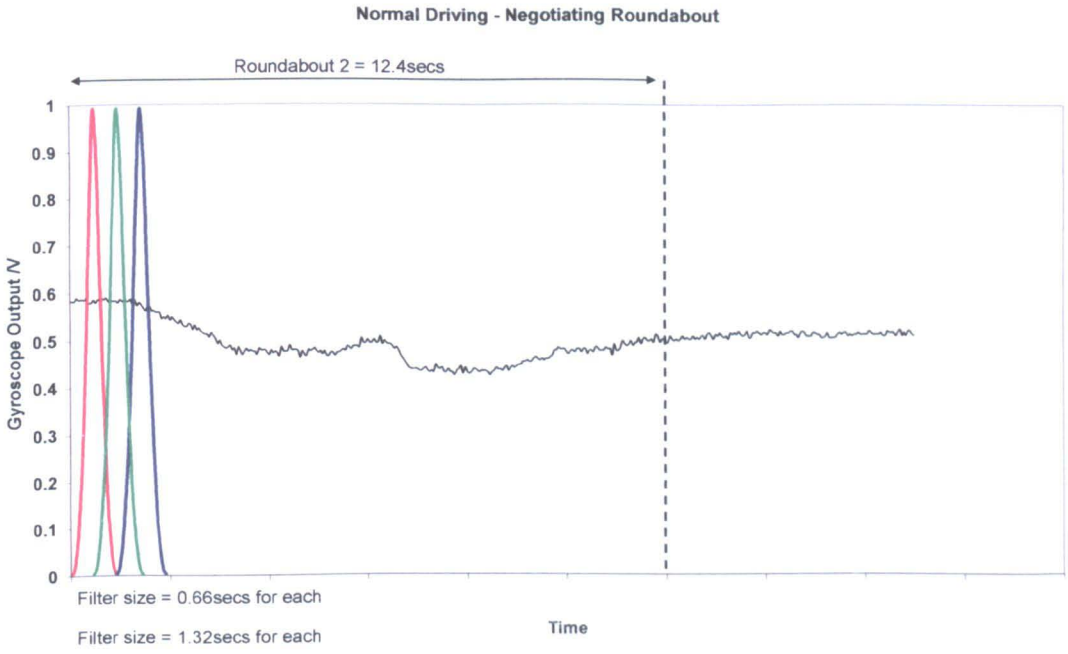

(c)

Figure 6.3.2.1.1 Deployment of the three overlapping filters (R, G and B) each with a width of 0.66s and a total time window of 1.32.

(a) fatigue related event (s1) from figure 5.3.3.2 (a)

(b) Left turn 1 from figure 5.3.2.1

(c) Roundabout 2 from figure 5.3.2.2

6.3.2.2 Chromatic Transformation

The second part of the chromatic analysis involves the chromatic transformation. The output values, r, g and b, from the chromatic filtering are used to calculate the chromatic parameters, H, L and S, using equation 2.6.3.2.1.

With a selected filter size of 0.66s for each filter, the chromatic filtering enables the fatigue related event to be detected and discriminated from other manoeuvres and enables values of the chromatic parameters to be determined. For this application only the L and S and not the H parameters are used. This is because the H parameter does not provide any useful information to detect the swerve and lane drifting manoeuvres. Therefore it is preferable to use Cartesian diagrams of L, S against time rather than polar diagrams of H-L and H-S (section 2.6.3.2) **[Jones et al, 2000; Zhang, 2004].**

For the dashboard unit application, the gyroscope output signal gave the angular rate associated with the yaw motion of the vehicle. Therefore the chromatic parameter L

can be defined as the nominal strength of the angular rate associated with the yaw motion of the vehicle.

The chromatic parameter S gives the spread of the gyroscope output signal with respect to time. The smaller the spread the higher the S values and vice versa. A schematic of the meaning of L and S with respect to a time varying signal is shown on figure 6.3.2.2.1.

In summary the chromatic output for this system can be defined as:-

L = Signal strength of the angular rate of the yaw motion of the vehicle
S = Spread of the signal, where high S defines a smaller spread and vice versa.

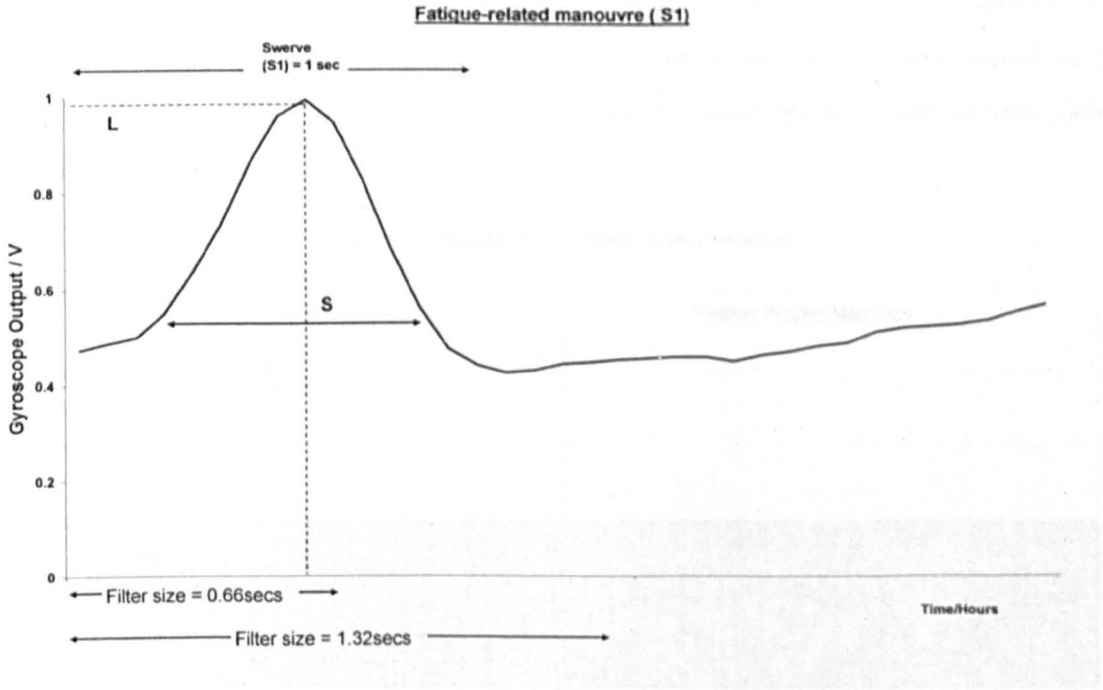

Figure 6.3.2.2.1 Chromatic S and L on the swerve 1 experimental output from figure 5.3.3.2 (a) (S=spread, L=strength ~ shaded area)

6.3.2.3 Comparison of normal and fatigue related driving manoeuvres

The results of the chromatic analysis for normal and simulated fatigue related driving manoeuvres (section 5.3) are compared. For this purpose, the maximum values of L and S were determined for all types of manoeuvres and are presented in figure 6.3.2.3.1 (a) and (b).

The graph on figure 6.3.2.3.1 (a) shows that for the angular rate changes of the vehicle, (L) varied within the range of 0.18 to 0.52 whereas when negotiating a roundabout the range was 0.11-0.14. Thus the angular rate of the vehicle produces lower L values for roundabouts compared to left and right turning. For acceleration and deceleration over speed bumps the maximum L level was less than 0.05 (figure 6.3.2.1 (a)). These values are the lowest compared to the other manoeuvres because there is little change on the yaw rotation during these types of bump based manoeuvres. For the fatigue related manoeuvres (lane drifts and swerves), the L ranged from 0.13 to 0.27. This shows that there is an indicative mid range for both the swerving and lane drifting actions.

The right and left turning exercises yielded a S range of values between 0.2 to 1 (figure 6.3.2.3.1 (b)). There was a larger spread in the signal for these manoeuvres compared to the roundabouts, speed bump, acceleration and deceleration which only have S values in a range less than 0.09. The fatigue related types of manoeuvres yield S values above 0.22.

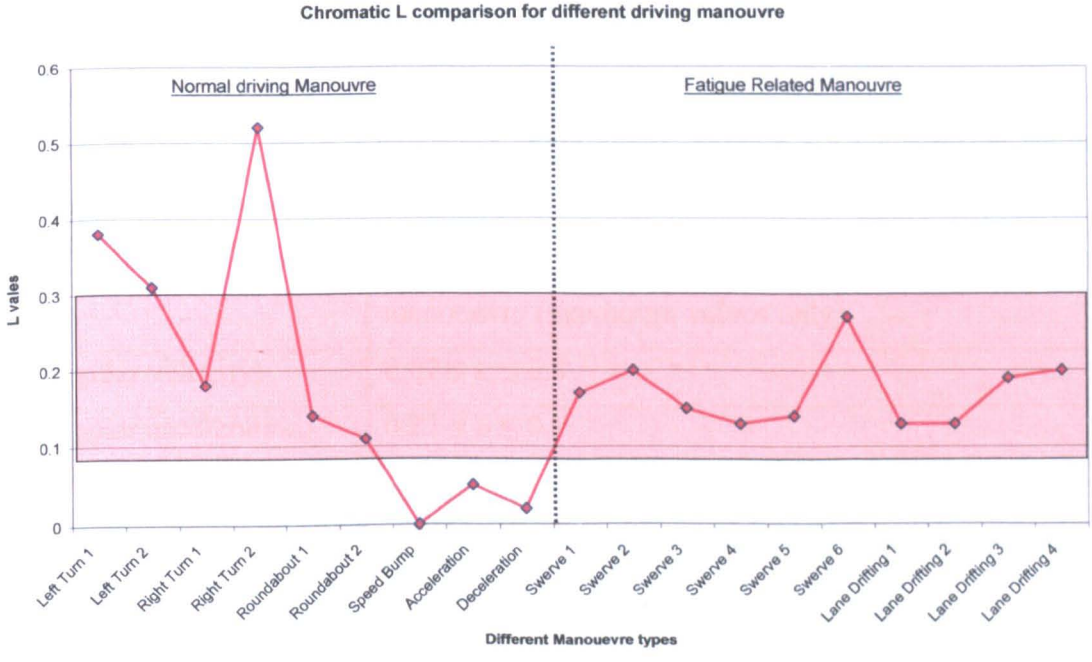

(a)

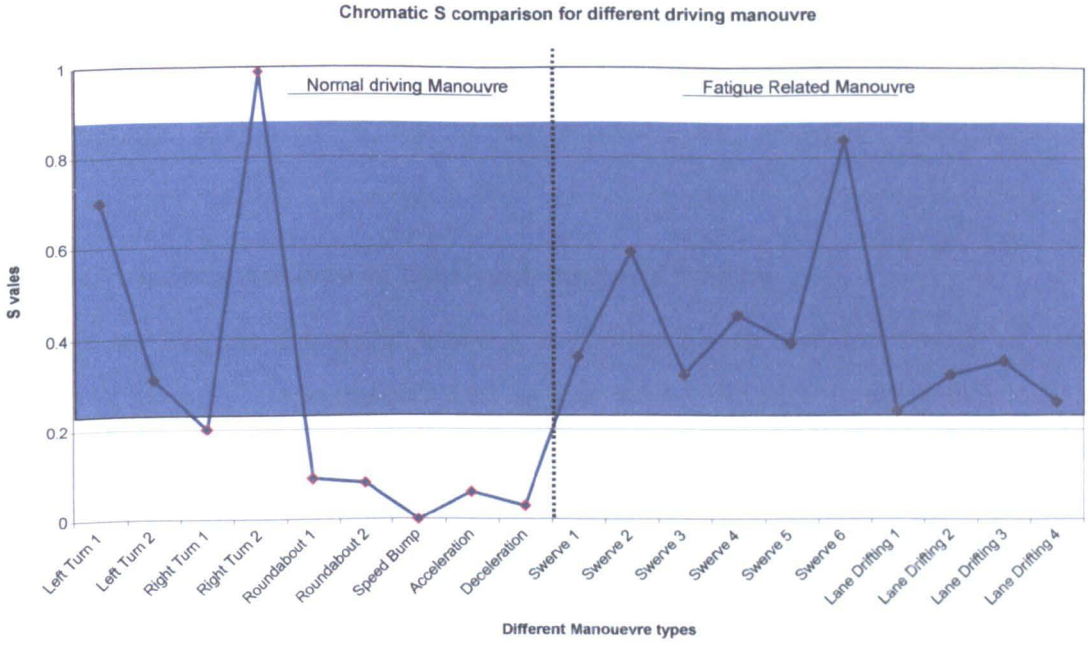

(b)

Figures 6.3.2.3.1 Chromatic parameter values for different types of manoeuvres

(a) Chromatic L comparison for different manoeuvres

(b) Chromatic S comparison for different manoeuvres

These comparisons, suggest that there are regimes for L and S within which fatigue signals reside identified by the colour zones on figures 6.3.2.3.1 (a) and (b) L comparison (pink zone), S comparison (blue zone). Table 6.3.2.3.1 summarises the fatigue boundaries for S and L

	Threshold level for detecting fatigue related driving manoeuvre (maximum values only)
L (angular velocity)	$0.07 \leq L \leq 0.3$
S (angular acceleration)	$0.22 \leq S \leq 0.9$

Table 6.3.2.3.1 Threshold levels for the fatigue related manoeuvres

The threshold information given on table 6.3.2.3.1, shows that both the L and S conditions for the threshold level need to be satisfied in order to classify the manoeuvre as a swerve or lane drift during a road drive. i.e. it is necessary to satisfy an L criterion of 0.07 to 0.3 and an S criterion of 0.22 to 0.9.

The next step is to apply this threshold level of L and S to the further road test experiments described in section 5.3.5. The list of the experiments can be found on table 5.3.5.1.

6.3.3 Chromatic Analysis of the Dashboard unit System

In this section, the chromatic analysis is applied to the road test results of section 5.2.3. A list of 17 experimental tests, conducted on the same route which lasted for approximately 40 minutes per experiment was presented on table 5.3.2.1. During these tests various drivers and vehicles were used. Also various types of weather conditions and traffic conditions were recorded as well as the specific days.

The main purpose of these experiments was to apply the chromatic analysis technique (section 6.3.2) and the threshold levels (table 6.3.2.3.1) to detect for simulated fatigue related manoeuvres (lane drifting and swerving) on real road conditions. There was also a need to understand the performance of the dashboard gyroscope system under different conditions (driver, vehicles, traffic and weather). The performance was to be considered in terms of how well the system detected the simulated fatigue related driving events under different conditions.

Figure 6.3.3.1 shows a flow chart for the detection of fatigue related events using the chromatic threshold levels defined by table 6.3.2.3.1. In addition to the factors described above there is also an element, "Driving mode" which checks whether the vehicle is moving and not idling and if so whether it is being driven on busy roads or a monotonous motorway.

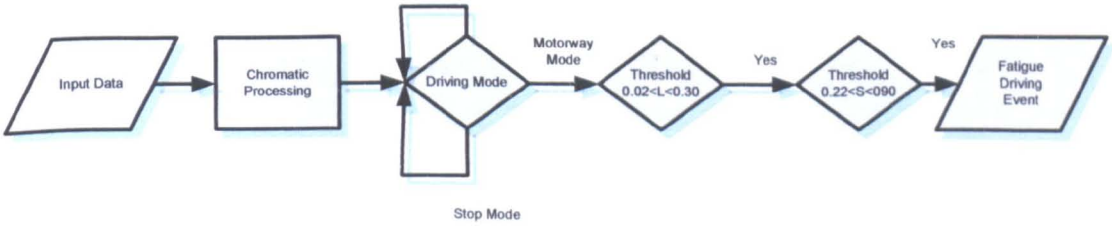

Figure 6.3.3.1 Flow chart for the real time fatigue event detector

6.3.3.1. Analysis for detection of event using the chromatic threshold level

Three experimental test have been selected from the results of table 5.3.5.1 illustrating the chromatic analysis procedure. The three test are tests 2, 3 and 7. The experimental results can be found in section 5.3.5. Data from the tests have been chromatically processed to obtain values of the parameters L and S (section 6.3.2) to which the threshold levels (figure 6.3.3.1) can be applied to test for fatigue events. This also enables the accuracy of the system to be assessed under these various conditions.

The time variation of chromatic L and S during a journey may be displayed graphically as shown on figure 6.3.3.1.1 (a) (b) (c). The chromatic parameter L is shown in red and S in blue. The detection of an event is flagged up as a yellow line to indicate the time at which it was detected. The events detected along with the corresponding L and S values are summarised on table 6.3.3.1.1.

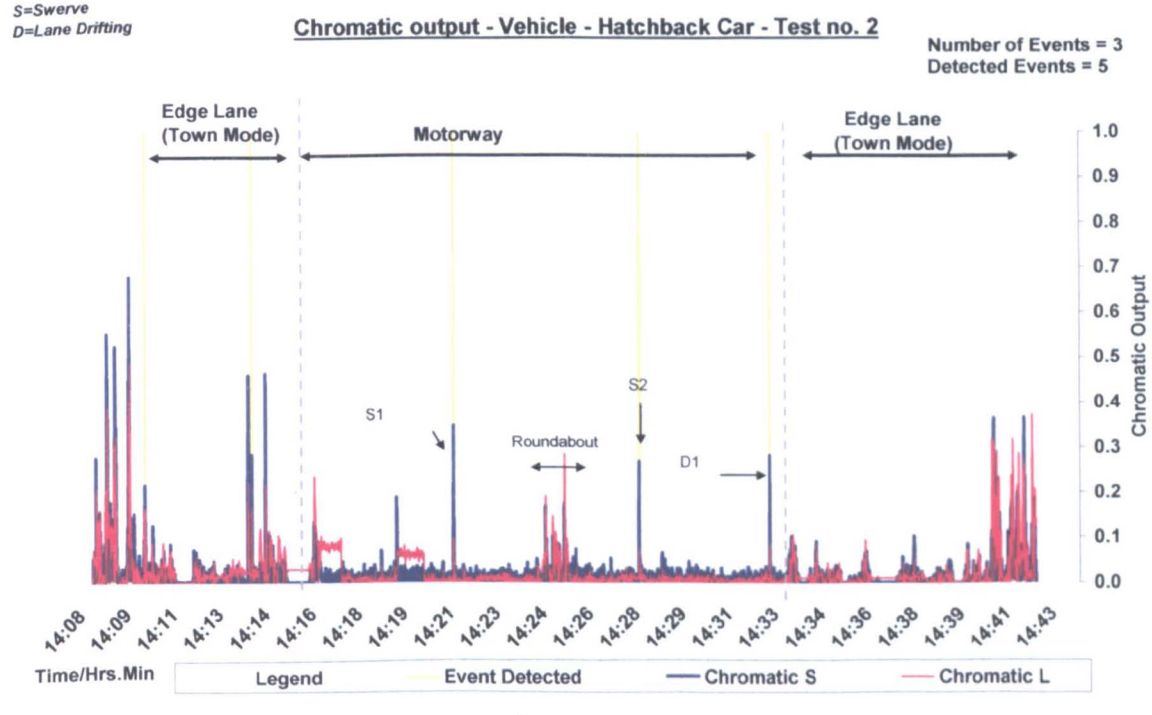

(a)

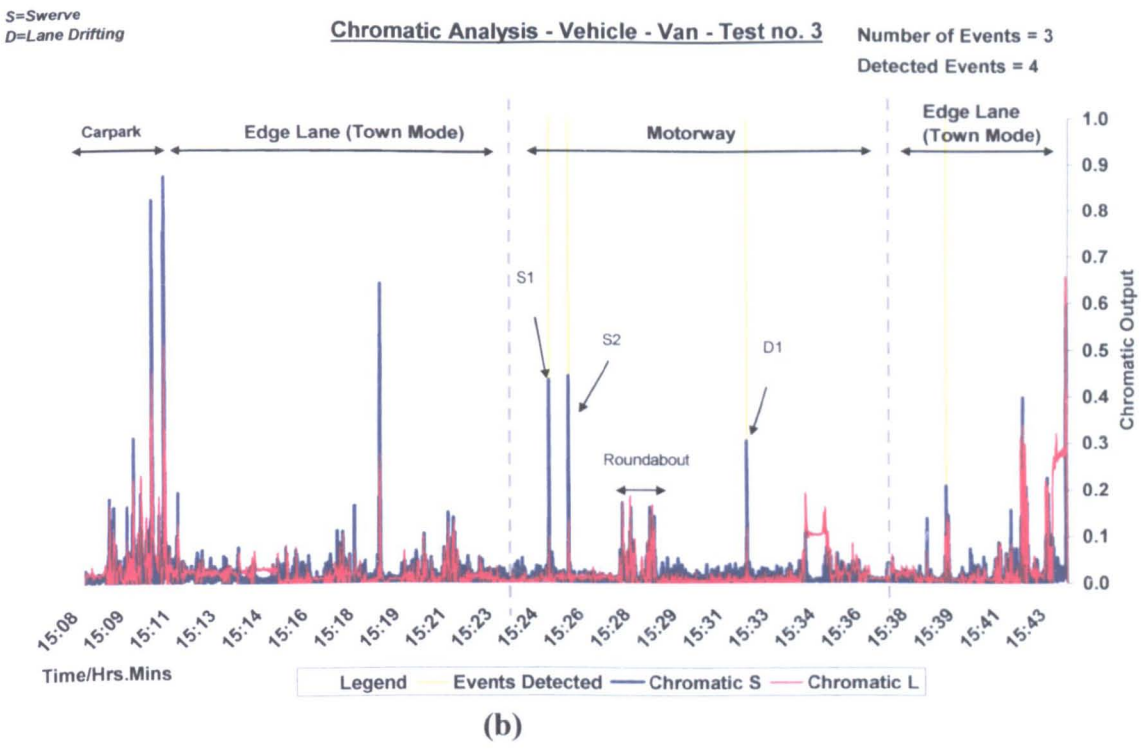

(b)

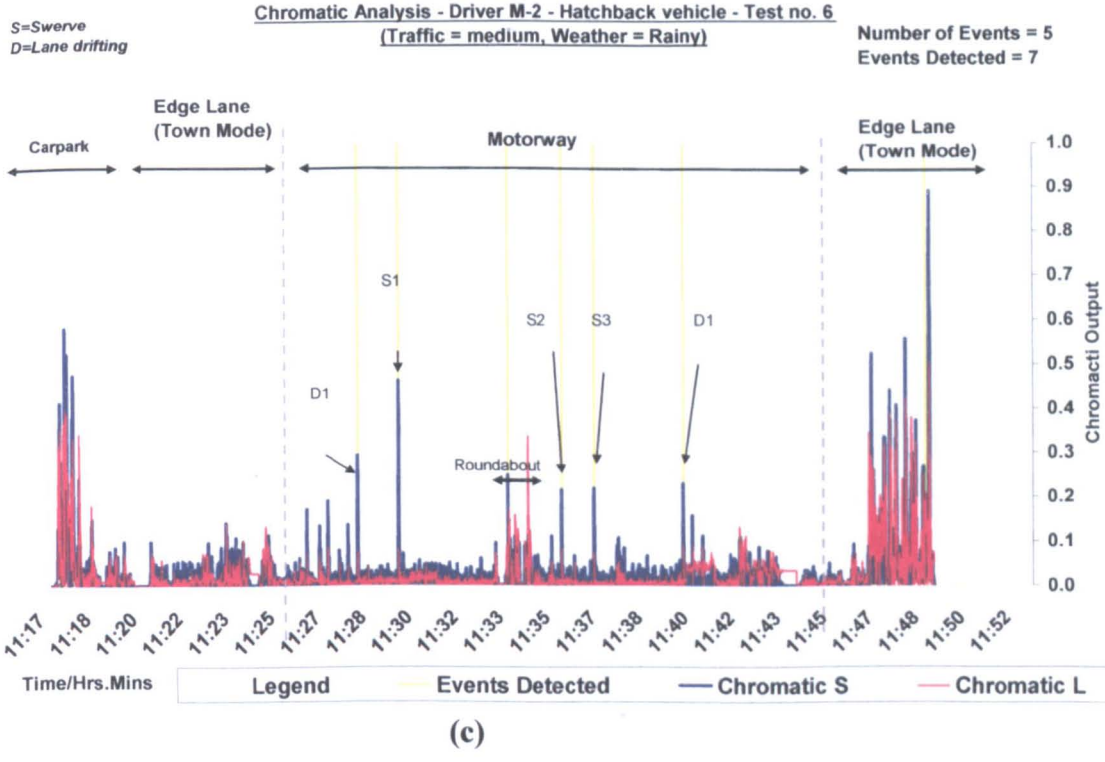

(c)

Figure 6.3.3.1.1 Chromatic of L and S as functions of journey time for the table 5.3.5.1

(a) Test 2

(b) Test 3

(c) Test 6

Driver	Events Detected	Chromatic L	Chromatic S
M-1 Hatchback Car (Test 2)	False Positive 1	0.15	0.22
	False Positive 2	0.23	0.43
	S1	0.09	0.34
	S2	0.07	0.27
	D1	0.08	0.28
M-1 Van (Test 3)	S1	0.10	0.44
	S2	0.12	0.45
	D1	0.11	0.31
	False positive 1	0.14	0.22
M-2 Hatchback Car (Test 6)	D1	0.07	0.29
	S1	0.08	0.46
	S2	0.08	0.22
	S3	0.07	0.25
	D2	0.09	0.23
	False Positive 1	0.15	0.22
	False Positive 2	0.25	0.28

Table 6.3.3.1.1 Summary of event detected during test 2, 3 and 6. The event detected consists of swerves, lane drifting and false positives.

On this table the events are described either as swerves, lane drifting or false positives. A false positive is defined as a test result which incorrectly implies that an event occurred. The event in this case was an indication of a fatigue reaction when none was deliberately simulated at that time instant.

The real events detected in test 2, include both swerves and lane drifting. However 2 false positives were also detected during the town mode in the first part of the journey when there were non-monotonous driving activities negotiating junction turnings, roundabouts and traffic lights. For the first false positive 1 result the S value is 0.22 which is barely over the threshold value. The false positive 2 was due to a bottle neck junction during road works where the vehicle moved into the next lane.

For test 3 all fatigue related events were registered by the system, but one false positive occurred towards the end of the journey. The S value is 0.22 which is the minimum level of the threshold.

For test 6, all the fatigue related events were detected but 2 false positives were also recorded. The first false positive recorded occurred during lane switching on a roundabout manoeuvre. The second false positive occurred during a parking manoeuvre into a parking bay.

It would be possible for the lower threshold of S (0.22) to be increased to exclude the above false positives. However this would also affect the actual fatigue related events such as swerve 2 of test 6 which would not have been detected. The results shows that all the false positives detected occurred only with non-monotonous driving i.e. town mode.

Table 6.3.3.1.2 shows the analysis of the results of the 16 experiments conducted (Table 5.3.5.1). The table shows results of the fatigue events simulated, events detected and the events missed by the system. From all 16 tests only during test 11 was a fatigue related event missed. The chromatic output for this experiment 11 are, S = 0.45 and L = 0.018. The event was not detected by the system because the chromatic L value did not exceed the lower threshold level of 0.2. All the fatigue simulations in the remaining 15 experiments were detected.

However there are numerous false positive events which occurred during 10 of the 16 tests. Thus although 15 out of 16 experiments detected 100% fatigue related swerves, the false positive events detected could cause the system to be less efficient and produce discrepancies. False positives occur more commonly under non-monotonous driving conditions such as parking and in slow moving traffic (vehicle changing lanes erratically during a traffic jam). However from the sleep research studies by Horne and Reyner, statistically fatigue related type accidents are most likely to occur during motorway or monotonous type driving **[Horne and Reyner, 1997]**.

Test No.	Driver (M=Male) (F=Female)	Vehicle Type	Simulated Fatigue event	Events Detected	Events Missed
1	M-1	Hatchback Car	4	5 (1 False Positive)	0
2		Hatchback Car	3	5 (2 False Positive)	0
3		Van	3	4 (1 False Positive)	0
4		Van	7	8 (1 False Positive)	0
5		Van	8	9 (1 False Positive)	0
6	M-2	Hatchback Car	5	7 (2 False Positive)	0
7		Van	3	3 (0 False Positive)	0
8		Van	7	7 (0 False Positive)	0
9	M-3	Hatchback Car	6	8 (2 False Positive)	0
10		Van	7	9 (2 False Positive)	0
11	M-4	Saloon Car	9	8 (0 False Positive)	1
12	M-5	Articulated Truck(Loaded)	4	5 (1 False Positive)	0
13		Articulated Truck(Unloaded)	4	4 (0 False Positive)	0
14	F-1	Van	1	1 (0 False Positive)	0
15		Van	4	4 (0 False Positive)	0
16	F-2	Van	4	5 (1 False Positive)	0

Table 6.3.3.1.2 Summary events detected, false positives and events missed for all 16 experiments from table5.3.5.1

6.3.3.2. Mode based driving effects.

As indicated in the introduction to section 6.3.3 in relation to figure 6.3.3.1, there were three different driving modes of interest, namely town, motorway and stop mode. Town mode driving involved several normal driving manoeuvres such as handling and leaving (including left and right turning), speed bumps, and roundabout

negotiation which are considered to be non-monotonous. Motorway mode driving involves fewer driving manoeuvres examples of which are, acceleration, deceleration and braking. Other motorway manoeuvres are vehicle over-taking, leaving or joining a slip road. These types of manoeuvres (motorway mode) do not induce much lateral changes to a monitoring gyroscope and the average output values are generally lower than the town mode based driving manoeuvres. For a stationary vehicle, the output of the gyroscope is approximately zero. Gyroscope outputs which are typical for each of these three modes are summarised on table 6.3.3.2.1

Driving Mode	**Average gyroscope output for previous 1 minute**
Town Mode	Gyro Output>0.25
Motorway Mode	0.001>Gyro Output>0.025
Stop Mode	Gyro Output<0.001

Table 6.3.3.2.1 Average gyroscope outputs for different driving modes

To take account of the different driving modes a further decision making flow chart needs to be introduced and is shown on figure 6.3.3.2.1. The thresholds for L and S shown on table 6.3.3.2.1 are used in conjunction with the mode based driving shown in the flow-chart (figure 6.3.3.2.1). Thus the fatigue decision making described in section 6.3.3..1 is only implemented if the driving mode is identified as being the motorway mode.

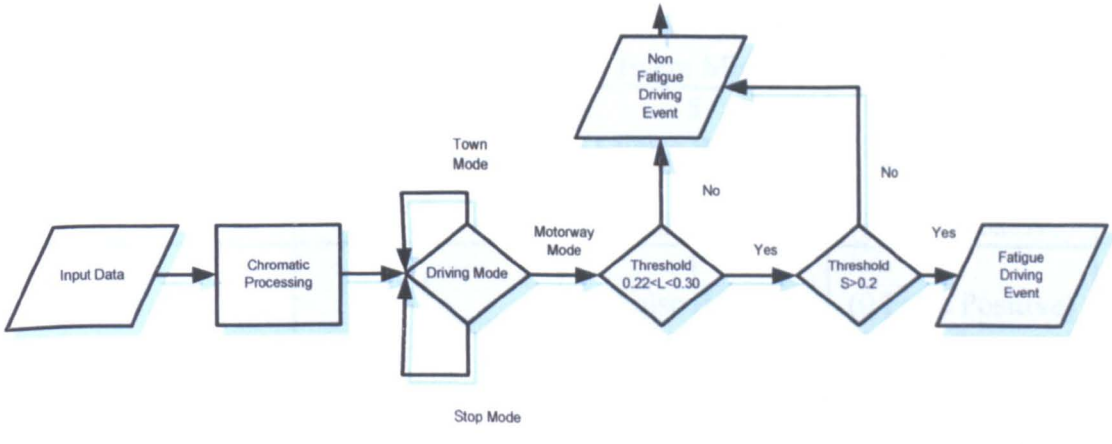

Figure 6.3.3.2.1 Flow chart for the real time fatigue event detector with mode base driving.

This procedure enabled many false positive identification to be eliminated. For example, there may be non-fatigue events that might qualify on the basis of the L and S thresholds. But if the system only detects that the vehicle is driving in a non-motorway mode (monotonous type driving) then the false positives could be removed. This mode base driving has been implemented and the results of the 16 experiments from table 6.3.3.1.2, reanalysed to give the results summarised on table 6.3.3.2.1.

Test No.	Driver (M=Male) (F=Female)	Simulated Fatigue event	Events Detected Without Mode base driving	Events Detected With Mode Base driving
1	M-1	4	5 (1 False Positive)	4 (0 False Positive)
2		3	5 (2 False Positive)	5 (0 False Positive)
3		3	4 (1 False Positive)	3 (0 False Positive)
4		7	8 (1 False Positive)	7 (0 False Positive)
5		8	9 (1 False Positive)	8 (0 False Positive)
6	M-2	5	7 (2 False Positive)	5 (0 False Positive)
7		3	3 (0 False Positive)	3 (0 False Positive)
8		7	7 (0 False Positive)	7 (0 False Positive)
9	M-3	6	8 (2 False Positive)	6 (0 False Positive)
10		7	9 (2 False Positive)	7 (0 False Positive)
11	M-4	9	8 (0 False Positive) (1 Event Missed)	9 (0 False Positive) (1 Event Missed)
12	M-5	4	5 (1 False Positive)	4 (0 False Positive)
13		4	4 (0 False Positive)	4 (0 False Positive)
14	F-1	1	1 (0 False Positive)	1 (0 False Positive)
15		4	4 (0 False Positive)	4 (0 False Positive)
16	F-2	4	5 (1 False Positive)	4 (0 False Positive)

Table 6.3.3.2.1 shows the comparison of the results of mode base driving introduced

This system of mode base driving effectively removes the entire false positive event for all 16 experiments. The reason is because the events detection has been disabled for town mode or non-monotonous driving conditions. All tests apart from test 11 have detected all events successfully. This is because the simulated fatigue related events have not qualified because of the predefined event detection threshold.

The 16 tests with the dashboard gyroscope system involved different driver gender, vehicle, weather and traffic conditions. The same chromatic algorithm, event detection and mode base driving parameters have been applied to all 16 tests. A total of 79 fatigue related events have been simulated on real road conditions with 78 events correctly detected. From this analysis successful detection by the system fatigue events could be determined to an accuracy of is 98.7%. Within the scope of these tests fatigue driving type manoeuvres appear to be similar for different vehicles, drivers, weather and traffic conditions investigated.

The results have shown that the chromatic analysis dashboard gyroscope system has been effective in detecting fatigue related driving manoeuvres (swerving and lane drifting) on real road conditions. However there are three recommendations for future research and experiments:-

1. More experiments for statistical comparisons. E.g. 50-100 experiments
2. Wider range of vehicles, different drivers and different countries
3. Experiments with drivers who are really fatigued under real road conditions (but in safe environments)

6.4 Chromatic Analysis of the Steering Wheel system

This section covers the analysis of the experimental results (section 5.4) of the steering wheel monitoring system. The chromatic processing analysis is similar to that applied to the Dashboard monitoring system and has been described in section 6.3.2. This is because both the dashboard and the steering wheel monitoring systems utilise the same principles as the gyroscope system.

Both laboratory and the road test results are analysed. Normal and simulated fatigue based driving manoeuvres were conducted for comparison in the analysis of both laboratory (section 6.4.1.1.1) and road (section 6.4.1.2.1) tests. The results of the steering wheel system may therefore be compared with those of the dashboard system in order to explore the implications of test results relative to the latter.

6.4.1.1 Analysis of the laboratory steering wheel results

The analysis of the laboratory steering wheel results has been undertaken with the same chromatic algorithms, event detection and town mode driving threshold levels which were applied to the dashboard unit (section 6.3).

Results for the time variation of L and S during a test are given on figure 6.4.1.1.1. The L variation is shown as a red curve, the S as a blue curve. Events detected are identified by dotted orange lines, and false positives are indicated by solid yellow lines. A total of 6 fatigue driving events were simulated on the laboratory steering wheel. The results of figure 6.4.1.1.1 show that a total of 9 events were detected of which 6 were false positive and 3 actual events detected. The 3 valid events detected were all during the 5th minute of the driving test when the swerves were simulated with a preceding lapse in concentration. Another 3 swerves during the 4th minute were not detected but indicated as false positives. The reason for this is because the swerve is registered as town mode driving and therefore does not satisfy the conditions (Table 6.3.2.2.1) for events detection. There are also 3 actual false positives detected during the 3rd and 4th minute intervals.

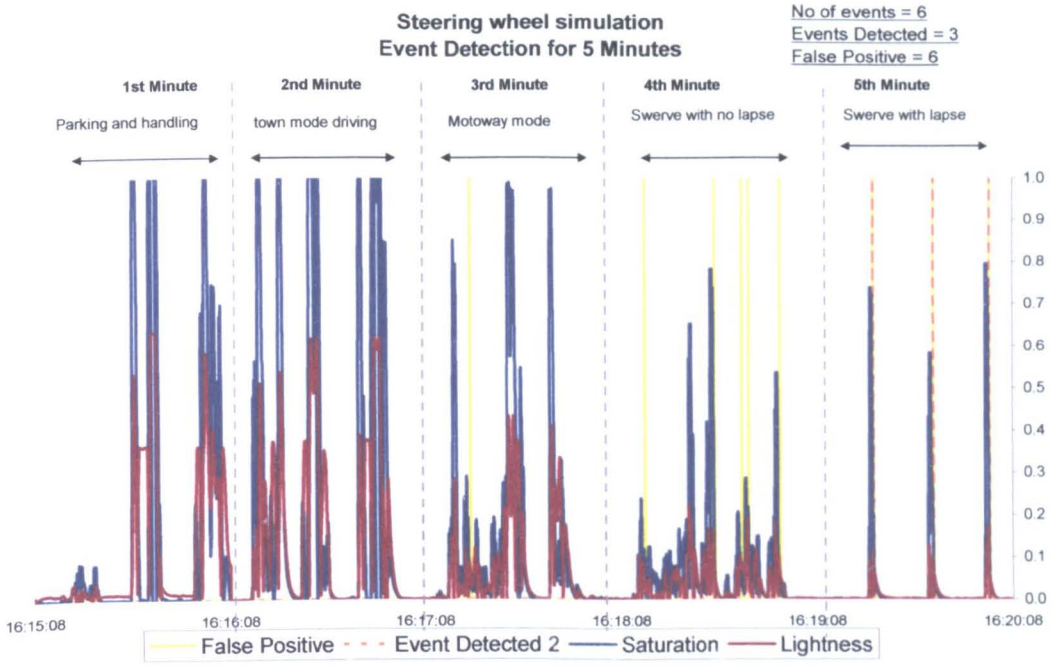

Figure 6.4.1.1.1 Events detection for the test results of figure 5.4.2.1

6.4.1.2 Discussion of the road test result

Both the dashboard and steering wheel systems were used in real road tests in order to capture the outputs from both systems simultaneously under the same conditions. The result of the analysis for the dashboard and steering wheel systems are shown respectively on figure 6.4.1.2.1 (a) and (b).

Comparison of the chromatic L and S results for the two systems shows that the steering wheel system results have higher amplitude excursions than the dashboard system. The implication is that the angular rate detected by the gyroscope on the steering wheel system is higher. This is because the gyroscope installed on the steering wheel experiences more rotational displacement around the steering column during manoeuvres compared to the dashboard unit.

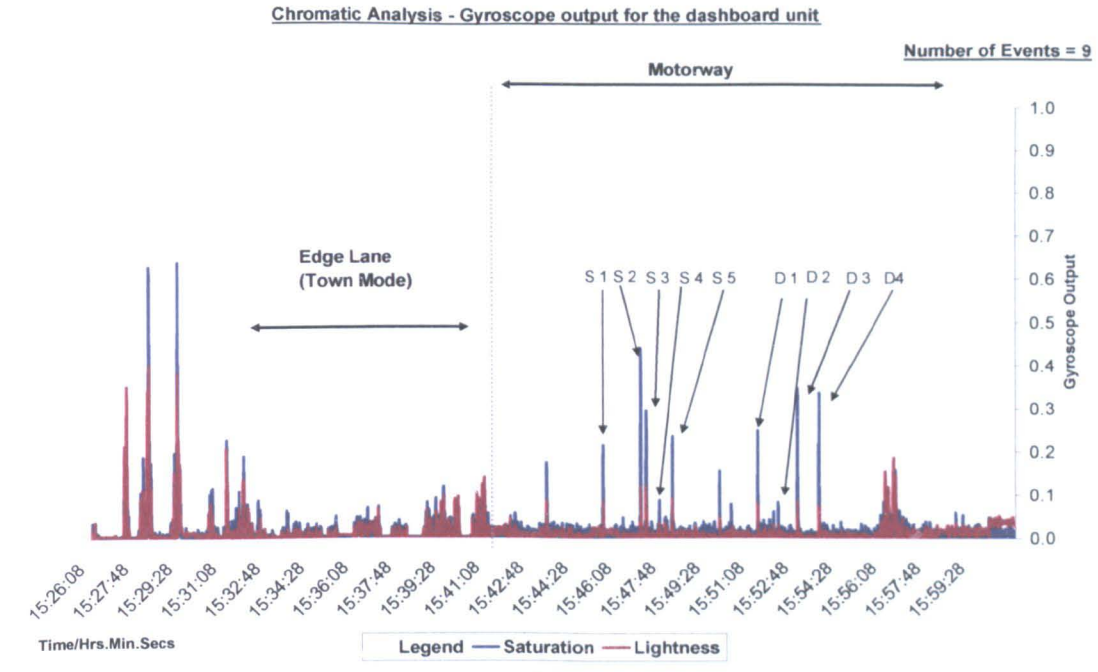

(a)

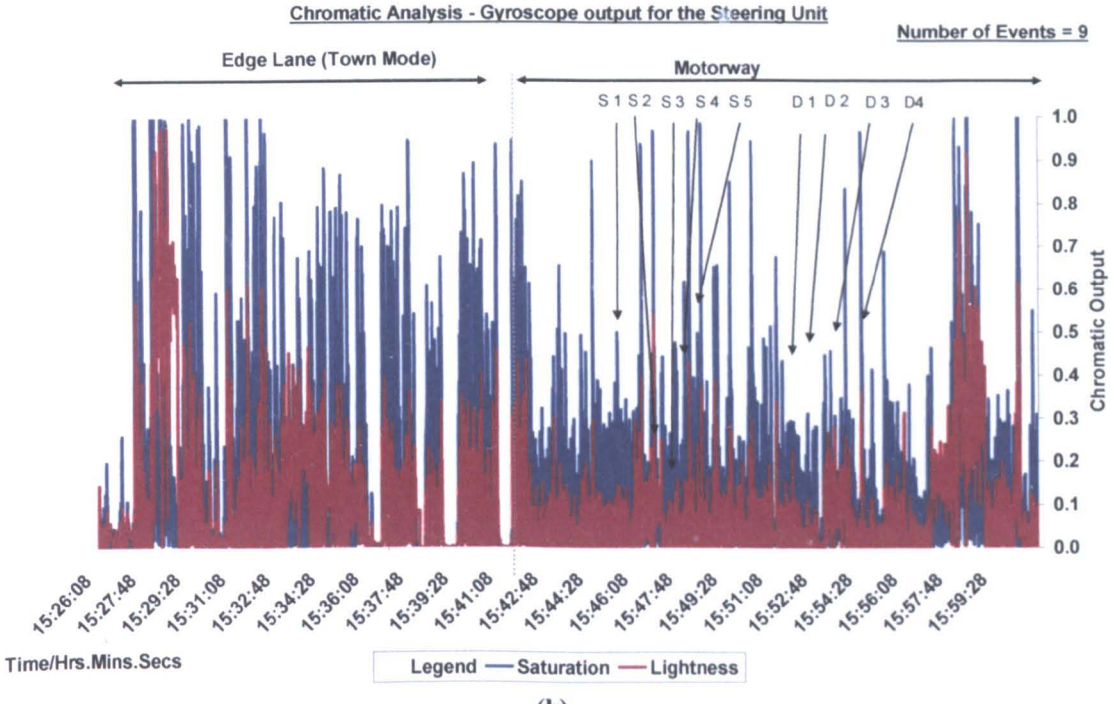

(b)

Figure 6.4.1.2.1 – Time variation of chromatic analysis parameters for the test results of figure 5.4.3.1

(a)Dashboard Unit (expt no. 8)

(b) Steering Wheel System

1. Swerving activities (S1)

Figure 6.4.1.2.2 shows a comparison of the swerve (S1) for the dashboard (figure 6.5.3.2(a)) and steering wheel systems (figure 6.5.3.2(b)). The maximum (L, S) values for the dashboard system (figures 6.4.1.2.2(a)) is (0.10, 0.21) whilst for the steering wheel system they are (0.14, 0.26). This shows that there is more activity observed on the results from the steering wheel system.

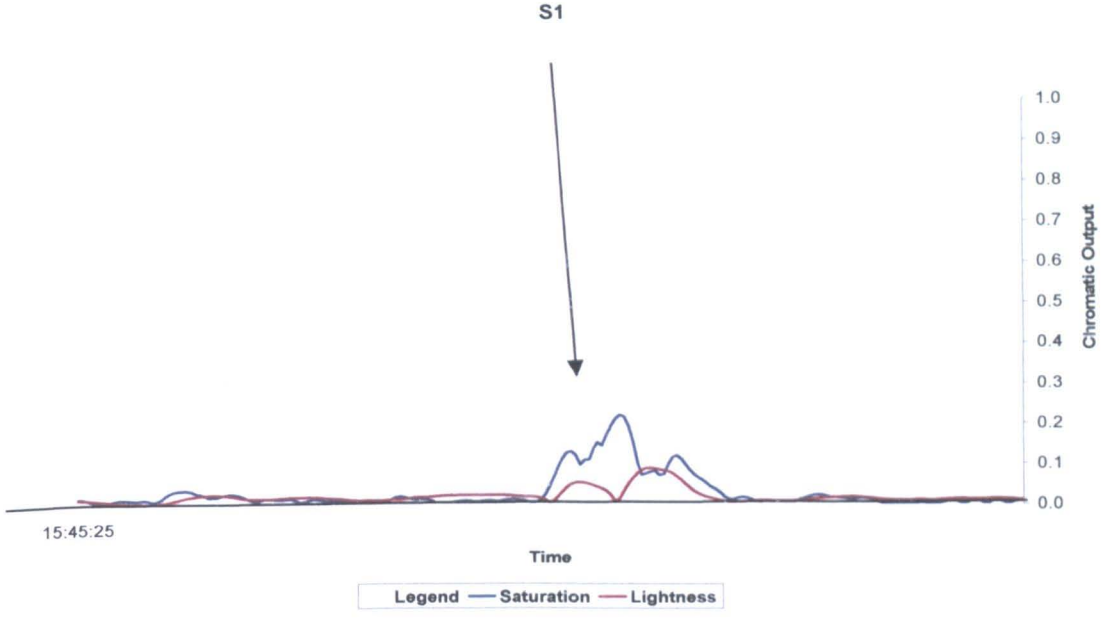

(a)

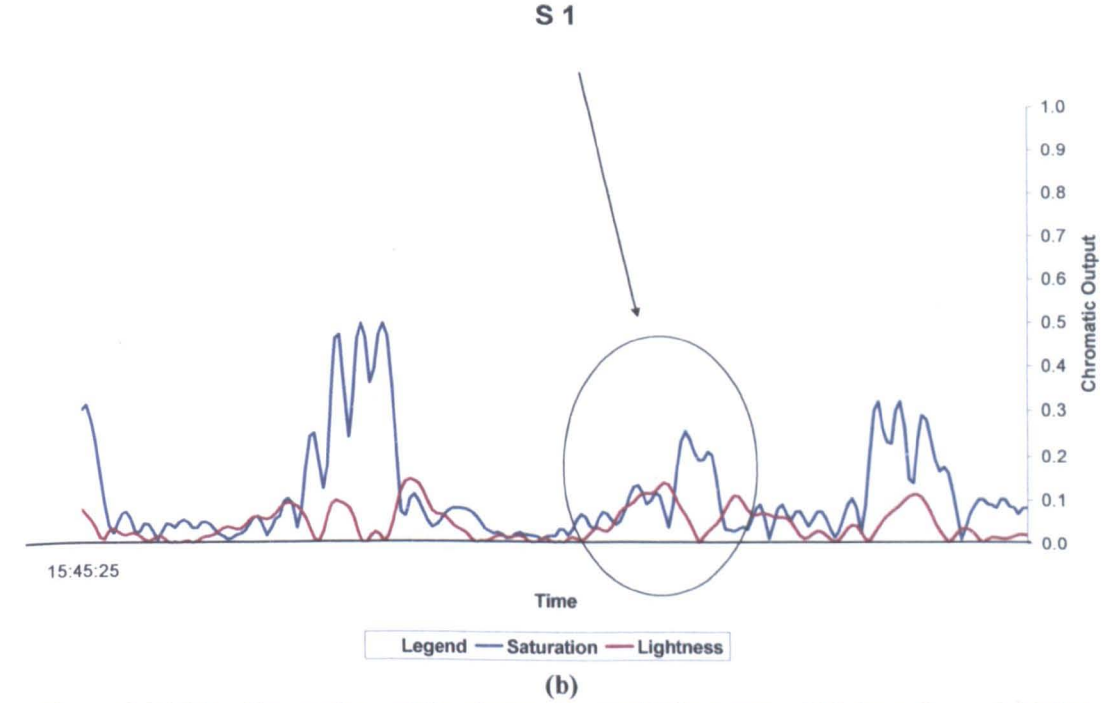

(b)

Figure 6.4.1.2.2 – Comparison of the chromatic results for swerve (S1) from figure 6.4.1.2.1

(a)Dashboard Unit (expt no. 8)

(b) Steering Wheel System

2. Lane Drifting

Figures 6.4.1.2.3 (a) and (b) show a comparison for lane drifting (D1) from figure 6.4.1.2.1 for the dashboard and steering wheel units respectively. The maximum (L, S) values for the dashboard system (a) are (0.09, 0.26) and for the steering wheel system (0.35, 0.68).

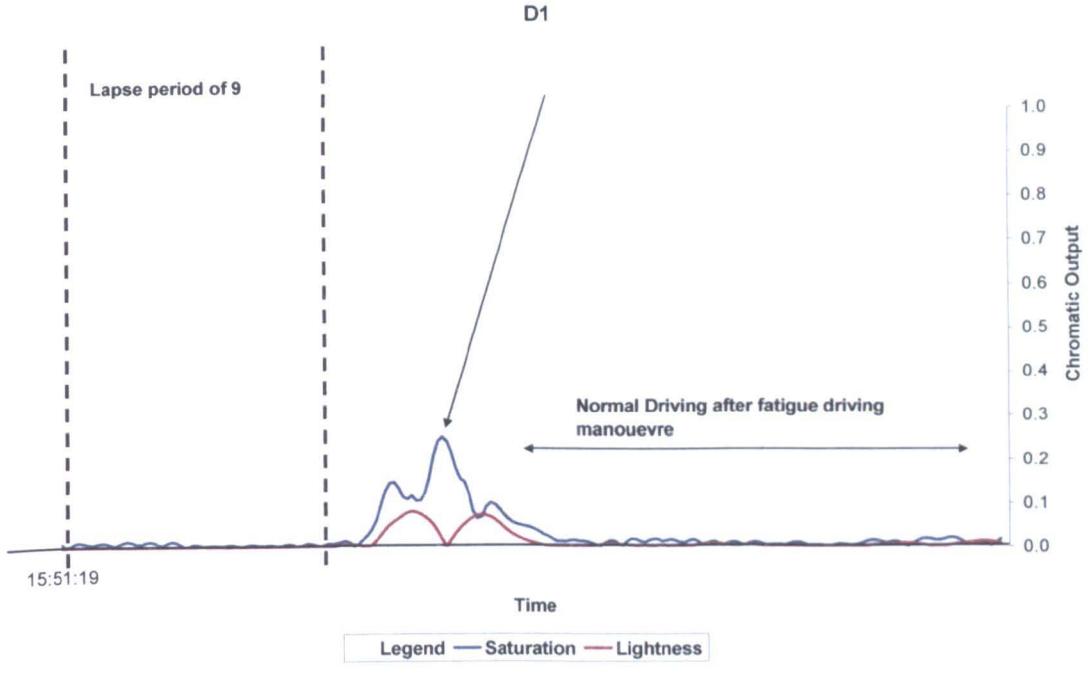

(a)

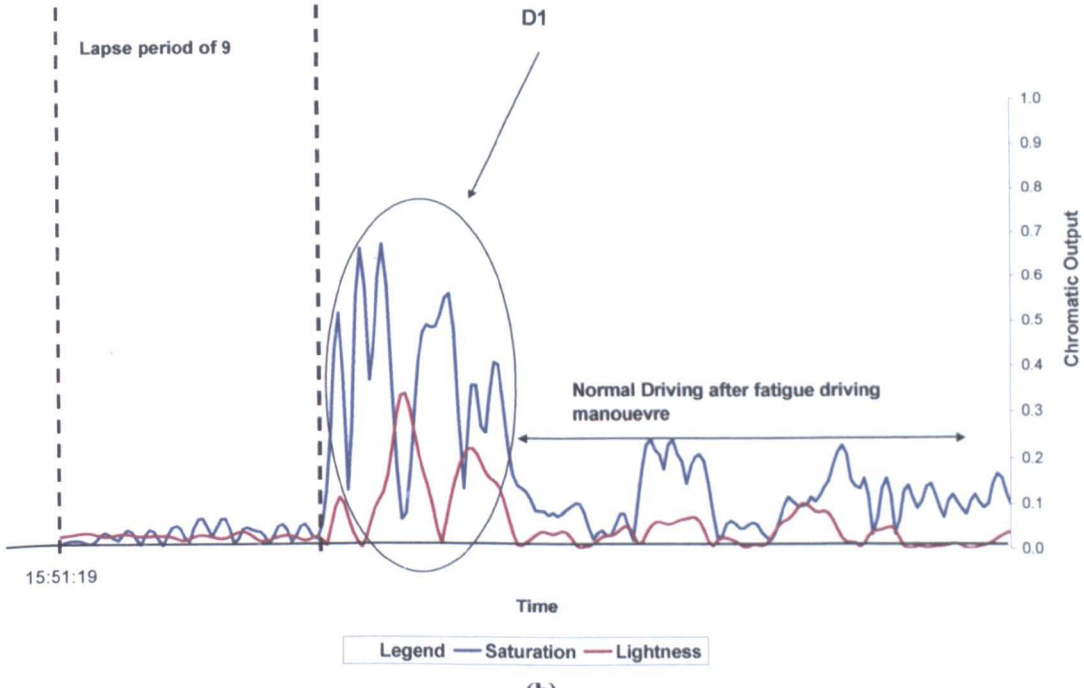

(b)

Figure 6.4.1.2.3 – Comparison of the chromatic results for lane drifting (D1) from figure 6.4.1.2.1

(a)Dashboard Unit (expt no. 8)

(b) Steering Wheel System

Also indicated on figure 6.4.1.2.3 (a) and (b) are the time period immediately prior to the lane drift which should correspond to a lapse phase. The lapse phase is a period during a driving fatigue event when there is a lack of activity on the steering wheel. This causes the vehicle to lane drift or wander away from the road. **[Horne and Reyner, 1997]**. For the present tests, the steering wheel was left unattended for 9 seconds to allow the vehicle to drift before the pull back swerve. A comparison of the figures 6.4.1.2.3 (a) and (b), shows that there are distinct differences in the response of the two monitoring systems during the lapse phase. For the dashboard (a) unit, the lapse and non-lapse periods appear similar with average lightness values of less than 0.05. For the steering wheel system (b) the lightness values for the lapse phase are less than 0.05, whilst the value for the non-lapse period is greater than 0.05 i.e. the steering wheel system is capable of detecting the lapse period of fatigue driving.

It may thus be concluded from this analysis that although it is more difficult to detect fatigue related events using the steering wheel system compared to the dashboard system, nonetheless the steering wheel system is capable of detecting the lapse period before the lane drift.

6.5 Combination of physiological and physical factors.

In this chapter, the chromatic analysis of results from two different systems (composite and gyroscope system) have been discussed separately. The composite system is concerned with physiological indications of driving fatigue based on information such as the human circadian rhythm and involving quality of sleep and duration of driving with emphasis on monotonous driving conditions. Application of chromatic analysis to the results of the composite system algorithm assists in identifying regions of fatigue (H) and magnitude of tiredness (L) based on chromatic polar diagrams (figure 6.3.3.1).

The gyroscope based systems are intended for the detection physical effects produced fatigued driving. Chromatic analysis of results from the two deployments of the gyroscope system, shows that the dashboard unit system is capable of detecting simulated fatigue related driving manoeuvres. The results have demonstrated that the chromatic analysis assists in discriminating between simulated fatigues induced lane drifting and swerving and normal driving manoeuvres. The analysis is capable of detecting simulated fatigue related events under various conditions such as different drivers, vehicles, traffic and weather conditions.

Horne and Reyner have suggested that if 3 fatigue events are detected within a span of 15 minutes, this indicate that the driver is fatigued **[Horne and Reyner, 2006]**. More than 3 fatigue event detected in the span of 15 minutes suggests that the tiredness level of the driver is critical and it is advisable to cease driving **[Horne and Reyner, 2006]**. This assists in furthering the design of an alarm raising capability of the dashboard gyroscope system.

Table 6.5.1 shows an alarm raising system based upon the number of events detected in the span of 15 minutes. For every event detected there is an increment of 0.1 in the value of a "Physical Tiredness Factor". If the registered fatigue event passes the 15 minute mark, there will be a reduction of 0.1 from the total score. There is no alarm action if only two or less events are detected within a 15 minute period. However 3 swerves in the span of 15 minutes produce a warning. If a fourth event is detected an

alarm will be raised indicating that the critical fatigue level of the driver based on the physical indication has been exceeded.

Fatigue Event Detected	Physical Tiredness Factor (Dashboard System) Duration of 15 minutes	Alarm Action
0	0	No
1	0.10	No
2	0.20	No
3	0.30	Warning
4	0.40	Yes Alarm
5	0.50	Yes Alarm

Table 6.5.1 Quantification of Physical Tiredness Factor based upon the number of events detected by a gyroscope and showing the various alarm levels.

The composite system (figure 4.2.1.2 based upon physiological factors has a separate alarm raising capability which is based upon a PTS threshold and 0.95 being exceeded.

6.5.2 Combination of Physiological and Physical Alarm system.

There is a need for combining the physiological and physical parameters to form an overall driving fatigue management system. In this section the combination of the composite system and dashboard unit are presented followed by a set of results.

The Chromatic Driving Fatigue Monitoring System consists of Physiological and Physical indicators in combination. Each indicator utilises Chromatic analysis differently. The main goal for the system is to be able to combine the information

from these two sub systems to yield a 'Total Tiredness Factor' (TTF) so that an alarm can be triggered above a threshold level.

Both the Physiological and Physical indicators may be regarded as semi-independent of each other, which implies that the alarms can be triggered based upon individual or combined threshold levels. With the combination of the composite and gyroscope (dashboard unit) analyses it is possible to form a fatigue management system that has been tested for real road conditions. The composite system contributes by identifying human physiological factors such as circadian rhythm based on the quality of sleep. The dashboard unit contributes by detecting fatigue related driving events such as swerving and lane drifting. A mathematical formula for the combination of the information from the two systems may be proposed as follows;

T.T.F = P.T.S + P.T.F ---------eqn 6.5.2.1

Where:

T.T.F is the total tiredness factor

P.T.S is the physiological tiredness factor

P.T.F is the physical fatigue detected by the dashboard gyroscope system

Table 6.5.2.1 provides a summary of the proposed values for the two terms of equation 6.5.2.1 and the manner in which they could be considered to give an overall integrated alarm level.

Table 6.5.2.1 shows two semi-independent sets of alarm. The 'Total Tiredness Factor' alarm and the dashboard unit alarm. The threshold for the TTF alarm is set at 0.95 which is similar to the PTS alarm. Basically the TTF is an addition of the PTS (physiological factor) and PTF (physical factor) values according to equation 6.5.2.1. The second alarm is the PTF alarm where this is independent of the physiological factor. As shown on table 6.5.2.1, a warning alarm is given when 3 events are detected and a full alarm when more than 4 fatigue related events are detected.

Table 6.5.2.1 shows the alarm criteria which can be used when combining information from both indicators. If the physiological indicator is at a minimal level, it will need a finite number of swerves (4) within 15 minutes to trigger the Dashboard

unit to initiate the alarm. Alternatively if the physiological indication is for critical tiredness, it will only require 1 swerve to trigger the total tiredness factor alarm. Using the semi independent alarm method helps to provide a fail safe margin for the system under different conditions. Examples of these conditions are:-

1. Driver experiencing jet-lag in a different time zone/country
2. Sleep apnoea patients
3. Drivers driving during dangerous Circadian periods (0200-0400hrs and 1400-1600hrs)

Physiological Indicators (Composite System)	**Physical Indicators (Dashboard Unit)**	**Semi-Independent Alarm**	
		Total Tiredness Factor Alarm	**Dashboard Unit Alarm**
Minimal Tiredness (PTS = 0)	4 events in last 15 mins (PTF = 0.40)	No (TTF = 0.40)	**Yes** (PTF = 0.40)
Low Tiredness (PTS = 0.30)	4 events in last 15 mins (PTF = 0.40)	No (TTF = 0.70)	**Yes** (PTF = 0.40)
Moderate Tiredness (PTS = 0.65)	3 events in last 15 mins (PTF = 0.30)	**Yes** (TTF = 0.95)	**Warning** (PTF = 0.30)
High Tiredness (PTS = 0.75)	2 events in last 15 mins (PTF = 0.20)	**Yes** (TTF = 0.95)	No (PTF = 0.20)
Critical Tiredness (PTS = 0.85)	1 events in last 15 mins (PTF = 0.10)	**Yes** (TTF = 0.95)	No (PTF = 0.10)

Table 6.5.2.1 Combination of physiological and physical indicators or driving fatigue

6.6 Summary

This chapter has described the chromatic analysis of the experimental results of chapter 5 for both physiological and physical systems followed by a discussion of their implications. The physiological indicators are based on the composite system results where the chromatic parameters H and L are used to determine the critical

tiredness level. Various H sectors on a H-L polar diagram (section 6.2.3) represent different tiredness situations with the critical tiredness level being in the 3rd sector (180^0 to 240^0). The L parameter represents the tiredness level whereby the higher L values indicate a more tired driver.

The physical indicator is based on the chromatic transformation of the gyroscope output signals. The gyroscope system has been deployed either on the vehicle dashboard or on the steering wheel. The dashboard implementation provides chromatic L and S values corresponding to the gyroscope output signal and whereby L is associated with the strength of the gyroscope angular rate and S with the spread of the signal. With the chromatic L and S values gathered for normal and simulated fatigue related manoeuvres, the threshold level for fatigue driving can be categorised. This can be further used for the detection of driving fatigue events to be identified autonomously. Initially the results detected numerous a false positive events which undesired effect was overcome through introduction of a mode based driving algorithm.

Analysis of the result for the steering wheel gyroscope was incapable of distinguishing the fatigue related simulated events as accurately as the dashboard gyroscope. This is because the gyroscope installed on the steering wheel experiences more rotational displacement around the steering column during manoeuvres compared to the dashboard unit. Therefore the magnitude of the output was higher which made it difficult to distinguish between normal and fatigue driving manoeuvres.

Finally the possibility has been addressed of combining the physiological and the physical factors from the chromatic analysis to provide a holistic means for identifying levels of driving fatigue. This is based upon combining the physiological tiredness score with the events detection (physical factor) to output the total tiredness factor alarm which triggers at a threshold level of 0.95. It is also important to include the physical factor independent to the physiological factor. Hence the system triggers the alarm when there are 3 or more fatigue related events regardless of the physiological factors such as circadian rhythm, quality of sleep and duration of the drive.

Chapter 7

Conclusions and Future Work

7.1 Conclusions

The main objective of this research was to develop a driving fatigue monitoring system which could be installed on a real vehicle operating on real roads. The system should be able to detect early signs of fatigue and advise the driver to cease driving when a tiredness threshold was approached. From knowledge of previous research, the driving fatigue monitoring system was based on both physiological and physical indications. With the application of a novel chromatic processing analysis, it has been possible to extract the required information (fatigue related conditions from normal driving) and also represent it in a simplistic form (chromatic polar diagrams).

Two separate systems have been designed to yield the physiological and physical indicators of fatigue. The two systems are:-

Composite System (Physiological Indicator)

The composite system was designed to detect early signs of fatigue from physiological factors such as the human circadian rhythm with regards to quality of sleep, the duration of driving and emphasising monotonous driving conditions. The composite system algorithm accumulates these factors and provides as an output a

'Physiological Tiredness Score' (PTS). An alarm threshold is implemented to trigger when the PTS exceeds a value of 0.95, indicating that the driver is over-fatigued and is advised to rest.

With the help of the chromatic analysis, data from the system output can be presented in a simplistic manner and divided into different categories of tiredness. . The Chromatic parameters H and L represent respectively the category of tiredness and the tiredness level. Four categories of tiredness have been identified on a H-L chromatic polar diagram from the 20 experimental tests conducted with professional drivers. The Chromatic physiological signatures which have been established are:-

- 1^{st} Sector (0-60^0) – represents a decreasing tiredness level. This region indicates the resting point of the driver when L, the tiredness level, reduces.
- 2^{nd} Sector (60^0-180^0) – represents the peak tiredness level. This region shows the tiredness level reaching its peak and then slowly reducing. The region usually indicates the effect of the circadian rhythm causing the driver to become more alert due to the time of day.
- 3^{rd} sector (180^0-240^0) - represents an increasing tiredness level. An L value of more than 0.8 in the 3^{rd} sector represents a high level of tiredness experienced by the driver and this will initiate an alarm to advise the driver to cease driving for an immediate rest
- 4^{th} Sector (240^0-360^0) – indicates rest periods where the PTS has minimal values.

Gyroscope System (Physical Indicator)

The gyroscope systems have been adapted to detect physical signs of driving fatigue. The physical indications of fatigue are erratic type driving during early stages of fatigue with the influence of such driving appearing via the steering wheel. The main sensor employed was a miniature vibrating gyroscope (Tokin NEC) which measured the angular rate of a moving body. The first system used a dashboard mounted gyroscope whereby the gyroscope was installed to detect the angular rate of the vehicle with reference to the yaw motion. The second system used a steering wheel

mounted gyroscope to measure the angular rate of the steering rotation. An analytical comparison of the two systems indicated that the dashboard gyroscope was able to distinguish simulated fatigue related events than the steering wheel gyroscope. The dashboard unit was tested and optimised to detect all fatigue related events accurately in 15 out of 16 experiments. Introducing a mode base driving consideration enabled all the false positive events which occurred during the non-monotonous driving conditions to be eliminated. It has been confirmed from previous research that driving fatigue is most likely to occur during monotonous driving conditions **[Horne and Reyner, 1997]**.

Outputs from the gyroscope system have been chromatically analysed for distinguishing driving fatigue from normal driving manoeuvres. The chromatic parameters L and S represent the signal strength of the angular rate and spread of the signal respectively.

Chapter 6.6 discussed the possibility of combining the physiological (composite) and physical (dashboard unit) system information. The method is based on two semi-independent alarms, the Total Tiredness Score (TTS) alarm and the Physical Tiredness Factor (PTF) alarm. The TTS alarm is based on the combination of the physiological parameters and the detection of events to gives for early warnings of the onset of fatigue. The threshold of the alarm is 0.95. The PTF alarm gives physical indications of fatigue in the absence of the physiological parameters. More than 3 swerves detected in 15 minutes indicate that the driver is highly fatigued regardless of time of the day **[Horne and Reyner, 2006]**. Therefore the PTF alarm should trigger when more than 3 swerves are detected in a span of 15 minutes.

This thesis has concluded that it is possible to design a monitoring system based on both the physiological and physical parameters for the detection of early signs of fatigue. More importantly this research has demonstrated that the experimental systems can operate under real road conditions and that the systems are unobtrusive to the vehicle and the driver during operation. An alarm system design has been discussed where the monitoring unit would act solely as an advisory system for the driver of the vehicle indicating high fatigue level. The cost of the system is economical whereby only a low cost sensor (gyroscope) and components are used.

7.2. Future Work

The experiments conducted with the gyroscope system are based on simulated driving fatigue manoeuvres conducted by non-fatigued drivers. This was done to ensure that there were no safety threats since experiments were conducted on real roads for the purpose of accommodating real environmental influences such as traffic, road and weather conditions. Future research (Section 6.3.3.2) should conduct experiments with fatigue or sleep deprived drivers on real road conditions, provided safety conditions are prioritised.

Circadian rhythm and duration of sleep requirements varies from one person to another. The current system only allows the driver to choose between 'Good', 'Bad' and 'Poor' quality of sleep the night before. Recently an American based company called 'Sleeptracker' **[Sleeptracker]** has developed a watch which stores information on previous sleep quality. The innovative product records the number of times a person is awake during the night and the average time between those moments. It also records the duration of sleep and compares the data from different nights to observe the restlessness during each night's sleep.

Future work on the physiological indicators needs to improve the quality of sleep estimate using information from such devices as the Sleeptracker **[Sleeptracker]** watch.

There is also the possibility of detecting driving effects other than those related to sleep. For example driving under influence of excess alcohol etc could be investigated. Clearly there would be a need to extrapolate the chromatic analysis to accommodate these other conditions.

Publications

1. [Koh et al, 2005]
Koh A, Dean.E., Zhang I, Jones G.R, , Spencer J.W
Effect of Chromatic filter characteristics in quantifying complex data
A Chromatic Approach to Complexity, Proceedings of the Complex Systems Monitoring Session of the International Complexity, Science and Society Conference, Liverpool, 11th - 14th September 2005, CIMS Centre for Intelligent Monitoring Systems, Dept. of Elec

2. [Koh et al, 2007]
Koh A, Jones G.R, Spencer J.W, Thomas I
Chromatic analysis of signals from a driver fatigue monitoring unit
Meas. Sci. Technol. 18 (2007) 747–754, 2007

3. [Jones et al, 2007]
Jones G.R, A., Deakin . and Spencer, J.W
A.Koh Chapter 11
Chromatic monitoring of complex systems
Taylor and Francis, ISBN: 9781584889885, (May, 2008)

Effect of chromatic filter characteristics in quantifying complex data

A. Koh, E.M. Dean, J. Zhang, G.R. Jones, J.W. Spencer

Centre of Intelligent Monitoring Systems (CIMS), Department of Electrical Engineering and Electronics, University of Liverpool, Brownlow Hill, Liverpool, L69 3GJ, UK

ABSTRACT

The use of chromatic processing is discussed for extracting information from the complexity of modulated pulsatile signals, which occur in many branches of medicine and engineering. A brief indication of the effect of changing the form of chromatic filters is given, followed by examples of the deployment of the method for yielding the signatures of some pulsatile signals.

1. INTRODUCTION

This contribution is concerned with the extraction of information from a complicated set of data representing a pulsatile condition. Such signals may occur as pulses in the circulation of blood in the human body, by faulty impeller blades on a mechanical pump or localised faults on the rotating tyre of a road vehicle. One approach for extracting information from pulsatile signals is to convert the signal from time variation into the frequency domain using Fourier based techniques. However the resulting frequency domain signal of such pulsatile signals is often as complicated if not more so than the original time domain signal. If in addition there are continuous periodic signals superimposed upon the pulsatile signals the Fourier transformed signals become even more complicated. An example of such a signal in the time domain and when Fourier transformed is shown on figures 1(a) and 1(b) respectively [2]. This shows that although the continuous signal frequencies are well below those of the pulsatile components, non-the less the pulsatile components are accordingly modulated complicating signal recognition.

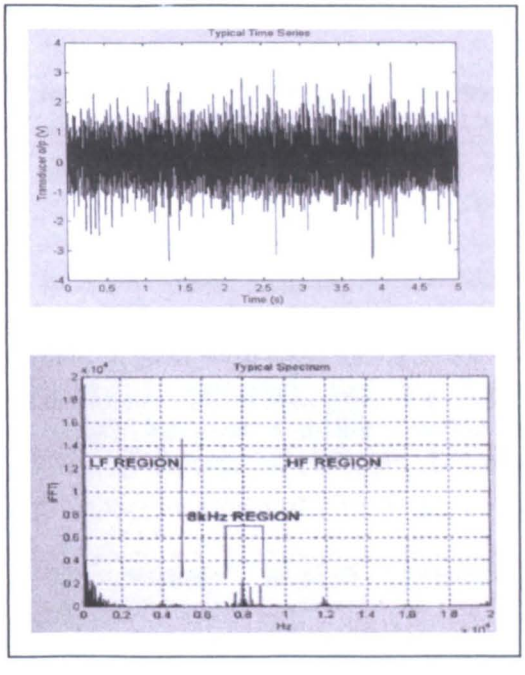

Figure 1: (a) Examples of Complex Pulsatile Signal time varying signal (b) Fourier Transform of figure 1(a)

Clearly additional techniques are needed to attempt to extract the information in an assimilable form. One method is based on chromatic processing which differs fundamentally from the Fourier approach in being non-orthogonal in

nature [1]. One way of implementing the approach is to chromatically process, the Fourier transform of the signal. This involves sampling the Fourier transform signal with non-orthogonal (overlapping) filters to yield three parameters, which then define the signal. The effect of the nature of the non-orthogonal processors on the signal defining parameters is considered before giving examples of the deployment of the approach for providing signatures of pulsatile signals

2. EFFECT OF FILTER PROPERTIES

This section discusses the manner in which different deployment of tristimulus filters (RGB) on the parameter axis translates into HLS space representation [2]. For clarity the input signal is assumed to be monochromatic (i.e. all values zero apart from a single parameter) so that S=1 and the performance can be tracked in terms of Hue. The manner in which the three filters are deployed will establish the region of overlap of the tristimulus filters, which in turn will determine the response of the system to the input signal.

2.1 Tristimulus filters at Half Height

Figure 2(a) shows a typical Blackman filter triplet, spanning the frequency range 0-22.5kHz. By tracking a series of monochromatic signals across this frequency range and calculating the H, L and S parameters in each case the variation of H with parameter (in this case frequency) for S=1 can be determined. The resulting variation is shown on figure 2(b). In this case, each of the chromatic filters overlapped at their half height values, the width and height of each filter being identical.

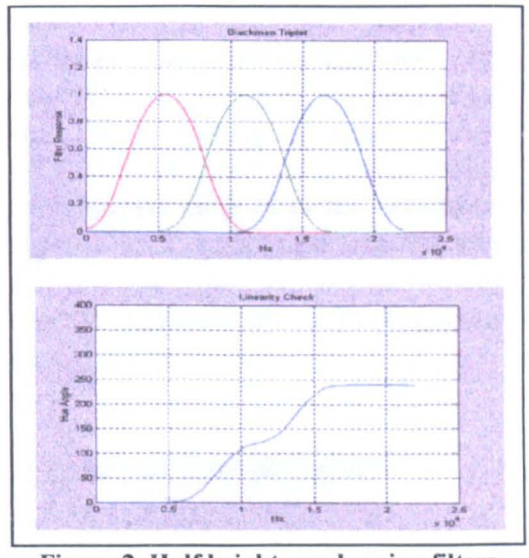

Figure 2. Half height overlapping filters (a) Response of filters (b) Hue: parameter characteristic

The result given on figure 2(b) shows that a H response is only obtained for the range of frequencies over which there is an overlap of the filter responses (i.e 5~17kHz). In between these limits H varies monotonically but in a non-linear manner with a reduced sensitivity in the range 10 – 12.5 kHz (the region where the R, B filter have minimal response) and the highest sensitivity where the filter overlap with a maximum rate of change (~8, 14kHz)

2.2 Widely Spaced Tristimulus filters

If the range of overlap of the filter responses is reduced as shown on the figure 3(a) a H: frequency characteristic of the form shown on figure 3(b) is obtained. This characteristic has an exaggerated non-linearity compared with figure 2(b) having a highly insensitive region (0.8 – 1.4 x 10^4Hz) due to the low level overlap of the R and B filters in that range. However there are two narrow regions either side of the insensitive

regions either side of the insensitive region that are highly sensitive.

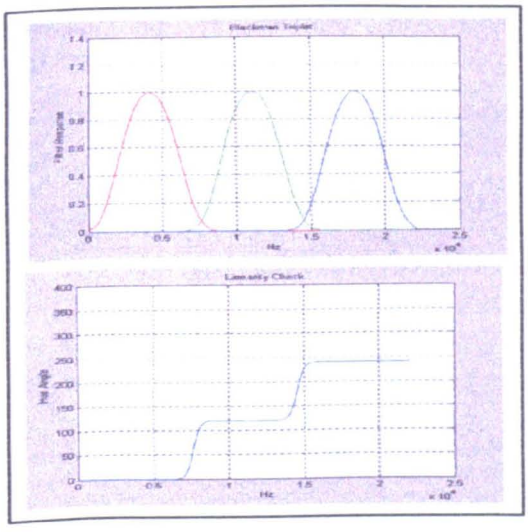

Figure 3: Filters with overlapping tails (a) Response of Filters (b) Hue: parameter characteristics

2.3 Truncated Triangular Tristimulus filters

A number of other filter arrangements can be envisaged. As an example a case is considered where the shape of the filter response is different and there is a truncation once the centre filter response reduces to zero. The filter shape is assumed triangular and the overlap is at half-height.

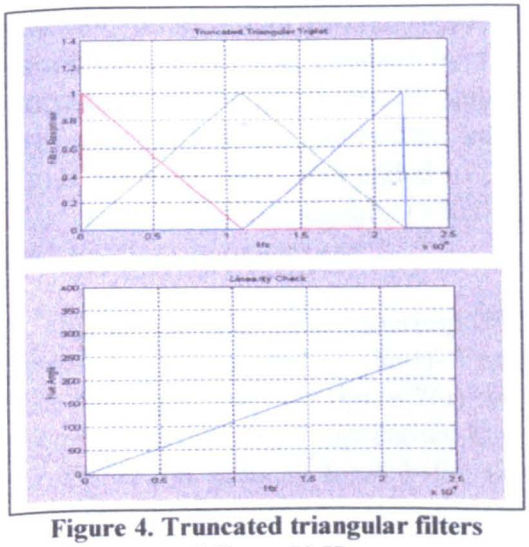

Figure 4. Truncated triangular filters (a) Response of filters (b) Hue: parameter characteristics

The resulting Hue: frequency characteristic in this case (figure 4) is highly linear extending throughout the range covered by the three-filter responses. Tests show that the best linearity occurred when the individual filters were spaced 2r apart (r=half width of filter) with the filter crossing points located at 0.07 of the maximum height. Filters implemented in this way give a result that is unconditionally linear throughout the entire frequency range, with no ambiguities.

2.4 Practical Considerations

The disadvantage of the triangular filter lies in the need for large kernels to accurately represent the discontinuities in the filter response. This can lead to greatly increased data processing.

In practise, this optimised filter is ideal for the processing of chromatic results from discrete data sets where a component of the data can be independent from another data point. On the other hand for continuous data, three Gaussians of the form shown in figure 2 are more practical because filter arrangements can be tailored to discriminate the data more at the centre of the Gaussian with less emphasis on the tail region.

Finally the information extracted in terms of H, L, S may be presented as each of two points on two polar maps in which H is the azimuthally angle and L, S are the radius respectively. An example of such a polar map representation of three monochromatic signals is given on figure 5. The chromatic filters are shown on figure 5(a) along with three monochromatic signals at frequencies of 150, 221 and 332kHz. The location of the chromatic point corresponding to each signal is

shown on a H-L map (figure 5(b)) [each signal having S=1 because of their monochromaticity but with a different H, respectively 30^0, 120^0, 240^0]

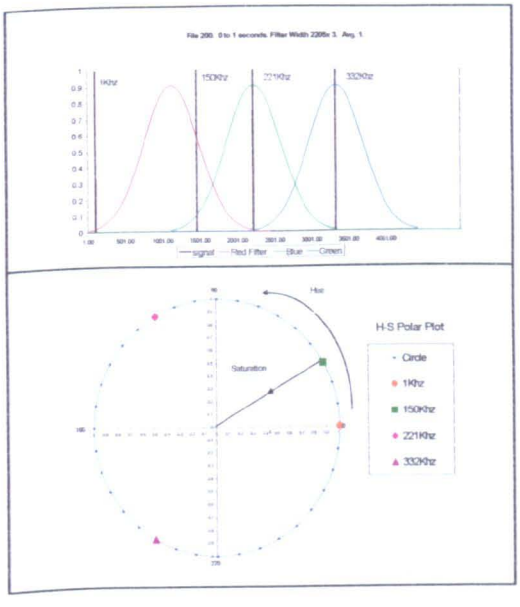

Figure 5 chromatic mapping
(a) Frequency domain signals (b) Chromatic domain representation

3. APPLICATION TO COMPLEX MONOCHROMATIC SIGNALS

3.1 Superposition Of Monochromatic Signals

Figure 6(a) and (b) show respectively two and three monochromatic signals superimposed on and coupled by the same three chromatic filters. In figure 6(b) an additional monochromatic signal (308kHz) has been added to the two monochromatic signals (150kHz and 250kHz) of figure 6(a)

A single, two and three superimposed signals are represented on the H-S and H-L chromatic maps of figure 7(a) and (b) respectively. Fig 7 (a) shows how the saturation reduces from 1 for the monochromatic signals to 0.78 for the two signals and 0.11 for the three signals. Figure 7(b) shows the manner in which L increases as the number of monochromatic signals increases. (Lightness Increases from 0.55 to 0.87)

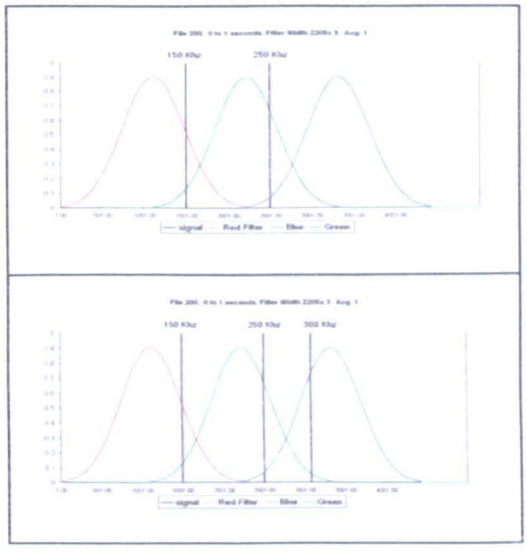

Figure 6. Superposition of monochromatic signals
(a) 2 superimposed monochromatic signals superimposed monochromatic signals

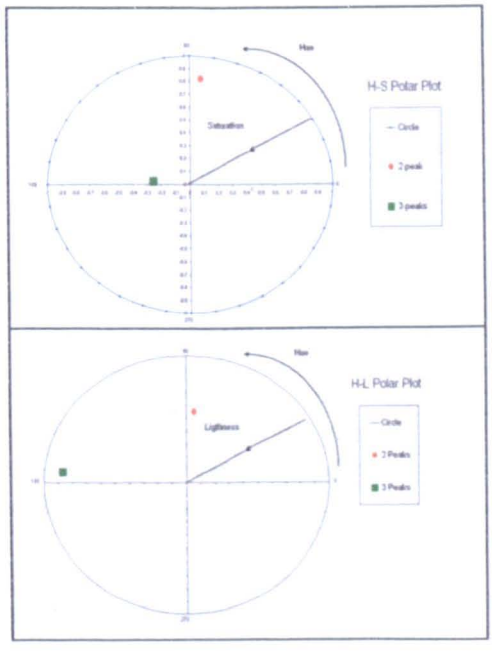

Figure 7. Chromatic maps of the monochromatic signals figure 6
(a) H-S polar map (b) H-L polar map

3.2 Amplitude variation of the composite monochromatic signal

3.2.1 Tristimulus Gaussian filters

Figure 8 shows the three monochromatic signals using tristimulus Gaussian filters of Figure 5(a) each with three different amplitudes forming three separate sets. Set A corresponds to the amplitudes set 1, 0.75, 0.5 for 150, 250 and 308KHz respectively; set B 0.5, 0.75, 1; Set C 0.75, 0.5, 1. This section considers the manner in which H, L and S values change with the relative amplitudes of the monochromatic signals.

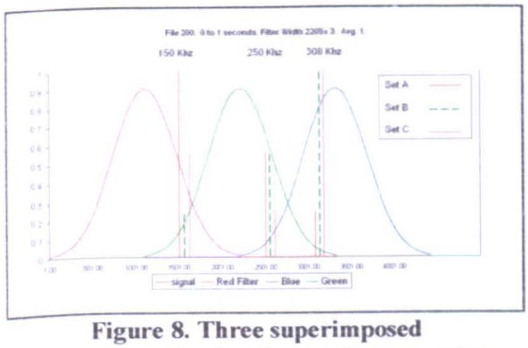

Figure 8. Three superimposed monochromatic signals with three varying amplitude using tristimulus Gaussian filters

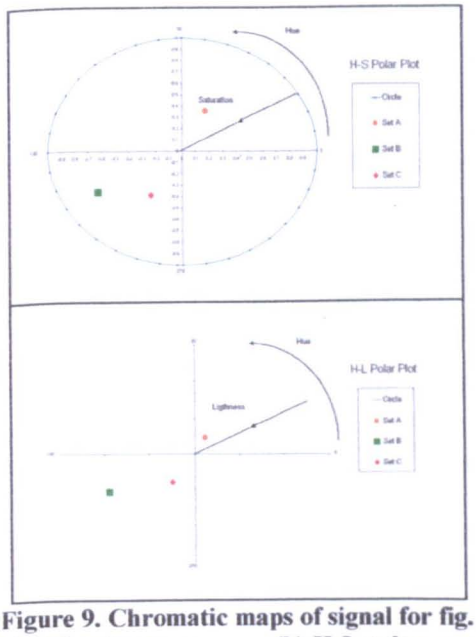

Figure 9. Chromatic maps of signal for fig. 8
(a) H-S polar map (b) H-L polar map

The three sets A, B and C of superimposed signals shown on figure 8 are represented on the H-S and H-L chromatic maps of Figure 9. Figure 9(a) shows saturation values of 0.39, 0.72, 0.46 for Sets A, B and C respectively. Figure 9(b) shows lightness values of 0.05, 0.22, 0.10 again for Sets A, B and C respectively. Thus Set B, has the highest saturation and lightness values and Set A, has the lowest saturation and lightness values

The Hue angles for Sets A, B and C are 64, 210 and 240 respectively. These results show that the difference in H, L and S values between each set A, B and C is sufficient for uniquely distinguishing between sets.

3.2.2 Tristimulus Triangular Filters

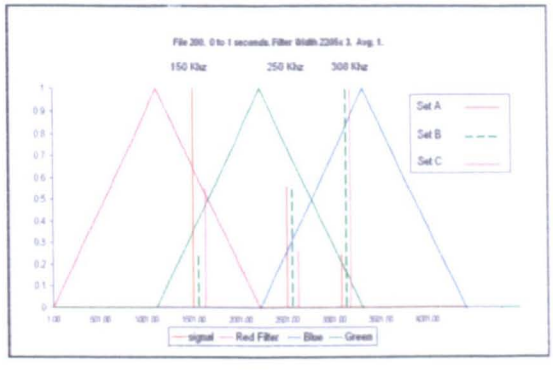

Figure 10. Three superimposed monochromatic signals with three varying amplitudes using tristimulus triangular filters

Figure 10 shows the three monochromatic signals similar to figure 8 however the filters used in this case are triangular filters.

The three sets A, B and C of superimposed signals shown on figure 10 are represented on the H-S and H-L chromatic maps of Figure 11. Figure 11(a) shows saturation values of 0.41, 0.71, 0.41 for Sets A, B and C respectively. Figure 9(b) shows lightness values of 0.06, 0.24, 0.11 again for Sets A, B and C respectively.

Thus Set B, has the highest saturation and lightness values and Set A, has the lowest saturation and lightness values

The Hue angles for Sets A, B and C are 83, 198 and 212 respectively. These results show that the difference in H, L and S values between each set A, B and C is sufficient for uniquely distinguishing between sets.

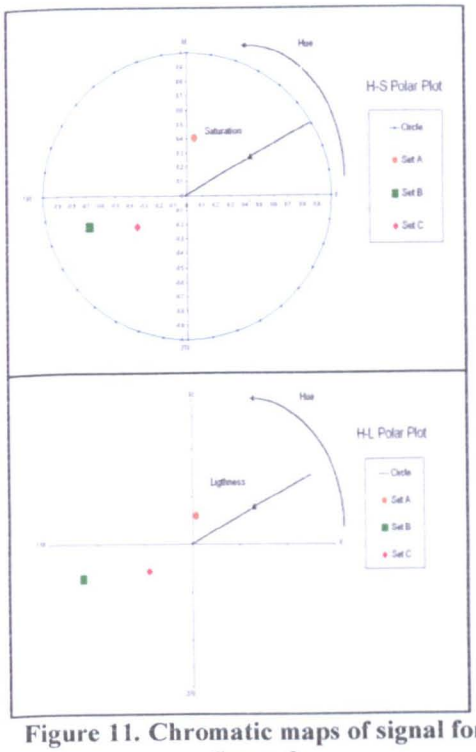

Figure 11. Chromatic maps of signal for figure 9

(a) H-S polar map **(b) H-L polar map**

3.2.3 Comparison of the two different filters configurations

The results for the different filters configurations Gaussian (fig. 8) and Triangular (fig. 10) are worth comparing. Firstly there is a large difference in the Hue angle results, where the discrimination for the Gaussian filters, figure 9, is greater than the triangular filters, figure 11. Thus hue angle results for Set A and Set B with the Gaussian filter has a difference of 210 – 64 =146, whereas for the triangular filters is only 198 – 83 = 115. With regard to Lightness the relative difference are 0.24 – 0.06 = 0.18 for the triangular filter and 0.22 – 0.05 = 0.17 for the Gaussian filters i.e. similar differences. The saturation values are 0.72 - 0.39 = 0.33 and 0.71 - 0.41 = 0.30 which are similar.

4. CONCLUSIONS

This contribution has shown how the form of the three chromatic filters affects the variation of the chromatic parameters for a given data set. For example a truncated tristimulus triangular filter produces uniformly linear response throughout the entire parameter range, with no ambiguities. However for many practical applications a half height Gaussian can be arranged to discriminate data in the centre region and with less emphasis on the tail regions.

Examples of the deployment of the filters to discriminate between pulsatile signals with superimposed continuously periodic signal are given. Comparing the output of the Gaussian and Triangular filters shows that in this case the triangular filters give higher hue discrimination mid range due to their better linearity.

Varying the relative amplitudes of the three chromatic filters can also be used to tune the chromatic response.

REFERENCES

[1] G R Jones, P C Russell, A Vourdas, J Cosgrave, L Stergioulas and R Haber, "The Gabor transform basis of chromatic monitoring" Meas. Sci. Technol. 11, 489–498, 2000

[2] E. M. Dean, PhD Thesis University of Liverpool, Non-Intrusive passive acoustic monitoring of Liquid Flow Systems, 2004

INSTITUTE OF PHYSICS PUBLISHING MEASUREMENT SCIENCE AND TECHNOLOGY

Meas. Sci. Technol. 18 (2007) 747–754 doi:10.1088/0957-0233/18/3/026

Chromatic analysis of signals from a driver fatigue monitoring unit

Alex Koh, Gordon R Jones, Joe W Spencer and Ian Thomas

Centre of Intelligent Monitoring Systems (CIMS), Department of Electrical Engineering and Electronics, University of Liverpool, Brownlow Hill, Liverpool, L69 3GJ, UK

E-mail: alexkoh@gmail.com

Received 22 August 2006, in final form 23 November 2006
Published 24 January 2007
Online at stacks.iop.org/MST/18/747

Abstract

The problem of extracting quantified information from physiological and physical indicators of the fatigue level of a vehicle driver is addressed. A chromatic approach has been used for processing the physiological and physical outputs from a driver fatigue monitoring system, the physical indicator being in the form of gyroscopic signals produced by the lateral movements of a vehicle. Some preliminary results are presented which show how the chromatic signatures of the physiological and physical indicators can be used to identify fatigue thresholds and provide a more optimized estimate of tiredness.

Keywords: chromatic processing, driver fatigue, data analysis, advisory system, circadian rhythm, gyroscope, Gaussian, monitoring, physiological, tiredness

(Some figures in this article are in colour only in the electronic version)

1. Introduction

There is an increasing awareness of the role of fatigue in reducing the effectiveness of everyday tasks such as vehicle driving. Drowsy driving encompasses several aspects, including falling asleep while driving or simply not paying attention due to fatigue or lack of sleep. There is therefore a need to provide assistive monitoring for vehicle drivers to reduce possible accidents etc, which might be caused by over-fatigued driving. Such monitoring needs to take account of both person based attributes and physical technology based indicators of fatigue. Regarding the former there is a need to respect the human biological clock which determines the fatigueness and is called 'circadian rhythm' [1, 2].

There are a number of methods which have been proposed for monitoring signs of fatigue of an individual whilst driving a vehicle. These include the detection of the driver's eye movement [3, 4], EEG (electroencephalogram) and EOG (electro-oculogram) [5, 6] etc. Whereas such methods are being tested at laboratory level, their reliability and implementation in real road situations remains to be proven and there are potential impediments such as cost and the complexity of the equipment to be addressed.

Another approach is to have a means which bridges the gap between physiological attributes and technical indicators. One such system is the ASTiD (advisory system for tired drivers) [7] system which is already in use on a number of vehicles. This system derives its output from the manner in which a vehicle is driven, inputted data by the driver and time of day related to circadian rhythm. The manner in which the vehicle is driven is determined from the vehicle response which is monitored in this system from the output of a gyroscope arranged to indicate the lateral movements of the vehicle. The research into fatigue and sleep shows that an early indicator of driver tiredness is given by a finite number of reactions resulting in particular corrective steering actions by the driver [2]. There is a need to better understand the capabilities of such systems with respect to their operation under real conditions. This contribution seeks to analyse the output signals from an ASTiD system. A chromatic processing technique [8, 9] is used for extracting relevant information from the complex data output relating to both the human physiological trends and those from the vehicle response.

It is shown that a chromatic transformation of the various data sets can enable significant signal patterns to be identified for providing an insight into a more rigorous approach for utilizing physiological and physical indications of fatigue.

0957-0233/07/030747+08$30.00

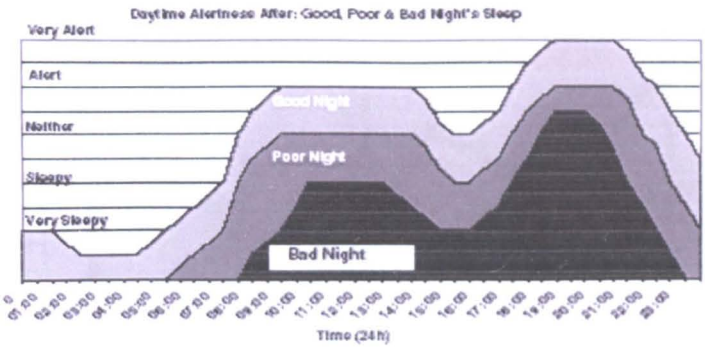

Figure 1. Circadian rhythm default plot for various sleeping conditions.

2. Test instrumentation

The instrumentation used consisted of an ASTiD (advisory system for tired drivers) [2]. This advisory system utilizes four sets of data which are

(a) the circadian rhythm representing diurnal variation in human tiredness;
(b) a driver's input about the quality of sleep before driving;
(c) a tiredness factor which increases with the continuous period of driving;
(d) a gyroscope output which indicates lateral movement of the vehicle being driven.

The circadian rhythm component (a) is derived from sleep research information from the University of Loughborough, Sleep Research Centre [1] and is embedded within a microprocessor in the ASTiD unit. Figure 1 shows the data for diurnal variation in alertness for different levels of sleep quality which is embedded in the ASTiD unit.

The quality of sleep judgement (b) 'good', 'poor', 'bad' is inputted into the ASTiD unit by the driver prior to commencing to drive. This chooses the appropriate circadian rhythm curve (figure 1) to be applied by the unit for that particular journey.

The quantification of the tiredness factor (c) is determined from studies on fatigue changes at the University of Loughborough and is again embedded within the microprocessor in the ASTiD unit. This yields the extent to which alertness decreases with the duration of driving and increases with period of resting from driving.

Whereas (a), (b), (c) are *a priori* determined physiological indicators approximately quantified, (d) is a direct measurement of a vehicle response to the driver's reactions. As such it forms the link between the physiological domain and real physical effects. This is achieved via a gyroscope embedded within the ASTiD unit which is appropriately mounted within the vehicle and firmly attached to the dashboard in such a manner that the gyroscope responds predominantly only to lateral movements of the vehicle (figure 2). The output of the gyroscope is mainly pulsatile in nature and is fed into the ASTiD embedded microprocessor. The number and extent of the pulsations are used in conjunction with the physiological indicators (a), (b), (c) to indicate the level of fatigue in order to alert when excessive thresholds are approached.

Figure 2. Shows the ASTiD system mounted on the dashboard of a vehicle.

The fatigue indications from each of the above components (a), (b), (c), (d) may be linearly summed to give an overall tiredness score (TS) given by

$$TS \cong C \cdot R(t) + D + (a_1\delta(t)_1 - a_2\delta(t)_2) + a_3 \sum_{t_w} P \qquad (1)$$

where

- $CR(t)$ is the time-dependent circadian rhythm tiredness score (a) (figure 1);
- D is the driver estimate of sleep quality received (b) (figure 1);
- $a_1\delta(t)_1$ is the time accumulating tiredness caused by continuous driving for a time interval $\delta(t)_1$, a_1 being constant (c);
- $a_2\delta(t)_2$ is the time accumulating resting effect after driving cessation for a time interval $\delta(t)_2$, a_2 being constant (c);
- $a_3 \sum_{t_w} P$ is the sum of the amplitudes P of the output pulses from the gyroscope during the driving time window t_w and a_3 is a numerical constant;
- t is time.

When the tiredness score (TS) exceeds a threshold predetermined from Sleep Research studies [1] the driver is alerted. The system at present yields a fail safe threshold with a good margin. A more precise estimate of the approach to the fatigue threshold might be achieved by better correlation of the data from the fatigue indicators (a), (b), (c) above.

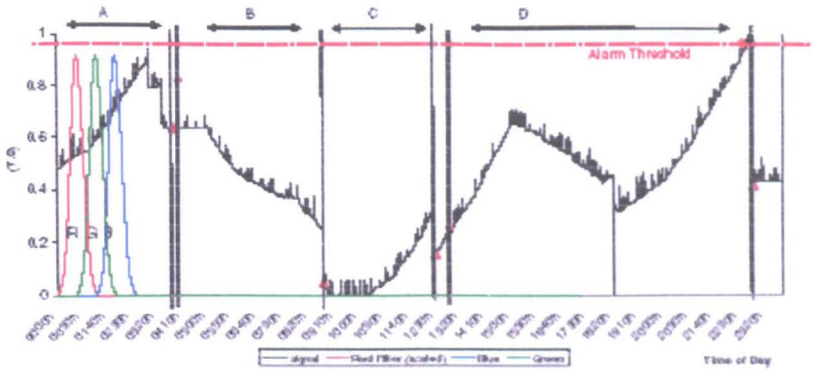

Figure 3. Typical output of the ASTiD system from a typical 24 h period test with several changes of drivers. (A, B, C, D different driver and shift periods.)

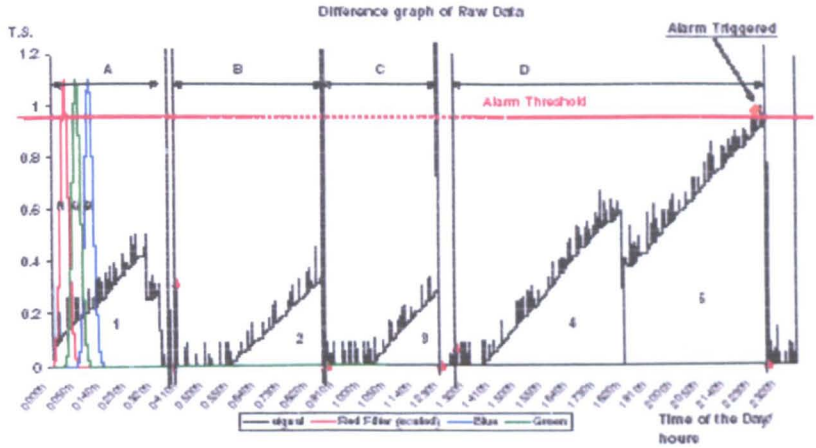

Figure 4. Difference graph of the raw data (figure 3). (Difference graph = raw data – circadian rhythm.) (A, B, C, D—drivers. 1, 2, 3, 4, 5—sectorial regions of increasing tiredness.)

3. Experimental tests

Two different sets of tests have been performed. The first set was with a commercial vehicle in routine use and driven by professional drivers with an ASTiD unit operating routinely. The second set was with a vehicle in which the output of the ASTiD gyroscope was monitored directly.

3.1. ASTiD unit output test

Experimental tests were performed with the ASTiD unit appropriately mounted on the dashboard of a commercial vehicle (figure 2) which was in routine use on normal roads, and when there were changes of drivers, rest periods and extensive road driving.

During such tests the overall output of the ASTiD unit was recorded as a function of time along with notes of major events such as time of start of driving, rest period, change of driver etc. The ASTiD unit also had inputted each driver's estimate of the quality sleep prior to driving. Also the outputs of the gyroscope as a function of time could be accessed retrospectively from the microprocessor embedded within the ASTiD unit.

Consequently test data could be retrieved after each test in the form of the time variation of the overall output of the ASTiD unit based upon the sum of the circadian rhythm curve appropriate to each driver, the fatigue increase during a driving session and the raw gyroscope output (equation (1)).

3.2. Gyroscope output tests

Tests were also undertaken whereby only the output of the gyroscope appropriately mounted on the dashboard of a vehicle was recorded directly in the absence of the circadian rhythm (a) and accumulative fatigue ((b) and (c)) outputs. During these tests, records of detailed observations of different driving conditions (e.g. different speeds, road conditions etc) were obtained by a passenger in the vehicle over a limited time interval (e.g. 6 min). During such tests the data sampling rate was 32 Hz.

4. Experimental results

Results from a typical 24 h test with driver changes obtained with the ASTiD system (figure 2) are shown in figures 3, and figure 4 corresponding respectively to the overall tiredness

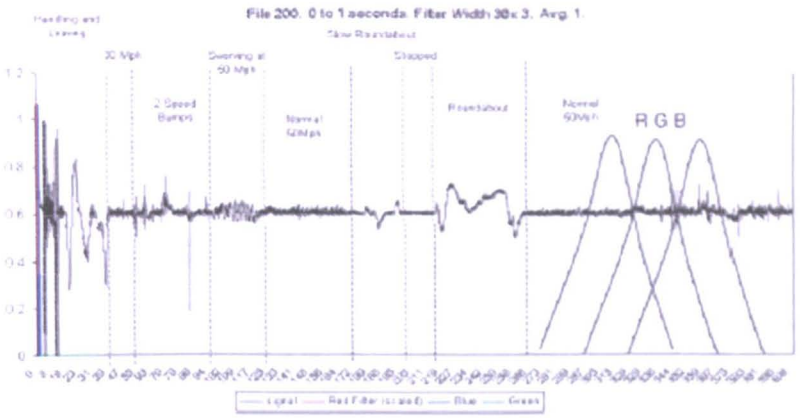

Figure 5. Gyroscope output showing different signals associated with various driving features.

score (equation (1)) and the tiredness score without the circadian contribution. More detailed results for a gyroscope test are shown in figure 5.

4.1. Overall output data

The overall output from the ASTiD unit (figure 3) shows a complex variation of *TS* with time. There are relatively slow variations due to the circadian rhythm ((a) section 2) combined with the continuous driving factor (b). There are also effects due to a total of four driver changes which occurred during different shift periods namely 03.30 (A), 08.46 (B), 12.30 (C) and 22.55 (D) hours. A change of driver is accompanied by the system resetting itself to the relevant point on the circadian rhythm. Likewise a driver resting reduces the tiredness score.

Superimposed upon the slower *TS* variations are short duration pulses which are the rapid response of the gyroscope to driver-induced lateral movement of the vehicle.

Based upon the Sleep Research conclusions of the University of Loughborough [1] a *TS* of 0.95 is regarded as the threshold for an unacceptably high tiredness level. This is shown as a dashed line in figure 3. In practice when $TS \geqslant 0.95$ an alarm is triggered to advise the driver to stop driving.

The circadian rhythm component (figure 1, (a), (b), section 2) may be removed from the overall *TS* in order to observe the effects of the other factors, i.e. fatigue increase with duration of driving ((c) section 2) and gyroscope output ((d) section 2).

The circadian rhythm [1] shows a daily cyclical pattern (figure 1) with a maximum tiredness at night time (03.00–05.00 hours) followed by a maximum period of awakeness (09.00–11.00 hours), a further tiredness peak (15.00 hours) and a wakeful period (17.30–20.00 hours). The absolute level of the circadian rhythm decreases with the quality of sleep leading to the three curves of figure 1.

Subtraction of the circadian rhythm component from the overall ASTiD output signal (equation (1)) leads to the time varying difference *TS* shown in figure 4. This graph shows that with fresh drivers (A, B, C, D figure 3) the tiredness score resets to zero. During the final phase of the day (sector D figure 3), there was no driver change therefore the tiredness score remained accumulative for prolonged periods (approx. 10 h) of driving with eventually the alarm being triggered at 22.33 hours.

Five time sectors of increasing tiredness can be identified in figure 4 which are designated by 1, 2, 3, 4 and 5. Each refers to a different driver apart from 4 and 5 which refers to a single driver D who reset at 18.20 hours so reducing the tiredness level (from 0.6 to 0.4) yielding the two regions of tiredness 4 and 5.

4.2. Gyroscope output data

Results for the time variation of only the output from the gyroscope during a test when detailed observations of driving conditions were made are shown in figure 5. The results which are typical of those obtained from such tests covered a total period of 6 min. The vehicle was deliberately driven through a number of phases (figure 5) which included the following:

(1) handling and leaving a stationary state;
(2) travelling at 30 mph;
(3) traversing two speed bumps;
(4) deliberate swerving for 20 s to simulate swerving due to fatigue;
(5) travelling at 50 mph;
(6) slow negotiating of a roundabout;
(7) vehicle stationary;
(8) more rapid negotiation of a roundabout (two circulations);
(9) travelling at 50 mph.

5. Analysis of results

The results given in figures 3, 4 and 5 show a number of features which are qualitatively distinguishable but warrant being examined quantitatively. For example discrimination of the 50 mph swerving detected by the gyroscope (figure 5) from the other driving artefacts would be particularly useful since it is generally recognized [1, 2] that a fatigued driver tends to drift off the road and swerve back as consciousness is regained. In order to explore the possibility of such quantified discrimination, chromatic techniques [8, 9] have been employed.

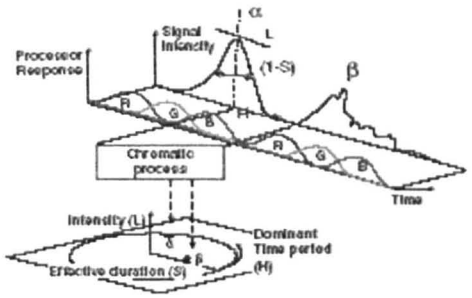

Figure 6. Time-dependent chromaticity showing time varying signals (α, β) during different times, each addressed by the chromatic processors (R, G, B) to yield H, L, S values. Each signal is replaced by a single point on the chromatic polar diagram.

5.1. Chromatic methodology

The deployment of chromatic processing was originally used with respect to optical wavelength [8] but subsequently it has been used for other parameters [9] and purposes [10]. In this application it is time-based chromatic processing which is deployed.

The time varying signal is addressed by three time based non-orthogonal filters R, G, B each of equal width and spanning a predetermined period (figure 6). The R, G, B outputs yield the chromatic parameters H, L and S defined by (equations (2)–(4) respectively), which in the present context have the following meaning. H represents the dominant signal time period, L is the nominal signal strength and S is the effective time duration of the signal within the monitored time window.

$$H = \begin{cases} 60\dfrac{G-B}{\max(R,G,B)-\min(R,G,B)}, & \text{if } R=\max \\ 60\left[2+\dfrac{B-R}{\max(R,G,B)-\min(R,G,B)}\right], & \text{if } G=\max \\ 60\left[4+\dfrac{R-G}{\max(R,G,B)-\min(R,G,B)}\right], & \text{if } B=\max \end{cases} \tag{2}$$

$$L = \frac{\max(R,G,B)+\min(R,G,B)}{2} \tag{3}$$

$$S = \begin{cases} \dfrac{\max(R,G,B)-\min(R,G,B)}{\max(R,G,B)+\min(R,G,B)}, & \text{if } L \leqslant 0.5 \\ \dfrac{\max(R,G,B)-\min(R,G,B)}{2-\max(R,G,B)-\min(R,G,B)}, & \text{otherwise} \end{cases}. \tag{4}$$

The H, L, S parameters may be displayed on a polar plot with $\theta \equiv H$, $r \equiv S$, $z \equiv L$, as shown in figure 6. Signal α (figure 6) is a simple Gaussian pulse in time which serves as an aide to indicate the physical meaning of H, L, S. In practice the three filters are time stepped using an appropriate step width relative to the filter width. Figure 6 shows how the Gaussian signal α is followed by a more complex signal envelope β and addressed by the three chromatic filters R, G, B n time steps later.

The chromatic coordinates of the point corresponding to β have a lower S value (more broadly spread signal) with its dominant time earlier (H lower) than α. This example shows how various signals can be discriminated in terms of their chromatic coordinates.

5.2. Chromatic processing of fatigue signals

The chromatic processing approach described in section 4.1 may be applied to the analysis of the time varying signals shown in figures 3–5. Also shown in the figures are R, G, B filters in time-domain mode. Each of the R, G, B filters of figures 3 and 4 has a width 75 min and were time stepped in increments of 1 min over the entire signal duration. The R, G, B filters of figure 5 each had a width 30 (0.9 s) and were time stepped with a step width of 0.03 s. Values of the chromatic parameters H, L, S equations (2)–(4) were obtained for each time window.

These H, L, S values may then be displayed on polar plots of H–L or H–S (H is the azimuthal angle and L, S are the radii, respectively) to highlight features of interest from the raw data. The choice between using H–L or H–S depends upon the information being sought.

5.2.1. Overall output signal. Applying the chromatic analysis to the overall data of figure 3 yields the H–L polar diagram of figure 7. Data for each driver are designated by A–D as shown in figure 3. An alarm which was triggered at 22.33 hours (figure 3) has H, L coordinates 210, 0.8. Arrows show the tiredness progression.

The results show loci for the various drivers with many convolutes on the $H \sim 30°$–$210°$ axes. Within the second quadrant (90°–180°) there are three arcs apparent (corresponding to drivers A, B, D) whilst within the fourth quadrant (270°–360°) there is only a single arc apparent (driver C).

5.2.2. Difference data analysis. Applying the chromatic analysis to the difference data of figure 4 yields the H–L polar diagram of figure 8. In this case the five different time stages of figure 4 (1–5) are distinguished by different symbols. The 22.33 hour alarm has H–L polar coordinates 210, 0.8 which are identical to the figure 7 values.

The results show a number of loci in the sector 90°–180° the length of whose radii are related to the magnitude of the tiredness factor of figure 4. The effect of a driver resting (separating region 4, 5, figure 4) appears as an excursion into the quadrant 270°–360° figure 8. The most rapid increase in tiredness score appears as a radial increase in L along the 210° radius.

5.2.3. Gyroscope data analysis. Chromatic analysis of the gyroscope output signal (figure 5) leads to the H–S polar diagram shown in figure 9. The nine different manoeuvres ((1)–(9) section 4.2, figure 5) are designated on figure 9 by different symbols.

Most of the manoeuvres appear as ellipses with major axes inclined along the $H \sim 30°$–$210°$ axis and with a minor axis value of $S \sim 0.2$. However, the swerving action (curve 4, figure 9) is circular with a radius $S \sim 0.3$–0.4.

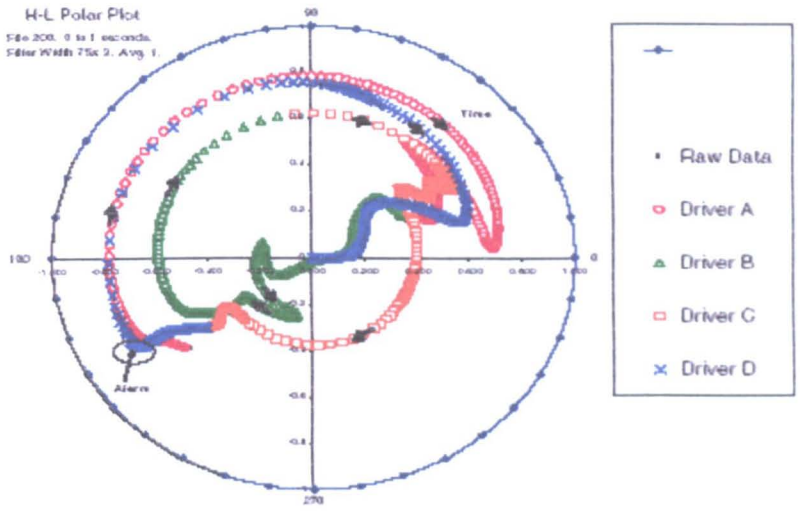

Figure 7. Chromatic polar-diagram $H-L$ for the overall output signal of figure 3. (Different symbols correspond to various drivers A–D, figure 3.)

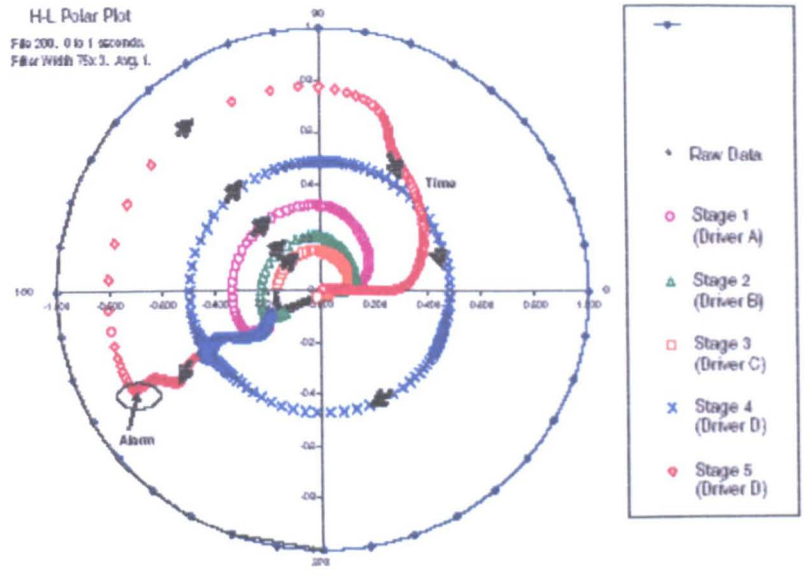

Figure 8. Chromatic polar-diagram of $H-L$ for the difference data of figure 4. (Different symbols indicate different stages of figure 4.)

6. Discussion of results

The results of the chromatic analysis presented in section 5 as $H-L$ and $H-S$ polar diagrams may be considered in terms of the extent to which various features are associated with different manoeuvres. The physiological components are considered first (figures 7 and 8) before discussing the gyroscope output figure 9 and the combined information.

6.1. Physiological results

The chromaticity transformed physiological trends (figures 7 and 8) may be interpreted by comparison with the raw time-domain data of figures 3 and 4. The $H-L$ polar diagram of figure 8 in conjunction with the difference graph figure 4 leads to the following conclusions:

- for no driver activity $L \sim 0, S \sim 0$;
- the locus of points on the $H-L$ diagram is sequenced in a clockwise direction (arrows);
- tiredness reduction (due to resting or a change of driver) leads to decreasing L values in quadrant 1 ($H \sim 0°$–$90°$);
- when the tiredness reduction does not lead to a complete recovery but is interrupted by a return to tiredness increasing (stages 4 and 5 in figure 4), the $H-L$ locus

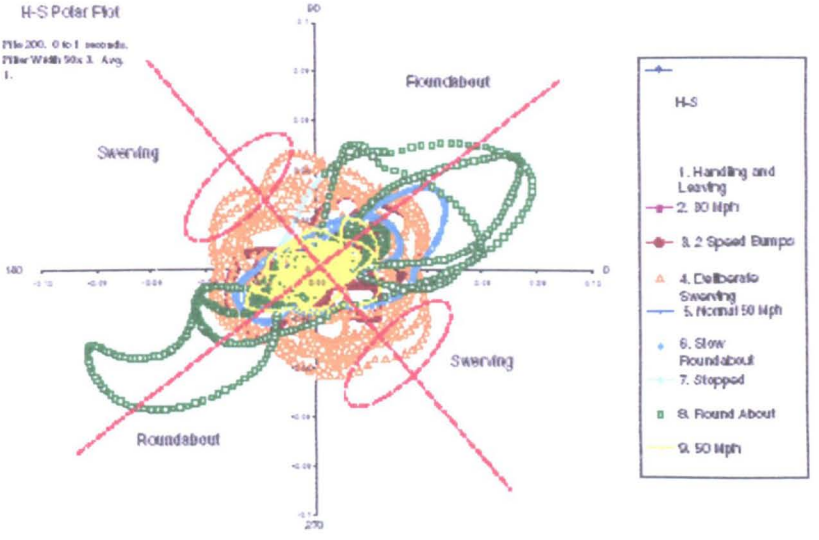

Figure 9. H–S polar diagram of the gyroscope output of figure 5. (Different symbols indicate different manoeuvres of figure 5.)

is within the fourth quadrant ($H \sim 270°$–$360°$) (figure 8) at approximately constant L;

- tiredness increasing is reflected in L increasing at constant H ($\sim 210°$) in quadrant 3 (figure 8);
- the magnitudes of the tiredness peaks in stages 1, 2, 3, 4, 5 (figure 4) are reflected by the L values of the arc in the second quadrant ($H = 90°$–$180°$) (figure 8).

The chromatically processed results for the combination of circadian rhythm and tiredness factor (figure 7) show similar trends to the difference results of figure 8. However the circadian rhythm component can contribute significantly in moving some trajectories further or closer to the critical threshold boundary. For example driver A's locus has a relatively low value of $L \sim 0.37$ in figure 8 but a higher value of 0.8 in figure 7.

These observations enable the implications of various sectors of the chromatically processed H–L signals to be appreciated as shown schematically in figure 10. The first quadrant of figure 10 corresponds to a progressive reduction in tiredness (i.e. decreasing tiredness, figure 4). The second quadrant of figure 10 corresponds to the tiredness level having passed through a peak. The third quadrant accommodates increasing tiredness trends whilst the fourth quadrant indicates a change in tiredness trends from initially decreasing (due to resting) to increasing (restart of driving).

Thus in general the lightness level L (radius in figure 10) represents the extent of tiredness whilst the H value is indicative of whether tiredness increases or decreases. A threshold for critical tiredness level may therefore be defined (figure 10) above which an alarm may be initiated.

6.2. Gyroscope results

In the case of the gyroscope results (figures 5 and 9), it is the H–S rather than the H–L chromatic map which provides a discrimination capability. Under 'normal' driving conditions

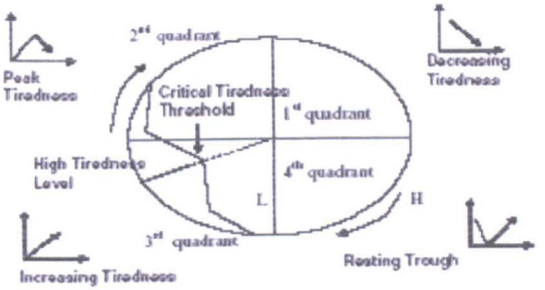

Figure 10. H–L polar diagram showing the critical tiredness threshold.

the H–S chromatically transformed data cluster about the origin. Manoeuvring roundabouts leads to lobes being formed along the 30° and 310° axis on the polar diagram (figure 8). However, the swerving motion in figure 5 produced more pronounced lobes within the second and third quartiles of the H–S diagram, where previously there had been only lower S levels. This implies that the time variation of the swerve signal (figure 5) is more regular than the other manoeuvre signals.

6.3. Combination of physiological and gyroscope signals

The results of figures 8 and 9 show that in the chromatic domain

- the physiological critical tiredness threshold has polar coordinates ($L > 0.8, 180° < H < 270°$);
- tiredness induced swerves (gyroscope signals) has polar coordinates ($S \geqslant 0.04, H = 120°, 300°$).

Thus whereas physiologically it is signal strength (L) combined with the L trend with respect to H which indicates the tiredness threshold, physically (gyroscope) it is the degree of monochromaticity ($1 - S$) at a particular part of the signal

(H) which is indicative of tiredness. Consequently summing the physiological and physical signal strengths (equation (1)) is rigorously inappropriate but provides a fail safe margin by taking all gyroscope pulses into account.

If a better optimized tiredness estimate is to be achieved, the difference in the chromatic domain physiological and physical indicators (section 6.3) needs to be respected implying that each needs to be treated separately and the two results then cross-correlated.

For the physiological case, the tiredness score may be expressed in chromatic terms as

$$(TS)_p = L(H) \tag{5}$$

with the critical tiredness threshold as

$$(TS)_{pT} = 0.8 \quad (180° < H < 270°). \tag{6}$$

In the physical case (gyroscope), it is the occurrence of a particular type of pulse defined by ($S \geqslant 0.4$, $H = 120°$, 300°) which is indicative of tiredness. Sleep research [1, 2] suggests that it is the number of such swerves within a given time window which is indicative of the degree of tiredness. Consequently, the physically based tiredness score $(TS)_g$ may be related to the occurrence of the identifying signal $S_g(S, H)$ by

$$(TS)_g = \sum S_g(\geqslant 0.4;\ 120°/300°) \tag{7}$$

with a critical physical tiredness threshold as

$$(TS)_{gT} = N_t \tag{8}$$

where N_t is an empirically determined number of the particular pulses detected in a given time window t to be unacceptable.

For the two extreme dominating cases

- physiological indicators,
- physical (gyroscope) signals,

the tiredness score compared to the relevant threshold [$(TS)/(TS)_T$] is conveniently given by equations (5)–(8) respectively.

For the cases when physiological and physical indicators both contribute, it is anticipated that the tiredness scores from equations (5) and (7) would correlate to indicate similar rates of increase of tiredness and approaches to each of the two critical tiredness thresholds as given by equations (6) and (8). Otherwise the most critical indicator might be adopted pending further experimentation and the possible use of additional chromatically based prognosis as used by Zhang *et al* [11].

7. Conclusions

It has been shown how time-domain chromatic processing may be applied to different types of signals from a driver fatigue monitoring system. Data are transformed into H–L or H–S chromatic maps on which signatures for different levels and trends of fatigue can be observed.

Physiologically based fatigue indicators have been shown to be distinguishable on an H–L polar diagram. Swerving motion associated with the onset of high levels of fatigue as detected by a gyroscope has been shown to be distinguishable from other types of lateral motions on an H–S polar diagram. This suggests that adding the magnitudes of the physiological and physical signals equation (1) is an over simplification but one which provides a high fail safe margin of fatigue estimation since it considers all rather than only some gyroscope outputs as significant.

In order to better optimize fatigue estimation, it is suggested that the physiological and physical indicators are treated separately in the chromatic domain pending the availability of additional test data to enable chromatic probability methods [11] to be invoked. Further tests are also needed to establish the extent to which swerve signals are discernible under other operating conditions (e.g. various drivers, vehicles, weather conditions etc). Such tests are currently ongoing.

Acknowledgments

The authors appreciate the provision of an ASTiD system and test data by Pennix which enabled the present work to be undertaken. Financial support provided by the EU via the IMS 2000 project is acknowledged. Discussions with Professor J Horne and Dr L A Reyner of the Sleep Research Unit of Loughborough University are also much appreciated as are the efforts of Ms S Kallio in producing this manuscript.

References

[1] Horne J A and Reyner L A 1995 Sleep related vehicle accidents *Br. Med. J.* 310 565–7

[2] Reyner L A and Horne J A 1998 Falling asleep whilst driving: are drivers aware of prior sleepiness? *Int. J. Legal Med.* 111 120–3

[3] Johns M W 2003 The amplitude–velocity ratio of blinks: a new method for monitoring drowsiness *Sleep* (Suppl.) 26 A51–2

[4] Leder R S, Stampi C and Webster J G 1996 Blink size and lid velocity from ambulatory subjects: an analog, retroflective eyelid sensor *J. Sleep Res.* (Suppl. 1) 121

[5] Held C M, Causa L, Estevez P, Perez C, Garrido M, Algarin C and Peirano P 2004 Dual approach for automated sleep spindles detection within EEG background activity in infant polysomnograms *26th Annual Int. Conf. Eng. Medicine and Biology Society (1–5 Sept)* vol 1 pp 566–9

[6] Peiris M T R, Jones R D, Davidson P R, Carroll G J, Parkin P J, Signal T L, Van DenBerg M and Bones P J 2005 Identification of vigilance lapses using EEG/EOG by expert human raters *27th Annual Int. Conf. Eng. in Medicine and Biology Society (01–04 Sept.)* pp 5735–7

[7] http://www.pennix.co.uk/

[8] Jones G R and Russell P C 1993 Chromatic modulation based metrology *Pure Appl. Opt.* 2 87–110

[9] Jones G R, Russell P C, Vourdas A, Cosgrave J, Stergioulas L and Haber R 2000 The Gabor transform basis of chromatic monitoring *Meas. Sci. Technol.* 11 489–98

[10] Brazier K J, Deakin A G, Cocke R D, Russell P C and Jones G R 2001 Colour space mining for industrial monitoring *Data Mining for Design and Manufacturing (Massive Computing Series* vol 3) ed D Braha (Dordrecht, The Netherlands: Kluwer)

[11] Zhang J, Jones G R, Deakin A G and Spencer J W 2005 Chromatic processing of DGA data produced by partial discharges for the prognosis of HV transformer behaviour *Meas. Sci. Technol.* 16 556–61

Chapter 11: Chromatic Monitoring of Activity and Behaviour

A. Koh

11.3 Physiological and Physical Indicators of Fatigue

11.3.1. Introduction

There is an increasing awareness of the influence of fatigue in reducing the effectiveness of individual in undertaking tasks such as vehicle driving. Drowsy driving encompasses several aspects, which include falling asleep or lacking concentration both of which can lead to fatal accidents [Reyner and Horne 1998] [Horne and Reyner 1995a] (Figure 11.3.1.1)

Figure 11.3.1.1 Hazard of driving when fatigue

Methods for assisting drivers to recognise indicators of the onset of disruptive fatigue are essential for preventing fatigue related road accidents which claim 1 in 5 of UK motorway accidents. [Horne 2001]

One such system is the Advisory System for Tired Drivers (ASTiD). This system incorporates the superposition of a Circadian rhythm [Horne and Reyner 1995b] upon signals from a gyroscope arranged to respond to the lateral movement of a vehicle [Koh et al 2007]. The Circadian rhythm is a diurnal variation in the level of alertness of a human. Amongst the lateral movements detected by the gyroscope are those produced as swerves in response to the impulsive reactions of a driver emerging from periods of micro-sleep. Also there are preceding quiescent periods consequent upon a fatiguing driver taking fewer minor corrective steering actions.

The output signal from an ASTiD unit is in the form of a time varying voltage composed of the addition of the three components: the Circadian rhythm curve, a component whose magnitude increases with duration of continuous driving and the gyroscope output (Figure 11.3.1.2). This particular record covers a period of 24 hours during which the vehicle was driven by 3 drivers and a high fatigue level being ultimately reached at 22.33 hours. The benefits provided by such a system can be

enhanced by improving the information extraction and correlation between the physiological and physical indicators.

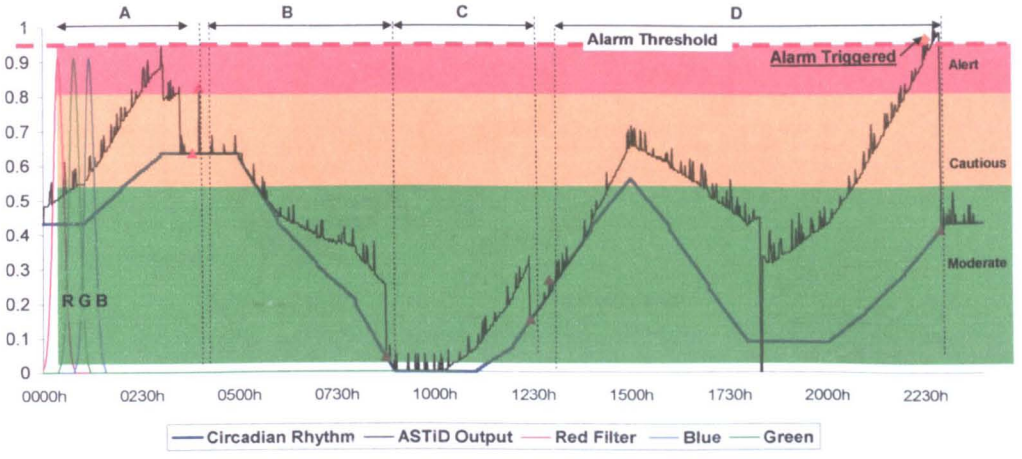

Figure 11.3.1.2 Typical output of the ASTiD system from a typical 24 h period test

with several changes of drivers.
(A, B, C, D different driver and shift periods.)
(Koh et al, 2007, With Permission)
(A, B, C, D different driver and shift periods.)
(Koh et al, 2007, With Permission)

11.3.2. Physiological Indicators

The time variation of the Circadian rhythm is shown on Figure 11.3.1.2 as a periodic continuous curve whilst the contribution due to the continuous driving is added to this curve to give the overall curve (neglecting the higher frequency pulses). Consequently this overall curve represents the total physiological signal.

The total physiological signal may be chromatically transformed by time stepping (1 min step) three chromatic processors (75 mins wide) along the signal. (e.g. chapter 10, section 10.2, figure 10.2.1 (iv)). The resulting chromatically transformed signal is shown on the H-L diagram of Figure 11.3.2.1 [Koh et al 2007] where the different symbols represent each of the four stages (A-D) (Figure 11.3.2.1). There are a number of phases to the curves which can be associated with different aspects of the physiological curves. Within the second quadrant (90-180 degrees) there are three arcs (A, C, D) which represent a change from increasing to decreasing fatigue. Within the fourth quadrant (270-360 degrees) there is a single arc (c) which represents the resting trough.

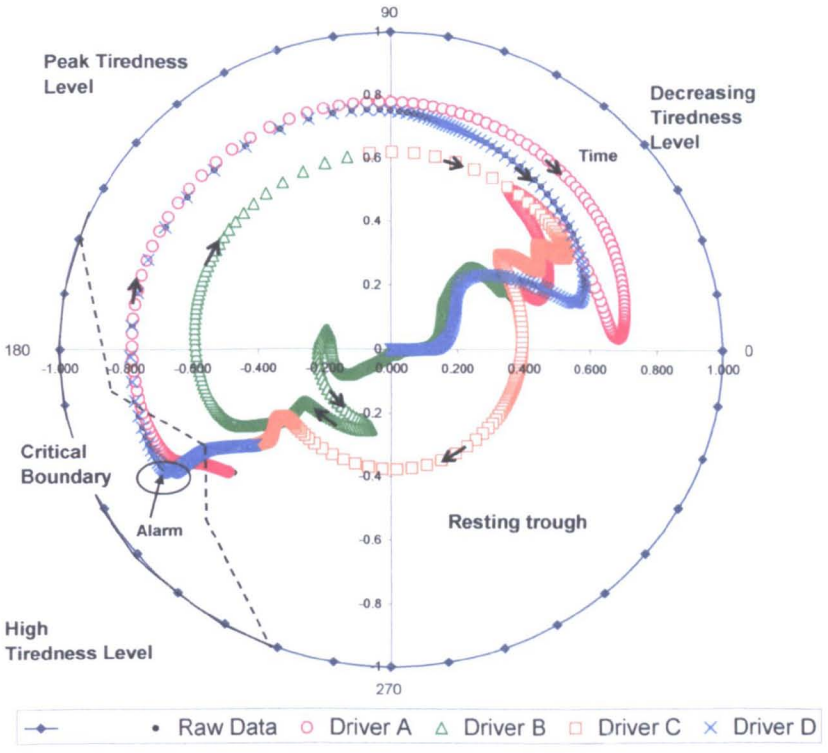

Figure 11.3.2.1 Chromatic polar-diagram H-L for the overall output signal of Figure

11.3.1.2.
(Different symbols corresponds to various drivers A-D, figure 11.3.1.2)
(Koh et al, 2007, With Permission)

The approach towards excessive fatigue is indicated by values of the H:L coordinates 210 degrees:0.8 which can raise an alarm [Koh et al 2007]. A threshold curve can be established mainly within the third quadrant (180<H<270 degrees) and with H~0.8 which serves to define the physiologically determined fatigue boundary.

11.3.3. Physical Indicators

The output signal from the gyroscope is in the form of a series of pulses as shown on Figure 11.3.1.2 superimposed upon the overall physiological curves. An expanded example of the gyroscope output in isolation and over a smaller time period, whose the existence of a number of different pulses produced by various road conditions (Figure 11.3.3.1(a)) These include signals when negotiating speed bumps, roundabouts etc as well as fatigue simulated swerves.

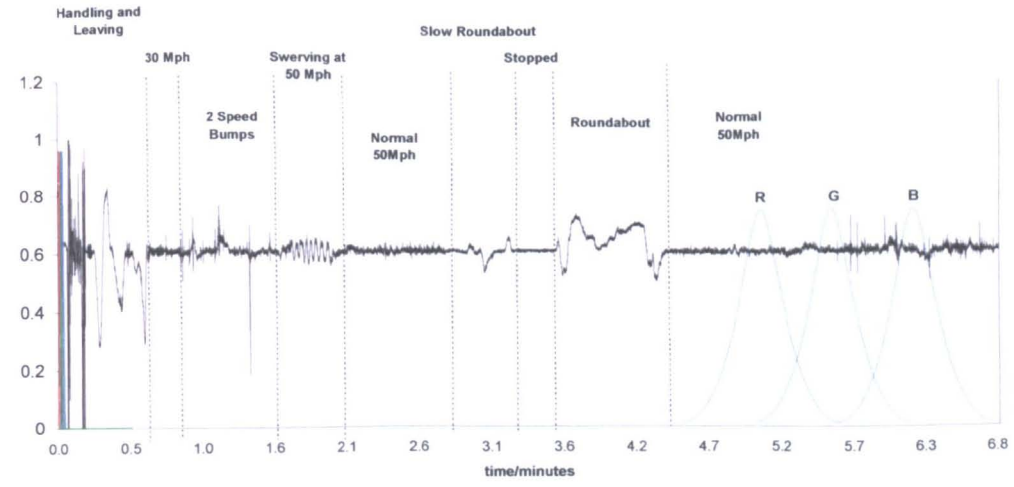

(a)

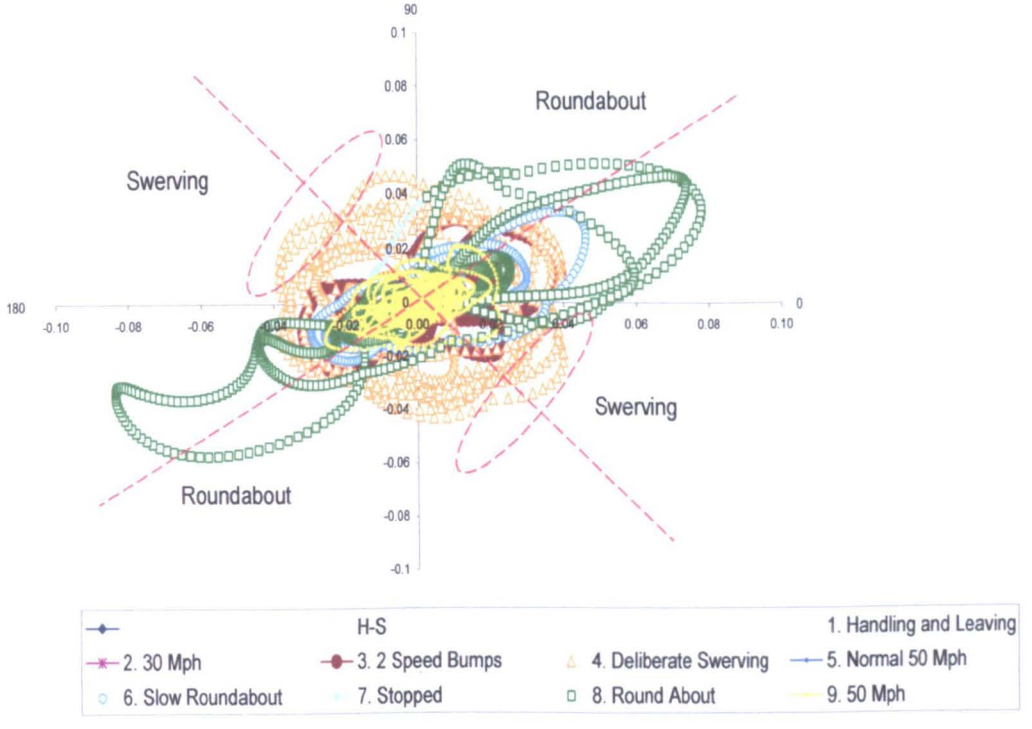

(b)

Figure 11.3.3.1 Chromatic Processing of gyroscope signals
(a) Gyroscope output showing different signals associated with various driving features
(b) H-S polar diagram of the gyroscope output of figure 11.3.3.1(a)
(Different symbols indicate different manoeuvres)
(Koh et al, 2007, With Permission)

Signals of the form shown on Figure 11.3.3.1(b) [Koh et al 2007] may be chromatically transformed by time stepping three non-orthogonal processors (R, G, B)

(Chapter 10, section 10.2, figure 10.2.1 (iv)) along the time axis. Such a procedure shows that the fatigue related swerves have particular chromatic H and S parameter variations which distinguish them from other gyroscope output signals. This results from the particular manner in which the vehicle steering wheel is moved during the impulsive response of a driver emerging from a micro sleep period. Figures 11.3.3.2 (a) (b) show the correlation between the time variation of the steering wheel acceleration and velocity with chromatic saturation and lightness respectively

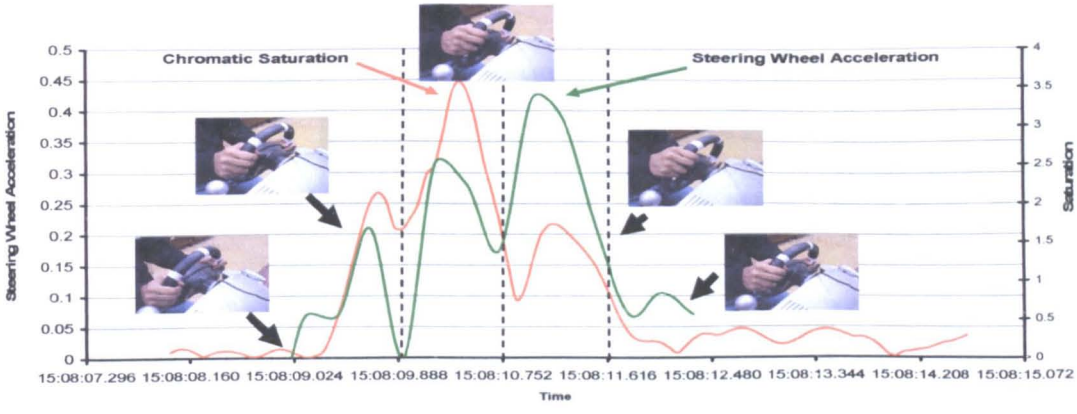

(a)

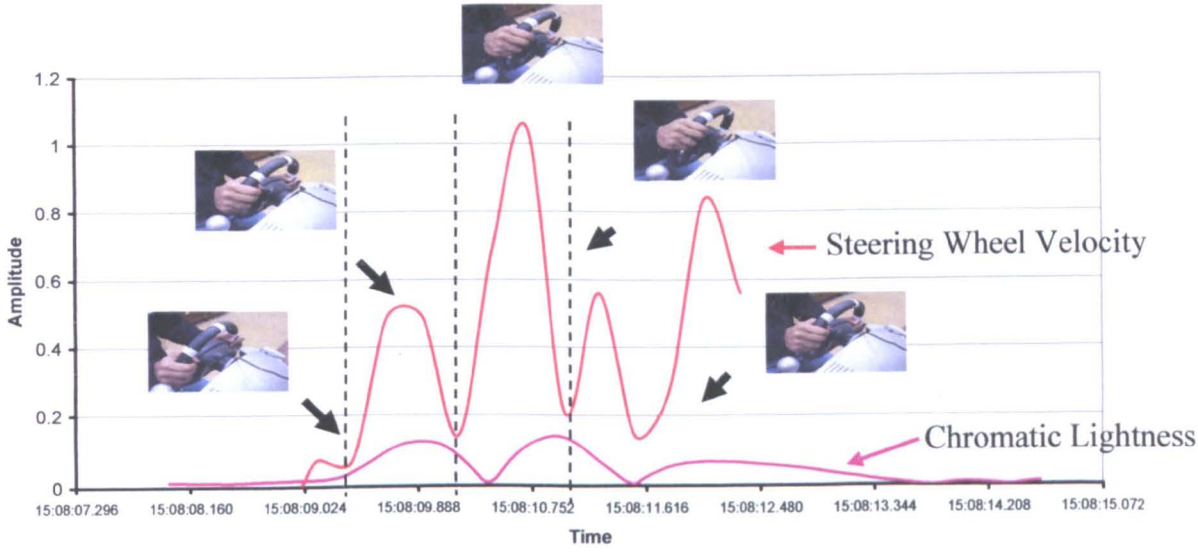

(b)

Figure 11.3.3.2 Correlation of gyroscope signals with steering wheel movement
(a) Correlation between the time variations of the steering wheel Acceleration and chromatic saturation
(b) Correlation between the time variations of the velocity and lightness

For real time, on line operation it is sufficient to set threshold to the magnitudes of chromatic L and S above which the signal is regarded as being due to fatigue induced swerving. An example of the application of this condition to real time gyroscope pluses transformed to S and L as functions of time, shows that fatigue induced signals can be identified (Figure 11.3.3.3)

A number of tests have shown that the L and S threshold apply regardless of change of driver, vehicle, weather conditions or traffic density [Koh et al 2007]

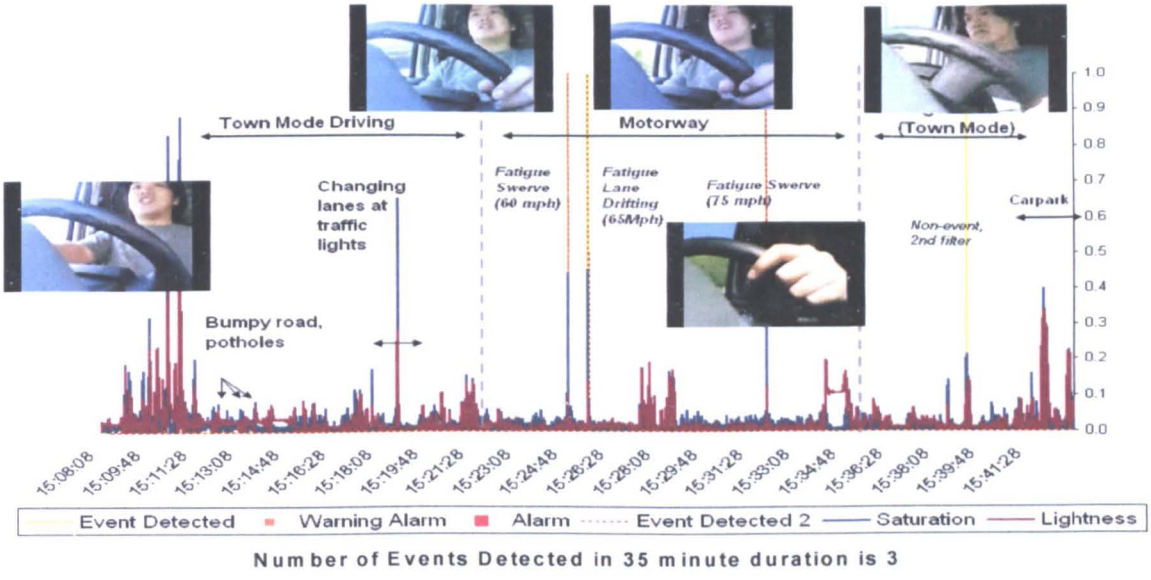

Figure 11.3.3.3 Real time chromatic analysis of the gyroscope output

11.3.4 Correlation between Physical and Physiological indicators

Whereas the physiological indicators of fatigue are that the relevant L and H chromatic parameters should exceed their threshold value. The physical indicator L and S not only need to exceed their threshold but need to do so a number of times. Correlation of the physiological and physical indicators may be considered in terms of chromaticity based probability factors [Zhang et al 2005] whereby the physiological factor depends upon L and H but the physical factor is based upon the number of L, S identified pulses in a given time period

This illustrates how a chromatic approach improves upon the simple expedient of summing the amplitudes of signal voltages without regard to distinguishing the cause of the latter (Figure 11.3.3.3).

11.4 Summary

The chromatic methodology may be deployed for addressing behavioural trends with minimal intrusion on personal privacy but in an economic and information efficient manner. Two examples (assistive care of the elderly and infirm; fatigue of road vehicle drivers) illustrate some of the different ways in which the methodology can be applied.

The assistive care application illustrates

- The use of chromatic signatures, in the optical domain, of a limited number of locations (~20) for indicating the presence of objects/persons (from the points eclipsed) and addressing specific functions at particular locations (e.g. temperature, TV on/off, door opening etc).
- The use of the chromatic space domain in conjunction with the time change of optical domain chromatic signatures at various locations for qualifying the general activity of an individual in terms of L (level of activity), H (dominant location of activity) and S (the extent to which activity is distributed amongst different locations)
- The combination of optical and space domain chromaticity with PIR space chromaticity to enhance the distinction between the movement of an individual and artefacts (such as ambient light changes, fluttering curtains etc), the level of immobility of an individual, the control of light switching for different levels of activity checking at night time etc.
- The conservative approach to information and system economics which enables multiplexing of several sites to occur within acceptable time scales and costs.

These various aspects are summarised on Table 11.4.1

Chromatic Domain	Individual Capabilities	Combined capabilities
Optical (Wavelength)	• Detailed locations • Specific functions (e.g. Door, TV, Temperature etc) • Moderate time response	
Optical (Spatial)	• Detailed Activity • Immobility (inc. Fall) • First Level Artefacts (e.g. Ambient Light, Inanimate Objects)	
Single PIR (none)	• Moving Person (NO spatial Resolution) • Stationary Person • Rapid Time Response	• Good time/location compromise • Activity/immobility confirmation • Much improved night operation (inc. light control) • Improved Artefact discrimination

Trefoil PIR (Spatial)	• Moving Person • Coarse Location/activity • Convenient night operation • Rapid time response	

Table 11.4.1 Comparison of Individual and Combined Capabilities of Various Chromatic Domains

The driver fatigue application indicates:

- the use of time stepped chromatic processing of the lateral movement of a vehicle can distinguish physiologically induced responses from drivers becoming increasingly fatigued independent of person, vehicle or weather.
- That empirically determined fatigue contributing factors (e.g. Circadian rhythm, period driving) may be transformed with chromatic time domain stepping to provide indications of fatigue variations.
- The trend towards high levels of fatigue may express in terms of probability functions based upon chromatic parameters form the vehicle movement and empirical considerations.

A summary of these aspects is given on Table 11.4.2.

Chromatic Domain	Fatigue Indicator	Chromatic Parameters	
		Individual	Combined
Time Stepped	Physical (Lateral Movement)	Number of Swerves (N) with Specific L, S values above threshold	
Time Stepped	Physiological (Circadian Rhythm, driving period)	H_{CR}, S_{CR} approaching threshold levels	

Table 11.4.2 Chromatic Parameters of Physical and Physiological Indicators of Fatigue

References

Carron T and Lambert P (1994)
Color Edge Detector Using Jointly Hue, Saturation and Intensity
IEEE Int. Conf. on Image Processing pp 977-981

Dony R D and Wesolkowski S (1999)
Edge Detection on Color Images Using RGB Vector Angle
Proc. IEEE CCECE'99 Canada

Horne, J.A.(2001)
Sleep-related vehicle accidents: *some guidelines for road safety policies.*
Transportation Research - Part F, 4: 63-74.

Horne J.A. & Reyner L.A. (1995(a))
Driver sleepiness.
Journal of Sleep Research, 4 (Suppl 2) 23-29.

Horne J.A. & Reyner L.A. (1995(b))
Sleep Related Vehicle Accidents.
British Medical Journal, 1995, 310, (6979), 565-567.

Koh, A., Jones, G.R., Spencer J.W. and Thomas I. (2007)
Chromatic analysis of signals from a driver fatigue monitoring unit,
Meas. Sci. Technol. 18, 1–8

Reyner L.A. & Horne J.A. (1998)
Falling Asleep Whilst Driving: Are Drivers Aware Of Prior Sleepiness?
International Journal of Legal Medicine. 111: 120-123.

Smith D.H. (2003)
Video Multiplexer Unit,
Private Communication

Smith D.H (2005)
Mechanical Fixtures for PIRCS,
Merton Projec

Wesolkowski S and Jernigan E (1999)
Color Edge Detection in RGB Using Jointly Euclidean Distance and Vector Angle
Proc. IAPR Vision Interface Canada pp 9-16

Wong K (2006)
Chromatic Monitoring of Living Environment,
PhD Thesis .

Wong K, Xu S, Jones G. R. (2005)
Chromatic Identification of Complex Movement Patterns,
Proceeding International Conference on Complexity in Science, Medicine and Sociology, the Centre for Complexity Research, Liverpoo

Xu S (2004)
Chromatic System For Care Society,
PhD Thesis

Xu S and Jones G R (2006)
Event and movement monitoring using chromatic methodologies
IoP J. of Measurement Science and Technology **17** 3204-3211

Yang C (2007)
Occupant's Behavioural Pattern Measurement,
Private Communication

Zhang J, Jones, G. R., Deakin, A. G. and Spencer, J. W. (2005)
Chromatic processing of DGA data produced by partial discharges for the prognosis of HV transformer behaviour, *Meas. Sci. Technol.* 16 556-561

References

A

[Australian Transport Safety Bureau, 1996]
Australian Transport Safety Bureau
Road Crash Costs in Australia Report 102, 1996

[Addision, 2002]
Paul S. Addison
'The Illustrated Wavelet Transform Handbook',
Institute of Physics, ISBN 0-7503-0692-0, 2002

[Altun, 2007]
Altun A, Ugur-Altun B
'Melatonin: therapeutic and clinical utilization',
Int. J. Clin. Pract. 61 (5): 835–45, 2007

B

[Bastiaas, 1994]
Bastiaas M.J.
'Gabor's signal expression and Zak transform',
Applied optics, Vol.33, no.23, pp. 5242-5255, 1994

[Baulk et al, 2001]
Baulk, S.D., Reyner L.A. & Horne J.A.
'Driver Sleepiness: Evaluation of Reaction Time Measurement as a Secondary Task',
Sleep, 24(6): 695-698. , 2001

[Brazier et al, 2001]
Brazier K J, Deakin A G, Cooke R D, Russell P C and Jones G R
'Colour space mining for industrial monitoring Data Mining for Design and Manufacturing',
Massive Computing Series vol 3 ed D Braha (Dordrecht,The Netherlands: Kluwer), 2001

[Bilcoe et al, 2002]
Blincoe, L. J., Seay, A., Zaloshnja, E., Miller, T. R., Romano, E., Luchter, S., et al.
'The economic impact of motor vehicle crashes',
Washington, DC: National Highway Traffic Safety Administration. , 2002

[Barroquiro and Jones, 2004]
S Barroqueiro and G R Jones,
'Chromatic single point sensor for aircraft fuel systems',
Meas. Sci. Technol. 15 814–820, 2004

C

[Cooper, 1986]
Cooper J
'Electrocardiography 100 years ago, origins, pioneers, and contributors',
N Engl J Med 315 (7): 461-4, 1986

D

[Dean, 2004]
Dean E.M
'Non-Intrusive passive flow acoustic monitoring of liquid flow systems',
PhD Thesis University of Liverpool, 2004

[Du, 2004]
Du X
'Application of Chromaticity',
PhD Thesis University of Liverpool, 2004

[Dinges, 2005]
David F. Dinges
'Pilot Test of Fatigue Management Technologies',
R&T:Today and Tomorrow, Washington, DC, TRB report, January 9, 2005

[Deakin et al, 2005]
Deakin, A.G, Rallis I, Zhang I, Spencer J.W & Jones G.R,
'Towards Holistic Chromatic Intelligent Monitoring of Complex system',
A Chromatic Approach to Complexity, Proceedings of the Complex Systems Monitoring Session of the International Complexity, Science and Society Conference, Liverpool, , CIMS Centre for Intelligent Monitoring Systems, 2005

[Dau et al; 2005]
Dau, V.T., Shiozawa , T., Dao, D.V., Kumagai, H. & Sugiyama, S.
'A dual axis gas gyroscope utilizing low-doped silicon thermistor'
Micro Electro Mechanical Systems, 2005. MEMS 2005. 18th IEEE International Conference, Issue , Page(s): 626 – 62, 930 Jan.-3 Feb. 2005

E

[Epstein, 1983]
Epstein, Charles M.
'Introduction to EEG and evoked potentials',

J. B. Lippincot Co. ISBN 0-397-50598-1., *1983*

[Evinger et al, 1991]
Evinger, C., K.A. Manning, P.A. Sibony
'Eyelid Movements: Mechanisms and Normal Data',
Invest Ophthal Vis Sci, vol. 32, pp.387-40, 1991

F

[Federal Motor Carrier Safety Adminstration, 2000]
Federal Motor Carrier Safety Administration
'Hours of service for drivers. Driver rest and sleep for safe operations'
DOT Report 49 CFR. Washington, DC: Department of Transportation. 2000

[Foster and Kreitzman 2004]
Russell Foster & Leon Kreitzman,
'Rhythms of Life',
Profile Books, London, 2004

G

[Gandevia et al, 1995]
Gandevia, S. C., Enoka, R. M., McComas, A. J., Stuart, D. G.and Thomas, C. K.
'Neurobiology of muscle fatigue - Advances and issues',
Advances in Experimental Medicine and Biology, vol. 384. pp. 515-25, 1995

[Gabarino et al, 2001]
Garbarino s, Nobili L, Beelke M, De Carli F, Balestra V, Ferrillo F
'Sleep related vehicle accidents on Italian highways',
G Ital Med Lav Ergon;23(4):430-4., 2001

[Gautschi, 2002]
Gustav H. Gautschi
'Piezoelectric Sensorics: Force, Strain, Pressure, Acceleration and Acoustic Emission',
Sensors, Materials and Amplifiers (Hardcover), ISBN-10: 3540422595, 2002

[Pavlath, 1994]
G.A. Pavlath,
'Fiber-optic gyroscopes',
IEEE Lasers and Electro-Optics Society (LEOS) Annual Meeting, Conference Proceedings, Volume 2, pages 237-238. 31 Oct-3 Nov 1994

H

[Hagberg 1981]
Hagberg, M.
'Muscular endurance and surface electromyogram in isometric and dynamic exercise',
Journal of Applied Physiology, vol. 51, pp. 1-7, 1981

[Hamelin, 1987].
Hamelin, P.
'Lorry drivers' time habits in work and their involvement in traffic accidents',
Ergonomics 30(9), 1323-133,. 1987

[Horne and Reyner, 1995]
Horne J.A. & Reyner L.A.
'Sleep Related Vehicle Accidents',
British Medical Journal, 310, (6979), 565-567, 1995

[Hawley and Reilly, 1997]
Hawley, JA & Reilly, T.
'Fatigue revisited',
Journal of Sport Science, vol. 15, pp. 245-246, 1997

[Horne, 2001]
Horne, J.A.
'Sleep-related vehicle accidents: some guidelines for road safety policies',
Transportation Research - Part F, 2001, 4: 63-74, 2001

[Halberg et al, 2003]
Franz Halberg , Germaine Cornélissen , George Katinas
'Tran disciplinary unifying implications of Circadian findings in the 1950',
Journal of Circadian Rhythms, 1:2 doi: 10.1186/1740-3391-1-2, 2003

[Horne and Baulk, 2003]
Horne J.A. & Baulk S.D.
'Awareness of sleepiness when driving',
Psychophysiology, 2003, 41: 161-165, 2003

[Horne et al, 2003]
Horne J.A., Reyner L.A., & Barrett P.R.
'Driving impairment due to sleepiness is exacerbated by low alcohol intake',
Occupational & Environmental Medicine, 60: 689-692, 2003,

J

[Jones and Russel, 1993]
Jones G R and Russell P C
'Chromatic modulation based metrology',
Pure Appl. Opt. 2 87–110, 1993

[Jones et al, 2000]
G.R. Jones, P.C. Russell, A. Vourdas, J. Cosgrave, L. Stergioulas and R. Harber
'The Gabor Transform Basis of Chromatic Monitoring',
Measurement Science and Technology, vol. 11, no. 5, pp.489-498, 2000

[Jones et al, 2003]
Jones G.R., Deakin A.G., Yan J.D. and Spencer J.W.

'Prognostic Intelligent Monitoring of Energy Systems',
Ed. Colette R. Benson, Proceedings of Euro TechCon 2003, pp 157-178, November 5-6, 2003, Manchester, TJ/H2b Analytical Services Inc, 2003.

[Johns 2003a]
Johns, M.W
'The Amplitude-Velocity Ratio of Blinks: A new Method for Monitoring Drowsiness',
Sleep, vol. 26 (Suppl), pp.A51-52, 2003

[Johns 2003b]
Johns, M.W
'Eyelid Closure, Visual Suppression and Hypovigilance in the Drowsy State: Lapses in Performance with Eyes Open or Closed',
Sleep, vol.26 (Suppl),p.A52. 2003

[Jones et al, 2005]
Jones G.R, Deakin, A.G, Spencer J.W,
'Multistimulus Chromatic Processing of Complex Signal',
A Chromatic Approach to Complexity, Proceedings of the Complex Systems Monitoring Session of the International Complexity, Science and Society Conference, Liverpool, , CIMS Centre for Intelligent Monitoring Systems, 2005

[Jammes 2006]
Bruno Jammes
'EEG/EOG processing for computing sleepiness level',
Abstract Book for International Conference for the EU 6th framework integrated project SENSATION on Monitoring Sleep and sleepiness- from physiology to new sensors 2006

[Jones et al, 2007]
Jones G.R, A., Deakin . & Spencer, J.W
'Chromatic monitoring of complex systems',
Taylor and Francis, ISBN: 9781584889885, In the press, 2008

[James, 1996]
Glyn James
'Modern Engineering Mathematics',
Addison Wesley, ISBN 0-201-87761-9, 1996

K

[Kecklund and Åkerstedt, 1995]
Kecklund, G. & Åkerstedt, T.
'Time of day and Swedish road accidents',
Shiftwork International Newsletter 12(1), 31, 1995

[Kolupula, et al, 2005]
'Chromatic Methodologies for information extraction from complex data sets',

A Chromatic Approach to Complexity, Proceedings of the Complex Systems Monitoring Session of the International Complexity, Science and Society Conference, Liverpool, , CIMS Centre for Intelligent Monitoring Systems, 2005

[Koh et al, 2005]
Koh A, Dean.E., Zhang I, Jones G.R & Spencer J.W
'Effect of Chromatic filter characteristics in quantifying complex data',
A Chromatic Approach to Complexity, Proceedings of the Complex Systems Monitoring Session of the International Complexity, Science and Society Conference, Liverpool, , CIMS Centre for Intelligent Monitoring Systems, 2005

[Koh et al 2007]
Koh A, Jones G.R, Spencer J.W, Thomas I
'Chromatic analysis of signals from a driver fatigue monitoring unit',
Meas. Sci. Technol. 18, 747–754, 2007

L

[Looe et al, 2005]
Looe H. M, Lappas C, Spencer, J.W, Jones, G. R,
'Location Determination of an Entity by remote chromatic processing of its emanations',
A Chromatic Approach to Complexity, Proceedings of the Complex Systems Monitoring Session of the International Complexity, Science and Society Conference, Liverpool, , CIMS Centre for Intelligent Monitoring Systems, 2005

M

[Miles, 1929]
Miles, Walter
'Sleeping with the Eyes Open',
Scientific American June, pp. 489-492. Reed, G. (1972)

[Mackie and Miller, 1978]
Mackie, R.R. & Miller, J.C. ()
'Effects of hours of service regularity of schedules and cargo loading on truck and bus driver fatigue',
DOT Report No. HS-803 799. Washington, US Department of Transportation, 1978

[Muller & Insua, 1995]
Muller, P. & Insua, D.R.
'Issues in Bayesian Analysis of Neural Network Models',
Neural Computation 10: 571–59, 1995

[Muzet 2004]
Muzet
'Precursors and Indicators of Driver Fatigue and Sleepiness Simulator Studies Fatigue, sleepiness and reduced alertness as risk factors in driving',

N

[National Sleep Foundation]
National Sleep Foundation
'Survey of Motorists' Attitudes to Road Safety: The Largest & Most Comprehensive Ever Undertaken in Ireland',
http://www.sleepfoundation.org/site/c.huIXKjM0IxF/b.2419073/k.77AF/Drowsy_Driving_Surveys.htm

[NEC]
http://www.nec-tokin.com/english/product/piezodevice2/ceramicgyro.html

[Namias, 1980]
V. Namias,
'The fractional order Fourier transform and its application to quantum mechanics',
J. Inst. Appl. Math. 25, 241–265, 1980.

[Norman, 2000]
Phillips, Norman A.,
'An Explication of the Coriolis Effect',
Bulletin of the American Meteorological Society: Vol. 81, No. 2, pp. 299–303. 2000

[New York State Department of Motor Vehicles, 2007]
New York State Department of Motor Vehicles
'Drowsy Driving & Fatigue',
Governor's Traffic Safety Committee Report, April 03, 2007

O

[Ohmi, 2006]
Takuhiro Ohmi
'Driver sleepiness detection by video processing',
Abstract Book for International Conference for the EU 6th framework integrated project SENSATION on Monitoring Sleep and sleepiness- from physiology to new sensors 2006

P

[Pernix 2005]
'White Paper',
http://www.pernix.co.uk/

[Papoulis and Pillai, 2002]
Papoulis A and Pillai S U
'Probability, Random Variables and Stochastic Processes' ,

4th edn Boston, MA:McGraw-Hill, 2002

[Paul et al, 2005 a]
Amit Paul, Linda Ng Boyl1, Erwin R. Boer, Jon Tippin, Matthew Rizzo
'Steering Entropy changes as a function of microsleeps',
Proceedings of the Third International Driving Symposium on Human Factors in Driver Assessment, Training and Vehicle Design, 2005

[Paul et al, 2005 b]
Amit Paul, Linda Ng Boyle, Jon Tippin, Matthew Rizzo
'Variability of driving performance during microsleeps',
Proceedings of the Third International Driving Symposium on Human Factors in Driver Assessment, Training and Vehicle Design, 2005

[Postnote, 2005]
'The 24 Hour Society',
Parliament office of science and technology report, Number 250, November 2005

R

[RAC]
'RAC's Fleet statistics'
http://www.rac.co.uk/business/information/fleet_statistics;jsessionid=8F5DCD3C7712992E2EF0DECDDC5484F1

[Reilly et al, 1982]
Reilly, D.L., Cooper, L.N. & Elbaum, C.
'A Neural Model for Category Learning',
Biological Cybernetics 45: 35–41, 1982

[Reyner and Horne 1997]
Reyner L.A. & Horne J.A.
'Caffeine combined with a short nap effectively counteracts driver sleepiness',
Psychophysiology, 1997, 34, pp 721-725, 1997

[Reyner and Horne 1998 a]
Reyner L.A. & Horne J.A.
'Falling Asleep Whilst Driving: Are Drivers Aware Of Prior Sleepiness?'
International Journal of Legal Medicine. 1998, 111: 120-123, 1998

[Reyner and Horne 1998 b]
Reyner L.A. & Horne J.A.
'Evaluation of "In Car" Countermeasures to Driver Sleepiness: Cold Air and Radio'
Sleep, Vol. 21, No.1, pp46-51 , 1998

[Russel et al, 1999a]
Russell P.C.1; Haber R.; Jones G.R.; McGrory W.
'A chromatically addressed optical fibre sensor for non-contact temperature monitoring',

Sensors and Actuators A: Physical, Volume 76, Number 1, 30, pp. 231-240(10), 1999

[Russel et al, 1999b]
Russell, P.C., Craven, A., Deakin, A., Cooke, R., Furlong, S., Spencer, J.W. and Jones, G.R.
'Intelligent chromatic monitoring of industrial plant',
Sensors and their Applications X, Eds. N M White and J T Augousti, Proceedings of the Tenth Conference on Sensors and their Applications, Cardiff, Institute of Physics Publishing, Bristol, pp. 245-250, 5-8 September 1999

[Reyner and Horne 2000]
Reyner L.A. & Horne J.A.
'Early Morning Driver Sleepiness: Effectiveness of 200mg Caffeine',
Psychophysiology, 37: 251-256, 2000

[Risser et al, 2000]
Risser, M. R., Ware, J. C., & Freeman, F. G.
'Driving simulation with EEG monitoring in normal and obstructive sleep apnoea patients',
Sleep, 23(3): 393-398, 2000

S

[Sleeptracker]
www.sleeptracker.com

[Stern et al, 1994]
Stern JA, Boyer D, Schroeder D.
'Blink rate: a possible measure of fatigue',
Hum Factors. Jun;36(2):285-9,. 1994

[Stergioulas 1997]
Stergioulas L.K.,
'Time-frequency methods in optical signal processing',
Ph.D Thesis, the University of Liverpool, 1997

[Stutts et al, 1999]
Jane C. Stutts, Jean W. Wilkins and Bradley V. Vaughn
'Why Do People Have Drowsy Driving Crashes?',
AAA Foundation for Traffic Safety report, 202/638-5944, November 1999

[Sagberg 1999]
Sagberg, F
'Road accidents caused by drivers falling asleep',
Accident Analysis and Prevention 31(6), 639-649. 1999

[Sagberg et al, 2004]
Fridulv Sagberg, Paul Jackson, Hans-Peter Krüger, Alain Muzet, Adrian Williams
'Fatigue, sleepiness and reduced alertness as risk factors in driving',

TØI report 739/2004

[Stengel, 2004]
Stengel R F:
'Flight Dynamics',
Princeton University Press, ISBN 0-691-11407-2, 2004

[Serway and Jewett, 2004]
Serway, Raymond A.; Jewett, John W
'Physics for Scientists and Engineers (6th ed.)',
Brooks/Cole. ISBN 0-534-40842-7, 2004

[Staner et al, 2005]
Staner Luc; Ertle Stéphane; Boeijinga Peter ; RINAUDO Gilbert
'Next-day residual effects of hypnotics in DSM-IV primary insomnia: a driving simulator study with simultaneous electroencephalogram monitoring',
Psychopharmacologia ISSN 0033-3158 2005, vol. 181, no4, pp. 790-798, 2005

T

[Turkingtona et al, 2001]
P M Turkingtona, M Sircara, V Allgarb, M W Elliotta
'Relationship between obstructive sleep apnoea, driving simulator performance, and risk of road traffic accidents',
Thorax;56:800-805 October, 2001

[Schilovsky, 1992]
Schilovsky P P
'The Gyroscope, Its construction and Practical Application',
E Spon Publications 1922

W

[Wilson, 1995]
R. G. Wilson,
'Fourier Series and Optical Transform Techniques in Contemporary Optics',
Wiley. ISBN-10: 0471303577, 1995

[Wright 2006]
Nicky Wright
'Use of the EEG and EOG to evaluate alertness devices: description of methodology and a demonstration',
Abstract Book for International Conference for the EU 6th framework integrated project SENSATION on Monitoring Sleep and sleepiness- from physiology to new sensors, 2006

[Wong et al, 2005]
K. Wong, S. Xu and G.R. Jones
'Chromatic Identification of Complex Movements Patterns',

A Chromatic Approach to Complexity, Proceedings of the Complex Systems Monitoring Session of the International Complexity, Science and Society Conference, Liverpool, , CIMS Centre for Intelligent Monitoring Systems, 2005

Y

[Y Hino et al, 2007]
Y Hino and T Kurosawa
'Traceability of radiation protection instruments',
Metrologia 44 S146-S152, 2007

Z

[Zhang et al, 2005]
J. Zhang, G.R. Jones, A. Deakin and J.W. Spencer ,
'Chromatic processing of DGA data produced by partial discharges for the prognosis of HV transformer behaviour',
Meas. Sci. Technol. 16 (2005) 556–561, 2005

Appendices

- **A- Nec Gyroscope Specification Sheet**
- **B- USB 1208FS Data Sheet**
- **C- ASTiD Data Sheet**
- **D- Sleeptracker Information**
- **E- Flow-Chart for the gyroscope system live-monitoring software**

Devices thru Material Innovation

NEC/TOKIN

Vol.01

NEW PRODUCT INFORMATION

Outline

Miniature angular rate sensors with a very simple construction are made of a single piezoelectric ceramic column printed with electrodes. High reliability is achieved by using Tokin's high performance piezoelectric ceramics.

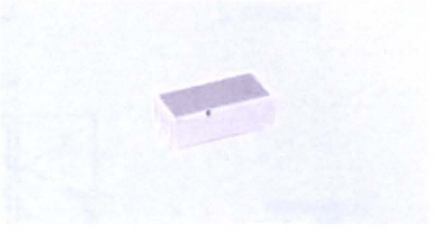

Features

- Miniature size
- High-speed response
- Magnetic field proof

Applications

- Shake detector for hand-held video cameras, cameras, and binoculars
- Gyroscope in radio-controlled helicopters
- Data entry equipment such as a mouse

Specifications

Model	Supply voltage (V)	Reference voltage output (V)	Current consumption (mA)max.	Maximum detectable angular rate (deg/sec) 25 °C	Sensitivity (mV/deg/sec) 25 °C	Output voltage at zero angular rate (mV)max. 25°C	Output voltage at zero angular rate (mV)max. Any temperature	Temperature characteristics of sensitivity (%)	Frequency response (Hz)min. -90deg	Dimensions (mm)
CG-L43	+3	+1.3	4	±90	0.66±20%	±300	±500	±15	100	8×16×5

* Operating temperature range -5~75℃
* Storage temperature range -40~80℃

Ceramic Gyro

■ Shapes and Dimensions

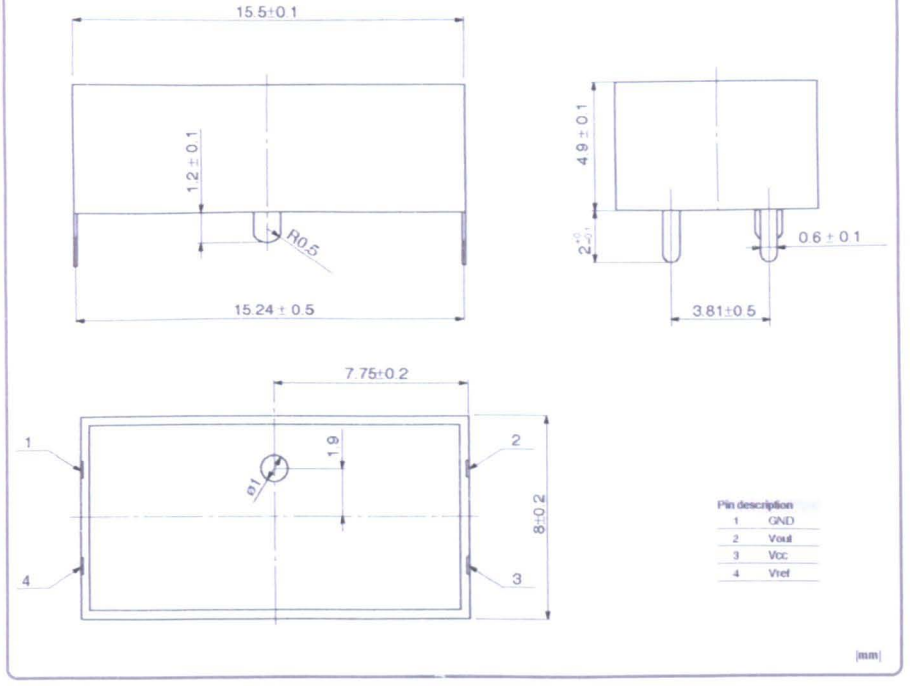

Pin description	
1	GND
2	Vout
3	Vcc
4	Vref

[mm]

NEC TOKIN Corporation

Precautions

- The names of the products and the specifications in this catalog are subject to change without notice for the sake of improvement. The manufacturer also reserves the right to discontinue any of these products. At the time of delivery, please ask for specifications sheets to check the contents before use.
- Descriptions in this catalog regarding product characteristics and quality are based solely on discrete components. When using these components, be sure to check the specifications with the component in question mounted on the products.
- The manufacturer's warranty will not cover any disadvantage or damage caused by improper use of the products that deviates from the characteristics, specifications, or conditions for use described in this catalog.
- The products in this catalog are intended for use in ordinary electronic products. If any of these products are to be used in special applications requiring extremely high reliability, where product defects might pose a safety risk, please consult your NEC TOKIN sales representatives.
- Though the manufacturer has taken all possible precautions to ensure the quality and reliability of its products, improper use of products may result in bodily injury, fire, or similar accident. If you have any questions regarding the use of the products in question, please consult your NEC TOKIN sales representatives.
- Please be advised that the manufacturer accepts no responsibility for any infraction by users of this manufacturer's products on third party patents or industrial copyrights. The manufacturer is responsible only when such infractions are attributable to the structural design of the product and its manufacturing process.
- Should any of these products be considered as strategic goods, and thereby governed by foreign exchange or foreign trade regulations, the Government of Japan will require an export license before said products can be exported outside Japan.
- This catalog is current as of March 2002.

International Business Headquarters Phone:81-3-3402-6179
Seoul Branch Phone:82-2-551-3693
NEC TOKIN America Inc. Phone:1-610-224-4110
Eastern Area Sales Office (Chicago Office) Phone:1-847-215-8802
Southwest Regional Sales (San Diego Office) Phone:1-760-494-5044
Southeast Regional Sales (Tampa Office) Phone:1-813-261-1163
NEC TOKIN Hong Kong Ltd. Phone:852-2730-3228
Shanghai Representative Office Phone:86-21-6415-0602
Shenzhen Representative Office Phone:86-755-246-9011
NEC TOKIN Singapore Pte.Ltd. Phone:65-6225-7076
Malaysia Branch Phone:60-3-620-10702
Bangkok Representative Office Phone:66-2-260-7017
NEC TOKIN Taiwan Co., Ltd. Phone:886-2-2521-3988
NEC TOKIN Europe GmbH Phone:49-2131-7998-0
NEC TOKIN UK Ltd. Phone:44-1926-410306
Cardiff Branch Phone:44-29-2078-6662

International Business Headquarters
5-9, Kita-Aoyama 7-chome, Minato-ku, Tokyo 107-8580, Japan
Phone: 81-3-3402-6179 Fax: 81-3-3402-6172

For inquiries, please call the Sales Promotion Department (Japan)
Phone: 81-3-0000-0000 Fax: 81-3-0000-0000

http://www.nec-tokin.com

Cat. No. PD-0E7E

Specifications

USB-1208FS

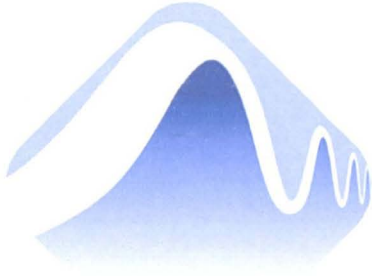

MEASUREMENT COMPUTING™

Document Revision 1.3, July, 2007

Specifications

Typical for 25°C unless otherwise specified.
Specifications in *italic text* are guaranteed by design.

Analog input

Table 1. Analog input specifications

Parameter	Conditions	Specification
A/D converter type		Successive approximation type
Input voltage range for linear operation, single-ended mode	CHx to GND	±10 volts (V) max
Input common-mode voltage range for linear operation, differential mode	CHx to GND	-10 V min, +20 V max
Absolute maximum input voltage	*CHx to GND*	*±28 V max*
Input impedance		*122KOhm*
Input current (Note 1)	Vin = +10 V	70 microamperes (µA) typ
Vin = 0 V	-12 µA typ	
Vin = -10 V	-94 µA typ	
Number of channels		8 single-ended / 4 differential, software selectable
Input ranges, single-ended mode		±10 V, G=2
Input ranges, differential mode		±20 V, G=1 ±10 V, G=2 ±5 V, G=4 ±4 V, G=5 ±2.5 V, G=8 ±2.0 V, G=10 ±1.25 V, G=16 ±1.0 V, G=20 Software selectable
Throughput (Note 2)	Software paced	250 samples per second (S/s) typ, PC-dependent
Continuous scan	50 kilosamples per second (kS/s)	
Channel gain queue	Up to 16 elements	Software configurable channel, range, and gain.
Resolution (Note 3)	Differential	12 bits, no missing codes
Single-ended	11 bits	
CAL accuracy	CAL = 2.5 V	±36.25 mV max
Integral linearity error		±1 least significant bit (LSB) typ
Differential linearity error		±0.5 LSB typ
Repeatability		±1 LSB typ
CAL current	Source	5 milliamperes (mA) max
Sink	20 µA min, 100 µA typ	
Trigger source	Software selectable	External digital: TRIG_IN
Pacer source	Software selectable	Internal External (SYNC), rising edge triggered Programmed IO

Input current is a function of applied voltage on the analog input channels. For a given input voltage, V_{in}, the input leakage is approximately equal to $(8.181*V_{in}-12)$ µA.

Maximum throughput scanning to PC memory is machine dependent. The rates specified are for Windows XP only. Maximum rates on operating systems that predate XP may be less and must be determined through testing on your machine

The AD7870 converter only returns 11-bits (0-2047 codes) in single-ended mode.

Table 2. Accuracy, differential mode

Range	Accuracy (LSB)
±20 V	5.1
±10 V	6.1
±5 V	8.1
±4 V	9.1
±2.5 V	12.1
±2 V	14.1
±1.25 V	20.1
±1 V	24.1

Table 3. Accuracy, single-ended mode

Range	Accuracy (LSB)
±10 V	4.0

Table 4. Accuracy components, differential mode - All values are (±)

Range	% of Reading	Gain Error at full scale (FS) (millivolts (mV))	Offset (mV)	Accuracy at FS (mV)
±20 V	0.2	40	9.766	49.766
±10 V	0.2	20	9.766	29.766
±5 V	0.2	10	9.766	19.766
±4 V	0.2	8	9.766	17.766
±2.5 V	0.2	5	9.766	14.766
±2 V	0.2	4	9.766	13.766
±1.25 V	0.2	2.5	9.766	12.266
±1 V	0.2	2	9.766	11.766

Table 5. Accuracy components, single-ended mode - All values are (±)

Range	% of Reading	Gain Error at FS (mV)	Offset (mV)	Accuracy at FS (mV)
±10 V	0.2	20	19.531	39.531

Table 6. Noise performance, differential mode

Range	Typical counts	Least significant bit $_{\text{root mean square}}$ (LSB_{rms})
±20 V	2	0.30
±10 V	2	0.30
±5 V	3	0.45
±4 V	3	0.45
±2.5 V	4	0.61
±2 V	5	0.76
±1.25 V	7	1.06
±1 V	8	1.21

Table 7. Noise performance, single-ended mode

Range	Typical Counts	LSB_{rms}
±10 V	2	0.30

Analog output

Table 8. Analog output specifications

Parameter	Conditions	Specification
Resolution		12-bits, 1 in 4096
Output range		*0 – 4.096 V, 1 mV per LSB.*
Number of channels		2
Throughput (Note 4)	Software paced	250 S/s single channel typical, PC dependent
Single channel, continuous scan	10 kS/s	
Dual channel, continuous scan, simultaneous update	5 kS/s	
Power on and reset voltage		Initializes to 000h code
Output drive	Each D/A OUT	15 mA
Slew rate		0.8V/microsecond (µs) typ

Maximum throughput scanning to PC memory is machine dependent. The rates specified are for Windows XP only. Maximum rates on operating systems that predate XP may be less and must be determined through testing on your machine.

Table 9. Analog output accuracy, all values are (±)

Range	Accuracy (LSB)
0-4.096 V	4.0 typ, 45.0 max

Table 10. Analog output accuracy components, all values are (±)

Range	% of FSR	Gain Error at FS (mV)	Offset (mV) (Note 5)	Accuracy at FS (mV)
0-4.096 V	0.1 typ, 0.9 max	4.0 typ, 36.0 max	1.0 typ, 9.0 max	4.0 typ, 45.0 max

Negative offsets will result in a fixed zero-scale error or "dead band." At the maximum offset of -9 mV, any input code of less than 0x009 will not produce a response in the output.

Digital input/output

Table 11. Digital I/O specifications

Digital type	CMOS
Number of I/O	16 (Port A0 through A7, Port B0 through B7)
Configuration	2 banks of 8
Pull up/pull-down configuration	All pins pulled up to Vs via 47K resistors (default). Positions available for pull down to ground. Hardware selectable via zero ohm (Ω) resistors as a factory option.
Input high voltage	2.0 V min, 5.5 V absolute max
Input low voltage	0.8 V max, –0.5 V absolute min
Output high voltage (IOH =	3.8 V min

-2.5 mA)

Output low voltage (IOL = 2.5 mA)	0.7 V max
Power on and reset state	Input

External trigger

Table 12. Digital trigger specifications

Parameter	Conditions	Specification
Trigger source (Note 6)	External Digital	TRIG_IN
Trigger mode	Software selectable	Edge sensitive: user configurable for CMOS compatible rising or falling edge.
Trigger latency		10 µs max
Trigger pulse width		1 µs min
Input high voltage		4.0 V min, 5.5 V absolute max
Input low voltage		1.0 V max, –0.5 V absolute min
Input leakage current		*±1.0 µA*

TRIG_IN is a Schmitt trigger input protected with a 1.5 kilohm (kΩ) series resistor.

External clock input/output

Table 13. External clock I/O specifications

Parameter	Conditions	Specification
Pin name		SYNC
Pin type		Bidirectional
Software selectable direction	Output (default)	Outputs internal A/D pacer clock.
Input		Receives A/D pacer clock from external source.
Input clock rate		50 KHz, maximum
Clock pulse width	Input mode	1 µs min
Output mode		5 µs min
Input leakage current	*Input mode*	*±1.0 µA*
Input high voltage		4.0 V min, 5.5 V absolute max
Input low voltage		1.0 V max, –0.5 V absolute min
Output high voltage (Note 7)	IOH = -2.5 mA	3.3 V min
No load		3.8 V min
Output low voltage (Note 7)	IOL = 2.5 mA	1.1 V max
No load		0.6 V max

SYNC is a Schmitt trigger input and is over-current protected with a 200 Ω series resistor.

Counter

Table 14. Counter specifications

Pin name (Note 8)	CTR
Counter type	Event counter

Number of channels	1
Input type	TTL, rising edge triggered
Input source	*CTR screw terminal*
Resolution	32 bits
Schmidt trigger hysteresis	*20 mV to 100 mV*
Input leakage current	*±1 μA*
Maximum input frequency	1 MHz
High pulse width	*500 ns min*
Low pulse width	*500 ns min*
Input high voltage	4.0 V min, 5.5 V absolute max
Input low voltage	1.0 V max, –0.5 V absolute min

CTR is a Schmitt trigger input protected with a 1.5K Ω series resistor.

Non-volatile memory

Table 15. Non-volatile memory specifications

EEPROM		1,024 bytes
EEPROM Configuration	**Address Range**	**Access** **Description**
0x000-0x07F	Reserved	128 bytes system data
0x080-0x1FF	Read/write	384 bytes cal data
0x200-0x3FF	Read/write	512 bytes user area

Microcontroller

Table 16. Microcontroller specifications

Type	*High performance 8-bit RISC microcontroller*
Program Memory	*16,384 words*
Data Memory	2,048 bytes

Power

Table 17. Power specifications

Parameter	**Conditions**	**Specification**
Supply current (Note 9)		80 mA
+5V USB power available (Note 10)	Connected to self-powered hub	4.5 V min, 5.25 V max
	Connected to externally-powered root port hub	
Connected to bus-powered hub	4.1 V min, 5.25 V max	
Output current (Note 11)	Connected to self-powered hub	420 mA max
	Connected to externally-powered root port hub	
Connected to bus-powered hub	20 mA max	

This is the total current requirement for the USB-1208FS which includes up to 10 mA for the status LED.

Self-powered hub refers to a USB hub with an external power supply. Self-powered hubs allow a connected USB device to draw up to 500 mA. *Root port hubs* reside in the PC's USB host controller. The USB port(s) on your PC are root port hubs. All externally powered root port hubs (desktop PCs) provide up to 500 mA of current for a USB device. Battery-powered root port hubs provide 100 mA or 500 mA,

depending upon the manufacturer. A laptop PC that is not connected to an external power adapter is an example of a battery-powered root port hub. *Bus powered hubs* receive power from a self-powered or root port hub. In this case the maximum current available from the USB +5 V is 100 mA. The minimum USB +5 V voltage level can be as low as 4.1 V.

This refers to the total amount of current that can be sourced from the USB +5 V, analog outputs and digital outputs.

General

Table 18. General specifications

Parameter	Conditions	Specification
Device type		USB 2.0 full speed
Device compatibility		USB 1.1, USB 2.0

Environmental

Table 19. Environmental specifications

Operating temperature range	0 to 70 °C
Storage temperature range	-40 to 70 °C
Humidity	0 to 90% non-condensing

Mechanical

Table 20. Mechanical specifications

Dimensions	79 millimeters (mm) long x 82 mm wide x 25 mm high
USB cable length	*3 meters max*
User connection length	*3 meters max*

Main connector and pin out

Table 21. Main connector specifications

Connector type	Screw terminal
Wire gauge range	16 AWG to 30 AWG

4-channel differential mode

Pin	Signal Name	Pin	Signal Name
1	CH0 IN HI	21	Port A0
2	CH0 IN LO	22	Port A1
3	AGND	23	Port A2
4	CH1 IN HI	24	Port A3
5	CH1 IN LO	25	Port A4
6	AGND	26	Port A5
7	CH2 IN HI	27	Port A6
8	CH2 IN LO	28	Port A7
9	AGND	29	GND
10	CH3 IN HI	30	PC+5V
11	CH3 IN LO	31	GND
12	AGND	32	Port B0

13	D/A OUT 0	33	Port B1
14	D/A OUT 1	34	Port B2
15	AGND	35	Port B3
16	CAL	36	Port B4
17	GND	37	Port B5
18	TRIGIN	38	Port B6
19	SYNC	39	Port B7
20	CTR	40	GND

8-channel single-ended mode

Pin	Signal Name	Pin	Signal Name
1	CH0 IN	21	Port A0
2	CH1 IN	22	Port A1
3	AGND	23	Port A2
4	CH2 IN	24	Port A3
5	CH3 IN	25	Port A4
6	AGND	26	Port A5
7	CH4 IN	27	Port A6
8	CH5 IN	28	Port A7
9	AGND	29	GND
10	CH6 IN	30	PC+5V
11	CH7 IN	31	GND
12	AGND	32	Port B0
13	D/A OUT 0	33	Port B1
14	D/A OUT 1	34	Port B2
15	AGND	35	Port B3
16	CAL	36	Port B4
17	GND	37	Port B5
18	TRIGIN	38	Port B6
19	SYNC	39	Port B7
20	CTR	40	GND

Measurement Computing Corporation
10 Commerce Way
Suite 1008
Norton, Massachusetts 02766
(508) 946-5100
Fax: (508) 946-9500
E-mail:
info@mccdaq.comwww.mccdaq.com

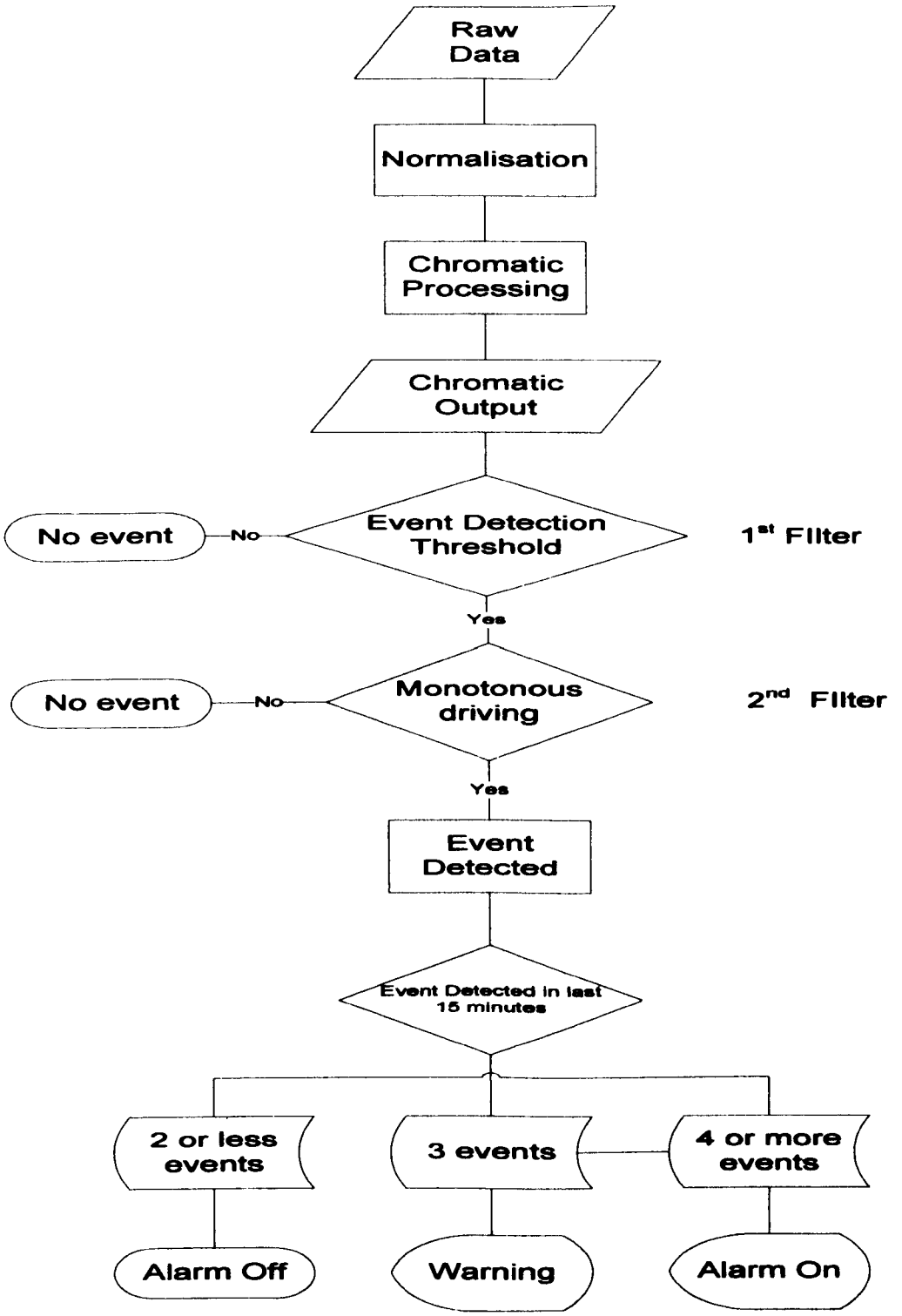
Raw Data
Normalisation
Chromatic Processing
Chromatic Output
Event Detection Threshold
No
No event
1st Filter
Yes
Monotonous driving
No
No event
2nd Filter
Yes
Event Detected
Event Detected in last 15 minutes
2 or less events
3 events
4 or more events
Alarm Off
Warning
Alarm On